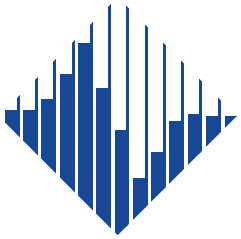

PACIFIC EARTHQUAKE ENGINEERING
RESEARCH CENTER

Seismic Evaluation and Retrofit of Existing Tall Buildings in California

Case Study of a 35-Story Steel Moment-Resisting Frame Building in San Francisco

Jiun-Wei Lai
Pacific Earthquake Engineering Research Center

Shanshan Wang
Department of Civil and Environmental Engineering
University of California, Berkeley

Matthew J. Schoettler
Pacific Earthquake Engineering Research Center

Stephen A. Mahin
Department of Civil and Environmental Engineering
University of California, Berkeley

PEER Report No. 2015/14
Pacific Earthquake Engineering Research Center
Headquarters at the University of California, Berkeley

PEER 2015/14
December 2015

Disclaimer

The opinions, findings, and conclusions or recommendations expressed in this publication are those of the author(s) and do not necessarily reflect the views of the study sponsor(s) or the Pacific Earthquake Engineering Research Center.

Seismic Evaluation and Retrofit of Existing Tall Buildings in California:

Case Study of a 35-Story Steel Moment-Resisting Frame Building in San Francisco

Jiun-Wei Lai
Pacific Earthquake Engineering Research Center
University of California, Berkeley

Shanshan Wang
Department of Civil and Environmental Engineering
University of California, Berkeley

Matthew J. Schoettler
Pacific Earthquake Engineering Research Center
University of California, Berkeley

Stephen A. Mahin
Department of Civil and Environmental Engineering
University of California, Berkeley

PEER Report No. 2015/14

Pacific Earthquake Engineering Research Center
Headquarters at the University of California, Berkeley

December 2015

ABSTRACT

The seismic performance of new tall buildings located in regions of high seismic hazard has been recently investigated by Pacific Earthquake Engineering Research Center (PEER) under its Tall Buildings Initiative (TBI) program. This program has now expanded to assess the seismic performance of existing tall buildings. Buildings being considered are 20 stories or more in height and were constructed on the west coast of the U.S. between about 1960 and 1990. During that period, several hundred tall buildings were constructed in California, but earthquake-resistant design procedures were not as fully developed as they are today.

A 35-story steel building located in San Francisco and designed in 1968 is selected as the subject of the detailed seismic evaluations presented in this report. Results from several three-dimensional (3D) nonlinear dynamic analyses are presented to examine the potential seismic performance of this structure in future earthquakes. Two primary earthquake hazard levels are used for these evaluations. Several different numerical models are developed for the building to represent different behavior characteristics for the as-built structure, as well as for the building following various retrofits. The models were developed in accordance with recommendations of ASCE 41-13 and other relevant guidelines, and simulations were carried out using the analysis framework OpenSees. Analysis results for the as-built and upgraded structure are interpreted considering the methodologies and performance criteria suggested in ASCE 41-13, FEMA 351, and FEMA P-58. With an understanding of the building's potential seismic vulnerabilities, the sensitivity of its behavior to ground motion and structural characteristics, and the capabilities of different guidelines, several retrofit strategies are identified and explored, focusing on modification of the existing structure and the addition of fluid viscous dampers (FVDs).

In terms of the evaluation of seismic response, performance objectives based on ASCE 41 were used; i.e., damage control under the BSE-1E hazard and limited safety under the BSE-2E hazard. The evaluations conducted indicate that the as-built case-study structure does not satisfy these objectives. Three major seismic deficiencies are identified as part of the ASCE 41 Tier 3 evaluations conducted: (1) the case-study building tends to form weak-story regions in the lower third of the building; (2) pre-Northridge beam-to-column connection details result in a high percentage of connection failures under BES-2E events; and (3) there is a high probability of brittle failures of column splices under BSE-1E and BSE-2E hazard-level excitations. Considering the oriented evaluation approach and performance criteria presented in FEMA 351, the case-study building in its as-built condition is found to be unable to achieve the global collapse prevention performance goal at the 90% confidence level for either a BSE-1E or BSE-2E hazard-level event.

Several retrofit scenarios are explored wherein modifications were made to the existing structure. These included replacing the heavy exterior cladding with a lightweight curtain wall system, retrofitting the column splices, and retrofitting the beam-to-column connections. Additional analyses are then carried out to assess enhanced retrofit schemes that introduce Fluid Viscous Dampers (FVDs) over the full or partial height of the building. In the studies presented, the FVDs improve the performance at the BSE-1E and BSE-2E hazard levels. They reduce the peak drift ratios, residual drift ratios, and localized connection fractures; in addition, they help suppress floor accelerations and lead to more rapid decay of seismic vibrations. However, the analysis results indicate that large damper force capacities are needed to achieve the desired

improvement in performance, especially in the most deformed stories. To obtain equal or better improvements in performance, and to reduce the number and size of the damping devices, a simplified optimization method is used to identify several more retrofit schemes that consider different damper properties, distribution of damper properties, and damper placement configurations. A simplified performance-based evaluation of the incremental costs and likely loss reductions is then made for the final retrofit strategies as well as for the as-built structure. Retrofit of the building is found to be very beneficial, but additional study is recommended to better estimate costs of implementing the retrofits, including costs associated with disruption of function during retrofit and business interruption losses following earthquakes. Recommendations are offered for changes that should be considered in developing future editions of ASCE 41 and for further research to improve the certainty with which response of existing tall buildings—in their as-built and retrofit condition—might be predicted. Because only a single structure is evaluated herein, it is finally recommended that other tall buildings be evaluated, and that a group of researchers and practitioners be gathered to develop improved guidelines for assessing and retrofitting existing tall buildings

ACKNOWLEDGMENTS

This study is supported in part by California Office of Emergency Services (CalOES) under Contract No. DR-1884: *Seismic Performance of Existing Tall Buildings and Development of Pilot Internet Database for Post-Earthquake Applications*. Additional funding was provided by the Pacific Earthquake Engineering Research Center (PEER) as part of its Tall Buildings Initiative and Next-Generation Attenuation Relation programs.

The assistance of Drs. Frank McKenna and Andreas Schellenberg in helping develop the OpenSees numerical models presented in this report is gratefully acknowledged. The authors especially appreciate the efforts of Professor Jack Baker of Stanford University for his efforts to develop the site-specific ground motions used in this study. In addition, the authors would like to thank Drs. Kit Miyamoto and Amir Gilani of Miyamoto International, Inc., for sharing their expertise and advice on the application of FVDs for seismic retrofit, Ronald Hamburger of Simpson Gumpertz & Heger, Inc., for sharing information about an earlier assessment of the case-study building, the owner of the case-study building for sharing structural and architectural drawings for the building, and several other engineering firms for providing information on the issues they encountered in the evaluation of similar older tall buildings.

Any findings, opinions, and conclusions or recommendations expressed in this report are those of the authors, and do not necessarily reflect the views of the sponsors, the Regents of the University of California, other organizations, or other individuals.

CONTENTS

LIST OF TABLES

LIST OF FIGURES

1 Introduction

1.1 MOTIVATION

The seismic performance of new tall buildings located in highly seismic areas of California has been recently investigated by the Pacific Earthquake Engineering Research Center (PEER) as part of a program referred to as the Tall Buildings Initiative (TBI). The first phase of the TBI program culminated in a set of engineering guidelines that allow new tall buildings to be designed with high confidence to achieve performance consistent with the basic performance objectives articulated by current building codes for typical buildings. It is expected that these guidelines will be updated as more experience and evidence is gathered from tests, analyses, and actual earthquakes, and guideline development efforts will be extended to refine these guidelines to address issues related to tall structures designed with the expectation that they achieve enhanced or special levels of performance.

A second phase of the TBI has been introduced recently to examine the performance of existing tall buildings. This phase was motivated because many existing tall buildings worldwide were designed and constructed when understanding of earthquake hazards and structural behavior were not advanced. This is especially true in California, where significant numbers of buildings greater than 20 stories in height were built between 1960 and 1990. Given the number and importance of these tall buildings in California, a preliminary study of a case-study building was undertaken and is reported herein. In addition, the feasibility of seismic retrofit to mitigate potential vulnerabilities was studied as part of the current effort. This report examines some of the potential seismic vulnerabilities of existing tall buildings in California, in general, and focuses on specific issues of a representative 1968-vintage, 35-story tall, steel moment-resisting frame building located in San Francisco.

This study is especially relevant for PEER in light of the major technical advances in the field of performance-based earthquake engineering (PBEE) that PEER has been leading since 1997, the development of the TBI guidelines, and the recent advances in quantification of seismic hazard in California through PEER's NGA programs [Bozorgnia et al. 2014].

1.2 TALL BUILDING INITIATIVE PROGRAM (TBI-1)

With the resurgence of tall building construction at the beginning of the twenty-first century, PEER embarked on a multidisciplinary, multi-institutional program of investigation to assess the seismic performance of newly constructed tall buildings, taking into account changes in architectural styles, height and configuration, structural and foundation systems, seismic hazards,

and acceptance criteria that had occurred since the previous generation of tall structures was constructed. The TBI program culminated in a set of background documents and design guidelines intended to provide designers, public officials, and occupants with high confidence that these structures would achieve the targeted seismic performance [PEER 2010a]. The TBI program was guided by a small Project Advisory Committee, and work was undertaken by a team of expert researchers, practitioners, and regulatory officials. Broad community engagement was sought through series of regular workshops and other outreach activities. The work plan was divided into a series of tasks:

- Establish Project Advisory Committee;
- Develop consensus on performance objectives;
- Baseline assessment of dynamic response characteristics of tall buildings;
- Select ensembles of ground motions representing different hazard levels;
- Review and validate ground motion records;
- Develop guidelines on selection and modification of ground motions records;
- Develop guidelines for modeling and acceptance values;
- Identify appropriate methods for inputting ground motions in tall buildings with basement levels;
- Dissemination of findings and solicit feedback;
- Develop performance based design guidelines for tall buildings; and
- Quantification of seismic performance expectations for tall buildings designed according to these new guidelines

The primary document produced by the TBI was the Guidelines for Performance-Based Seismic Design of Tall Buildings [PEER 2010a]. This document synthesized the results and findings from the remainder of the project. It was intended to support ongoing guidelines and code-writing activities of collaborating organizations, as well as being a stand-alone reference for designers of high-rise buildings. The TBI Guidelines contain information on:

- Design performance objectives;
- Documenting design criteria;
- Selecting the seismic input for (a) service-level evaluation, (b) design-level earthquake shaking evaluation, and (c) maximum considered earthquake shaking evaluation;
- Preliminary design – Typically, the initial design would be based on regular building code prescriptive measures assuming that these are appropriate for the new tall building;
- Service-level evaluation – The design developed in the preliminary design process is then evaluated, considering its performance when subjected to less intense ground shaking. The design is revised as needed to meet

acceptance criteria established for the performance expected at this level of excitation. Thus, the structure is expected to have relatively small lateral displacements and nearly elastic behavior;

- Maximum considered earthquake shaking evaluation – The revised structure is then subjected to earthquakes corresponding to the highest level of seismic excitation considered. Recommendations are provided on numerical modeling and acceptance criteria;
- Documentation of results – The documentation needed to substantiate the adequacy of the design is outlined; and
- Project review – It is presumed that a structural peer review process would be used in conjunction of the performance-based design of a tall building. The TBI Guidelines discuss the qualifications of the reviewer and the scope of his/her work.

Several technical reports were also developed to substantiate the recommendations contained in the TBI guidelines and to assist users of the guidelines in applying them to real-world projects. These reports include:

- Seismic Performance Objectives for Tall Buildings [Holmes et al. 2008];
- Modeling and acceptance criteria for seismic design and analysis of tall buildings [PEER 2010b];
- Input Ground Motions for Tall Buildings With Subterranean Levels [Stewart and Tileylioglu 2010]; and
- Case Studies of the Seismic Performance of Tall Buildings Designed by Alternative Means: Task 12 Report for the Tall Buildings Initiative [PEER 2011].

The TBI Guidelines and supporting documents are widely used in designing tall buildings for performance levels not addressed in normal building codes, or in cases of design where the building or design approach do not satisfy basic code prescriptive requirements. In such cases, the TBI Guidelines are used as a part of a framework for using alternative means to demonstrate that a structure satisfies the basic safety and other requirements for buildings.

Two other guidelines are often used specifically for the design of tall buildings. These are:

- *An Alternative Procedure for Seismic Analysis and Design of Tall Buildings Located in the Los Angeles Region* [LATBSDC 2014], Los Angeles Tall Buildings Structural Design Council, and
- *Requirements and Guidelines for the Seismic Design of New Tall Buildings using Non-Prescriptive Seismic-Design Procedures* [SFDBI 2014.

1.3 TALL BUILDING INITIATIVE PROGRAM PHASE 2 (TBI-2): ASSESSING EXISTING TALL BUILDINGS

The inventory of existing tall buildings (taller than 20 stories) in California, with emphasis on buildings located in Los Angeles, Oakland, and San Francisco, is discussed in Chapter 2. The first wave of the post-World War II tall building construction in California covered the period from the late 1960s through the 1990s. During this period, the understanding of earthquake hazards and structural behavior was not as advanced as now. Many changes have been made since then to improve modern building codes. These changes have identified several known vulnerabilities of existing tall buildings, including:

- Low required design base shear forces;
- Few or no drift limits imposed on the building during the design process;
- Use of simplified equivalent static lateral load analysis and design methods that were not able to address the complexities of dynamic response;
- Vertical irregularities, especially near the base of tall buildings, where partial mezzanines, tall ground-story columns, discontinuous columns, large transfer girders, and sudden changes in framing systems may occur;
- Plan irregularities, including L, T, or other irregular floor plan layouts, and asymmetrical placement of lateral load-resisting systems;
- Member proportions and sizes not passing the "strong-column–weak-beam" checks;
- Capacity design principles not used in design;
- Column splice and similar details not being able to develop member capacity;
- Beam-to-column and panel zones not seismically designed;
- Built-up sections not being able to develop their full flexural or shear capacities, and
- Column loads not adequately transferred to foundations.

Furthermore, tall buildings constructed in California during this period predominately, although not exclusively, employed welded steel moment-resisting frames as their lateral load-resisting system. At that time, these systems were believed to be among the very best for providing ductile seismic resistance to strong earthquake ground shaking. However, the 1994 Northridge, California, earthquake caused previously unexpected brittle ruptures to these structures in the vicinity of the welds of the beams to the columns [FEMA 2000h].

Although none of the welded steel moment-resisting frame buildings shaken by the Northridge earthquake collapsed, many sustained substantial damage, and required expensive and disruptive efforts to inspect and repair damaged connections. The following year, the Hyogo-ken Nanbu (Kobe) earthquake produced similar damage in welded steel moment-frame structures. While the structural details used in Japan differed from those in the U.S., Japanese

engineers expected these structures to exhibit highly ductile behavior as well; however, many of these buildings exhibited behavior similar to that seen in the U.S. According to the Architectural Institute of Japan (AIJ), as many as 10% of the low-rise steel moment-resisting frames collapsed in this more intense earthquake.

Given the number and importance of these older tall buildings in California, it is prudent to evaluate their seismic performance and assess the feasibility of retrofitting these buildings to address seismic vulnerabilities. This is especially relevant now in light of the major technical advances in numerical simulation techniques and PBEE. Phase 2 of the Tall Building Initiative focuses on the seismic performance of existing tall buildings.

1.4 OBJECTIVES AND SCOPE

In view of the total number of existing tall buildings in California, the significant number of potential seismic deficiencies in the existing tall buildings, and the damage to steel buildings observed in past earthquakes, the fundamental goal of the research reported herein is to investigate the seismic performance of a representative existing tall building under recorded ground motions corresponding to hazard-levels, and to identify and evaluate cost-efficient and effective seismic retrofit schemes. The specific objectives and scope of the study presented in this report are as follows:

- Provide a preliminary overview of the inventory of existing post-World War II tall buildings in California, examine the general behavior of tall buildings in past earthquakes, identify potential deficiencies in early design methods that might lead to poor seismic behavior in future earthquakes, and review various methods available to assess the seismic behavior of existing tall buildings;
- To select a case-study building that represents the typical configuration and structural details used in the existing tall buildings, particularly those constructed before the 1994 Northridge earthquake;
- To conduct comprehensive structural analyses of the case-study building;
- To assess seismic performance of the case-study building using the up-to-date national standard ASCE 41-13 [ASCE 2014] evaluation procedures along with earlier procedures developed for steel moment frames FEMA 351 (FEMA 2000c) and recent advanced PBEE concepts contained in FEMA P-58 [FEMA 2012a, b, c];
- To examine the feasibility and cost-effectiveness of retrofit schemes to achieve targeted performance levels for the case-study building; and
- To identify best practices and guideline improvements, as needed, in conjunction with advice from the profession.

1.5 REPORT OVERVIEW

In order to achieve the research objectives described in Section 1.4, a series of analytical studies were conducted on the case-study building using the state-of-the-art simulation tools. A brief review of literature related to such studies is presented in Chapter 2. This review provides a better understanding of the inventory of existing tall buildings in California, damage observed in tall buildings following past earthquakes, the changes in building code provisions, the evolution of seismic performance evaluation methodologies, and previous studies of existing tall buildings similar to the case-study building.

A representative case-study building is identified in Chapter 3. The geometry of the building is described along with the structural systems used to carry vertical and lateral loads. Typical structural details are also described.

Chapter 4 examines the seismic performance evaluation procedures used in this study, along with the performance objectives considered. While the case-study building is based on an actual building, several simplifying assumptions were made consistent with the intent of this study. Several different mathematical models were developed to understand the contributions of different structural and ground motion characteristics to seismic performance, also described in Chapter 4. Several of these models examine basic retrofit strategies based on simple modifications to the model of the as-built structural system. These include reducing the mass of the building by replacing the heavy exterior cladding used on the building with a lightweight curtain wall, preventing a brittle failure of column splices, and upgrading the beam-to-column connections in the building to preclude premature brittle failures.

The seismic hazard levels used in the ASCE 41-13 and FEMA 351 evaluations and in the more refined FEMA P-58 assessments are described in Chapter 5. This chapter also describes the site-specific ground motions used in the study, including the selection, scaling, and modification criteria used. Ground motions were selected from the recently developed NGA West2 Ground Motion Database [PEER 2015].

The characteristics and parameters used to numerically model different structural components, loading case definitions, and other relevant modeling assumptions are described in Chapter 6. Limitations of the numerical models used in the study are also discussed.

The results of the ASCE 41-13 evaluation are presented in Chapter 7. Potential seismic deficiencies are identified from the Tier 1 screening procedure outlined in ASCE 41-13 and are presented in this chapter. Results for several nonlinear static pushover analyses are also presented to better understand the general behavior trends exhibited by the case-study building, and to highlight the different behavior among the various numerical models used in the dynamic analyses. Results of time-history response analyses of seismic response (Tier 3 evaluations) are then described for the different structural models described in Chapter 4, and for sets of ground motions representing different hazard levels presented in Chapter 5. Results are presented for individual models and records, and for cases with and without the vertical component of ground shaking. Statistical results showing the median response for a set of motions at a particular hazard level for each mathematical model are also presented, as well as information on the dispersion of results for different records. Results are presented for global response quantities (such as floor displacements, story drifts and shear forces, and floor accelerations) for three hazard levels defined in ASCE 41-13 (BSE-1E, BSE-2E, and 50%/30yrs). Local results such as

member chord rotations, plastic strains or rotations, member axial loads, etc., are also presented. FEMA 351 is then used to evaluate the probability of achieving local and global collapse of the building at different seismic hazard levels. Overall, Chapter 7 summarizes the findings and seismic deficiencies identified from the evaluations using ASCE 41-13 and FEMA 351.

Chapter 8 discusses several additional strategies to mitigate the specific vulnerabilities identified in the dynamic analyses presented in Chapter 7. Among those strategies suggested, the addition of fluid viscous dampers is considered to be the most promising; as such, it is the primary approach examined in this chapter. Several analytical methods for selecting the size and characteristics of the supplemental dampers are described. An iterative design and evaluation approach is followed. In the first phase, several studies are undertaken for a limited number of ground motions to assess the overall feasibility of improving behavior. In the second phase, the results of these studies are used in conjunction with the distribution and properties of supplemental dampers to optimize performance and cost considerations. A number of remaining issues are also identified, and suggestions for enhancing the performance of the retrofit structure are discussed. In these studies presented, few considerations are given to aesthetic, programmatic, or constructability issues. However, the implications of the performance of the as-built and retrofit structure for various seismic hazards is assessed in terms of initial costs, repair costs, downtime, and likely tagging decisions. Notwithstanding these investigations, further study is needed.

The last chapter summaries the overall findings of this study, and specifically contains recommendations for improving ASCE 41-13 and other evaluation guidelines, the need for improved modeling and component testing of members and connections, and opportunities for further research related to existing tall buildings in general.

Several appendices are provided that contain detailed information on ground-motion selection and scaling, ASCE 41 Tier 1 checklists, and more comprehensive sets of plots of the results of the dynamic response analyses.

2 Review of Literature

2.1 INTRODUCTION

This chapter presents background information related to the assessment of the potential seismic risk to older tall buildings in California. This material includes results of a preliminary inventory of existing tall buildings in the State, which identified the number of buildings involved and their general characteristics (e.g., age, height, structural system, etc.). As a guide for the failure mechanisms of interest to be studied in this research, the behavior of tall buildings of the type constructed in California after the Second World War during several major earthquakes is then examined to better understand the types of damage exhibited by these types of structures.

The occasional poor behavior in these and other buildings, and improvements in science and engineering knowledge underpinning seismic-resistant design resulted in rapid changes in building codes over the past three decades. These changes are reviewed to help identify the particular vulnerabilities that might be associated with various vintages of construction. This assessment is followed by a review of the evolution of criteria used to assess the response and performance of existing buildings, with a focus on tall buildings. Information is then presented on past evaluations that have been carried out on tall buildings. These past studies provide a basis for assessing the results presented in this report. Lastly, a few preliminary observations are presented relative to the needs for future research.

2.2 BUILDING INVENTORY OF EXISTING TALL BUILDINGS

In order to assess how many potentially vulnerable tall buildings are located in California, a preliminary inventory of these buildings was conducted. The inventory was developed primarily from building databases available on two websites: *www.skyscraperpage.com* and *www.emporis.com*.

Buildings with 20 or more stories and whose construction was completed before 2012 were included in the inventory. Only Los Angeles, San Francisco, and Oakland were included in the preliminary inventory, as these cities contained by far the majority of the tall buildings constructed during the time period of interest. It is assumed that older tall buildings of similar vintage and construction exist in Sacramento, San Diego, and other sites throughout Northern and Southern California. The inventory includes buildings with any type of lateral force-resisting system.

To help select the case-study building to be evaluated, the data was then grouped based on building construction era, building height, and lateral load-resisting system. Figure 2.1 illustrates the grouped inventories for the three selected cities. From the initial statistics shown in Figure 2.1, there are 371 existing tall buildings taller than 20 stories in the three cities, with San Francisco having the greatest number of buildings of interest.

About 55% of these tall buildings in San Francisco and more than 65% of these buildings in Los Angeles were constructed between 1960 and 1989. This period was one of exceptional growth for the state, as reflected in the significant number of tall buildings constructed during that time. Unfortunately, the understanding of earthquake hazards and structural behavior then was nowhere as advanced as it is now.

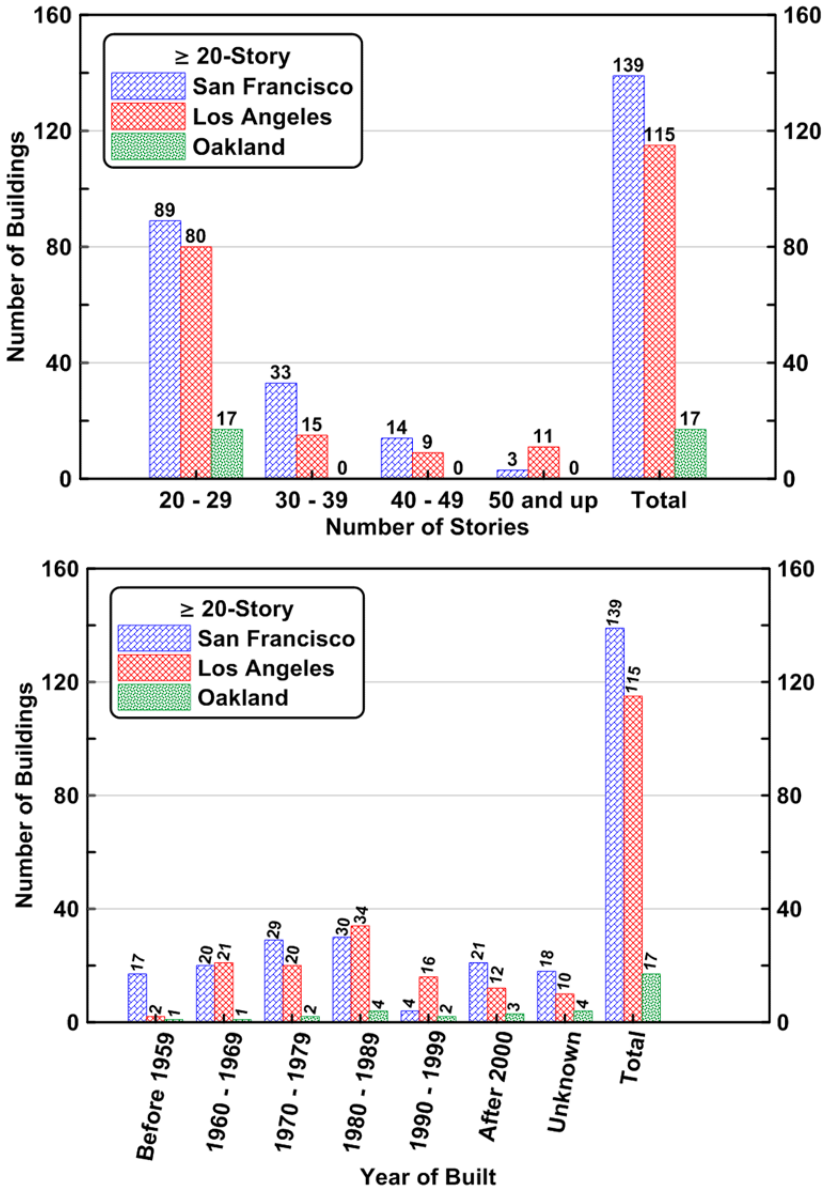

Figure 2.1 **Inventory of tall buildings at three major cities in California (San Francisco, Los Angeles, and Oakland).**

The overall inventory shows that nearly 70% of the tall buildings are between 20 and 29 stories. Note that 14 buildings (3%) in the inventory are taller than 50 stories. Many of these buildings are iconic structures that dot the skylines of these cities.

It is difficult to break up the data in the current existing tall building inventory based on the type of lateral force-resisting system. The two databases used to construct the inventory only list the construction materials used (e.g., concrete, steel, etc.). Information on the type of lateral force-resisting system for a few buildings was gathered from a literature review of research papers and technical reports available in public domain, or was obtained in meetings with structural engineers practicing design before 1990.

A previous survey in San Francisco by Almufti et al. [2012] revealed that the steel moment-resisting frame system was the most prevalent type used between 1960 and 1990. This appears consistent with discussions with engineers practicing during that period. To narrow down the search for the case-study building, the study focused on buildings located in San Francisco built between 1970 and 1989 with steel moment-resisting frame systems that are 20 or more stories high.

2.3 DAMAGE TO TALL BUILDINGS AND STEEL MOMENT-RESISTING FRAME BUILDINGS IN PAST EARTHQUAKES

2.3.1 Background

As reported in the literature, a few relatively modern buildings have collapsed or partially collapsed in earthquakes. Examples, including damage and failures of mid-rise to tall buildings, have been reported following the 1985 Valparaiso, Chile, earthquake [Wyllie (ed.) 1986]; 1985 Mexico City earthquake (e.g., Osteraas and Krawinkler [1989]); 1988 Armenia earthquake [Wyllie and Filson (eds.) 1989]; 1993 Guam earthquake [Comartin et al. (eds.) 1995]; 1994 Northridge, California, earthquake [Hall (ed.) 1994]; 1995 Kobe, Japan earthquake [Comartin et al. 1995; Nakashima et al. (eds.) 1998]; 1999 Kocaeli, Turkey earthquake [Youd et al. (eds.) 2000]; 1999 Chi-Chi, Taiwan earthquake [Uzarski and Arnold (eds.) 2001]; Canterbury, New Zealand, earthquakes [EERI 2010a]; and 2010 Chile earthquake [EERI 2010b]. In addition, considerable damage to nonstructural elements and contents was noted in modern high-rise buildings during the 2010 Chile and 2011 Great East Japan earthquake [EERI 2012], and substantial movement and distress to occupants in high-rise buildings located at large distances from the causative fault ruptures were reported during the 2008 Wenchuan earthquake [Liang et al. 2009], the 2010 Chile earthquake [EERI 2010b], and 2011 Great East Japan earthquake.

This section examines the seismic response of mid-rise to high-rise buildings to some of these earthquakes. Because of the focus on steel moment-frame structures in this report, emphasis will be placed on earthquakes and structures that shed light on the behavior of steel structures during severe earthquake ground shaking. It is useful to note that statistically very few partial or complete collapses of tall steel buildings have been observed worldwide.

2.3.2 1985 Mexico Earthquake

During the 1985 Mexico earthquake, adjacent 21-story and 14-story tall steel buildings in the Pino Suarez Complex in Mexico City collapsed. Analysis of these structures [Osteraas and

Krawinkler 1989; Osteraas 1990; and Ger et al. 1993] identified the failure mechanism. The complex consisted of five steel buildings, three 21-story buildings, and two 14-story buildings (Figure 2.2). During this earthquake, one of the 21-story buildings (Bldg. D in Figure 2.2) collapsed onto the adjacent 14-story building (Bldg. E in Figure 2.2), resulting in its collapse. The two remaining 21-story buildings and one 14-story building sustained significant damage but did not collapse (Figure 2.3). One of the remaining 21-story buildings had significant permanent lateral displacement following the earthquake. All of the buildings were subsequently demolished.

Unlike steel moment-resisting frame buildings common in the U.S., the structural system of those buildings was a combination of steel moment-resisting frames and steel braced frames. The moment-frame portion of the structures incorporated many details not typically found in the U.S. For example, columns were built-up box sections fabricated from thin plates, and the beams were built-up truss girders. The top and bottom chords of these truss girders were constructed from angle sections and were connected to the columns by welding to form moment connections. A conventional plastic hinge in the beams was thus not possible.

Typical failure modes observed are shown in Figure 2.4. It is believed that several factors contributed to the 21-story building's collapse. These factors included poor built-up section welding details in the box columns and truss girders, column over loading (including P-Δ effects), torsional effects (plan irregularity), excessive live loads at the time of the earthquake, and long-duration ground motions [Krawinkler and Martinez-Romero 1989].

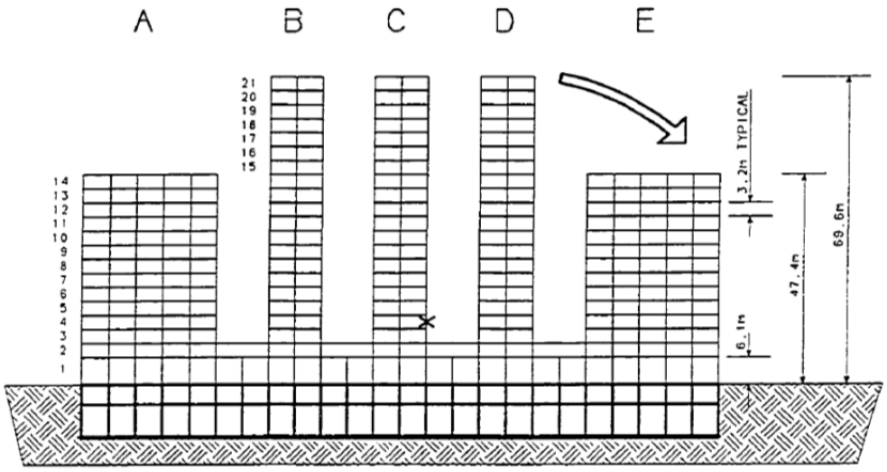

Figure 2.2 **Elevation view of the Pino Suarez Complex (extracted from Osteraas [1990]).**

(a)

(b)

Figure 2.3 Collapse of a 21-story steel building onto a 14-story building during the 1985 Mexico earthquake; (a) aerial view (source John Osteraas); and (b) side view (source: *www.skyscrapercity.com*).

(a) (b)

(c) (d)

Figure 2.4 **Typical failure modes observed Pino Suarez Complex in the 1985 Mexico earthquake: (a) plate buckling and fracture of welds in a built-up box column [EERI 1997]; (b) temporary supports for the buckled box columns (source: John Osteraas): (c) truss girder to box column connection bottom chord fracture (source: John Osteraas); and (d) buckling of web-lacing bars in a built-up truss girder (source: John Osteraas).**

2.3.3 1994 Northridge Earthquake

The 1994 Northridge earthquake identified serious and previously undetected problems related to welded steel moment-resisting frame buildings. These problems were associated with premature brittle fractures of the beam-to-column connections that occurred in the vicinity of the welds of the beam flanges to the column flanges. Damage was not immediately obvious because steel components are typically covered with fireproofing and architectural elements; none of earthquake-affected steel buildings collapsed, and few had appreciable permanent drifts.

However, in the months following the earthquake, more and more damage to steel moment-resisting frame buildings was being reported. Researchers and design professionals from the California Universities for Research in Earthquake Engineering (CUREe), the Structural Engineers Association of California (SEAOC), and the Applied Technology Council (ATC) banded together to study the causes of the unprecedented damage, and to develop and validate guidelines to design new steel moment frames and to evaluate, retrofit, and upgrade existing steel buildings [FEMA 2000b–2000f]. This effort was initially funded by the California Office of Emergency Services (OES), and subsequently by the Federal Emergency Management Agency (FEMA). This program, generally known as the SAC Steel Program, resulted in major changes in the design and detailing of steel frame structures, and in the risk assessment of buildings in general. Widespread public concern did not occur for several more months until an article appeared in the Los Angeles Times after the earthquake [EERI 1997].

Post-earthquake inspections identified several types of damage in the beam-to-column connections of steel moment-resisting frame buildings, ranging from very small cracks visible only with crack detection equipment to large cracks that were visible to the naked eye [FEMA 2000b]. Several types of damage are illustrated in Figure 2.5. It was remarkable that none of the connections damaged in the earthquake demonstrated the ductile behavior intended for these types of connections. Instead, the failures all appeared to be quite brittle. This was true in short as well as tall buildings, in new as well as older buildings, and in conventional buildings as well as special-purpose structures like hospitals. The observed brittle fractures extended from the beam flange-to-column flange welds or heat-affected zones (HAZ) through the beam or column. In some cases, cracks extended through adjacent column flanges and progressed into the column web; see Figure 2.5. This type of failure mode was of particular concern.

Because of the increasing amount of reported damage, the Los Angeles City Council adopted an ordinance in 1995 to inspect nearly all steel moment-resisting frame buildings in the most heavily damaged areas of the city. The mandatory inspection later reported about 100 damaged steel buildings in Los Angeles alone, with a total of nearly 2300 damaged beam-to-column connections. These damaged connections comprised about 19% of all of the inspected connections. The averaged repair cost per connection was about $12,400 dollars (at the time of the repair).

From the perspective of this report, it is important to note that no failures of column splices were identified during the post-earthquake inspections. This may be due to the premature failure of the beam-to-column connections, which limited the axial and bending forces that could be developed at the splices, and the relative moderate level of shaking felt by the damaged steel buildings in Los Angeles.

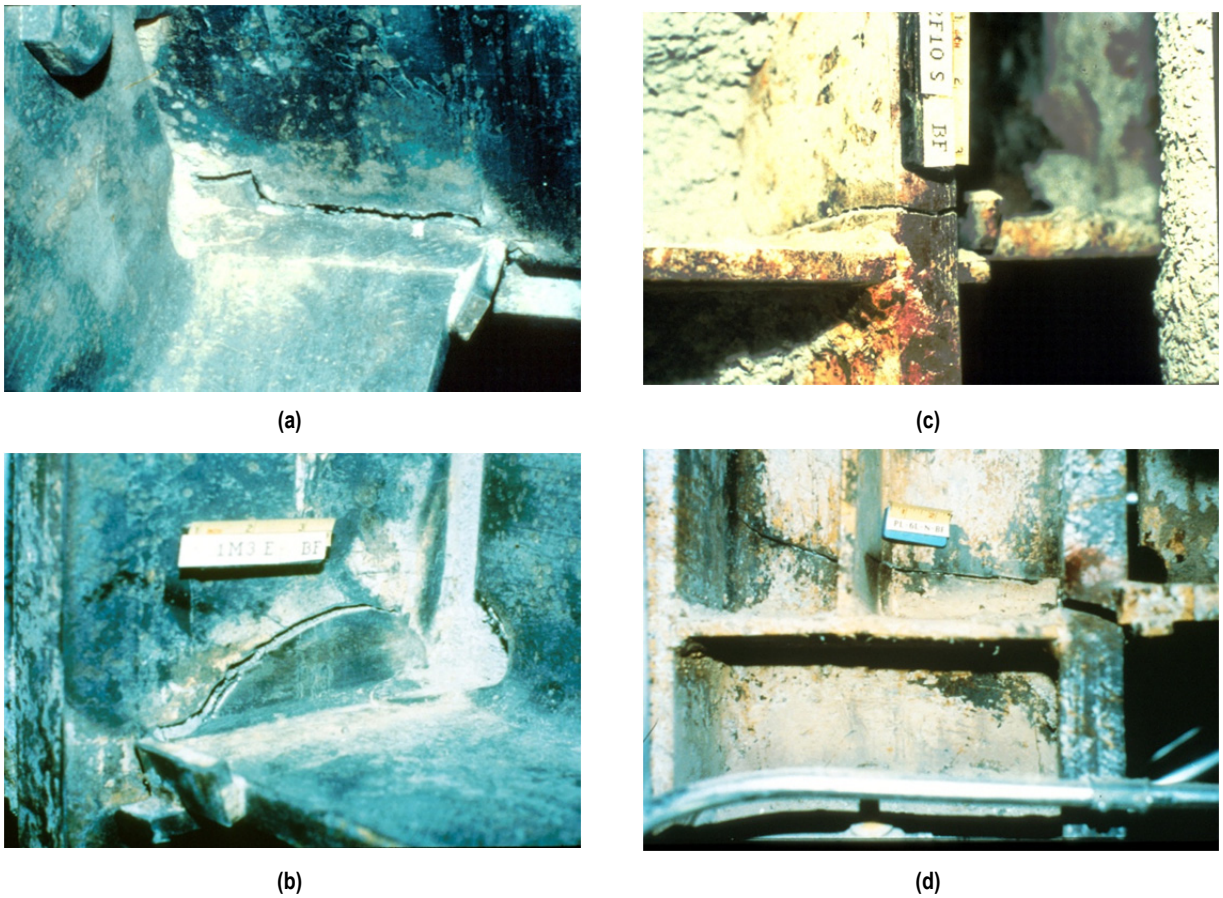

(a) (c)

(b) (d)

Figure 2.5 **Types of connection damage in steel moment-resisting frame buildings observed after the 1994 Northridge earthquake: (a) fracture at heat-affected zone; (b) column flange fracture; (c) fracture through column flange; and (d) fracture through column flange and web (sources: AISC and FEMA-355E).**

The SAC Steel Program carried out inspections and evaluations of damaged buildings, carried out tests and analyses of materials, welds, joints and complete beam-to-column sub-assemblages, and undertook analyses to assess seismic demands and capacities to identify effective methods to evaluate and retrofit or upgrade existing structures. From this process, five principal documents were developed:

- FEMA-350 – *Recommended Seismic Design Criteria for New Steel Moment-Frame Buildings* [FEMA 2000b].
- FEMA-351 – *Recommended Seismic Evaluation and Upgrade Criteria for Existing Welded Steel Moment-Frame Buildings* [FEMA 2000c].
- FEMA-352 – *Recommended Post-Earthquake Evaluation and Repair Criteria for Welded Steel Moment-Frame Buildings* [FEMA 2000d].

- FEMA-353 – *Recommended Specifications and Quality Assurance Guidelines for Steel Moment-Frame Construction for Seismic* Applications [FEMA 2000e].
- FEMA-354 – *A Policy Guide to Steel Moment-Frame Construction* [FEMA 2000f].

In addition, a series of six state-of–the-art reports were prepared as part of the program that summarize the findings of more than 100 individual research reports.

The brittle connection failures were not found to the result of a single type of defect but from the inherent characteristics of moment frames. The connection detail permitted by the then-current building code concentrated stress and strain demands at the welded connection at the location where the beams were attached to the columns, further concentrated demands in potentially brittle zones within these connections, and employed strong but brittle weld materials. Through the use of notch-tough weld materials, the introduction of a variety of detailing changes (the critical regions were moved away from the susceptible welds, localized stress concentrations were reduced, and plastic deformations in panel zones, which compounded inelastic demands on critical locations in the connection, were limited) and improved welding processes and inspection requirements, such welded steel beam-to-column connections, are now expected with high confidence to behave in a ductile manner.

Another unexpected failure observed after this earthquake was the fracture of heavy steel base plates at the Oviatt Library on the campus of the California State University, Northridge. This building utilized a multi-story steel braced frame with X-braced bays as its lateral load-resisting system. The uplift forces imposed on the steel base plates resulting from overturning moments fractured the 4-in.-thick plates at some locations; see Figure 2.6. It was believed that fracture initiated at the welds between columns and base plates.

(a) (b)

Figure 2.6 **Steel column base plate damage observed at Oviatt Library; (a) overview of column base and (b) closed view of crack in the base plate (sources: NISEE and EERI [1997)].**

2.3.4 1995 Kobe Earthquake

The Kobe earthquake (formally known as the Hyogo-Ken Nanbu earthquake) occurred about one year after 1994 Northridge earthquake. Kobe is a major industrial city in southeast Japan. There were many welded steel moment-resisting frame buildings in the city, ranging from low-rise buildings constructed in 1950s and 1960s to high-rise buildings constructed between 1985 and 1995. Unlike the common practice in the U.S., many of the low-rise welded steel moment-resisting frame buildings in Japan utilized cold-formed tubular steel columns rather than hot-rolled wide flange columns or welded built-up sections for the columns. In addition, the beams in those moment frame buildings were connected directly to diaphragms that ran through the beam-to-column moment connections; see Figure 2.7.

Shortly after this earthquake, a detailed investigation of the damage sustained by 988 steel buildings in Kobe was conducted under the Architectural Institute of Japan [AIJ 1995]. This investigation revealed that about 30% of inspected steel buildings had no significant damage, 30% had minor damage, and 30% had severe damage. About 10% of the modern welded steel moment-frame buildings had collapsed partially or completely. Several failure modes were identified in the AIJ report [1995]. Failure modes related to these Japanese steel moment-frame buildings included: column base failure, column splice failure, local buckling of column sections, and beam-to-column connection fractures. Photographs from that report showing typical damage are shown in Figures 2.8–2.11. The results of this report prompted the Japanese government and building officials to call for significant research on the cause of these unexpected failures, combined with an urgent need to develop design guidelines for new construction and evaluation procedures for existing moment frame buildings.

Figure 2.7 **Typical Japanese beam-to-column moment connection detail (source: *www.atlastube.com*).**

Figure 2.8 Beam bottom flange and partial web fractures in a 5-story moment frame [AIJ 1995].

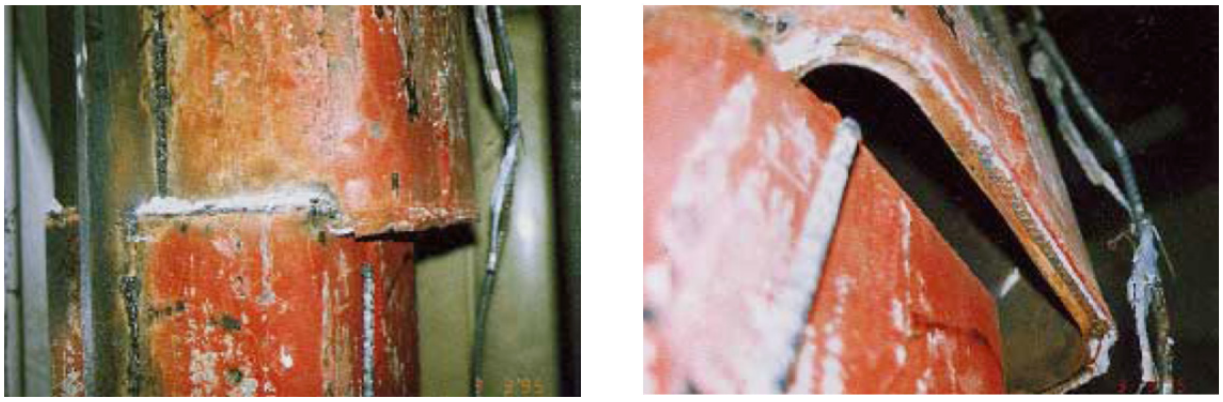

(a) (b)

Figure 2.9 Cold-formed square hollow section column splice failure in a 5-story tall welded steel moment-resisting frame: (a) side view and (b) view from bottom side [AIJ 1995].

Figure 2.10 Local buckling at the top of a cold-formed square hollow section column in a 5-story moment-resisting steel frame [AIJ 1995].

Figure 2.11 Fracture of anchor bolts and shifting of base plate in a 6-story steel moment-resisting frame [AIJ 1995].

Column failures were also observed in a group of high-rise residential steel buildings (Figure 2.12) at Ashiya, a seaside town near Kobe in Japan. Twenty-one out of 52 residential buildings had severe column damage. Constructed in 1975, these buildings ranged from 14 to 29 stories in height whose structural system consisted of mega-truss moment-resisting frames (Figure 2.13). Among all the buildings investigated, the tallest (29-story) building had no column fractures; the shortest (14-story) building had only a few fractures [AIJ 1995]. Most fractures were observed in buildings having 19 or 24 stories. Three types of fracture were observed: (a) fracture in the base metal of built-up box columns (up to 20 in. wide with 2.2-in.-thick walls; see Figure 2.14); (b) fracture in or immediately adjacent to the column-to-brace connections (Figure 2.15); and (c) fracture of column splices (Figure 2.16). All fractures were brittle in nature, with little evidence of significant yielding. Subsequent investigations suggested that the fractures in the base metal (type "a" failures noted above) may have been associated with discontinuities in the backing bars placed longitudinally in the four corners of the box to facilitate welding of the built-up box section. While numerous columns completely fractured, the maximum residual offset of the box columns at the fractures was about 0.8 in. Although serious damage to steel box columns and wide-flange braces in the vertical trusses were observed, the buildings remained plumb and did not appear to have significant damage to other structural or non-structural elements.

The structural system of these buildings was exposed on the exterior of the buildings, and fireproofing was not placed over the structural members. As such, damage was very visible, and inspection and repair of damage to these structures was relatively easy compared to more typical steel buildings.

Figure 2.12 **Aerial view of the buildings in Ashiya, a seaside town in Japan (source: *building-pc.cocolog-nifty.com*).**

Figure 2.13 Side view of one typical 19-story residential building in Ashiya (source: NISEE).

(a) (b)

Figure 2.14 Fracture in the base metal of built-up box columns: (a) source AIJ [1995] and (b) EERI [1995].

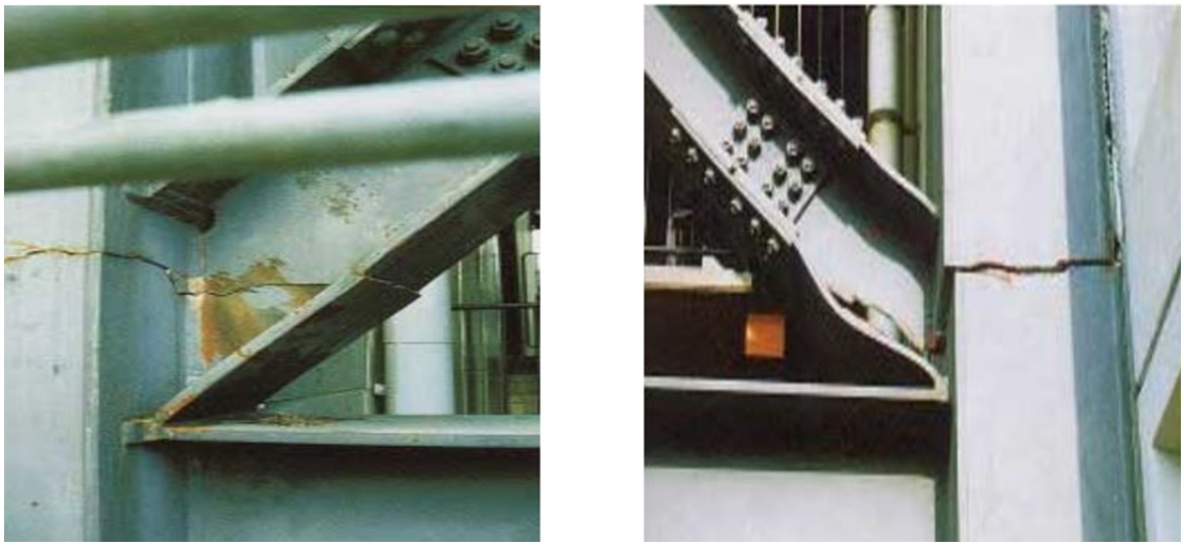

(a) (b)

Figure 2.15 **Fracture at the brace-to-column connection in a residential building in Ashiya [AIJ 1995].**

(a) (b)

Figure 2.16 **Column splice fractures in a residential building in Ashiya (source [AIJ 1995]).**

2.3.5 Other Earthquakes

After the 1994 Northridge and 1995 Kobe earthquakes, engineers and building officials became concerned that similar but undetected damage might have occurred in other welded steel moment-frame buildings during previous earthquakes in California. The SAC Steel Project noted that any steel building of the type damaged in the Northridge earthquake and subjected to ground accelerations in excess of 25%*g* should be inspected for potential brittle fracture of connections.

As a result, voluntary inspections of steel buildings were carried out across the state of California where earthquakes had occurred between 1980 and 1994.

As reported by the investigators working on the SAC steel project [FEMA 2000h], approximately thirty steel welded steel moment-resisting frame buildings shaken by the 1989 Loma Prieta earthquake in the San Francisco Bay Area were inspected. Of these, five were found to have brittle beam-to-column connection fractures. Three of the buildings were in downtown Oakland (which is one of the reasons why Oakland was included in the development of existing tall building inventories), and two were located on the San Mateo Peninsula. The height of the damaged buildings ranged from 6 to 20 stories. The cost for inspecting and repairing fractured connections in a six-story building was estimated to be as high as $2,500,000 USD.

In another study, Anderson and Bertero [1997] reported that a two-story steel moment-resisting frame building sustained damage during the 1992 Landers–Big Bear earthquake. Although connection fractures were not discovered immediately after the 1992 earthquake, damage to steel structures in the 1994 Northridge earthquake prompted additional inspections of this building. The discovery of severe cracking resulted in a seismic upgrade implemented by adding steel braces.

The damage to welded steel moment-resisting frame buildings throughout the state indicates that the potential brittle connection failures observed in the 1994 Northridge earthquake were not isolated phenomena associated with that earthquake, but rather a more fundamental issue related to the welded steel moment-resistant framing system constructed prior to 1994.

2.4 EVOLUTION OF SEISMIC PROVISIONS IN BUILDING CODES

During the past four or more decades, tremendous advances have been made in understanding of seismic hazards, structural analysis, and the inelastic behavior of structures. These leaps of knowledge have been reflected in building codes. However, buildings designed in earlier eras remain seismically vulnerable and developing retrofit strategies to combat this vulnerability is critical.

During the period in question, many structures, including tall steel moment-resisting frame buildings, were designed using allowable stress design methods; limited understanding of the inelastic dynamic response of structures during severe earthquakes was available. In addition, the computational facility that we take for granted today was not widely available when the earliest of these buildings were designed. As a result, members and connections were often designed to only develop forces that resulted from simplified elastic analyses of the structure based on design forces that were quite small compared to what we would expect these structures to withstand today.

For example, Figure 2.17 compares response spectra developed for the design of steel moment-resisting frames in downtown San Francisco constructed from the 1960s to the present. In particular, the two levels of earthquake hazard suggested by ASCE 41-13 for the evaluation of existing buildings, BSE-1E and BSE-2E, are much higher than those considered in the designs executed in the 1990s and earlier. Most of the early design codes specified the earthquake intensity to be consistent with allowable stresses in members rather than the yield values currently considered in the load and resistant factor design approach (LRFD) used in modern codes. However, even if these corrections are made, it is apparent that older steel moment frame

buildings may have been designed for less than one-quarter of the design forces of what would be used to evaluate their performance today.

The use of allowable stress design methods also resulted in member strengths greater than those required to resist seismic lateral loads to satisfy stiffness requirements that limit vertical displacements under gravity loads. This resulted in a member stronger than needed, but the connections might be inadequate to sustain the computed seismic loads. As a result, when computed seismic design loads are exceeded, the member might not yield but the connection could fail. Similarly, as seen in several tall building designs, where structural members are constructed from plates and other structural sections, the welds holding these components together might only be sized for the shear and other forces needed to withstand the computed seismic design forces and not the actual capacity of the member acting like the intended composite section. As such, a variety of poorly understood failure mechanisms are possible.

Table 2.1 shows an evolution of various code provisions, focusing on the introduction of provisions related to the equations used to compute base shear, and the limit imposed on story drifts; special provisions provided to insure ductile behavior are listed for different editions of the building code. It can be seen that drift limits were not explicitly introduced until the 1976 UBC [ICBO 1967]. Some of the prior codes indicated that limits would be desirable, but that the limit should be set by the Engineer of Record (EOR). Thus, it is possible that many older buildings have could have very long fundamental periods, which results in low design forces according to the spectra shown in Figure 2.17, thus developing large lateral displacements in moderate to severe earthquake ground shaking.

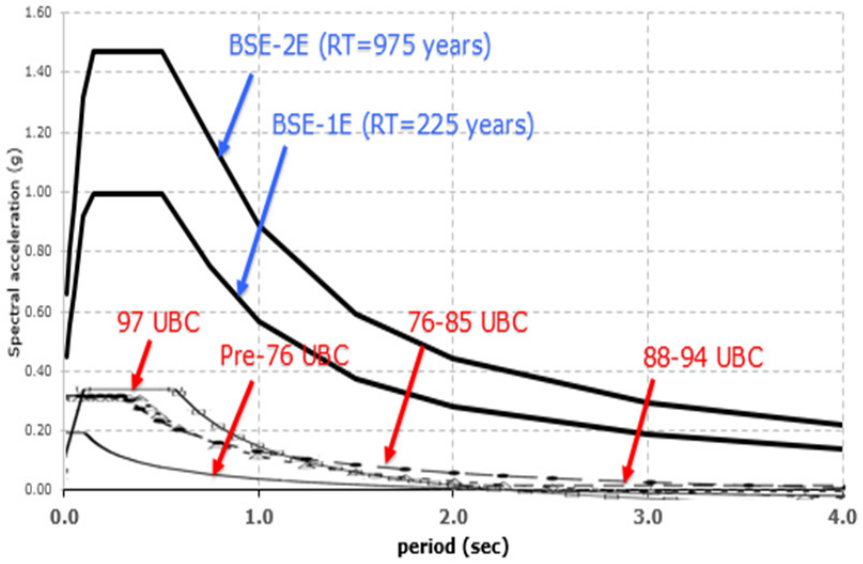

Figure 2.17 **Design response spectra for special moment-resisting frames corresponding to various building codes for San Francisco (modified based on Freeman [2007]).**

Table 2.1 Summary of major additions to building code requirements [FEMA 2000g].

Code Editions	Base Shear	Story Drift Limit	Ductility Requirements
1958	$F = CW$ (C≈0.02)	None	none
1961, 1964, 1967	$V = ZKCW$ K = 0.67 (SMRF)	EOR decide	none
1970, 1973	$V = ZKCW$ K = 0.67 (SMRF)	EOR decide	**Connections should be able to develop full plastic capacity of members** and **plastically compact sections**
1976, 1979, 1982, 1985	$V = ZIKCSW$ K = 0.67 (SMRF)	**0.005**	
1988, 1994	$V = ZICW/\boldsymbol{R_w}$ R_w = 12 (SMRF)	For T > 0.7 sec **Min. (0.03/R_w, 0.004)** at working stress level	**Panel zone** strength and **strong column–weak beam** requirements

Note that no particular requirements were included in early codes to insure that sections could develop and maintain their flexural strength through moderate inelastic rotations. These were not introduced until the 1970 UBC [ICBO 1970], and they have been substantially strengthened since that time. In addition, the 1970 UBC introduced provisions that joints and connections be stronger than the members being joined.

It was only with revisions to the 1988 UBC [ICBO 1988] that two additional important concepts were added. One of these related to the notion that yielding in steel moment-resisting frames should occur in beams rather than in the columns. Today, this is accepted as a logical and essential aspect of the design of moment-resisting frame structures. However, this "strong-column–weak-beam" design concept was not introduced until many tall buildings had been constructed in California and elsewhere. As a result, these older structures might be expected to have a tendency to form weak story mechanisms when loaded into the inelastic range by severe earthquake ground shaking.

A related provision concerning the strength beam–column connections was also added in 1988 for the first time. This explicitly called out for connection panel zones to be designed for shears and other forces corresponding to beam plastic moment capacities being developed under lateral sway of the building. Without this provision, it was possible for moment-frame buildings to have lateral strengths smaller than intended by the code, since yielding might occur prematurely within the beam–column connections.

Thus, during the period of rapid construction of tall buildings in California before 1990, building codes did not require many of the design features taken for granted today. Many structural engineers, aware of these issues, took independent action to limit story drifts by

providing a complete load path to develop the capacities of members and incorporating ductile details. However, this may have not been done comprehensively, or at all, and a wide variety of seismic vulnerabilities might exist today in these structures. Thus, it is important to have available practical and reliable methods to assess the seismic response and performance of such structures.

2.5 EVOLUTION OF SEISMIC PERFORMANCE EVALUATION METHODS

2.5.1 From ATC-14 to ASCE 31-03

Before the 1987 publication of ATC-14 [1987], *Evaluating the Seismic Resistance of Existing Buildings*, the seismic evaluation and upgrade of existing building was based mainly on engineering judgment. This report was one of several pioneer documents [Wright et al. 1973, Veterans Administration 1973; Freeman et al. 1975; Culver et al. 1975; and Bresler et al. 1977] that explicitly addressed seismic evaluation methodology of existing buildings. ATC-14 presented a consensus-based methodology intended to guide engineers in evaluating existing buildings to identify potential seismic deficiencies and vulnerabilities that could endanger human lives. As such, the primary goal of the evaluation methodology was to evaluate and upgrade an existing building to achieve the minimum life-safety performance goal. To this end, it provided a catalog of possible weak links in existing buildings based on past observations of seismic performance. The procedures recommended in ATC-14 extended analysis methods and evaluation concepts developed in ATC-3 [ATC 1978] and ATC-6-2 [ATC 1983]. In particular, the capacity-to-demand ratio concept was used to identify and prioritize the weak links in the structural system. Prototype evaluation checklists for existing buildings within regions of high seismicity were developed and presented in the Appendix C of ATC-14.

In 1992, FEMA published FEMA 178 [1992a], a handbook for the seismic evaluation of existing buildings based on ATC-14. In this document, general sets of evaluation statements (similar to checklists) were developed for areas of high seismicity. A companion FEMA handbook, FEMA-172 [1992b], provided additional information on techniques to mitigate seismic deficiencies for different construction types. Shortly thereafter, the ATC 28 [ATC 1992] and ATC 28-2 [ATC 1993] projects were undertaken to help identify remaining technical and policy issues and suggest approaches for their resolution.

Based on FEMA-178, FEMA 310 [1998] was developed as a pre-standard to help enable turning these guidelines into a national consensus standard. This pre-standard was the result of a joint ASCE and FEMA effort. It provided a three-tiered procedure for seismic evaluation of existing buildings considering multiple levels of seismicity and two performance levels (i.e., life safety and immediate occupancy). An extensive discussion on performance-based evaluation methods and techniques was also included in this document. FEMA 310 was subsequently accepted as a national standard and published as ASCE 31-03 [ASCE 2003].

2.5.2 Moving Toward the Performance-Based Era: Vision 2000, FEMA 273, FEMA 356, and ASCE 41

Following the 1994 Northridge earthquake, the Vision 2000 Committee of SEAOC developed the first generation framework and methodology for performance-based seismic engineering.

Intended to be used for the design of new buildings and for the evaluation and upgrade of existing buildings [Poland et al. 1995], this was the first document that fully outlined performance-based methodologies, and attempted to establish quantitative means of reconciling seismic hazard, performance levels, and building use. As with prior attempts, the methods developed were deterministic (issues of uncertainty were not explicitly treated), and many of the modeling procedures and acceptance criteria used were based on judgment.

Two years later, another landmark document, FEMA 273, the *NEHRP Guidelines for the Seismic Rehabilitation of Buildings*" [1997], was published to serve as a reference document and a tool for structural engineers. This document was originally developed to serve as a base for future development and implementation of performance-based building codes. The developed guidelines contained several significant new features that were very different from the existing seismic design procedures. Displacement-based methodologies were included for the first time in this document [Pekelnicky and Poland 2012]. Other features included: (1) methods and design criteria to achieve different seismic performance levels and ranges were defined; (2) simplified and systematic rehabilitation methods were presented; (3) four distinct analytical procedures for different types of structures were incorporated; (4) structural component behavior was examined quantitatively; and (5) the procedures for incorporating new technologies into rehabilitation were discussed.

Several years later, the FEMA 273 document was expanded and updated technically through joint effort of FEMA and ASCE and released as FEMA 356 [2000a], a pre-standard for use in developing a nationally applicable standard for evaluating and retrofitting existing buildings. Subsequently this pre-standard was revised, balloted, and accepted as a national consensus standard and eventually published as ASCE/SEI 41-06 standard [ASCE 2007]. The intent of developing ASCE 41-06, primarily based on the FEMA 356 pre-standard, was to demonstrate the procedures to rehabilitate existing building to achieve a variety of different performance levels. More detailed discussion on the improvements reflected in the ASCE 41-06 standard can be found in Mitchell and Poland [2007].

2.5.3 ASCE 41: Combining ASCE 31-03 and ASCE 41-06

The first generation of national standards for seismic evaluation and retrofit of existing buildings, ASCE 31-03 and then ASCE 41-06, were used as the basis for seismic evaluation and retrofit of existing buildings, but also for the performance-based design of new buildings. As these standards gained use, several inconsistencies between them were discovered, as well as with ASCE 7-10 [ASCE 2010]; see Pekelnicky and Poland [2012]. As a result, in 2009 the ASCE standards committee decided to combine the ASCE 31-03 and ASCE 41-06 standards into a single integrated and updated standard. The combined standard ASCE 41-13 was published in 2014 [ASCE 2014]. The integrated ASCE 41 methodology now incorporates a three-tiered approach to evaluate an existing and retrofitted structure. For a complex high-rise structure, like the case-study building, the ASCE 41 Tier 1 simplified screening evaluation is not required. Instead, the Tier 3 systematic evaluation procedure is automatically required. ASCE 41-13 is widely used today for the evaluation and retrofit assessment of existing buildings, and for the performance-based design by alternative means of new buildings; see Chapter 4 for a detailed discussion of the ASCE 41 approach.

2.5.4 Guidelines for New Tall Buildings (the PEER TBI and Other Guidelines)

With the resurgence of tall building construction at the beginning of the twenty-first century, PEER embarked on a multidisciplinary, multi-institutional program of investigation to assess the seismic performance of tall buildings. This investigation took into account changes in architectural styles, height and configuration, structural and foundation systems, seismic hazards, and acceptance criteria that had occurred since the previous generation of tall structures was constructed. The tall building initiative (TBI) program culminated in a set of background documents and design guidelines intended to provide designers, public officials, and occupants with high confidence that these structures would achieve the targeted seismic performance. The primary document produced by the TBI project was the *Guidelines for Performance-Based Seismic Design of Tall Buildings* [PEER 2010a]. This document synthesized the results and findings from the remainder of the project. It was intended to support ongoing guidelines and code-writing activities of collaborating organizations, as well as being a stand-alone reference for designers of new high-rise buildings. Several technical reports were also developed to substantiate the recommendations contained in the TBI guidelines and to assist users of the guidelines in applying them to real-world projects [Holmes et al. 2008; PEER 2010b; Stewart and Tileylioglu 2010; and PEER 2011]. The TBI Guidelines and supporting documents are widely used in designing new tall buildings for performance levels not addressed in normal building codes, or in cases of design where the building or design approach do not satisfy basic code prescriptive requirements. In such cases, the TBI Guidelines are used as a framework for the use of alternative means to demonstrate that a structure satisfies the basic safety and other requirements for buildings.

Two other guidelines are often used specifically for the design of new tall buildings. These are:

- *An Alternative Procedure for Seismic Analysis and Design of Tall Buildings Located in the Los Angeles Region* [LATBSDC 2014[, Los Angeles Tall Buildings Structural Design Council, and
- *Requirements and Guidelines for the Seismic Design of New Tall Buildings using Non-Prescriptive Seismic-Design Procedures* [SFDBI 2014].

While these approaches appear in many respects to be a specialized and focused application of performance-based evaluation methods such as those used in ASCE 41-13 and its predecessors, they differ in certain key aspects. Based on computed dynamic responses, a rather practical member-by-member evaluation approach is used, and limits are placed on global drifts; however, special provisions are included to encourage a hierarchy of behavior modes occurring during dynamic response. That is, a desired inelastic deformation mechanism is identified for a structure, with yielding assigned to specific displacement controlled regions, and other mechanisms and elements are designed so that their yielding or failure is delayed until the structure reaches its full capacity or system's lateral displacement demands are conservatively achieved. For a moment-resisting frame structure, one might want to have a structure where flexural plastic deformations occur at or near the ends of the beams. In this case, the beams would be evaluated considering their expected moment capacity, but the beam shear and columns would be provided with strengths corresponding to the median plus a number of standard deviations. The amount of over-strength required depends on the nature of the failure

mode. More brittle elements would require a high over-strength compared to the median demand, whereas more ductile but not preferred inelastic modes of behavior would be provided with smaller over-strengths compared to median demands. To limit the large number of analyses that might be required to compute statistically reliable standard deviations for member demands, most of the cited guidelines incorporate default values based on a limited number of analyses of model buildings. Therefore, beams in a moment-resisting frame might be designed and evaluated for their median moment and rotation demands, but the design of columns would be based on the median axial load demand multiplied by a factor ranging from about 1.2 to 1.5.

2.5.5 Towards Risk-Informed, Performance-Based Evaluation: The SAC Steel Project

The 1994 Northridge earthquake had shaken structural engineers' confidence in the safety and performance of existing moment-resisting frame buildings. As a result, SEAOC, ATC, and CUREe formed a joint venture to develop consensus-backed guidelines to reduce the earthquake risks posed by steel moment-resisting frame buildings. One of several objectives of the SAC Steel Program was to develop and validate professional practices and recommendations for evaluation of existing steel moment frame buildings so they could provide reliable performance in future earthquakes.

Several difficulties were identified in applying the evaluation and retrofit guidelines available at that time. These included the lack of a mechanics-based theory to explain the observed brittle behavior of steel beam-to-column connections and scarcity of data to assess the mechanical behavior of existing and retrofit connections. Thus, a series of field, laboratory, and numerical studies were undertaken to better understand and predict the behavior of these structures and their critical connections.

However, several major theoretical issues were identified related to the application of then-existing performance-based evaluation procedures. According to the PBEE methodology of that time, structures were analyzed for expected ground shaking, and structural performance was checked member by member. In this way, the expected demands on an element were compared with their expected capacities. If any member was found to be deficient for a particular performance level, the entire structure was deemed unable to achieve this level of performance. This provided a conservative approach to performance evaluation but did not reflect the realities of the situation following the 1994 Northridge earthquake. First, attempts to correlate locations of damage in actual buildings with numerical simulations of those buildings indicated that available computer simulation methods were unable to reliably predict damage severity and locations, even ones based on advanced nonlinear dynamic analysis and modeling techniques. Second, while nearly 200 steel moment-frame buildings were found to have brittle fractures in their connections, which would have triggered a violation of the collapse prevention limit state criteria using the member-by-member evaluation approach used in FEMA and ASCE documents at the time, none of these buildings collapsed or injured occupants.

Thus, a new approach to performance assessment was needed that considered and accounted for uncertainties in the seismic hazard, analysis methods and models, seismic response and member behavior, and one that considered global system level response as well as local member behavior in assessing seismic performance. During the SAC Steel Program, a series of guidelines were developed to conduct probabilistic performance-based evaluation, design, repair,

and upgrading of welded steel moment-resisting frame buildings: FEMA 350, FEMA 351, and FEMA 352. As noted previously, a series of state-of-the-art reports and technical background reports were published to describe the basis of the guidelines.

One of the SAC guidelines, FEMA 351 [FEMA 2000c], specifically provides engineers with recommended criteria to evaluate the performance of existing welded steel moment-resisting frame buildings. Unlike the ASCE 41 procedure, which uses a deterministic approach to evaluate individual member demand-to-capacity ratios, the FEMA 351 performance evaluation procedure is a reliability-based, probabilistic approach. The evaluation procedure explicitly includes different source of uncertainties and defines confidence levels through factored-demand-to-capacity ratios for particular building performance parameters (or failure modes), such as story drift, column compression axial load and column splice tension force.

FEMA 351 permits the use of four different analysis approaches (linear static, linear dynamic, nonlinear static, and nonlinear dynamic), incorporated test- and analysis-based estimates of connection and member deformation capacities, and, as noted earlier, explicitly accounted for uncertainties in predicting and evaluating performance. Only two performance levels were included: collapse prevention and immediate occupancy. The SAC criteria required that the user estimate the confidence that a structure would achieve a prescribed performance level; the engineer needed to compute the median and dispersion for several important engineering demand parameters (EDPs), including story drift, and minimum and maximum column axial load as a minimum. This is shown for FEMA 351 in Table 2.2. A theoretically derived procedure is used to compute the confidence of achieving both system-level and local-level behavior. The global behavior examined was the peak story drift, and the local behavior examined was related to the damage in plastic hinges, and the peak tension and compression axial loads in columns. As can be seen in Table 2.3, a higher (90%) confidence was required for behavior modes that might adversely affect global stability of the structure. A lower confidence of 50% was required for behavior modes that were believed would not to lead to global collapse of the structure. Note that the absence of damage to column splices in the Northridge earthquake led to the use of a 50% confidence criterion for column splice failures in tension.

Table 2.2 Performance parameters requiring evaluation of confidence per FEMA 351 [2000c].

Parameter	Discussion
Interstory drift	The maximum interstory drift computed for any story of the structure shall be evaluated for global and local behavior (for Collapse Prevention and Immediate Occupancy).
Column axial load	The adequacy of each column to withstand its calculated maximum compressive demand shall be evaluated both for Collapse Prevention and Immediate Occupancy.
Column splice tension	The adequacy of column splices to withstand their calculated maximum tensile demands shall be evaluated both for Collapse Prevention and Immediate Occupancy.

Table 2.3 Recommended minimum confidence levels from FEMA 351 [2000c].

Behavior	Performance Level	
	Immediate Occupancy	Collapse Prevention
Global Behavior Limited by Interstory Drift	50%	90%
Local Connection Behavior Limited by Interstory Drift	50%	50%
Column Compression Behavior	50%	90%
Column Splice Tension Behavior	50%	50%

2.5.6 Next-Generation Performance-Based Design Methodologies: PEER PBEE, ATC-58, and FEMA P-58

In the previously cited evaluation procedures, performance was defined in terms of limit states, such as collapse prevention, life safety, immediate occupancy, and continued occupancy. Acceptance criteria were developed in terms of engineering response or demand parameters such as story drift, plastic or total rotations in plastic hinges, axial loads in columns, etc. While newer methods such as FEMA 350 consider system response and uncertainty in the evaluation process more explicitly, these limit states are most useful for design professionals focusing on structural behavior. For instance, the limit state evaluation criteria is not related directly to tagging considerations that would indicate whether a building might be able to be occupied following an earthquake, nor to the expected downtime, cost of inspections, design services, repairs, recovery management, and business interruption losses associated with a damaged structure, and the number of injuries and casualties. These variables are likely more meaningful and relevant to an owner or occupant than predictions of plastic hinge rotations.

As such, the past two decades has seen the rapid development of the second-generation PBEE methodology, where probabilistic aspects of hazard characterization and response prediction are explicitly taken into account, and seismic performance objectives are expressed in terms of decision variables of interest to stakeholders such as owners, occupants, public officials, insurance companies, etc. Figure 2.18 illustrates the PBEE methodology developed by PEER during a ten-year project funded by the U.S. National Science Foundation. This methodology is based on the total probability theorem, allowing performance evaluation to be divided into a number of steps (Figure 2.18), and involves conditional probabilities to propagate the uncertainties from one level of assessment to the next, resulting in a probabilistic prediction of overall performance.

The four primary steps of the PEER PBEE—hazard analysis, structural analysis, damage analysis, and loss analysis—are illustrated in Figure 2.18 and by Equation (2.1). The following terminology is used: $p[X|Y]$ denotes the probability density of X conditioned on Y, $\lambda[X|Y]$ denotes the mean exceedance rate (mean frequency) of X given Y, *IM* denotes an intensity measure, *EDP* denotes engineering demand parameters, *DM* denotes damage measures, and *DV* denotes decision variables. Equation (2.1) is also conditioned on the facility definition and site, but this is excluded from the equation for clarity.

$$\lambda[DV] = \iiint p[DV \mid DM] \cdot p[DM \mid EDP] \cdot p[EDP \mid IM] \cdot d\lambda[IM] \tag{2.1}$$

For the hazard analysis, the mean annual rate of exceedance of a particular ground motion intensity measure (IM) is evaluated, considering nearby earthquake sources and site conditions. A suite of acceleration histories is then selected and scaled to be compatible with the site hazard.

The next step involves performing a suite of nonlinear response time history analyses. The computed responses are used to establish the conditional probabilistic response, $p[EDP|IM]$, for *EDP*s of interest, conditioned on *IM*. As discussed previously, some examples of *EDP*s are peak story drift, peak floor acceleration, and peak plastic-hinge rotation.

The third step is damage analysis, in which fragility functions are utilized to express the conditional probability, $p[DM|\ EDP]$, that a component (e.g., beam, column, partition, elevator, etc.) is in, or exceeds, a particular damage state specified by *DM*. The selected damage states reflect the repair efforts needed to restore the component to an undamaged state. The fragility functions are compiled based on laboratory experiments, analytical investigations, expert opinion, or some combination of these.

The last step of PBEE establishes the conditional probabilistic losses, $p[DV|\ DM]$, where *DV* may include repair cost, business interruption costs, repair duration, and loss of life. By integrating numerically all the conditional probabilities along with the ground-motion hazard function, the mean annual rate, $\lambda[DV]$—with which various *DV* levels are exceeded—can finally be calculated. The analysis results expressed in this form can be used to inform risk-management and design decisions.

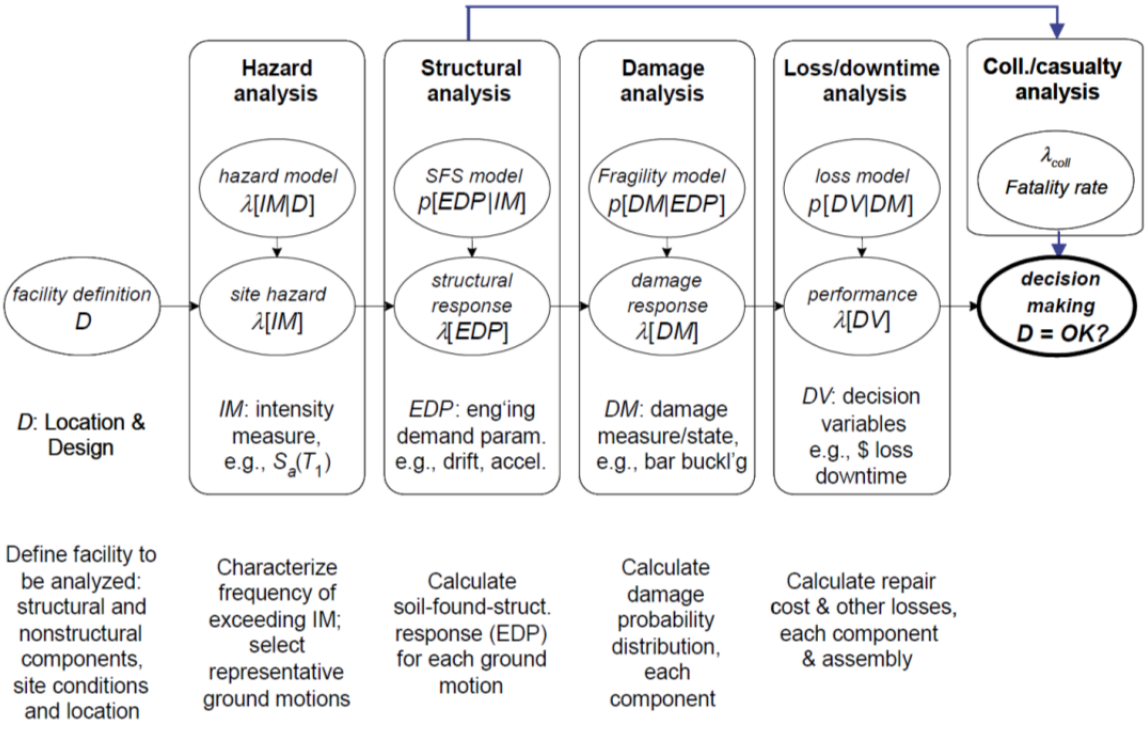

Figure 2.18 PEER PBEE framework (adapted from Porter [2003]).

To move this risk-informed, performance-based evaluation process to the point that it could be applied in practice, in 2001 FEMA funded a 10-year, three-phase project known as ATC 58 [FEMA 2006]. The objective of Phase 1 was to adapt the performance assessment methodology and develop engineering guidelines to predict the probable performance of new buildings or existing buildings in future earthquakes. The Phase 2 objectives contained the development of refined procedures for designing buildings to achieve desired performance, quantification of performance provided by current prescriptive procedures, assessment of adequacy of performance, and development of guidance on selecting appropriate structural systems, strength, stiffness, and so on during the design process that is likely to be able to meet performance objectives. The ATC-58/ATC-58-1 projects culminated in a set of documents [FEMA 2012a; FEMA 2012b; and FEMA 2012c] describing the general methodology, the implementation tool, Performance Assessment Calculation Tool (PACT), and the background documents. A third phase is currently underway, which is refining as well as simplifying the methodology, examining methods to encourage its implementation in design practice and apply it to a variety of real world cases.

For more information, considering the cost of repair, downtime, and business interruption costs associated with disruption or loss of occupancy, see Porter [2003], FEMA [2012], and Terzic et al. [2015].

2.6 PREVIOUS SEISMIC EVALUATIONS OF EXISTING TALL BUILDINGS

Most tall buildings have performed satisfactorily during moderate to strong ground shaking, but some notable failures have been noted worldwide. While engineering evaluation, analysis, and design methods currently exist to address some of these issues, and some of the features found in older tall buildings may be proscribed in modern building codes, it is likely that existing tall buildings designed under older codes are vulnerable to strong earthquake ground shaking. As such, several studies have previously been undertaken to evaluate the safety of different types of existing tall buildings.

An extensive study of existing steel moment-resisting frame buildings was undertaken as part of the SAC Steel Project following the 1994 Northridge earthquake. *The State-of-the-Art Report on Performance Prediction and Evaluation of Steel Moment-Frame Structures* [FEMA 2000g] utilized the evaluation methods outline in FEMA 351 to examine the behavior of 3-, 9-, and 20-story welded steel moment frame structures designed according to older building codes. The study was carried out for buildings constructed in Boston, Los Angeles, and Seattle. For these studies, two principal sets of ground-motion records were considered for each city, one corresponding event to a 2% probability of exceedance in 50 years (2475-year recurrence period), and one corresponding to a 50% probability of exceedance in 50 years (72-year recurrence period).

Table 2.4 summaries results presented in FEMA 355F for 20-story tall buildings located in Los Angeles. In this table, confidence values are shown for the 20-story building achieving the collapse prevention limit state. The building was designed according to the 1997 NEHRP seismic design recommendations as well as to the 1994, 1985, and 1973 editions of the UBC. Considering the continual improvements that have occurred in building codes (see Section 2.4), it was estimated that for very rare earthquakes, corresponding to a 2% probability of exceedance in 50 years, that a 20-story building designed according to the 1997 NEHRP provisions could

achieve the collapse prevention limit state (considering both local and global response criteria) with more than 90% confidence. As shown in Table 2.4, this confidence decreases progressively with each earlier version of the building code. For instance, for 20-story buildings designed according to the 1973 UBC, the confidence that the collapse prevention limit state could be achieved for this level of shaking reduces to less than 50%. Moreover, the confidence of avoiding a complete local failure of at least one beam-to-column connection reduces to between 19% and 27% for these earlier codes.

Table 2.5 presents similar results, but for cases where the earthquake hazard corresponds to an occasional event having a 50% probability of exceedance in 50 years. In this case, there is at least a 99% confidence of avoiding collapse for all vintages of buildings considered. However, it appears that 20-story moment-frames built according to the 1994 and earlier editions of the UBC would not satisfy the immediate occupancy requirements of FEMA 351, and might well be red or yellow tagged, thus limiting their use and requiring inspections and repairs.

Several other similar studies have been undertaken (e.g., Hall et al. [1995], Hall [1998], and Krishnan and Muto [2011], etc.), which have focused on an examination of the cause of significant story drifts in tall steel moment-resisting frame buildings at sites where forward directivity, near-fault ground pulses occur. They demonstrated that for structural systems having shear-wave velocities lower than the peak ground velocity during near-fault related velocity pulses, seismic response resembles waves propagating up a shear beam. Thus, substantial story drifts can occur due to potentially large ground displacements and the constructive reinforcement of waves passing up and down the building.

Table 2.4 **Performance confidence values for 20-story building in Los Angeles for earthquakes with 2% probability of exceedance in 50 years.**

Performance Goal	1997 NEHRP	1994 UBC	1985 UBC	1973 UBC
Global collapse	93%	75%	71%	46%
Local collapse	96%	19%	26%	27%

Table 2.5 **Performance confidence values for 20-story building in Los Angeles for earthquakes with 50% probability of exceedance in 50 years.**

Performance Goal	1997 NEHRP	1994 UBC	1985 UBC	1973 UBC
Global collapse	99%	99%	99%	99%
Immediate Occupancy	97%	22%	22%	5%

In a recent related investigation by Muto and Krishnan [2011], three model buildings were subjected to ground-motion records at 784 sites around greater Los Angeles. These records correspond to the motions at different locations during a single realization of a hypothetical **M**7.8 earthquake occurring on the San Andreas fault east of metropolitan Los Angeles. This effort was carried out as part of the 2008 Great Southern California Shakeout scenario investigation. Thus, while many records were considered, their work did not consider the range of earthquakes that might be expected in the area, nor the probability of the event considered actually happening.

The Model Building 1 was based on an actual 18-story tall, welded steel moment-resisting frame building designed according to the 1982 UBC. Model Building 2 was similar, but the design was updated to reflect the provisions of the 1997 UBC. This building had more moment-resisting bays, and the lateral load-resisting system was modified to eliminate some of the torsional irregularities present in Model Building 1. Model Building 3 was a 19-story tall steel moment-frame building with an L-shaped plan.

Computer models were developed for all three model buildings, and beam-to-column connections were modeled as being ideally ductile or susceptible to premature fracture. In addition, the three dimensional (3D) models of the building were not identical in the NS and EW directions, so the models were rotated by 45 or 90° to assess the effects of directivity and directionality in the ground shaking on seismic response. Results obtained from this research are shown in Table 2.6, where the inferred performance of the buildings is based the computed peak story drift ratio (DR).

These studies reached a similar conclusion to that presented in FEMA 355F. That is, for the older (1982) UBC design with fracture susceptible connections, only about 5% of the sites achieved a continued occupancy status. Moreover, the older building would experience collapse at between 18% and 24% of the sites. For this older building, Muto and Krishnan suggested that the 1982 design would be red tagged or collapse at between 30% and 32% of the sites considered. Although the newer design performed better, the two 1997 UBC-based designs would still be red tagged or experience collapse at between 8.1% to 20.3% of the sites considered, depending on the quality of the connections and the orientation of the building relative to the site.

Table 2.6 **Model building performance levels for base and rotated orientations, with susceptible and perfect beam-to-column connections [Muto and Krishnan 2010].***

Model	Orientation	Connections	Performance Level				
			IO	LS	CP	RT	CO
Building 1 (1982 UBC)	Base	Susceptible	5.2	28.3	36.5	11.7	18.3
		Perfect	5.4	29.7	46.0	11.9	7.0
	Rotated	Susceptible	4.8	29.7	33.8	7.5	24.2
		Perfect	4.9	31.0	42.2	10.7	11.3
Building 2 (1997 UBC)	Base	Susceptible	8.5	36.4	35.5	9.8	9.8
		Perfect	8.5	37.2	42.0	7.7	4.7
	Rotated	Susceptible	7.7	36.0	36.0	8.2	12.1
		Perfect	7.7	37.4	41.2	10.0	3.8
Building 3 (1997 UBC) (L-Shaped)	Base	Susceptible	8.2	42.4	39.0	6.6	3.9
		Perfect	8.2	42.8	40.9	6.6	1.5
	Rotated	Susceptible	9.9	45.5	34.2	4.6	5.7
		Perfect	9.9	46.0	35.9	5.5	2.7

*Numbers indicate the percentage of analysis sites at which performance can be categorized as: (a) immediately occupiable (IO) with DR<0.007; (b) life-safe (LS) with 0.007<DR<0.025; (c) collapse-prevention (CP) with 0.025<DR<0.05; (d) red-tagged (RT) with 0.05<DR<0.075; or (e) collapsed (CO) with DR>0.075. DR = story drift ratio.

2.7 CONCLUDING REMARKS

Steel moment-resisting frame systems comprise the majority of tall buildings constructed in California prior to 1990. These older buildings have variety of vulnerabilities, as demonstrated by past earthquakes and earlier studies. In particular, steel moment-resisting frame systems are vulnerable to brittle fracture of beam-to-column connections and column splices. Modern building codes have addressed many of these seismic deficiencies, and building code provisions now consider these older buildings to be seismically inadequate. The rapid advancement of evaluation methods and more modern and complex analysis methods has made assessing the adequacy of older tall buildings, especially tall steel moment-resisting frame buildings, possible.

3 The Case-Study Building

It is theoretically impossible to select a case-study building that represents the entire inventory of existing tall buildings and comprehensively addresses potential seismic deficiency issues. However, several issues that exist in older tall steel buildings are of high priority to address, including pre-Northridge moment connection details and brittleness of partial joint penetration weld details in column splices. This chapter describes the case-study building selection criteria, the site condition of the selected building, and its structural details.

3.1 CRITERIA FOR SELECTION THE CASE-STUDY BUILDING

Many factors were considered during the selecting process of the case-study building, including: the total number of stories of building, existing building site, design era, construction era, type of structural system used, type of structural material used, structural details, instrumentation availability, structural drawing accessibility, importance (from an economical and societal standpoint), and potential seismic vulnerability foreseen.

Based on the inventory discussed in Section 2.2, San Francisco has the most—on the order of 140—among the three major cities in California considered in terms of the total number of existing tall buildings taller than 20 stories. Furthermore, more than one-half of the existing tall buildings within the inventory of San Francisco were designed and constructed between 1960 and 1990 or before.

In light of unexpected damage to the welded steel moment-resisting frame systems during 1994 Northridge earthquake [Mahin 1998; FEMA 2000h] and observed damage in the San Francisco Bay Area (Oakland and South Bay) after 1989 Loma Prieta earthquake [Phipps 2000], existing tall buildings with welded steel moment-resisting frame systems and pre-Northridge connection details were selected to be candidate buildings for the case study. To validate the mathematical model, instrumented buildings were considered a top priority. A key factor in selection process was the availability of both the detailed structural drawings as well as the recorded seismic response data of the existing building from the past earthquakes since building owners might be reluctant to release information or allow researchers to perform site inspections. This study had access to the structural drawings of the building selected for this case study and felt its seismic response would be representative of a class of older buildings of concern.

3.2 SITE

With the aforementioned screening criteria, a 35-story case-study building in downtown San Francisco was selected. The building site is located about nine miles from the San Andreas fault, 9.7 miles from the Hayward fault, and 14.3 miles from the San Gregorio fault. All of these three major faults are capable of producing magnitude 6.7 or greater strong ground motion; see Figure 3.1. The site is not in the earthquake fault zone defined by the Alquist-Priolo Earthquake Fault Zone Act.

The report [Sexton & Associates 1968] prepared for the case-study building should be referred to for building site geology. According to this report, the site is located on manmade land and is underlain with loose sandy fill (from datum 0~-20 ft), soft clay (-20~-40 ft), medium clay (-40~-55 ft), dense silty fine sand (-55~-80 ft), stiff clay (-80~-235 ft), decomposed shale (-235~-245 ft), and Franciscan bedrock (-245 ft and beyond). Figure 3.2 illustrate the site ideal soil profile. Note that the building site is inside the regions that have potential for liquefaction during a seismic event [CGS 2000].

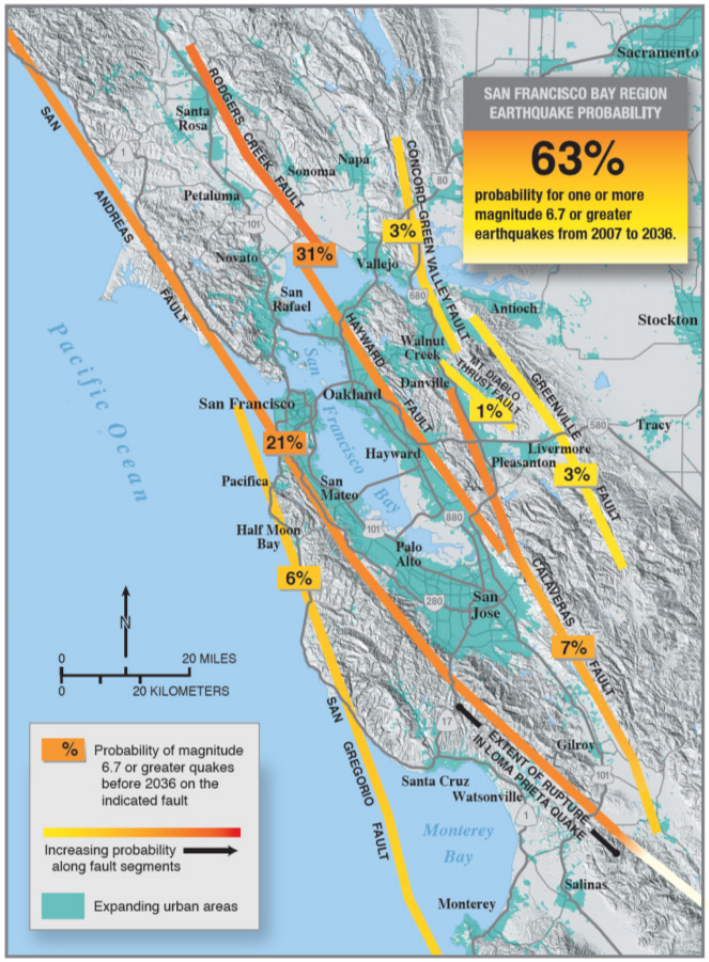

Figure 3.1 **San Francisco Bay region earthquake probability prediction by the United States Geologic Survey (source: USGS web site, 2008).**

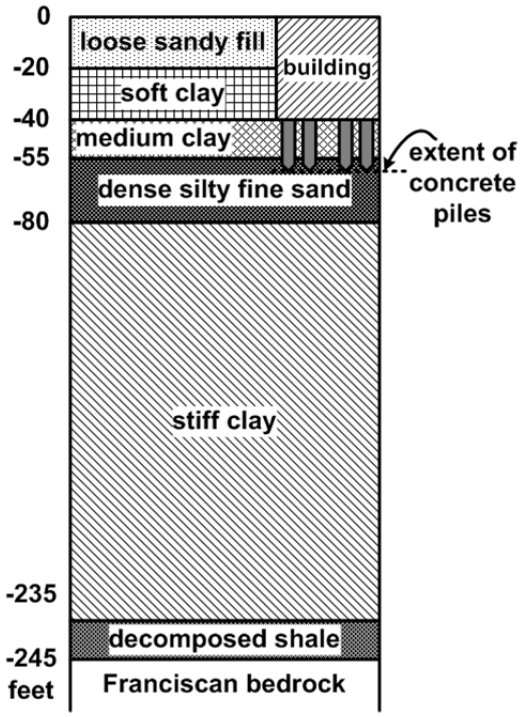

Figure 3.2 Building site soil profile (reproduced from Sexton [1968]).

3.3 EXISTING BUILDING DESCRIPTION

The case-study building (see Figure 3.3) considered herein located in San Francisco; it is a 35-story tall (about 490-ft in height) and 185 ft × 135 ft in plan. The building consists of a main tower, a four-story podium (for boiler room and mechanical rooms), and an atrium at north side of main tower. The building has three basement levels (one basement and two sub-basement levels). Structural evaluation was limited to the main tower above the ground in this study. The building was designed in 1968 and finished construction in 1971. The structural system consists of complete 3D welded steel moment-resisting space frames in both longitudinal and transverse directions. These steel frames consist primarily of built-up box columns (either single-cell or two-cell), wide flange columns, and beams (either built-up or hot-rolled sections). Figure 3.4 shows the typical built-up section details. All column lines (a total of 34 columns) within the main tower region serve as gravity columns and the seismic force-resisting system. A typical 6-in.-thick concrete slab on metal deck is provided at each floor. No shear studs were welded through metal deck; only 3/4-in. puddle welds were provided to connect metal deck and beam top flange. The typical beam span is 30 ft, and the typical story height is 13 ft [except the mezzanine level (22 ft), 3rd level (15 ft), 4th level (15 ft), and 32nd level (17 ft)].

Figures 3.3(b), 3.3(c), 3.3(d) illustrate a typical frame elevation, a typical floor plan, and the mezzanine level floor plan. Note that the perimeter precast concrete façade, non-structural concrete elevator core walls, a non-structural concrete smoke tower, and moveable interior partition walls were not simulated in the analytical model; see Chapter 6 for mathematical modeling details. Minimum distance to the adjacent building is about 80 ft at the north side of main tower. A site investigation was not performed before the structural evaluation.

The building foundation consists of a 7-ft-thick foundation mat located 40 ft below grade, which is supported by more than 2500 18-in.-diameter concrete piles extended to about 20 ft below the foundation mat; see Figure 3.2. The 7-ft-thick foundation mat is connected to the 3-ft-thick bulkhead wall around the entire site. Member sizes, structural details, foundation details, and other information were collected from the City of San Francisco's Department of Building Inspection [DBI 2013] and the building owner.

Beam-to-column moment connection details are pre-Northridge, and the partial joint penetration (PJP) weld column splice details are used in the case-study building. Typical wide-flange beam-column connection details and column splice details for wide-flange columns are shown in Figures 3.5 and 3.6. Typical column base details are shown in Figure 3.7. Note that the column (built-up section) is bolted, not welded, to base plate, and there are no anchor rods connecting base plate to the mat foundation.

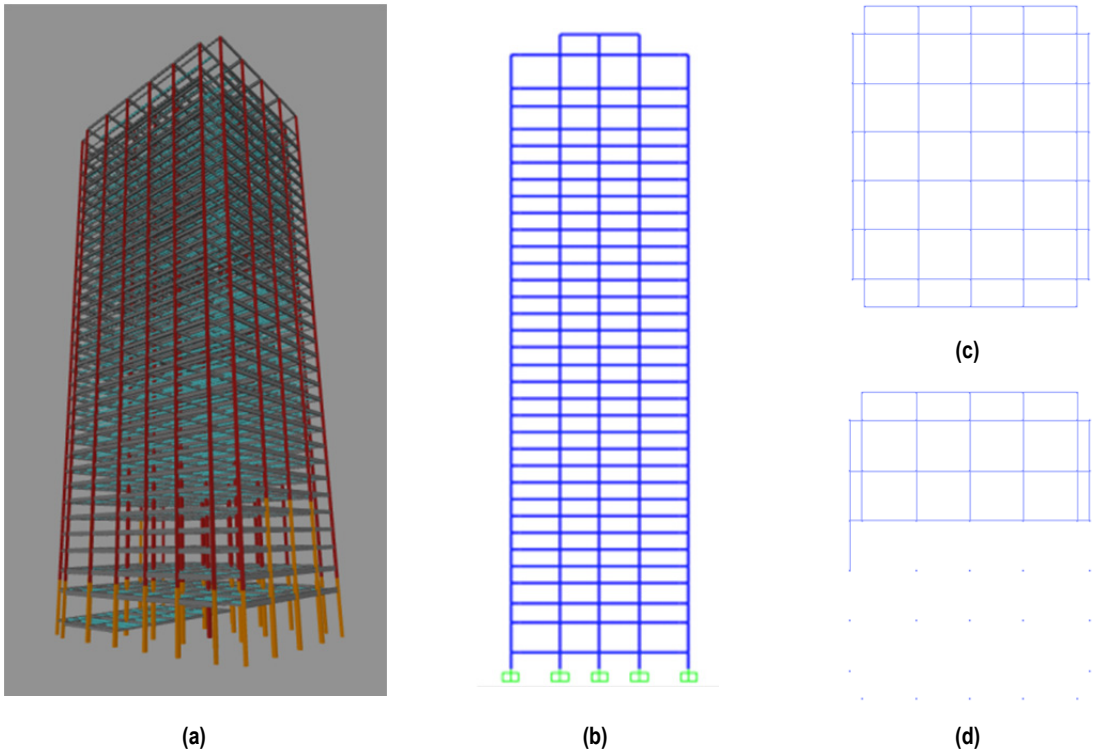

Figure 3.3 **The case-study building: (a) perspective view (basements not shown); (b) typical frame elevation; (c) typical floor plan; and (d) mezzanine level floor plan.**

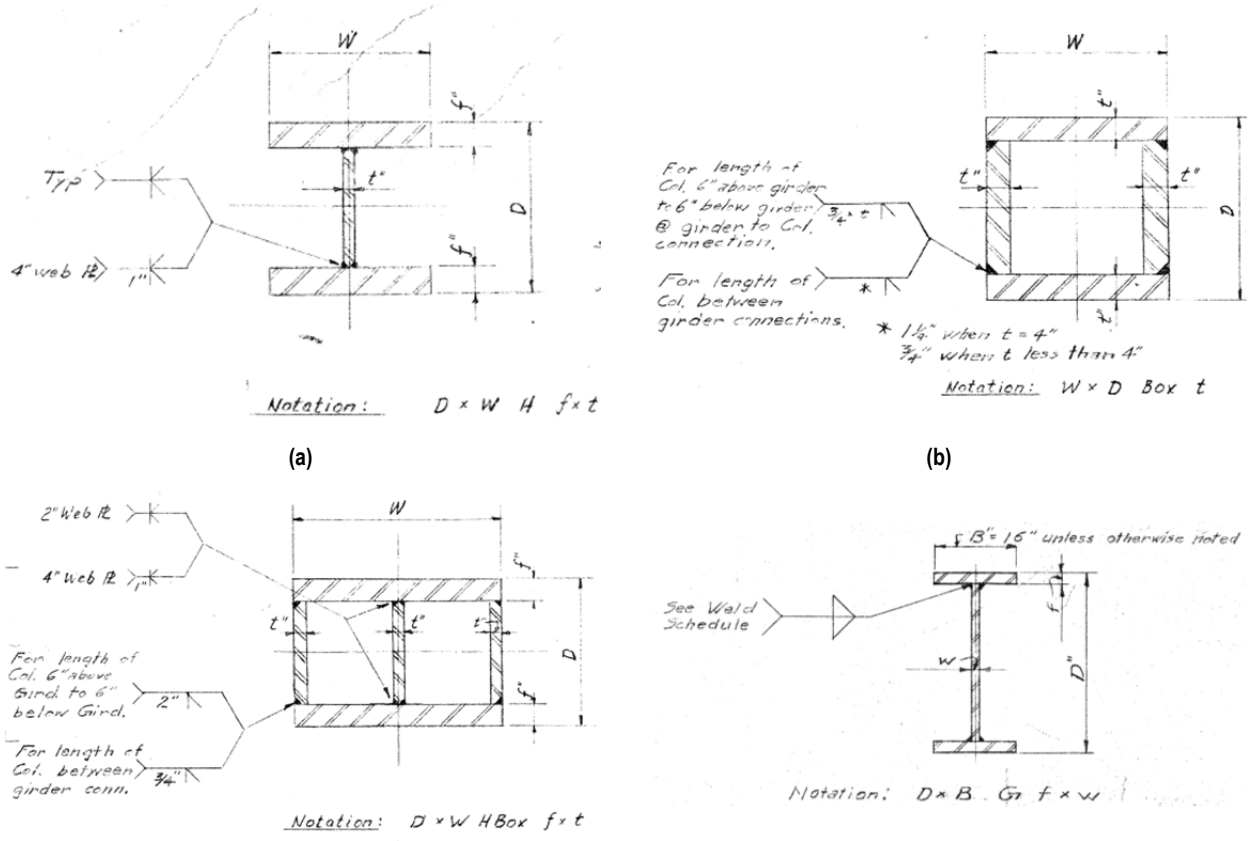

Figure 3.4 **Typical built-up section details: (a) built-up wide-flange column section detail; (b) built-up box column section detail; (c) built-up H-Box (two-cell) column section detail; and (d) built-up wide-flange girder section detail.**

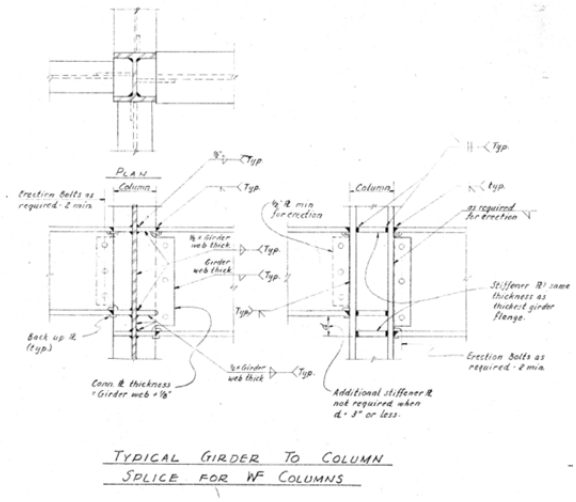

(a)

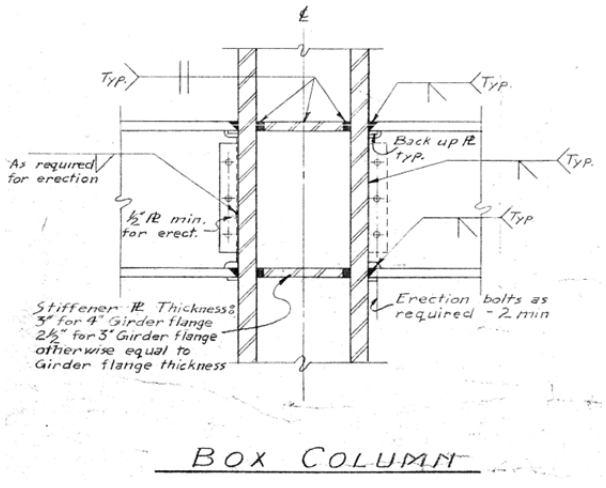

(b)

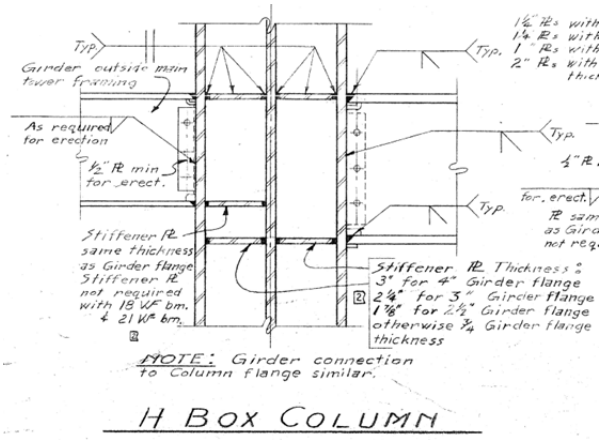

(c)

Figure 3.5 **Typical connection details: (a) girder to wide-flange column connection details; (b) girder to box column connection details; and (c) girder to H-box two-cell) column connection details.**

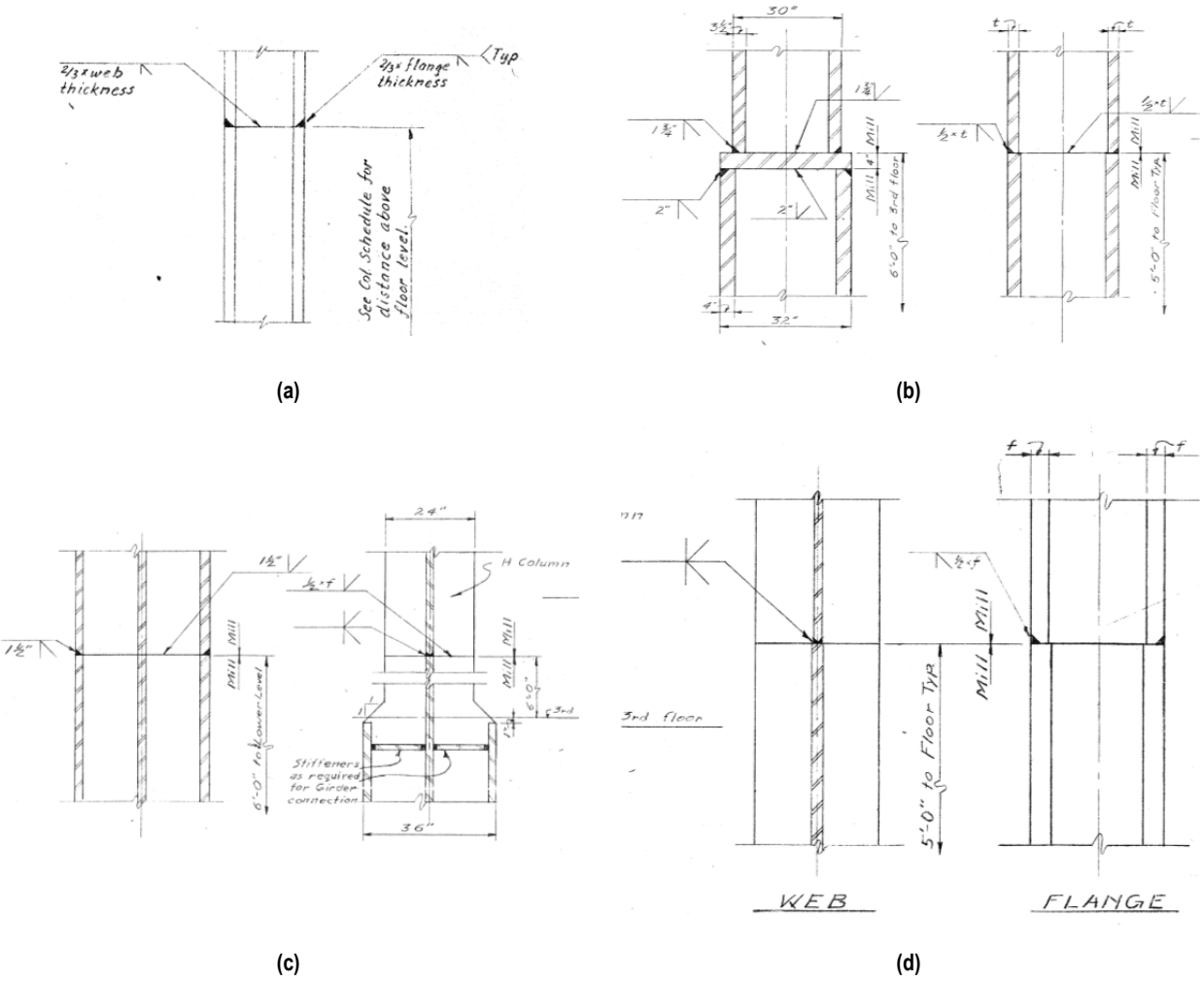

Figure 3.6 **Typical column splice details: (a) wide-flange column; (b) built-up box column; (c) built-up H-box column; and (d) built-up H-columns.**

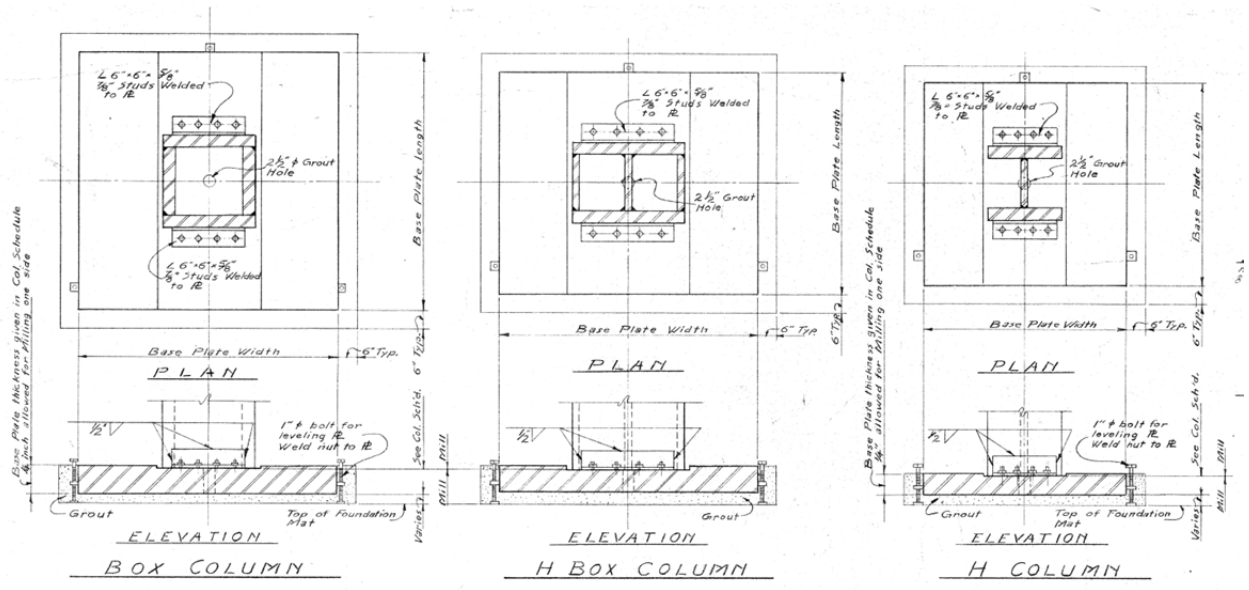

Figure 3.7 Typical column base detail.

3.4 CONCLUDING REMARKS

A 1970-era 35-story steel moment-resisting space frame having typical pre-Northridge beam-to-column moment connection details and column splice details was investigated. The building selected here addresses several key issues that are of particular interest in examining the performance of older existing tall buildings in future earthquakes.

4 Seismic Performance Assessment

Chapter 2 reviewed several well-documented methodologies available for evaluating existing buildings. This chapter examines in more detail the primary evaluation procedure used in this study: *Seismic Evaluation and Retrofit of Existing Buildings* [ASCE 2014], ASCE 41-13. This specific evaluation procedure was chosen for the following reasons:

- ASCE 41-13 is a contemporary nationwide standard consistent with many of the features of the ASCE 7-10 standard [ASCE 2010];
- The standard reflects the most current state of knowledge and practice;
- It integrates previous standards (i.e., ASCE 31-03 and ASCE 41-06), thus enhancing the consistency between evaluation and retrofit procedures; and
- It was adopted by California Building Code [CBSC 2013]; most engineers in California follow this standard when evaluating existing buildings.

The following sections describe the outline of the evaluation procedure, selection of performance objectives, and modeling matrix.

4.1 SEISMIC PERFORMANCE EVALUATION PROCEDURES

4.1.1 ASCE 41-13

The seismic performance evaluation procedure presented in this report follows the ASCE 41-13 standard. As mentioned in Chapter 2, it is a combined product of two existing national standards, ASCE 31-03 and ASCE 41-06, and is based on the performance-based methodology. This new standard differentiates experience-based and systematic evaluations; it maintained the three-tier evaluation framework from ASCE 31-03. Tier 1 was completely transferred from ASCE 31-03, Tier 2 was combined from both standards, and Tier 3 was mainly extracted from ASCE 41-06. For consistency's sake, it removed the distinction between evaluation and rehabilitation. Although this standard may create difficulties when evaluating existing buildings, it does have several benefits:

- provides consistencies between evaluation and retrofit procedures;
- is more consistent with the ASCE 7-10 standard;
- includes up-to-date technical information;

- equivalent new design code performance objectives are explicitly defined;
- procedures for existing buildings having different risk categories are explicitly described; and
- a less conservative Tier 1 life-safety provisions has been updated [Pekelnicky and Poland 2012].

The combined standard provides a flow chart to help users understand the evaluation process, and the procedure includes component level evaluations of the building performance. Figure 4.1 shows an abridged flowchart of the evaluation procedure used. For the particular building selected in this study, the seismic performance evaluation was based on the available existing as-built drawings (see Chapter 3) and engineering judgment regarding behavior of pre-Northridge era steel construction.

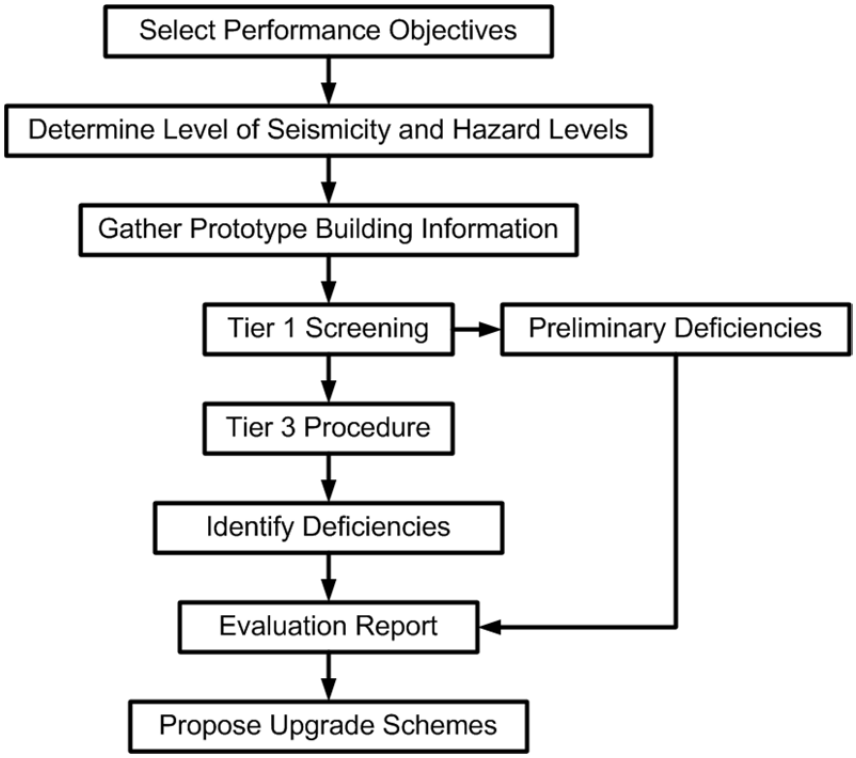

Figure 4.1 Evaluation flowchart for this study.

4.1.2 Tier 1 Screening (Checklist)

The selected case-study building conforms to common building type S1 (steel moment frames with stiff diaphragms) but exceeds the height limit permitted for this type; therefore, Tier 3 systematic procedures are automatically required. To rapidly identify potential seismic deficiencies, a Tier 1 screening evaluation was performed prior to a Tier 3 evaluation. A Tier 2 "deficiency-based" procedure was not used in this study. The Tier 1 procedure utilizes checklists to evaluate the adequacy of a building's lateral force-resisting system. The "Basic Configuration Checklist" was followed, which is applicable to all building types. ASCE 41 has additional checklists for Life Safety (LS) and Immediate Occupancy (IO) performance levels. As described

later, the basic performance objective for existing buildings (BPOE) recommended by ASCE 41 requires the case-study building to meet the Life Safety (S-3) performance level. Therefore, the checklists for the LS performance level were also completed. Checklists related to non-structural elements were not utilized. Complete checklists required for a Tier 1 screening procedure are shown in Appendix B. Screening results are discussed in Section 7.1.

4.1.3 Tier 3 Systematic Evaluation

Since the case-study building has a taller first story level and a mezzanine level that does not extend the entire area of a typical floor, it is considered to have an irregularity in the seismic-force-resisting system; thus, linear procedures are not permitted in the Tier 3 analysis. Considering that the higher mode effects are significant in this case, the nonlinear dynamic procedure (NDP) was used to evaluate the case-study building's performance. The nonlinear static procedure (NSP) was used before performing the NDP to investigate the likely building performance and the mechanical behavior of the connections. See Chapter 5 for ground-motion selection procedures for each hazard level (BSE-1E and BSE-2E).

4.2 PERFORMANCE OBJECTIVES

The performance objective of the case-study building was selected to be the BPOE as defined in ASCE 41, which depends on the risk category of the building and the evaluation procedure used. The risk category of the case-study building was selected as III, per ASCE 7-10 [ASCE 2010]. As an office building in Risk Category III, the BPOE performance criteria for a Tier 3 procedure are structural performance measure S-2 at BSE-1E seismic hazard level, and structural performance measure S-4 at BSE-2E seismic hazard level. Table 4.1 shows the selected (or target) building performance levels for the study. Non-structural performance measures N-B and N-D are also listed for a loss evaluation study (or PACT analysis). The building is evaluated at both BSE-1E and BSE-2E performance levels (Tier 3 procedure); note that more restrictive requirements (in terms of performance criteria selection) can be applied. For the Risk Category III, the Tier 1 screening checklist is based on LS performance level (S-3), except that checklist statements using the Quick Check procedures described in ASCE 41-13 were used but for a different performance level. Table 4.2 describes three structural and four nonstructural performance levels defined by ASCE 41-13. Level S-2 is an intermediate level between the IO and LS levels, while Level S-4 is an intermediate level between the LS and CP levels.

Table 4.1 Target building performance levels.

Risk Category III (Tier 3 Assessment)		Damage Control (2-B)	Limited Safety (4-D)
Seismic Hazard Level	(BSE-1E (20%/50yrs, MRP* = 225 yrs)	✓	
	BSE-2E (5%/50yrs, MRP = 975 yrs)		✓

* MRP: mean return period.

Table 4.2 Building performance levels (extracted from ASCE 41-13, Table C2-3).

Target Building Performance Levels				
Overall damage	**Collapse Prevention Level (5-D)**	**Life Safety Level (3-C)**	**Immediate Occupancy Level (1-B)**	**Operational Level (1-A)**
	Severe	**Moderate**	**Light**	**Very light**
Structural components	Little residual stiffness and strength to resist lateral loads, but gravity load-bearing columns and walls function. Large permanent drifts. Some exits blocked. Building is near collapse in aftershocks and should not continue to be occupied.	Some residual strength and stiffness left in all stories. Gravity-load-bearing elements function. No out-of-plane failure of walls. Some permanent drift. Damage to Partitions. Continued occupancy might not be likely before repair. Building might not be economical to repair.	No permanent drift. Structure substantially retains original strength and stiffness. Continued occupancy likely.	No permanent drift. Structure substantially retains original strength and stiffness. Minor cracking of facades, partitions, and ceilings as well as structural elements. All systems important to normal operation are functional. Continued occupancy and use highly likely.
Nonstructural components	Extensive damage. Infills and unbraced parapets failed or incipient failure.	Falling hazards such as parapets, mitigated, but many architectural, mechanical, and electrical systems are damaged	Equipment and contents are generally secure but might not operate due to mechanical failure or lack of utilities. Some cracking of facades, partitions, and ceilings as well as structural elements. Elevators can be restarted. Fire protection operable.	Negligible damage occurs. Power and other utilities are available, possibly from standby sources.
Comparison with performance intended for typical buildings designed to codes or standards for new buildings for the design earthquake	Significantly more damage and greater life safety risk.	Somewhat more damage and slightly higher life safety risk.	Less damage and low life safety risk.	Much less damage and very low life safety risk.

4.3 MODEL MATRIX

As mentioned in a study by Rodgers and Mahin [2003] on the effects of connection hysteretic degradation on the seismic behavior of steel moment-resisting frames, the brittle fracture of beam-to-column connections is not the only type of hysteretic degradation that may have negative effects on global system behavior. Other types of hysteretic behavior that can occur in beam-to-column connections include deformation softening (negative post-yielding stiffness) and strength degradation. Similarly, other hysteretic behavior types can occur in column splices. Thus, there are benefits in examining the effects of connection mechanical behavior on global system behavior and identifying the influence hierarchy on system behavior. For example, it can be beneficial to know if the mechanical behavior of a beam-to-column connection has more influence on the global behavior than does the column splice mechanical behavior or vice versa.

Based on the feedback of practicing engineers who have performed seismic retrofits, another issue that arose was the use of heavy cladding. The seismic retrofit of an existing 29-story steel moment-resisting frame building in San Francisco is one example where the structural engineer removed its heavy cladding as a retrofit strategy. Note that the issue of heavy cladding is also an issue in mid-rise and low-rise buildings.

Thus, a total eight models were proposed based on the combination of connection mechanical behavior as well as the absence of cladding weight. Model 1d* represents the as-built structure, and the other seven models represent a modification of the structure to enhance its performance. Table 4.3 illustrates the modeling matrix used in the study and different types of analyses performed on each model; see Chapter 6 for detailed discussions on the mathematical modeling used in each model for the simulated connection hysteretic behavior.

Table 4.3 Model matrix.

Model ID	Beam-to-column connection behavior	Column splice behavior	Nonlinear static procedure (NSP)	Nonlinear dynamic procedure (NDP)	Including cladding weight
1a*	fully ductile	fully ductile	✓	×	Yes
1b*	fully ductile	brittle	✓	×	Yes
1c*	per ASCE 41	fully ductile	✓	×	Yes
1d*	per ASCE 41	brittle	✓	✓	Yes
1a	fully ductile	fully ductile	✓	✓	No
1b	fully ductile	brittle	✓	×	No
1c	per ASCE 41	fully ductile	✓	✓	No
1d	per ASCE 41	brittle	✓	✓	No

* Star (*) represents a model including the full cladding mass.

4.3.1 Model 1a*

This is an ideal fully ductile model. The force-deformation relationships of steel beam-to-column connections and column splices are bilinear, and have infinite deformation ductility without strength degradation. No connection fracture was modeled.

4.3.2 Model 1b*

This model is similar to Model 1a*, except the hysteretic behavior of the column splices was considered to be brittle fracture. Fracture at the column splice was defined as reaching an allowable tension strain.

4.3.3 Model 1c*

The Model 1c* is similar to Model 1a*, except the hysteretic behavior of beam-to-column connections had strength degradation capabilities (capping model) where the moment-rotation relationship was defined following ASCE 41-13 modeling parameters.

4.3.4 Model 1d*

This model is presumed to be more accurate and closer to current as-built conditions of an actual building than the previous three models. The simulated hysteretic behavior of connections, both beam-to-column connections and column splices, is closer to the actual behavior observed in the past earthquakes or laboratory tests. The hysteretic behavior of beam-to-column connections was considered to be strength degradation (capping model), where the moment-rotation relationship was defined following ASCE 41-13 modeling parameters. The hysteretic behavior of column splices was considered to be brittle fracture, where the column splice was defined as fracture after reaching an allowable tension strain.

4.3.5 Model 1a

Similar to Model 1a*, this model is an ideal fully ductile model except that the cladding weight is not included in the model. This model represents the extensive retrofit work performed on the case-study building (compared to the original condition), e.g., heavy cladding removed and pre-Northridge beam-to-column connections and column splice connections repaired and upgraded.

4.3.6 Model 1b

Model 1b is similar to Model 1a* except the hysteretic behavior of the column splices was considered to be brittle fracture, and the weight of exterior cladding was not included in the model. This model represents moderate retrofit of the case-study building, e.g., heavy cladding removed and pre-Northridge beam-to-column connections repaired and upgraded.

4.3.7 Model 1c

The Model 1c is similar to Model 1c* except the cladding weight was not included in the model. This model represents moderate retrofit of the case-study building, e.g., heavy cladding replaced and all column splices repaired.

4.3.8 Model 1d

Model 1d is similar to Model 1d* except the cladding weight was not included in the model; minor retrofit works must be performed to replace the heavy cladding.

4.3.9 Selection of the Baseline Model

Model 1c was selected as the baseline model for the study. It represents a model without heavy cladding and no vulnerabilities of brittle fracture in column splices. It was chosen as the baseline for two reasons:

1. Replacing heavy cladding is an accepted retrofit strategy that can be done as an alternative to or in tandem with an upgrade. It is a relatively simple and inexpensive way to improve the seismic performance of existing buildings. From the architectural point of view, removing cladding from an existing building provides opportunities to give the building an updated look. This is particularly feasible (excluding historic buildings) when the enforced seismic upgrade of an existing building is triggered when the occupancy of building is changed. Furthermore, seismic retrofit strategies often involve repairs of beam-to-column connections or column splices, which typically require opening of non-structural covers around connection regions and include opening of nearby cladding.
2. There are a limited number of analytical tools to simulate brittle failure in column splices and lack of large-scale test data to validate the mathematical model. Moreover, there are no specific modeling requirements mentioned in ASCE 41-13 standard for column splices in moment-resisting frame buildings.

4.4 CONCLUDING REMARKS

The up-to-date national standard ASCE 41-13 was selected as the primary guideline to evaluate the seismic performance of the case-study building. The basic performance objectives for existing buildings (BPOE) were selected per ASCE 41. Both Tier 1 screening and Tier 3 systematic procedures were performed in this study. Eight mathematical models were developed to capture the potential dynamic responses of case-study building that considered the different mechanical behavior of beam-to-column moment connections and column splices, as well as the effect of cladding weight on global response. Additional retrofit measures are considered in Chapter 8.

5 Seismic Hazard and Ground Motions

5.1 SEISMIC HAZARDS

The seismic hazard for a site in downtown San Francisco was assessed considering a soil profile having V_{S30} of 217 m/sec. This site was very near the current case-study building, as well as two other candidate case-study buildings. Probabilistic uniform hazards were generated for five exceedance probabilities; 50% in 30 years, 20% in 50 years, 10% in 50 years, 5% in 50 years, and 2% in 50 years. Corresponding return periods are provided in Table 5.1. In addition, three code-based spectra were developed for the site; one corresponding to the current design level in ASCE 7 [ASCE 2010] and two for the basic safety earthquake levels 1 and 2 (BSE-IE and BSE-2E) for existing buildings in accordance with ASCE 41 [ASCE 2014]. The corresponding return period for the code spectra is provided in Table 5.1. The hazards are represented in terms of pseudo-acceleration response spectra; see Figure 5.1. Characterization of the hazard in the vertical direction was designated by a two-third factor on the horizontal component's response spectrum. The vertical response spectrum was not taken into account during ground-motion selection or scaling.

Table 5.1 Seismic hazard levels.

Hazard level	Return period
50% in 30 years	43 years
20% in 50 years	224 years
10% in 50 years	475 years
5% in 50 years	975 years
2% in 50 years	2475 years
ASCE 7-10 Design	475 years
ASCE 41-13 BSE-1E	224 years
ASCE 41-13 BSE-2E	975 years

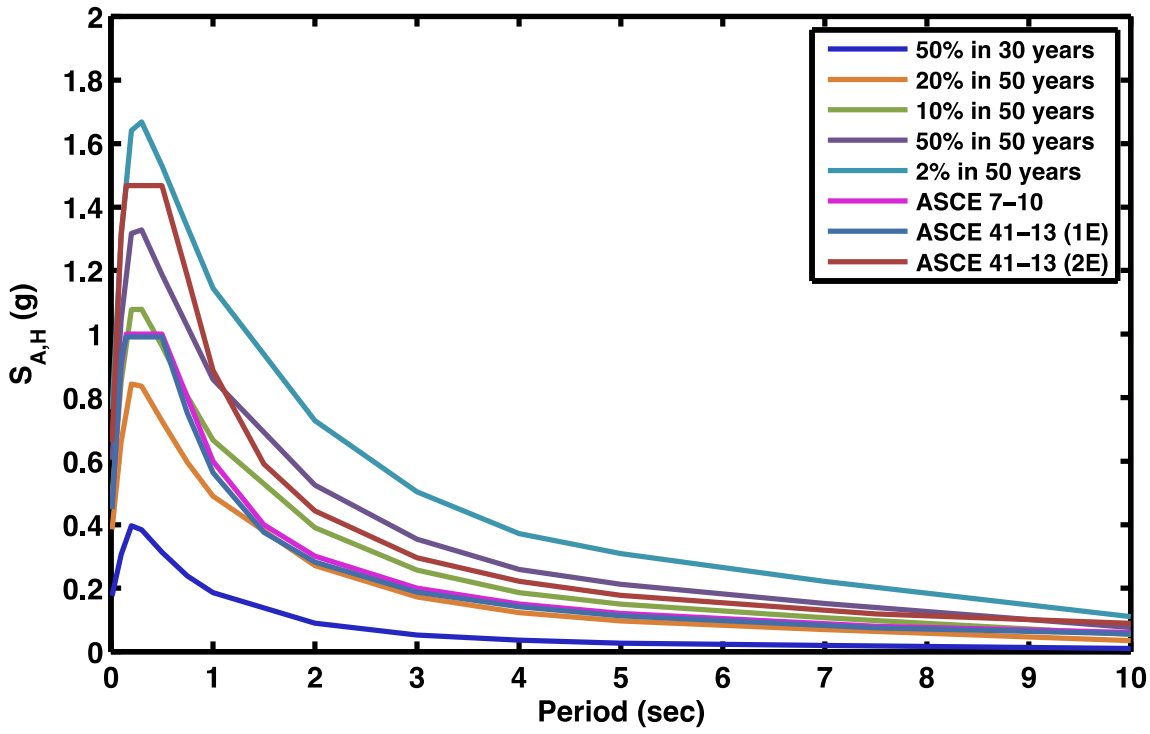

Figure 5.1 **Target horizontal acceleration response spectra at 5% critical damping.**

5.2 GROUND-MOTION SELECTION METHODOLOGY

Ground-motion selection and scaling was completed by J. Baker (*personal communication*, October 29, 2014). Ground motions were obtained from the PEER NGA-West-2 database [Ancheta et al. 2014]. Each hazard level contained a unique set of twenty, three-component recordings (two horizontal and a vertical), which were amplitude scaled to the targeted hazard spectrum following ASCE [2010] recommendations.

Records were scaled such that all three components were modified by the same scale factor. Scaling was based on the geomean or square-root-of-sum-of-squares (SRSS) of the two horizontal components, depending on whether the hazard was probabilistic or code compliant, respectively. Consequently, the average vertical response spectrum is not in agreement with the target spectrum. Scale factors were minimized to the extent possible given the selection criteria in Table 5.2. The magnitudes and distances of the selected ground motions were constrained to reflect typical earthquakes that controlled the seismic hazard in each hazard level.

Table 5.2 identifies the number of ground motions available in each hazard level based on the selection criteria. From the immense database with approximately 30,000 possible recordings, a maximum of 150 records meet the criteria for the 20% probability of exceedance in 50 years. At lower probabilities of exceedance, this number reduces to as few as 45. This restricts the characterization of the hazard and results in the reoccurrence of the same ground motion in multiple hazard levels, but the number of records matching the criteria sufficiently generated an average response with good agreement to the target spectra with the desired number of 20 ground motions.

A long fundamental period coupled with significant higher modes is a characteristic feature of tall buildings. The frequency content of the ground motions must therefore encompass a wide range to capture the uniform hazard spectra and code spectra. Selection and scaling was executed with this in mind. The maximum usable period was required to exceed 8.4 sec and the minimum usable period was set to 0.2 or 0.8 sec; see Table 5.2.

Table 5.2 Ground motion selection criteria.

		ASCE 41-13		Probabilistic				
	ASCE7-10	**BSE-1E**	**BSE-2E**	**2% in 50 yrs**	**5% in 50 yrs**	**10% in 50 yrs**	**20% in 50 yrs**	**50% in 30 yrs**
Min. magnitude	6.8	6.8	6.9	6.9	6.8	6.5	5.9	5.9
Max. magnitude	7.9	7.9	7.9	7.6	7.9	7.6	7.9	7.3
Min. distance (km)	0	5	0	1	5	2	0	4
Max. distance (km)	29	28	29	29	29	28	70	44
Min. Vs30 (m/s)	187	229	199	186	187	192	175	128
Max. Vs30 (m/s)	650	726	566	650	650	566	516	638
Min. period (s)	0.8	0.2	0.8	0.2	0.2	0.2	0.2	0.2
Max. period (s)	8.4	8.4	8.4	8.4	8.4	8.4	8.4	8.4
Lowest usable freq (Hz)	0.12	0.12	0.12	0.12	0.12	0.12	0.12	0.12
Max. scale factor	2.0	2.6	3.3	6.0	5.0	2.0	2.0	1.6
Num. available	46	45	58	50	50	94	150	133
Num. from NGA-W1	25	25	32	26	27	51	82	69
Num. from NGA-W2	21	20	26	24	23	43	68	64

Key steps in the ground-motion selection methodology were as follows:

- Site conditions and earthquake characteristics followed the criteria of Table 5.2;
- No more than four recordings from any single earthquake were used within a given set of 20 ground motions;
- Only ground motions with maximum usable periods greater than 8.4 sec were considered;
- The selected ground motions came from recordings in parts of the world with similar seismic and geological conditions to the study area. Many recordings come from California, but some were from Taiwan, Turkey, and other regions where scientific consensus is that ground motions have similar properties to those in the western U.S. These non-U.S. ground motions were used due to the lack recordings from large U.S. earthquakes

at nearby distances with response spectra matching the target spectra considered here;

- For the code spectra, ground motions were selected and scaled so that their SRSS spectra matched the target Design Response Spectrum between 0.8 and 8.4 sec; thus, the average of the SRSS spectra exceeded the target spectrum over this period range per the requirements of the reference code documents. Closeness of the spectral match was computed as the sum of squared differences between the record's geometric mean spectrum and the target spectrum over a discretized set of periods in the specified range;
- For the probabilistic spectra, ground motions were selected and scaled so that their geometric mean spectra matched the target spectrum between 0.8 and 8.4 sec. This is because the probabilistic spectra are "GMRotI50" spectra (approximately equivalent to the spectra of the geometric mean of two-component motions); this approach was used to maintain consistency between the target spectrum definition and the ground motion spectrum definition. Closeness of the spectral match was computed as the sum of squared differences between the record's geometric mean spectrum and the target spectrum over a discretized set of periods in the specified range. Unlike the code spectra cases, the average of the ground motions' spectra was not required to exceed the target spectrum at all periods (i.e., it is slightly above at some periods and slightly below at other periods); and
- An initial automated selection process was performed as follows:
    - Ground motions were screen based on their magnitude, distance, V_{s30}, and maximum usable period values. Ground motions not falling within acceptable ranges of these properties were discarded;
    - Twenty ground motions were selected that best fit the target spectrum after scaling (i.e., those with a minimum sum of squared errors), subject to the constraint that the scale factor not exceed the specified maximum amount; and
    - If more than four of the 20 selected ground motions came from a single earthquake, the worst-fitting ground motions from that earthquake were discarded and replaced with new ones.

After the initial automated selection, the results were manually reviewed, and any problematic ground motions were discarded. Reasons for discarding ground motions included:

- Ground motions with unreasonable spectral values at periods outside of the range considered for automated selection;
- Ground motions that had been previously selected for another similar set (i.e., for ASCE 7-10 and ASCE 41-13 1E, where the spectra are nearly identical and unique records were desired for each set); and
- Ground motions that had other unusual properties deemed to be unrepresentative of expected motions at the target site.

The "unreasonable spectral values" criterion above was primarily used to remove ground motions where scaling produced high spectral amplitudes at short periods. This removal was done in some cases via manual screening, and in some cases was achieved by re-running the automated selection while considering spectral values down to 0.2 sec when selecting ground motions with close spectral matches. The resulting ground motion selections and scale factors are provided in Appendix A. The scaled response spectra are provided in Figure 5.3–5.9.

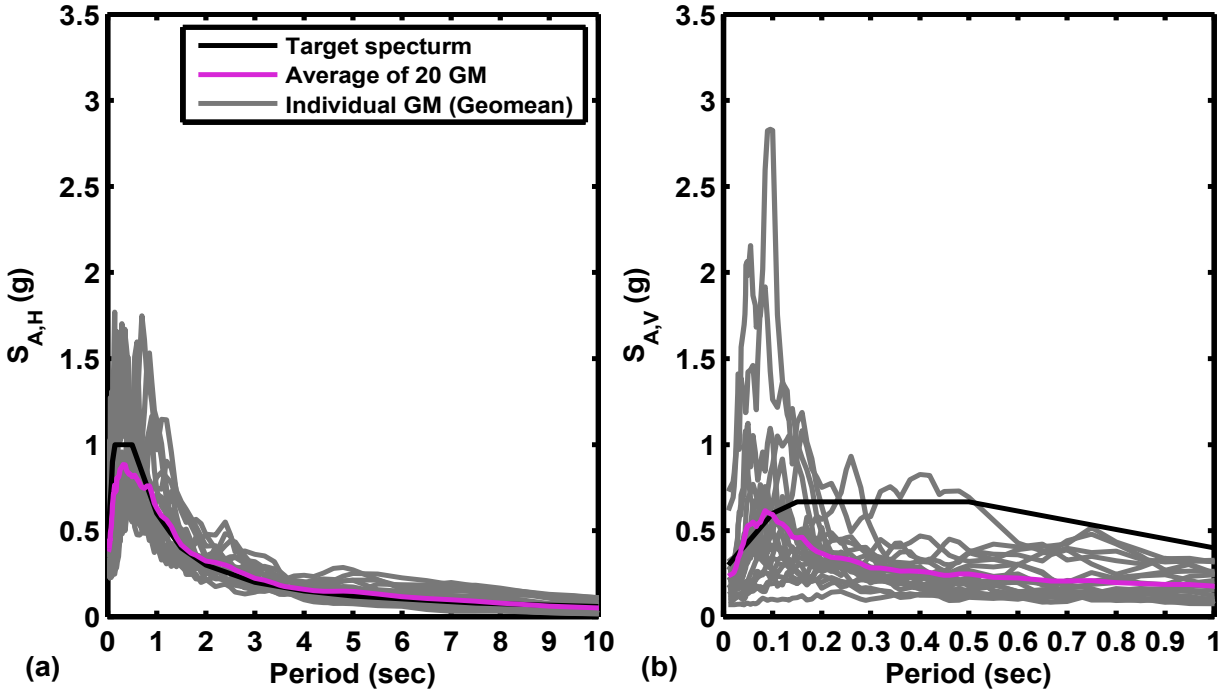

Figure 5.2 **Design level [ASCE 2010] hazard in terms of (a) horizontal and (b) vertical acceleration response spectra at 5% damping.**

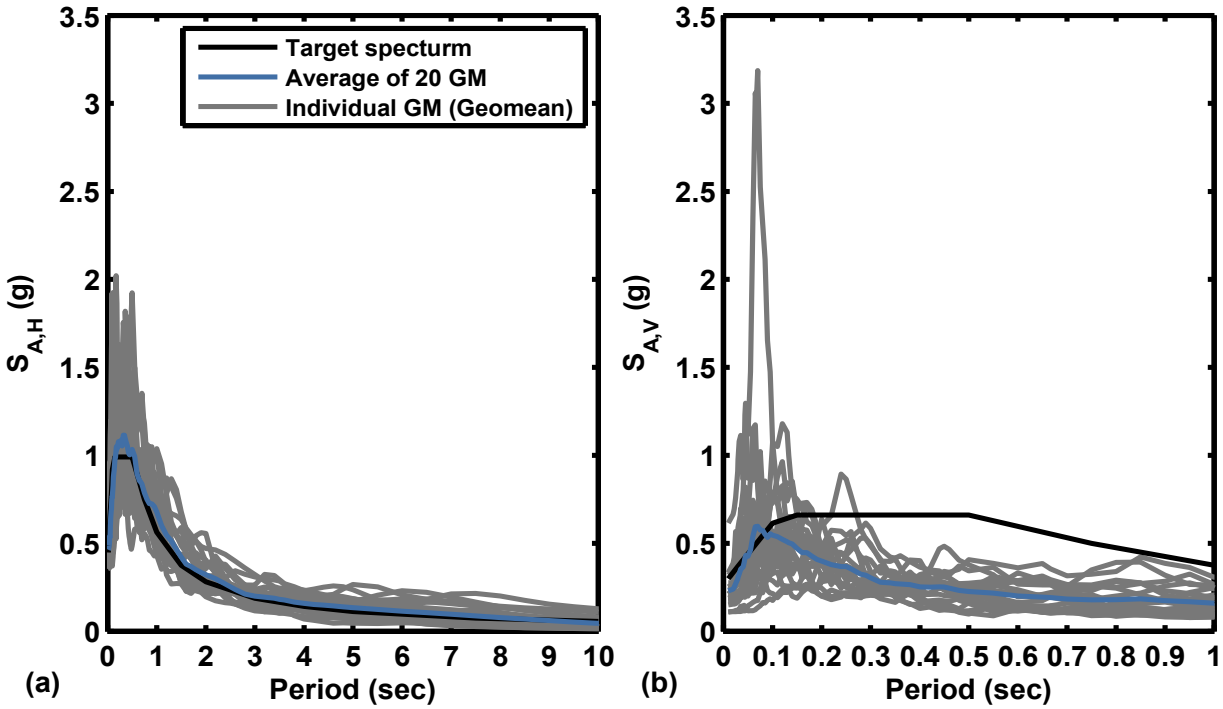

Figure 5.3 BSE-1E [ASCE 2014] hazard in terms of (a) horizontal and (b) vertical acceleration response spectra at 5% damping.

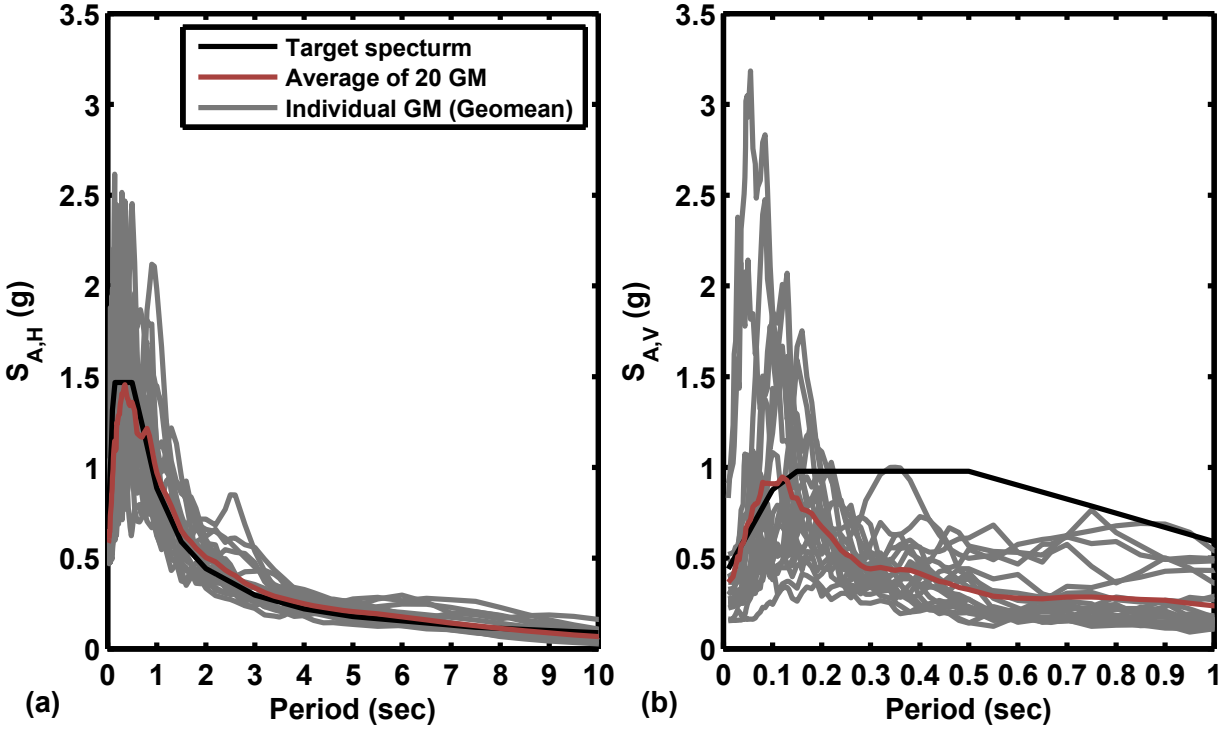

Figure 5.4 BSE-2E [ASCE 2014] hazard in terms of (a) horizontal and (b) vertical acceleration response spectra at 5% damping.

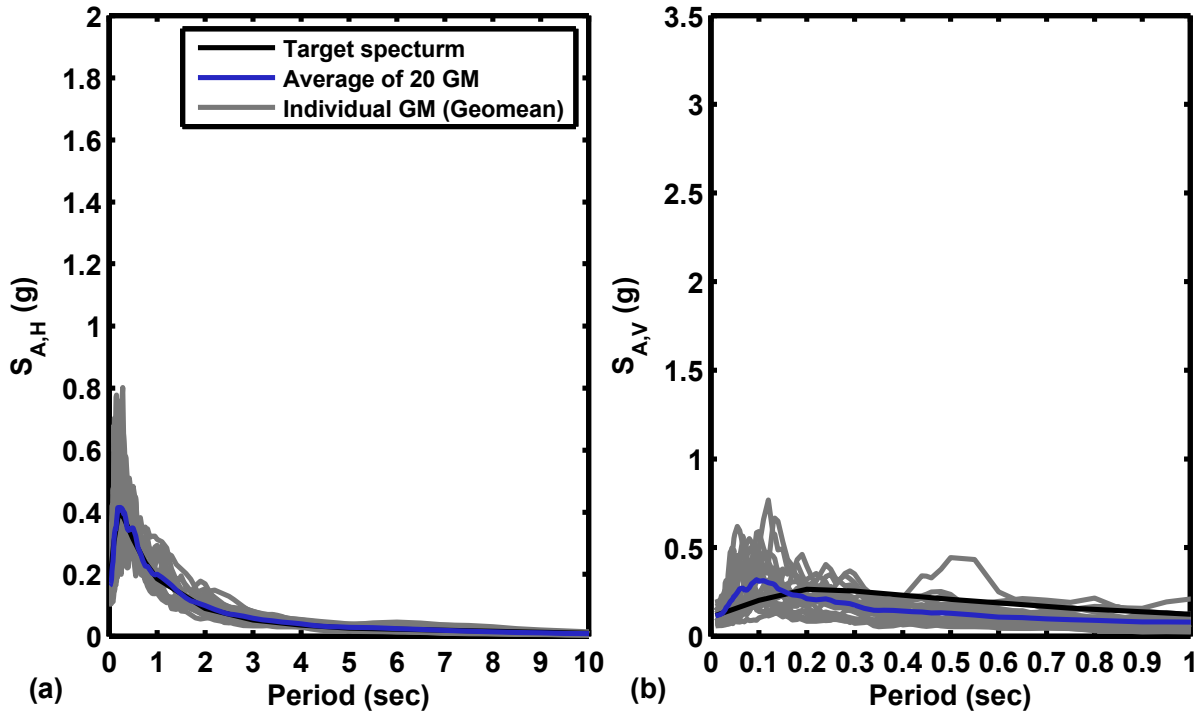

Figure 5.5 A 50% in 30-year (43-year return period) probabilistic hazard in terms of (a) horizontal and (b) vertical acceleration response spectra at 5% damping.

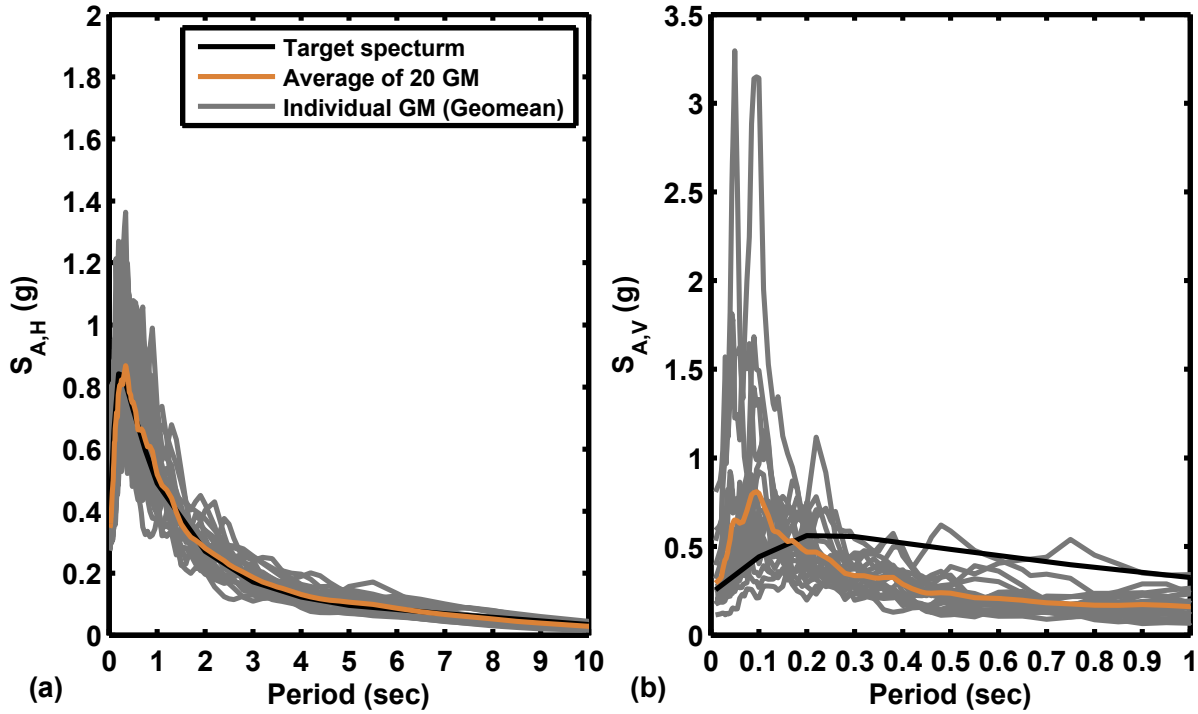

Figure 5.6 A 20% in 50-year (224-year return period) probabilistic hazard in terms of (a) horizontal and (b) vertical acceleration response spectra at 5% damping.

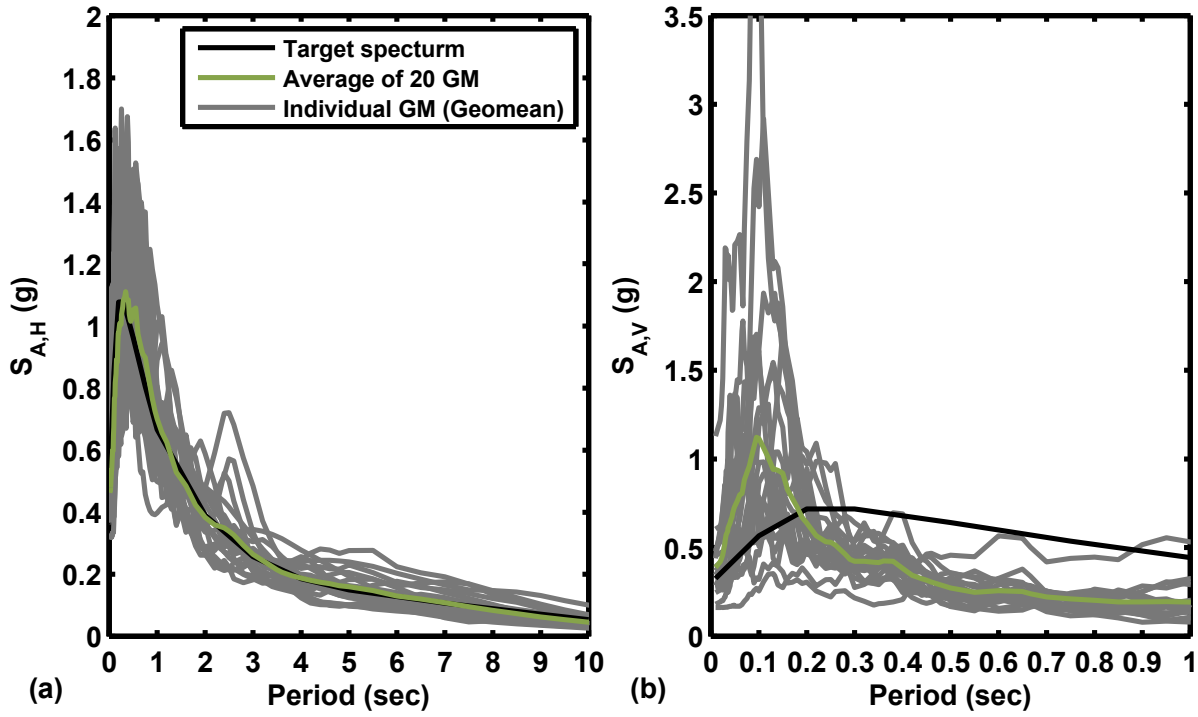

Figure 5.7 A 10% in 50-year (475-year return period) probabilistic hazard in terms of (a) horizontal and (b) vertical acceleration response spectra at 5% damping.

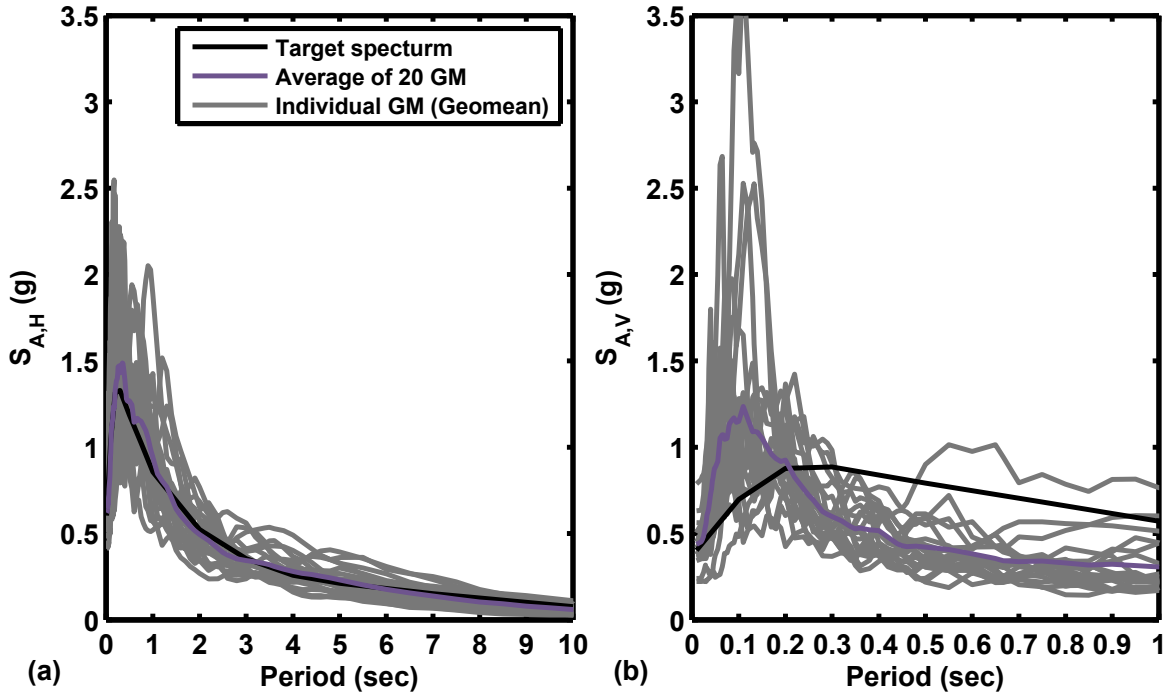

Figure 5.8 A 5% in 50-year (975 year return period) probabilistic hazard in terms of (a) horizontal and (b) vertical acceleration response spectra at 5% damping.

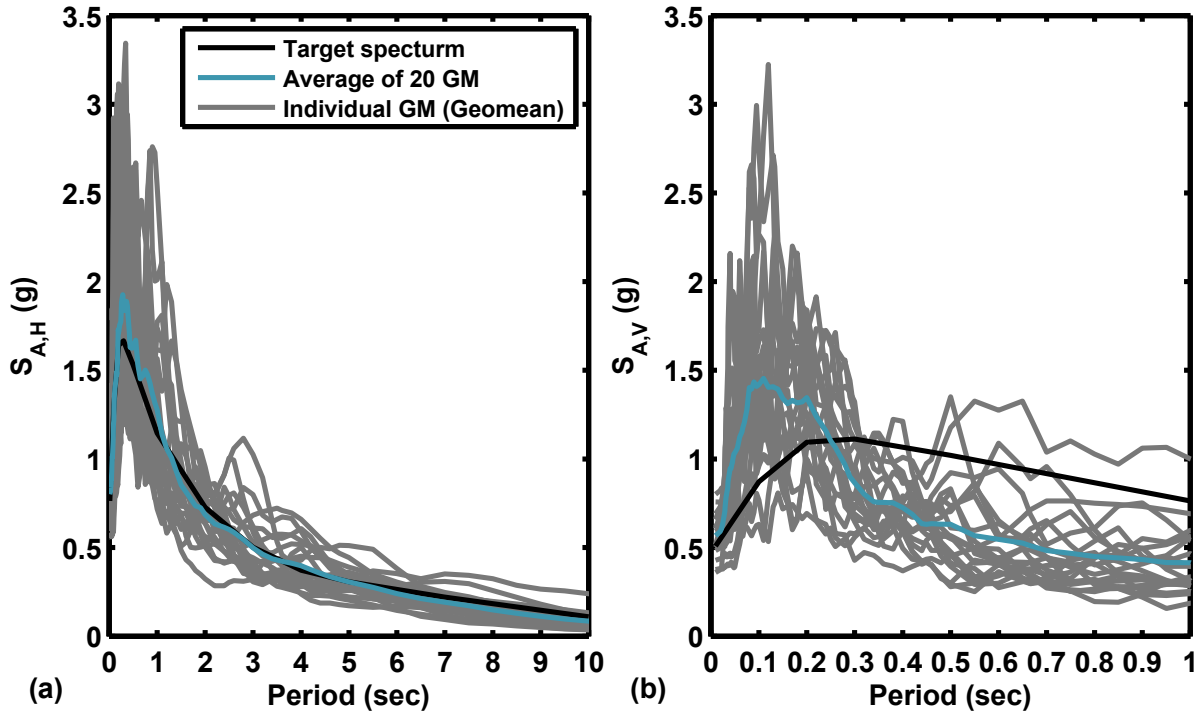

Figure 5.9 **A 2% in 50-year (2475 year return period) probabilistic hazard in terms of (a) horizontal and (b) vertical acceleration response spectra at 5% damping.**

5.3 NGA-WEST-2 ENHANCEMENTS

Table 5.2 identifies the number of records available that were added by NGA-West-2 and those previously available from NGA-West-1. The number of newly available records has been expanded on those previously available by nearly a factor of 2. This great enhancement is, however, understated. Record processing procedures of the NGA-West-2 exanded the usable frequency content, in some cases, of older records available from NGA-West-1. This improvement is reflected in Table 5.3, which includes the number of records included in each ground-motion set (20 records for each hazard level) that were previously available. Of these, the number of records that previously had inadequate frequency content, but were re-processed during NGA-West-2 to satisfy the criteria of Table 5.2, are identified. These ranged between two to ten records that previously would have been excluded from characterization of the hazard. Eliminating these records reduces selected ground motions usable from NGA-West-1 by 20% to 91%. Consequently, re-processing enhanced records previously available and increased the number that satisfied the selection criteria. Therefore, the number identified in Table 5.2 as being available from NGA-West1 is overstated because of the re-processing enhancment.

Table 5.3 Selected ground motions previously available from NGA-West-1.

		ASCE 41-13		Probabilistic				
	ASCE 7-10	BSE-1E	BSE-2E	2% in 50 yrs	5% in 50 yrs	10% in 50 yrs	20% in 50 yrs	50% in 30 yrs
No. selected from NGA-West-1	9	10	9	13	12	13	14	11
No. in NGA-West-1 with inadequate frequency content	2	2	4	5	3	8	10	10
Total usable from NGA-West-1	7	8	5	8	9	5	4	1

5.4 GROUND MOTION RECORD FROM THE LOMA PRIETA EARTHQUAKE

A case study was used to validate the numerical model. The model's response was evaluated subjected to a recording from the 1989 Loma Prieta earthquake to determine if the seismic performance was consistent with expectations of what occurred during the historic earthquake. The CSMIP station 58480 recording obtained from the CESMD [2015]. The station is located in downtown San Francisco and is consistent with the generic location used to generate the hazards. Three-component basement recordings from the 18-story, mixed reinforced concrete shear wall and steel frame structure were used as input for this case study; see Section 2.3.4. Acceleration response spectra of the Loma Prieta record are provided in Figure 5.10 along with the 30% probability of exceedance in 50-year hazard level. The horizontal SRSS response spectrum of the recording shows the low-period content far exceeds that of the 43-year return period hazard. At a 3-sec period, the historical record matches the probabilistic hazard but then drops below the probabilistic hazard at longer periods. Figure 5.11 illustrates this deviation more dramatically in the displacement response spectrum. Near the fundamental period of the building, the Loma Prieta record is 25–30% below the probabilistic hazard.

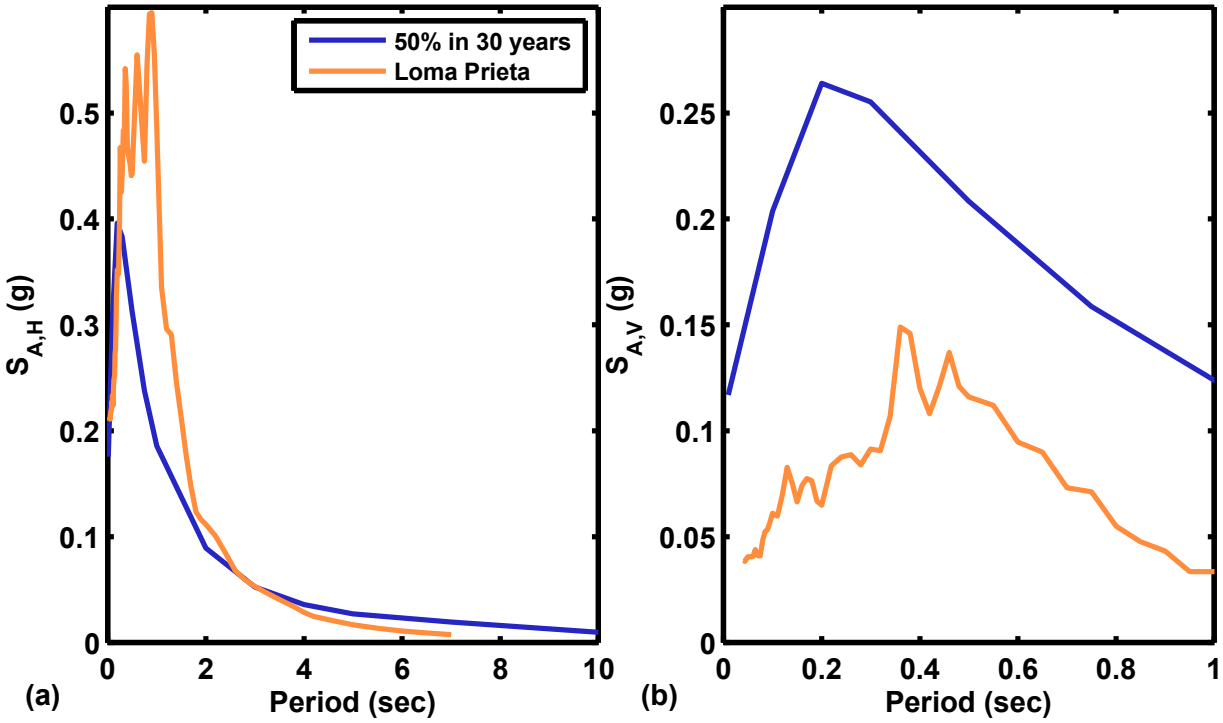

Figure 5.10 Loma Prieta case study ground motion in terms of (a) horizontal and (b) vertical acceleration response spectra at 5% damping.

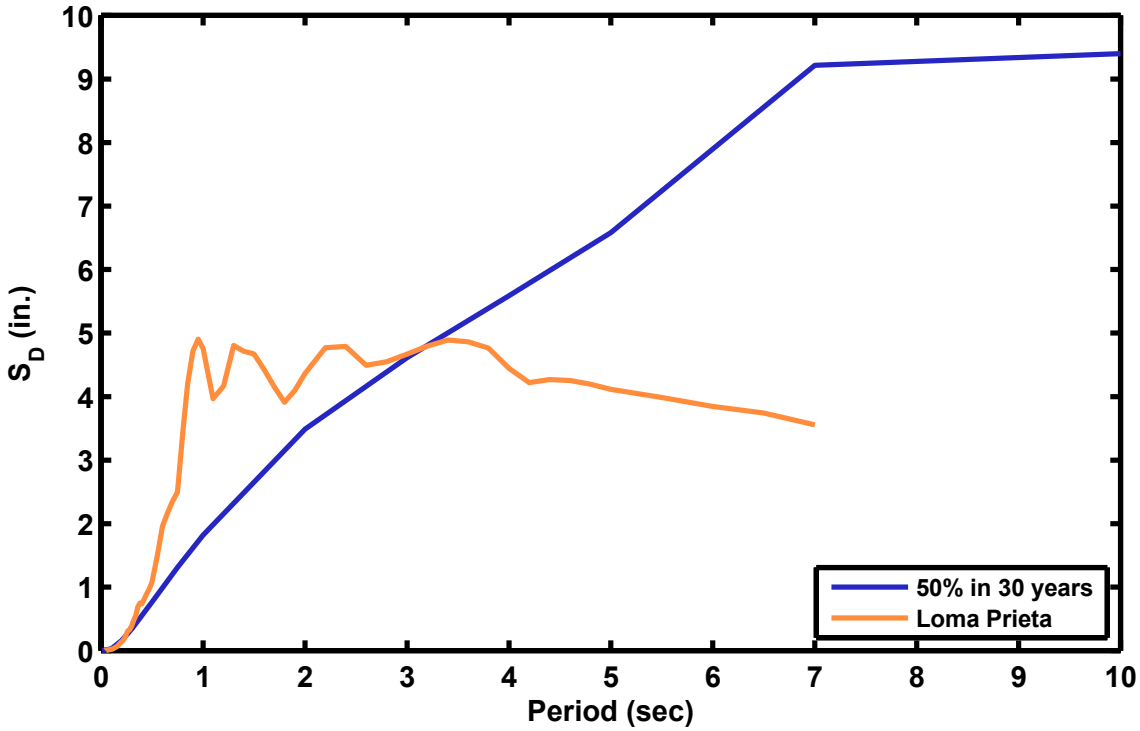

Figure 5.11 Loma Prieta case study ground motion in terms of horizontal displacement response spectra at 5% damping.

5.5 CONCLUDING REMARKS

The selected ground motions and scaling methods used were obtained from the PEER NGA-West-2 database. Enhancements from the NGA-West-1 database were identified as beneficial to the selection procedure by increasing the number of records available. Each hazard level contained a unique set of twenty, three-component recordings (two horizontal and a vertical), which were amplitude scaled to the targeted hazard spectrum following ASCE [2010] criteria. The selected ground motions contain a wide range of frequencies that could encompass the low-frequency range that are of particular importance for tall buildings. A case study recording from the 1989 Loma Prieta earthquake was also introduced.

6 Mathematical Modeling

The mathematical modeling details and assumptions used for this study are described in this chapter. Following the basic assumptions described in ASCE 41-13, a 3D computer model of the case-study building was constructed using OpenSees [McKenna et al. 2010] to investigate its nonlinear dynamic behavior. The seismic lateral force-resisting system of the case-study building is a bi-directional moment-resisting space frame system. As shown in Figure 6.1, all above-ground main framing members contributing to the seismic lateral force resisting systems were included in the model. The elevation, typical floor plan, and mezzanine level floor plan of the case-study building are illustrated in Figure 3.3. Mathematical modeling details and the simulation assumptions used in OpenSees for different structural components are described below.

6.1 STEEL MATERIAL STRENGTHS

Generally, the material properties of structural elements in the numerical model were modeled per ASCE 41-13, Section 9.2.2. For structural sections made of ASTM A36 steel manufactured between 1961 and 1990 (see ASCE 41-13, table 9-1), the yield strength was based on the AISC structural shape size groupings (see Table 1-2 [AISC 1994]). For Group 1, Group 2, and Group 3, the yield strength was taken as 44 ksi, 41 ksi, and 39 ksi, respectively. The expected steel material strength was estimated as the multiplication of lower bound strength (see ASCE 41-13, table 9-1) and modification factors for each material class (see ASCE 41-13, Table 9-3). The modification factor was 1.1 for ASTM A36 steel and ASTM A441 steel (since this value is not listed in Table 9-3 per ASCE 41-13).

A Giuffré-Menegotto-Pinto uniaxial stress–strain constitutive model with isotropic strain hardening (*Steel02)* was used in OpenSees to define the hysteretic behaviour of the steel. The strain-hardening ratio used in the *Steel02* uniaxial material was 0.003 (for fiber sections) and the Young's modulus of elasticity of steel was taken as 29,000 ksi.

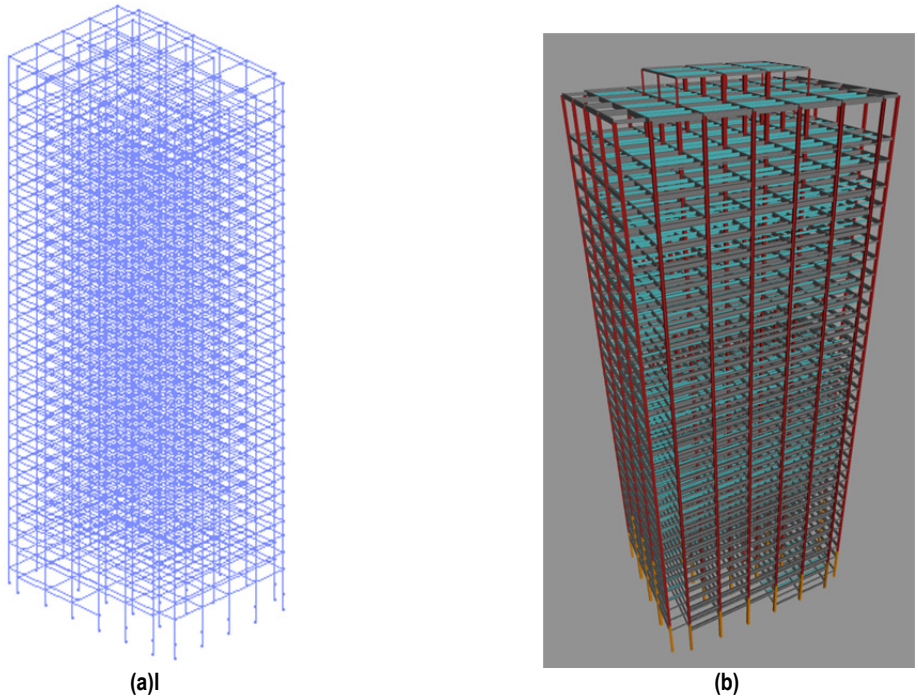

(a)I (b)

Figure 6.1 **Perspective view of OpenSees model; (a) bare frame view of the model and (b) rendered view of the model.**

6.2 STRUCTURAL COMPONENT MODELS

6.2.1 Columns and Column Splices

In this study, columns were modeled with displacement-based beam–column elements with fiber sections at five integration points (NIP = 5) along the length of the element. Each fiber section had four layers in the width (or depth) direction and four layers in the thickness direction. Structural materials were modeled per ASCE 41-13, Section 9.2.2. The expected steel material strength was estimated as the multiplication of lower bound strength and modification factor for each material class. Column P-M-M interaction was considered directly through the use of fiber sections. Shear and torsional deformations of typical column sections were considered through aggregating elastic *uniaxialmaterial* objects containing shear rigidity (GA) and torsional rigidity (GJ) to the corresponding column fiber sections. No interactions between moment, shear, and torsion were simulated.

Column splices were modeled using *zerolengthsection* elements and were assumed to be either fully ductile (no failure) or brittle. To capture the brittle behavior, a maximum permitted tension fiber strain [Kanvinde, *personal communication*, 2012] for each column splice location was derived and assigned to the corresponding fiber section within the *zerolengthsection* element. The maximum permitted strain at fiber rupture was determined using Equation (6.1) shown below.

$$\varepsilon_{allowable} = \frac{K_{IC}}{E \cdot \left[9.91\left(\frac{a}{t_f}\right)^2 - 1.12\left(\frac{a}{t_f}\right) + 1 \right] \cdot \sqrt{\pi a}} = \frac{4.72 \times 10^{-4}}{\sqrt{t_f}} \tag{6.1}$$

where t_f is the thickness of column flange; $a = 0.5t_f$ according to typical column splice welding detail as shown in the shop drawings (also, see Figure 6.2); $K_{IC} = 50 \text{ ksi}\sqrt{\text{in.}}$ is the assumed fracture toughness of weld consumables, and E = 29,000 ksi is the Young's modulus of steel.

To investigate the effect of mechanical behavior of various connections on building seismic responses (see Chapter 4), another set of modeling parameter for an ideally ductile column splice using the *Steel02* uniaxial material was used for comparison on the effect of connection mechanical behavior on the global responses.

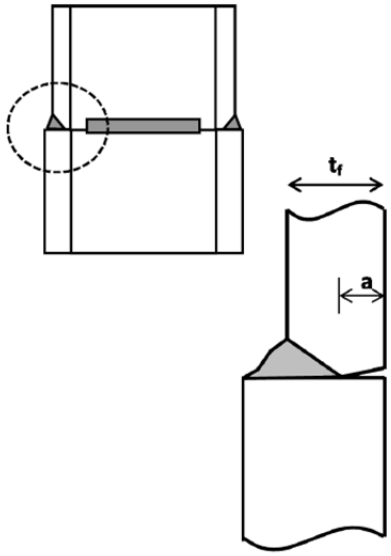

Figure 6.2 **Typical column splice weld detail and geometry (extracted from Stillmaker et al. [2016]).**

6.2.2 Beams, Beam-to-Column Connections, and Panel Zones

Beams were modelled using force-based nonlinear beam-column elements with finite-length plastic hinges at both ends as proposed by Ribeiro et al. [2015]. The moment-curvature behavior of plastic hinge was assigned as the hysteretic uniaxial material with the *fatigue* material wrapper to account for low-cycle fatigue. Plastic hinge length was selected as 1/6 of the beam length, such that no correction of moment of inertia for the elastic portion of the beam element was required [Ribeiro et al. 2015]. As illustrated in Figure 6.3, if using a plastic hinge length other than 1/6 of the beam length, it is assumed that the typical plastic hinge length to beam span ratios are between 1/10 and 1/20, and the flexural stiffness modification parameters β_1 and β_3 are negative; this will create numerical stability problems during the dynamic analysis. This is the main reason for selecting a plastic hinge length to beam span ratio of one-sixth in the study.

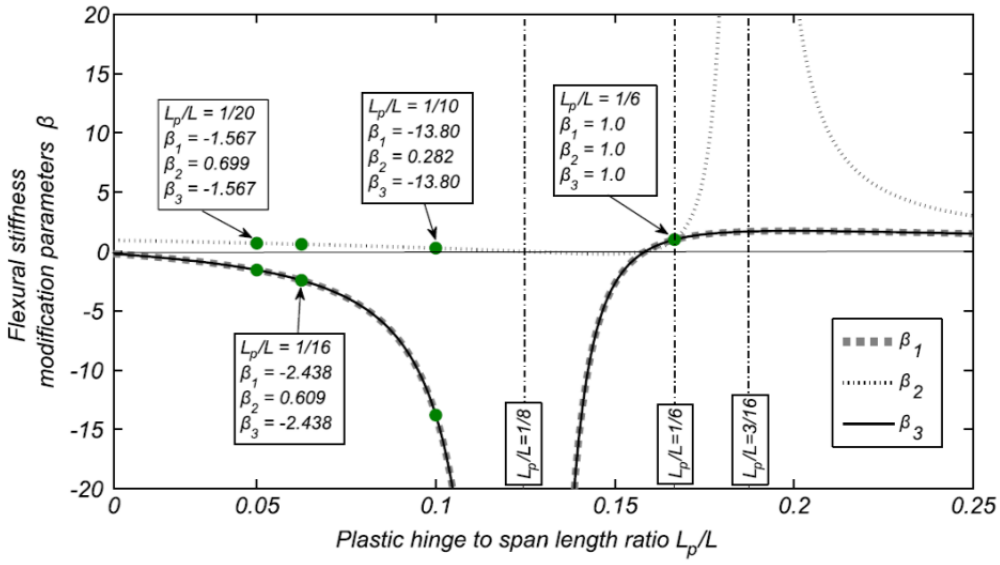

Figure 6.3 **Flexural stiffness modification factors as a function of the plastic hinge length to span ratio (extracted from Ribeiro et al. [2015]).**

ASCE 41 modeling parameters for welded unreinforced flange (WUF) beam-to-column connections were used to simulate the connection behavior. A 3% strain-hardening slope of the elastic slope for beams was used as permitted by ASCE 41. Figure 6.4 illustrates one example of simulated beam-to-column assembly responses (per ASCE 41 modeling parameters) under monotonic and cyclic loading conditions of a wide flange beam (W33×118) to box column connection. As mentioned in Chapter 4, another set of modelling parameter for an ideally ductile connection (using bilinear *Steel01* uniaxial material) was used for comparison on the effect of connection mechanical behavior on the global responses.

Panel zones were not explicitly modeled. Instead, as permitted by FEMA 451 [2006], the center-to-center elements model was used.

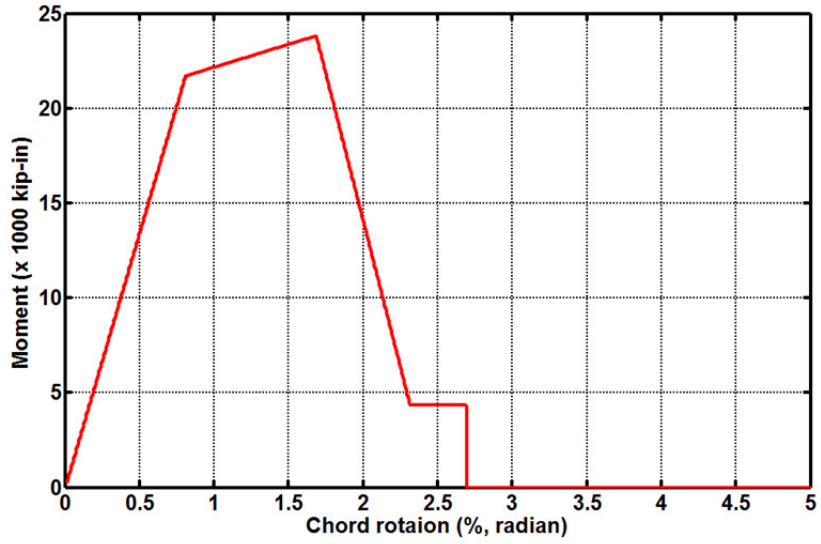

(a) Monotonic

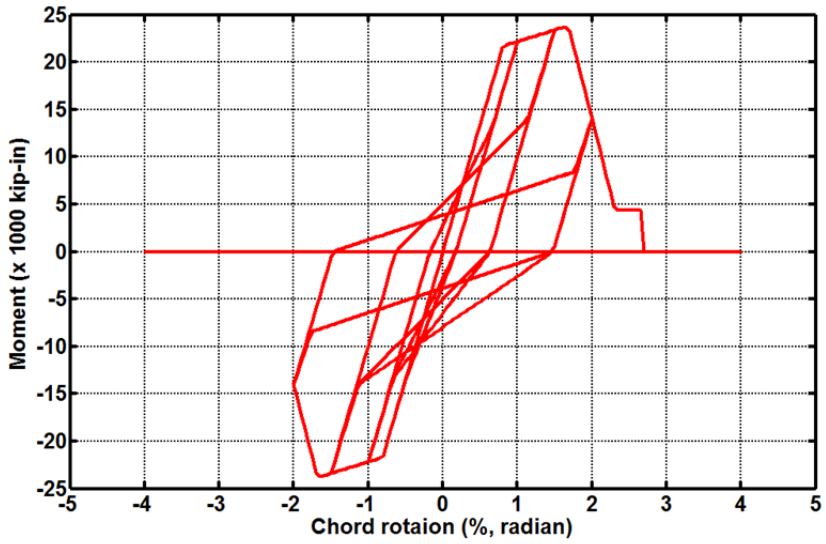

(b) Cyclic

Figure 6.4 **Simulated beam-to-column connection response (per ASCE 41 modeling parameters).**

6.2.3 Floor Diaphragms

As mentioned in Chapter 3, the typical floor diaphragm of the case-study building consisted of a 6-in.-thick, lightweight, reinforced concrete slab on top of a metal deck. From the structural drawings, there were no shear studs welded through the metal deck; only 3/4-in. puddle welds were provided to connect the metal deck and the beam top flange. From the available design information about the case-study building, it is not clear if the floor slab was designed as a diaphragm; however, rigid diaphragm constraints were included in the numerical model for simplicity.

6.3 SEISMIC LOADS AND LOAD COMBINATIONS

Similar to the PEER TBI guidelines for new tall buildings [PEER 2010], Section 7.7.2 of ASCE 41-13 calls for consideration of full gravity dead loads along with 25% of live loads when combined with seismic effects for evaluation using the nonlinear dynamic procedure. Thus, dead loads plus 25% of the design live loads were included in the seismic analyses. A typical floor live load was assumed to be 100 psf everywhere, and the sources of superimposed dead load (not including the structural member self-weight) are listed in Table 6.1. Note that dead loads and live loads on beam elements are specified through the uniform line distribution along the elements in OpenSees based on the tributary area. No gravity beams—the beams that are not in the lateral force-resisting system—were simulated in numerical model.

Seismic masses were assigned as joint masses per tributary area and converted from the element self-weight, concrete slab weight, superimposed dead loads, and 25% of live loads. Note that the estimated weight of the 8-in.-thick exterior cladding (6-in.-thick precast lightweight concrete panels plus 2-in.-thick granite) was 15% of the entire building weight; the effect of cladding weight is discussed in detail in Chapter 7.

Table 6.1 Source of dead load assumed in the study.

Source	Value (psf)
Light weight concrete slab (6-in.-thick)	56
Metal deck	5
Partitions	20
Mechanical and MISC	20

6.4 DAMPING

Rayleigh damping coefficients were derived assuming the first- and the 24th-mode critical damping values both equal to 1.71 % (α/N = 60/35) according to the Equation (2-10) in ATC 72-1 (ATC, 2010).

6.5 BOUNDARY CONDITIONS

A fixed-base boundary condition was used at the column bases at the ground level for the results shown herein; see Figure 6.1. The soil-structure interaction (SSI) effects, both inertial and kinematic interactions, were not considered here. However, according to the recommendations in the ATC-83 [NIST 2012], if possible, inertial interaction effects and kinematic interaction effects should be considered. For the inertial interaction, the most important factor is the ratio of structure-to-soil stiffness, which is related to the $h/(V_s \cdot T)$ ratio, where h is the effective height of the center-of-mass for the first-mode shape, V_s is the soil shear-wave velocity, and T is the fundamental period of the structure. Typically, inertial SSI effects are negligible when this ratio is less than 10% [NIST 2012]. For the case-study building considered herein, the estimated minimum soil shear-wave velocity to determine if the inertial SSI effect can be neglected is computed as follows:

$$T = 0.028 \cdot \left(\frac{5690}{12} \right)^{0.8} = 3.87 \text{ (sec)}$$

$$V_S \geq \frac{h}{0.1 \cdot T} = \frac{\frac{2}{3}\left(\frac{5690}{12} \right)}{0.1 \cdot 3.87} = 817 \text{ (ft / sec)}$$

From the above estimates, as long as the soil shear-wave velocity of the site is larger than 817 ft/sec, the effect of inertial SSI can be neglected. Recall that V_{s30} for site class D for a stiff soil site in ASCE-7, Table 20.3-1 [ASCE 2010], is between 600 and 1200 ft/sec. From the report by H.J. Sexton & Associates, Engineers [1968], the site–soil condition of the case-study building is Zone 3 (S3), which is equivalent to the site class E (V_{s30} < 600 ft/sec) in ASCE-7 [Dobry and Iai 2000]. For the kinematic interaction, the transfer function in frequency domain is required to convert the free-field ground motions to foundation input motions. Since the effects of damping and flexibility at the foundation–soil interface are not expected to be significant because of the building's long fundamental period [NIST 2012], and because soil properties at the site were not well-established, SSI effects were not considered in this report. However, the above discussion suggests that there may be a benefit of investigating SSI effects more fully.

6.6 SELECTION OF ENGINEERING DEMAND PARAMETERS

The structural response parameters (EDPs) of interest in the study are identified below. Table 6.2 presents the typical EDPs monitored during the nonlinear dynamic analyses and the derived EDPs obtained from the raw output data of OpenSees recorders.

Table 6.2 Engineering demand parameters of interest.

Engineering demand parameters (EDPs)	Data type (raw date from OpenSees recorder outputs or derived data)
Floor (control node) relative displacement	Raw
Floor (control node) relative acceleration	Raw
Floor (control node) relative velocity	Raw
Story drift ratio (SDR)	Raw
Floor (North-East corner) relative displacement	Raw
Floor (North-West corner) relative displacement	Raw
Floor (South-East corner) relative displacement	Raw
Floor (South-West corner) relative displacement	Raw
Base reaction forces	Raw
Column elements forces	Raw
Column elements deformations	Raw
Column elements plastic deformation envelope	Raw
Column splices forces	Raw
Column splices deformations	Raw
Column splices damage indices	Raw
Beam elements forces	Raw
Beam elements deformations	Raw
Beam elements plastic deformations	Raw
Beam elements force envelope	Raw
Beam elements deformation envelope	Raw
Beam elements plastic deformation envelope	Raw
Roof orbital displacement history	Derived (relative and absolute)
Roof displacement history	Raw
Peak story drift ratio (PSDR)	Derived
Peak roof drift (PRD)	Derived
Peak floor acceleration (PFA)	Derived (relative and absolute)
Peak floor velocity (PFV)	Derived (relative and absolute)
Residual roof displacement	Derived
Residual story drift (ResDR)	Derived
Story shear forces	Derived
Story moment	Derived
Column splice failure percentage	Derived (damage indices)
Peak chord rotation demand at beam ends	Derived
Connection hysteresis loops	Derived (force-deformation)
Peak story displacement envelope	Derived
Peak story drift envelope	Derived
Peak story shear envelope	Derived

6.7 LIMITATIONS OF MATHEMATICAL MODELS

The mathematical models developed and used in the study are not comprehensive and are not intended to predict all possible behavior of case-study building under given excitations. Several, but not all, limitations of current mathematical models are listed below.

- The member models used to model beams and columns did not simulate local buckling behavior of the structural sections;
- The fixed base model did not consider soil-structure interaction effects;
- Composite actions between the beams, metal deck, and floor slab were not considered;
- Stiffness contribution from non-structural concrete elevator core wall, non-structural concrete smoke tower, building façade, and exterior cladding were not included in current models;
- Panel zone regions were not simulated, although permitted by FEMA 451 [FEMA 2006];
- Possible column base rocking (tension force transfer between column base plate and the foundation mat was not explicitly detailed) behavior could not be captured using the current model;
- Subterranean basement levels and the perimeter retaining walls were not included in the mathematical model; and
- Contact behavior between fractured surfaces (in column splices or beam-to-column connections) was not captured using the current model.

6.8 CONCLUDING REMARKS

The mathematical models used in the study followed the basic requirements described in ASCE 41-13 standard. An attempt to explicitly simulate the brittle fracture of column splices was incorporated into the OpenSees model to examine the effect of the mechanical behavior of column splices on the dynamic responses of case-study building. Several modeling limitations were pointed out and briefly discussed.

7 Evaluation of Results and Discussion

This chapter summarizes the results of ASCE 41-13 and FEMA 351 performance evaluation procedures. The seismic deficiencies identified during the ASCE 41-13 Tier 1 screening process are discussed first. Then, pushover analysis results according to the nonlinear static procedure (NSP) are presented. Modal analysis results are introduced before discussing building responses under a series of different hazard level ground excitations and one historical event. The global and local responses of the case-study building under BSE-1E and BSE-2E hazard-level ground-motion sets per ASCE 41-13, Tier 3 systematic procedure, nonlinear dynamic procedure (NDP), are then discussed in detail. Effects of vertical component of ground motion, cladding weight, and mechanical behavior of connections on the building dynamic responses are discussed. Deficiencies identified in the Tier 3 evaluations are summarized. Finally, the probabilistic approach used in FEMA 351 is used to assess likely performance.

7.1 SEISMIC DEFICIENCIES IDENTIFIED FROM TIER 1 SCREENING

The Tier 1 structural evaluation identified a number of possible deficiencies, including a potential soft story at the mezzanine level. Other deficiencies included high column stress levels, pre-Northridge beam-to-column connection details, panel zone details, inadequacy according to the strong-column–weak-beam (SCWB) check, column bases are not anchored to the foundation, diaphragm openings at the mezzanine level, and metal decks connected to steel frames with only puddle welds (no shear studs were used). In some cases, welds used to fabricate built-up sections were insufficient to develop member flexural capacities. Capacity checks of the partial joint penetration welds at column splice regions were also found to be problematic. Detailed checks carried out in accordance with Tier 1 procedures, as well as weld capacity checks, are provided in Appendices B, C, and D.

7.2 MODAL ANALYSIS

Elastic range Eigen-analyses were performed to determine the vibration modes of the case-study building. Vibration modes are useful to understand the dynamic behavior of the building and to visually check that elements are properly connected. In the study, the first 24 vibration modes were determined using the OpenSees Eigen-analysis. For these analyses, realistic cladding weight was incorporated in the model. Figure 7.1 shows the deflected shapes of the first three modes. The first mode, shown in Figure 7.1(a), is a translational mode in the *X*-direction, which has a period of 4.70 sec. The second mode, shown in Figure 7.1(b), is a translational mode in the

Y-direction, which has a period of 4.53 sec. The third mode, shown in Figure 7.1(c), is a torsional mode having a period of 4.15 sec. Table 7.1 lists the periods of the first 24 modes. The vertical mode of vibration is associated with mode number 18 with a period of 0.43 sec.

Table 7.1 Modal periods of the case-study building (with cladding weight).

Mode	Period (sec.)	Mode	Period (sec.)	Mode	Period (sec.)	Mode	Period (sec.)
1	4.697	7	0.935	13	0.538	19	0.430
2	4.532	8	0.922	14	0.535	20	0.388
3	4.151	9	0.870	15	0.522	21	0.385
4	1.623	10	0.687	16	0.436	22	0.365
5	1.571	11	0.683	17	0.433	23	0.360
6	1.424	12	0.662	18	0.431	24	0.358

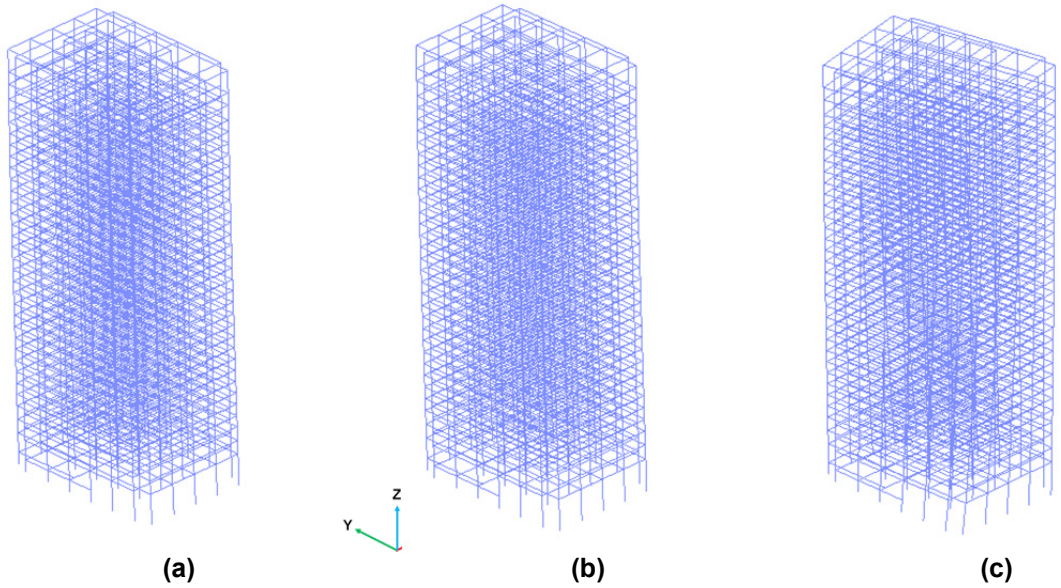

Figure 7.1 Mode shapes of the first three modes (with cladding weight); (a) Mode 1 (*X*-translation); (b) Mode 2 (*Y*-translation); and (c) Mode 3 (*Z*-twisting).

7.2.1 Effect of Cladding Weight on Modal Analysis Results

As mentioned in Section 4.3, three of the models (Model 1a, 1c, and 1d), used in the parametric study of the effect of the mechanical behavior of connections on the system response, considered the case where the heavy cladding was completely removed. Reduction of the weight of the building might be a strategy for improving the response of the building. Removing the entire weight of the cladding provides a lower bound on the amount of weight that could be removed.

Figure 7.2 shows the deformed shapes of the first three modes without the cladding weight. The first mode, shown in Figure 7.2(a), is a translational mode in the *X*-direction, which has a period of 4.33 sec. The second mode, shown in Figure 7.2(b), is a translational mode in the

Y-direction, which has a period of 4.18 sec. The third mode, shown in Figure 7.2(c), is a torsional mode having a period of 3.59 sec. Table 7.2 lists the periods of the first twenty-four modes. The vertical mode of vibration is associated with mode number 16 with a period of 0.41 sec.

The weight of the cladding is about 15% of entire building weight. Including it increases the fundamental period from 4.33 sec for the case without cladding to 4.70 sec in the *X*-direction $\left[4.70/4.33 \approx \sqrt{1/(1-15\%)} = 1.085\right]$ Similarly, the fundamental period in *Y*-direction increased by 8.5% $\left(4.53/4.17 \approx 1.085\right)$. Note that the period of the torsional mode increases slightly more than 15% (rather than by 8.5%), since the cladding is distributed around the perimeter of the building (rather than being uniformly distributed in plan). There are no visible differences of modal shapes between models with or without cladding weight; see Figures 7.1 and 7.2.

Table 7.2 Modal periods of the case-study building (without cladding weight).

Mode	Period (sec.)	Mode	Period (sec.)	Mode	Period (sec.)	Mode	Period (sec.)
1	4.329	7	0.867	13	0.501	19	0.396
2	4.179	8	0.856	14	0.497	20	0.356
3	3.585	9	0.761	15	0.465	21	0.341
4	1.499	10	0.640	16	0.408	22	0.338
5	1.451	11	0.636	17	0.404	23	0.332
6	1.234	12	0.587	18	0.399	24	0.325

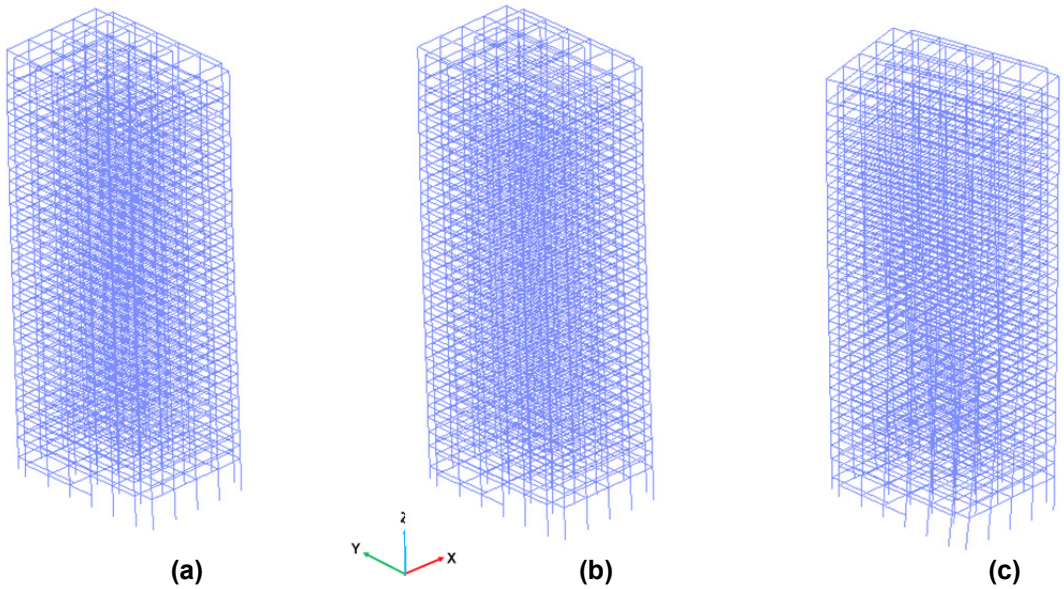

Figure 7.2 Mode shapes of the first three modes (without cladding weight) (a) Mode 1 (*X*-translation); (b) Mode 2 (*Y*-translation); and (c) Mode 3 (*Z*-twisting).

7.3 NONLINEAR STATIC PUSHOVER ANALYSIS

Nonlinear static pushover analysis is not permitted in ASCE 41-13 for tall buildings since higher mode effects are not taken into account. However, such analyses provide basic comparative information on post-yielding behavior. Figures 7.3 and 7.4 show pushover curves and deformed shapes at selected roof displacements of Models 1a*, 1b*, 1c* and 1d* (see Section 4.3 for detailed description of the models) with loads applied in either the *X*- or *Y*-directions. The lateral load pattern used for each push direction was the same as the first-mode shape along the corresponding direction; see Figure 7.1. The peak base shear capacity in *X*-direction is about 13,500 kips (equivalent to about 8.7% of building weight), and the peak base shear capacity in the *Y*-direction is about 13,700 kips (equivalent to about 8.8% of building weight). Significant *P*-Δ effects were observed. Note that the minimum design base shear (2993 kips) per UBC 1967 [ICBO 1967] for the case-study building is only 1.9% of building weight, about 45% of the required design base shear (6650 kips) per ASCE 7-10.

The star symbol markers on the pushover curves indicate roof displacements correspond to either first significant yielding or first column splice failure. Upward-pointing triangle makers indicate the roof displacements at peak base shear. Downward-pointing triangle makers indicate the roof displacements when significant *P*-Δ effects took place. Cross markers indicate the roof displacements when the simulation was terminated or the numerical model became unstable. In addition, the same makers are used to show the corresponding deformed shape profiles for each model. Clearly, story drifts concentrated between floor levels five and ten in all models. However, the mechanical behavior of the beam-to-column connection had a significant effect on the degree of concentration and system deformability.

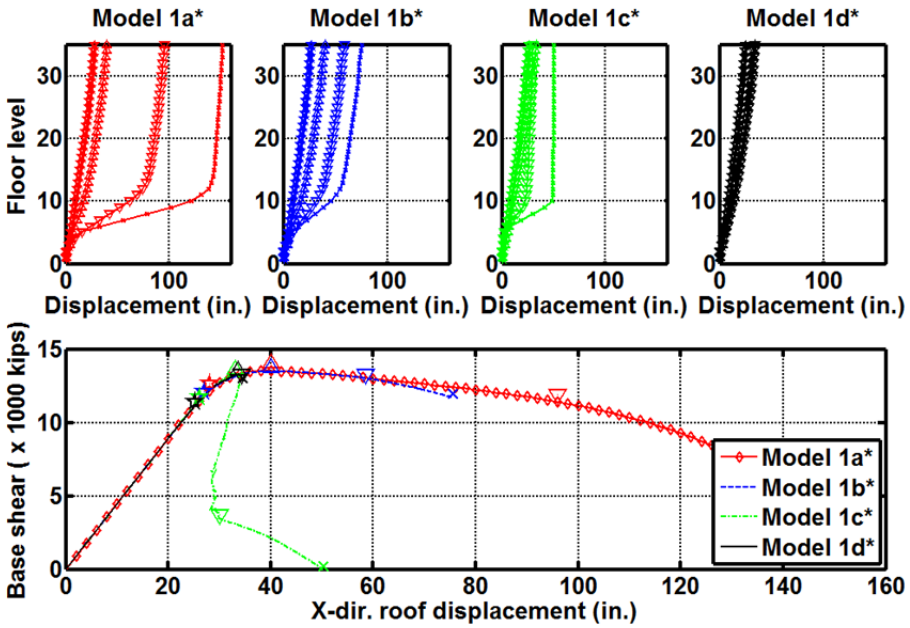

Figure 7.3 **Static pushover curves and deformed shapes of four models (*X*-direction, with cladding weight included).**

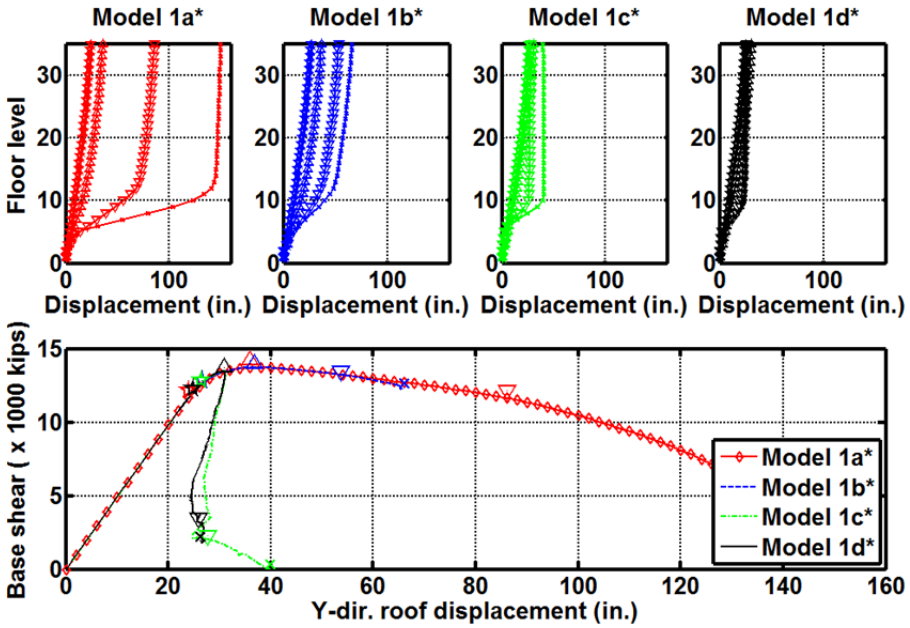

Figure 7.4 **Static pushover curves and deformed shapes of four models (*Y*-direction, with cladding weight included).**

7.3.1 Effect of Cladding Weight on Pushover Curves

The effect of cladding weight on nonlinear static responses was also examined. Figures 7.5 and 7.6 show pushover curves and deformed shapes at selected roof displacements of Models 1a, 1b, 1c, and 1d (not including cladding weight), with loads applied in either the *X*- or *Y*-directions. The lateral load pattern used for each push direction was the same as the first-mode shape along the corresponding direction (see Figure 7.2). A comparison of the *X*-direction pushover curves shows that there are fewer *P*-Δ effects observed in the models without cladding weight, as evidenced by comparing the negative slope of pushover curves; see Figures 7.3 and 7.5. A similar observation applies to *Y*-direction pushover curves.

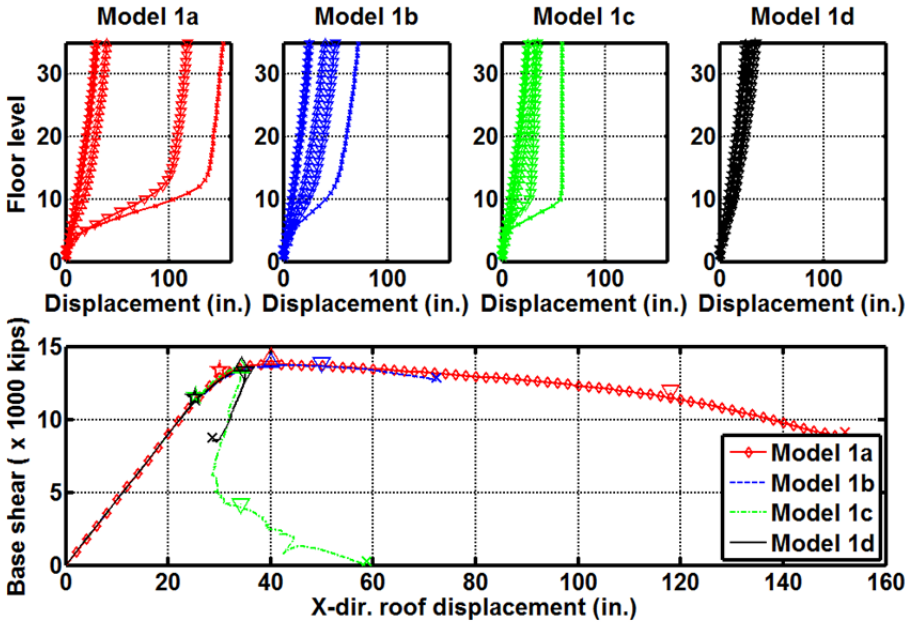

Figure 7.5 Static pushover curves and deformed shapes of four models (*X*-direction, without cladding weight considered).

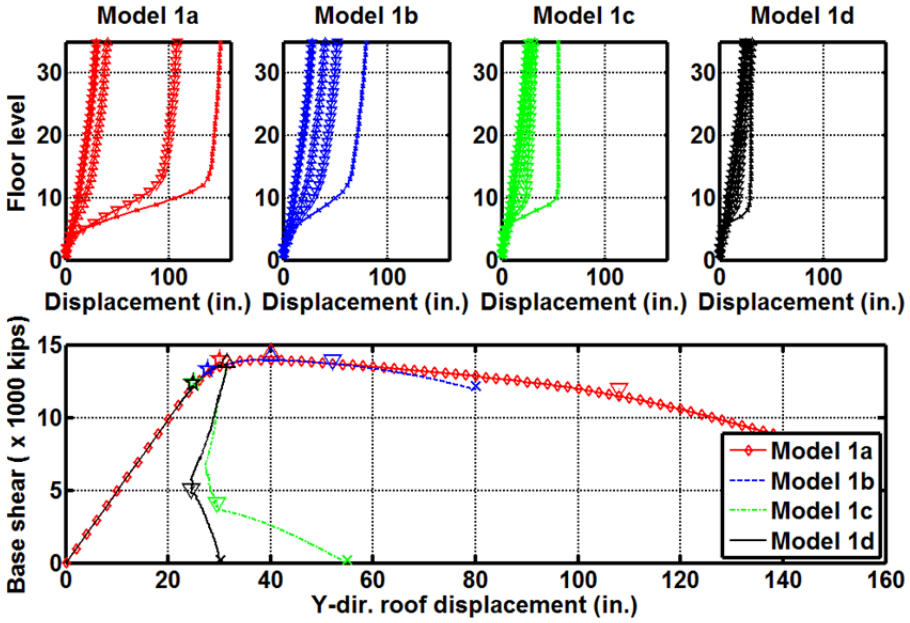

Figure 7.6 Static pushover curves and deformed shapes of four models (*Y*-direction, without cladding weight considered).

7.4 NONLINEAR DYNAMIC ANALYSIS

To help calibrate the numerical models to observed behaviour, this section first presents the results of a dynamic response analysis of the case-study building subjected to a record obtained near the building site during the 1989 Loma Prieta earthquake. Next, results are presented for nonlinear dynamic analyses carried out per ASCE 41-13 recommendations using excitations corresponding to BSE-1E, BSE-2E, and 50% probability of exceedance in 30 years (43-years mean return period) hazard levels. For each hazard level, twenty 3-component ground motion records were considered; see Chapter 5 for the selection process and a detailed list of ground motion records.

7.4.1 Dynamic Responses under a 1989 Loma Prieta Earthquake Record

The 1989 Loma Prieta earthquake had a tremendous impact on the San Francisco Bay Area. For downtown locations near the case-study building, relatively little structural damage was observed. However, some nonstructural damage was observed in the case-study and nearby buildings. No recordings of the ground motions or the building response at the case-study building are available. Nonetheless, it is beneficial to examine the dynamic response of the case-study building under a record obtained at a site near the building. Comparison of observed damage with results of the dynamic analyses will help calibrate the numerical model. Model 1d* (the as-built model with the cladding present) was used to represent realistic conditions at the time of the Loma Prieta event. The selected ground-motion record was obtained at station CSMIP 58480, located in another building in downtown San Francisco about 0.2 miles away from the site of case-study building. During the 1989 Loma Prieta earthquake, three components (two horizontal and one vertical motion were obtained at the basement level) of ground accelerations The duration of the records is 60 sec; see Figure **7**.7. The distance between the recording station and the epicenter is 59.3 miles (***www.strongmotioncenter.org***). As shown in Figure **7**.7, the peak recorded horizontal ground acceleration was 0.17*g*.

Figure 7.8 shows the computed roof displacement response histories (relative to the ground) and computed roof displacement orbits for this recorded ground acceleration history. The peak roof displacement is about 8 in. in the *Y*-direction, while the peak roof displacement is smaller (5.2 in.) in the *X*-direction. Both peak displacements are well within the elastic range, as can be inferred from the results of the static pushover analyses; see Figures 7.3 and 7.4. No permanent roof displacement was observed at the end of the simulation. Note that the plotted responses in the Figure 7.8 after 60 sec are free-vibration responses computed with significantly increased damping (so residual displacements could be more easily be estimated). From the same figure, it is clear that the translational vibration modes in both *X*- and *Y*-directions govern the dynamic response, especially after 40 sec. The estimated vibration period of the case-study building model is about 4.44 sec (10/2.25) from the displacement response histories shown in Figure 7.8. The amplification factor of peak horizontal acceleration is about 2.4 at the roof level (0.4*g*/0.17*g*) as shown in Figure 7.9. The peak story drift ratio along the height of the building is around 0.48% (see Figure 7.10), which is just slightly less than the typical 0.5% limit considered for immediate occupancy. Peak story drifts occurred in the mezzanine level and near the roof. As shown in Figure 7.11, the peak base shear force (maximum of both directions) is 7743 kips, indicating that the building essentially remained elastic during this earthquake, as evidenced by

comparing the base shear force and the peak roof displacement with the static pushover results shown in Figures 7.3 and 7.4.

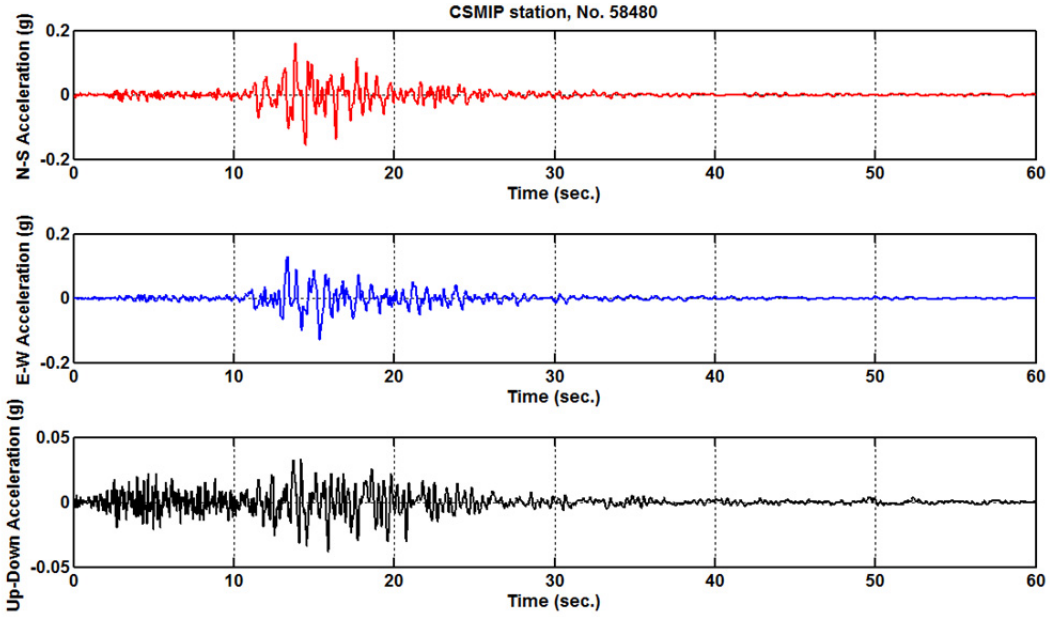

Figure 7.7 **Ground acceleration histories recorded at CSMIP 58480 station during 1989 Loma Prieta earthquake.**

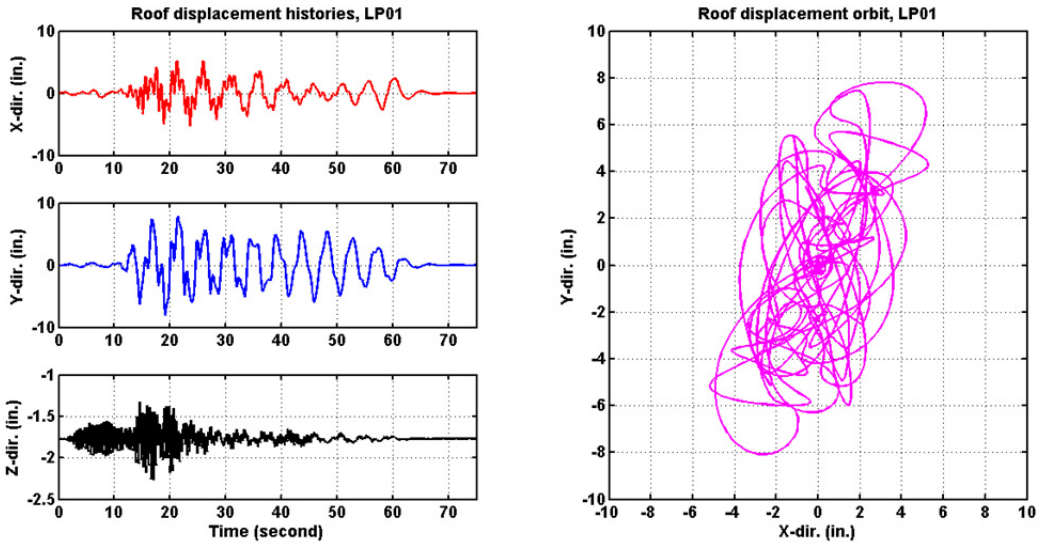

Figure 7.8 **Computed roof displacement histories and orbital responses for an actual ground motion recorded during the Loma Prieta earthquake (Model 1d*). Amplified structural damping considered after 60 sec.**

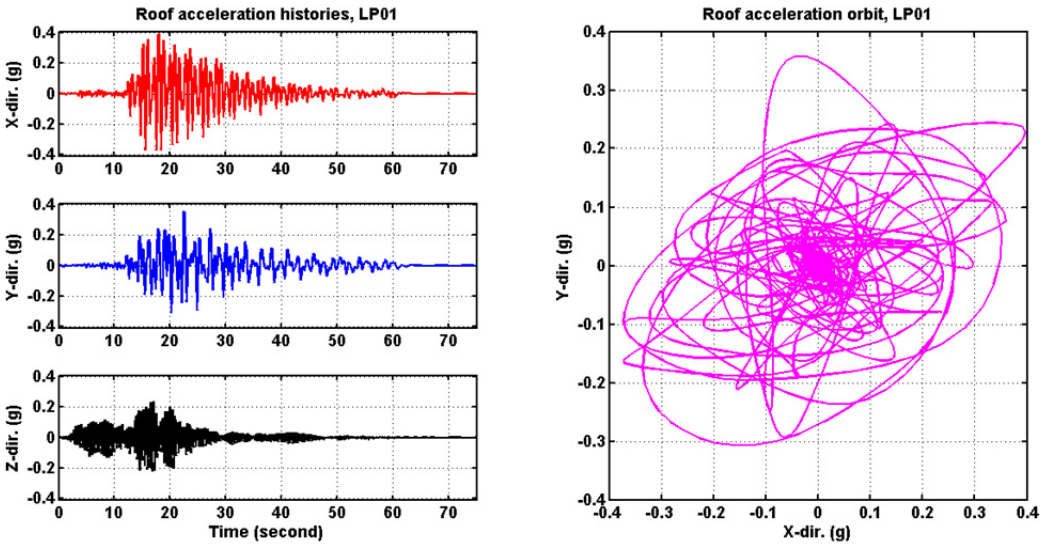

Figure 7.9 Computed roof absolute acceleration histories and orbits of the case-study building subjected to an actual recorded ground motion (Model 1d*).

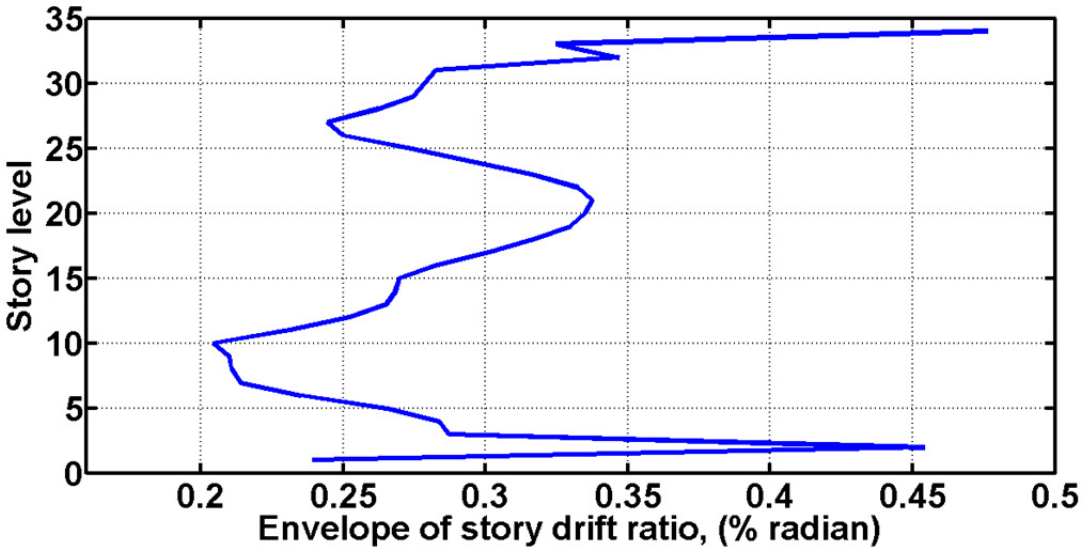

Figure 7.10 Computed peak story drift ratios for an actual recorded Loma Prieta ground motion record (Model 1d*).

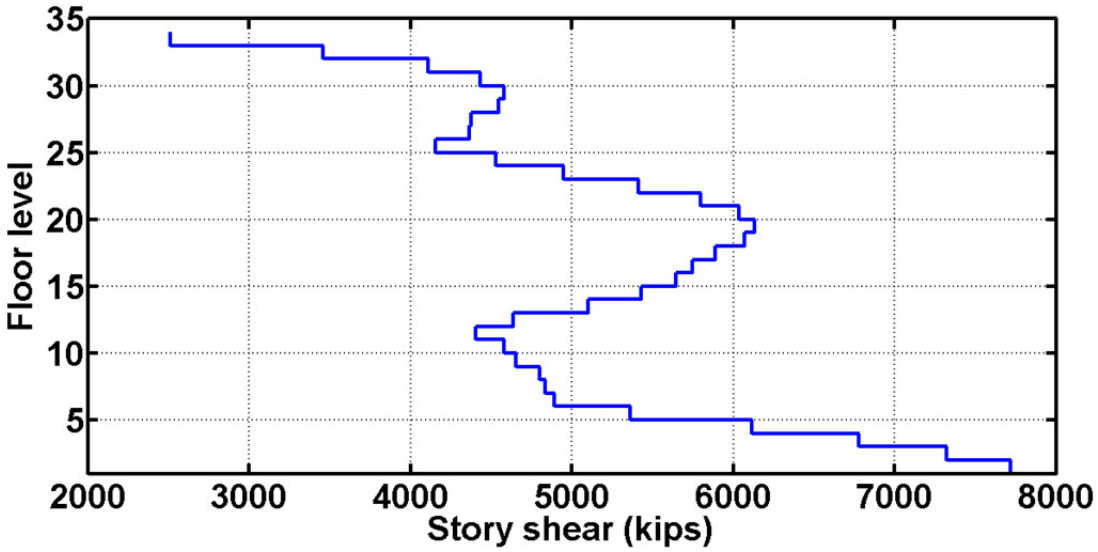

Figure 7.11 **Computed story shear force envelope under an actual ground motion recorded during Loma Prieta earthquake (Model 1d*).**

7.4.2 Dynamic Responses under BSE-1E Hazard-Level Ground Motions

7.4.2.1 General Responses

Figure 7.12 displays the distribution of median peak story drift ratios over the height of the case-study building for Model 1d* subjected to the BSE-1E hazard level records. The results used in constructing Figure 7.12 included only the simulation cases where the analysis program terminated normally. Normal termination of the analysis program is defined as cases where either the simulation ran through the entire duration of ground motion or where any story reached 10% story drift ratio. Simulations that failed to converge were not included in the plot or computation of median values. In future editions of the ASCE 7 standard (2016 draft), failure of an analytical solution to converge is taken as unacceptable structural response. Under the BSE-1E hazard-level ground motions, there were 11 normal termination cases. Nine of the twenty cases failed to converge. Reasons for the large number of motions for which analytical convergence was not possible are discussed later.

The results show a tendency towards weak story behavior in the bottom one-third of the structure. In these stories, the median peak story drift ratios of the 11 cases that terminated normally were nearly 9.5%. The maximum peak story drift ratio was as large as 20% over all of these 11 ground motions, which is significantly larger than the peak drift of 4.5% permitted in several criteria (e.g., LATBSDC, 2014).

The story-shear envelope in Figure 7.13 shows that the median base shear demand for the 11 BSE-1E level ground motions is about 15,000 kips, or five times the original design base shear (see Section 7.3). Median peak beam end total rotation demand for the 11 BSE-1E level events that converged was as large as 10%; see Figure 7.14. Similar to the story drift responses, the beam end rotation demands have a tendency to concentrate in the bottom one-third of the building. In terms of the percentage of failed beam-to-column connections at a floor level in the weak story region, the peak median percentage is about 30%; see Figure 7.15. Here, failure is

defined as a connection that completely loses its moment capacity (beam ends rotation demands are larger than collapse prevention criteria per the ASCE 41 standard). In terms of median residual story drift ratio (from the 11 converged records), the maximum value obtained under BSE-1E hazard-level earthquakes was about 9.1%. A large dispersion in the story residual displacements is noted from **Figure 7.16** for stories between floor levels 5 and 10. It should be recalled that in these analyses, a story drift ratio of 10% was set as a limit to terminate the simulation. Had the analyses continued to larger displacement amplitudes before automatic termination, or if difficulties associated with convergence were resolved, the actual residual drifts and dispersions are expected to be even larger.

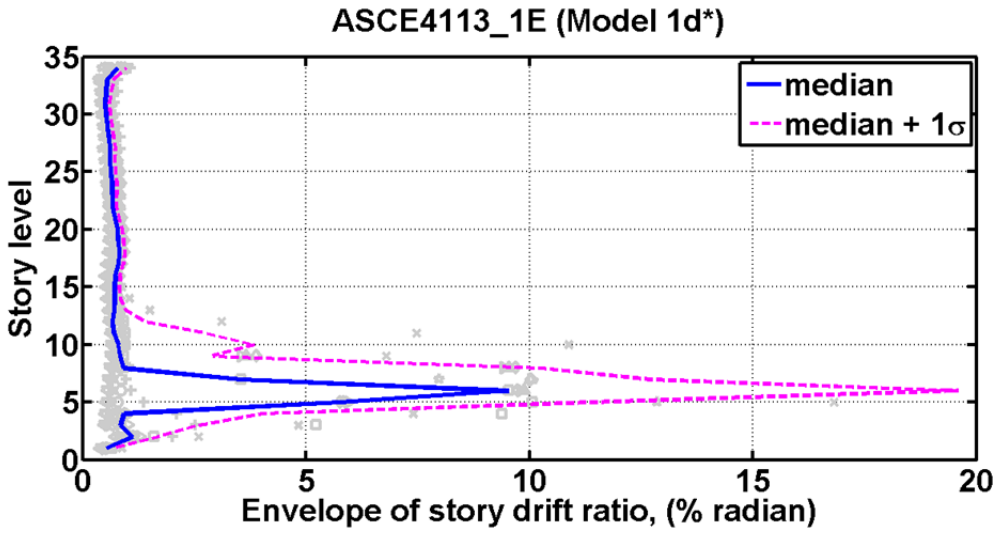

Figure 7.12 **Story drift envelope of Model 1d* under BSE-1E hazard-level ground motions.**

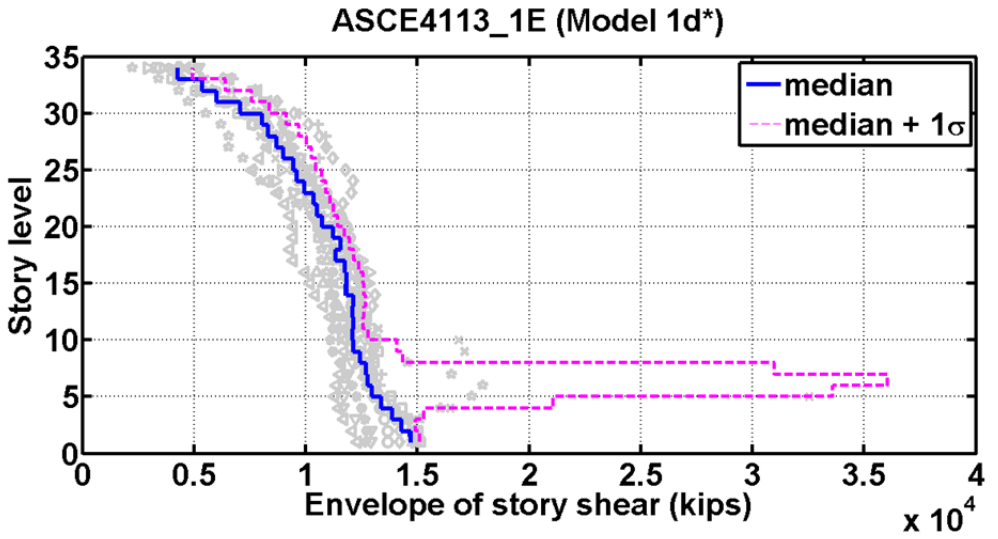

Figure 7.13 **Story shear envelope of Model 1d* under BSE-1E hazard-level ground motions**

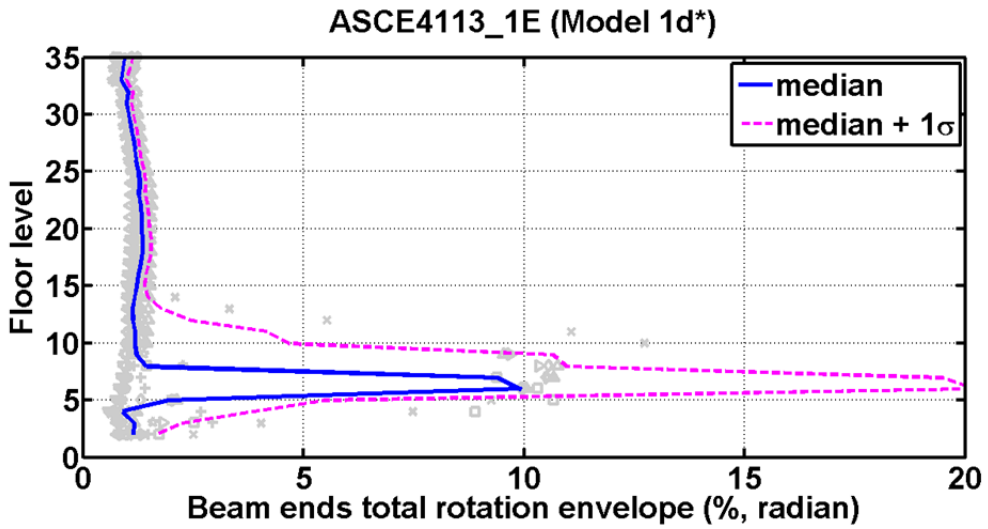

Figure 7.14 Beam ends total rotation envelope of Model 1d* under BSE-1E hazard-level ground motions.

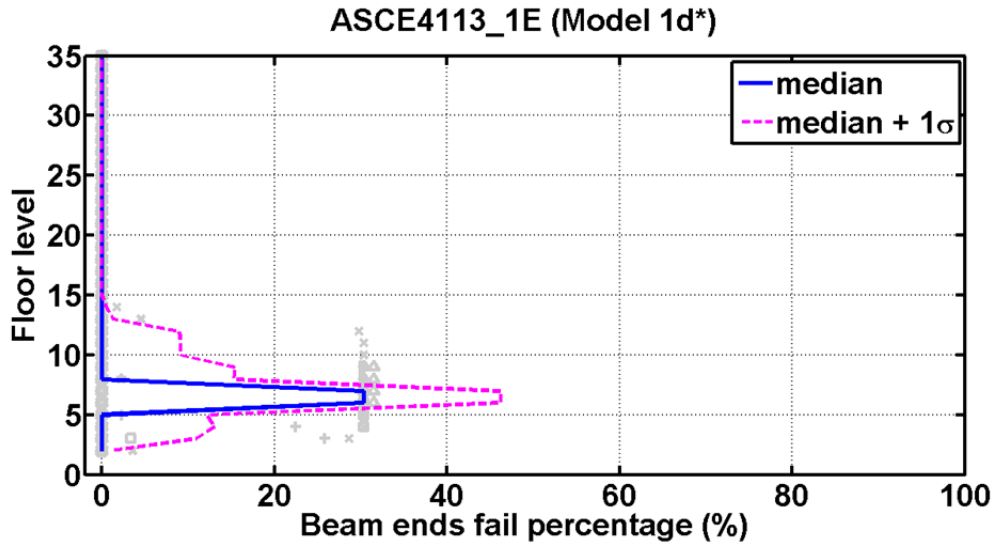

Figure 7.15 Beam ends failure percentage of Model 1d* under BSE-1E hazard-level ground motions.

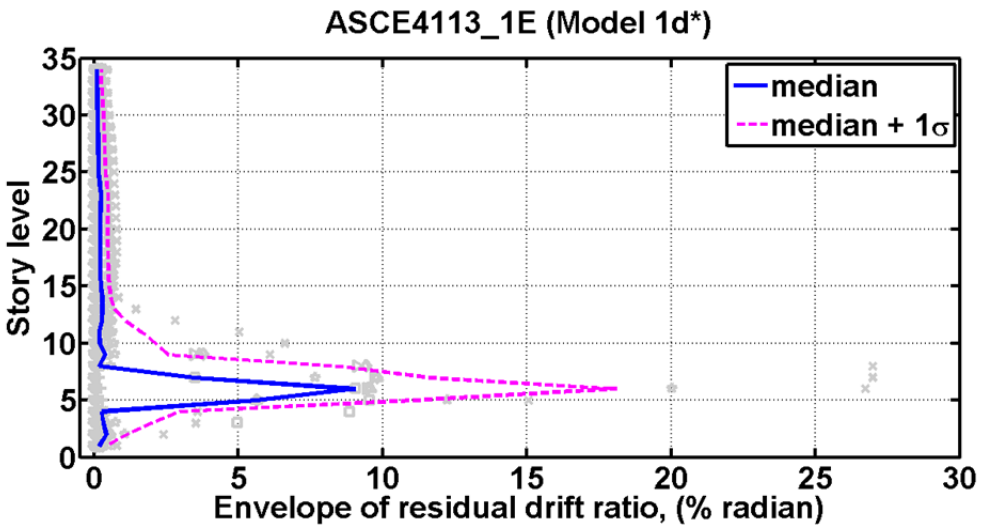

Figure 7.16 **Residual drift envelope of Model 1d* under BSE-1E hazard-level ground motions.**

7.4.2.2 Responses under Selected Ground Motion Records

Dynamic responses of the 1d* model to three ground motions from the twenty BSE-1E records are selected for more detailed examination. A comprehensive set of response plots for all 20 ground motions for the BSE-1E hazard level (and for BSE-2E as well) is included in Appendix E (electronic file) for Model 1d*. Table 7.3 lists three ground motion records selected from the BSE-1E set and three from the BSE-2E set selected for detailed examination. All of these motions were recorded in California.

Figures 7.17, 7.18, and 7.19 show *X*- and *Y*-direction beam end plastic rotation envelops for ground motion record numbers 1, 11, and 18 from the BSE-1E ensemble (Table 7.3). The envelops are presented in the form of horizontal stacked bar charts that summarize the condition of the beam ends status based on ASCE 41-13 performance criteria. Table 9-6 in ASCE 41 lists the response criteria for three discrete performance levels, which are immediate occupancy (IO), life safety (LS) and collapse prevention (CP), but two additional intermediate performance levels are introduced in the accompanying text. These two additional performance levels, damage control (DC) and limited safety (LS), have acceptance criteria halfway between the three discrete performance levels defined in Table 9-6 of the ASCE 41 standard. That is, damage control acceptance criterion is halfway between immediate occupancy and life safety; the limited safety acceptance criterion is halfway between life safety and collapse prevention. Thus, acceptance criteria for five discrete performance levels divide the beam end deformation condition into six performance states, as shown in the bar chart legend of Figure 7.17.

From Figure 7.17 and the target performance levels shown in Table 4.1, beam ends plastic rotation responses of the case-study building under this particular ground motion seem to satisfy the damage control performance level. However, the BSE-1E ground motion number 1 simulation terminated early at 12.5 sec instead of running through the entire duration of 60 sec; this was due to the numerical instability issues caused by column splice failures. Although the beam ends deformation condition satisfies the performance criteria based on rotation, the failure of column splices observed during the simulation clearly created serious structural stability

problems that in turn made numerical simulation difficult. In some floor levels, complete or partial fracture of column splices was predicted for many columns at several stories, as can be seen in Figure 7.20. Note that 34 columns are spliced at a story. The large number of column slice fractures shown in this figure near the top of the building is associated with a large change in column size and shape at this level.

Under BSE-1E ground motion numbers 11 and 18, the simulations predict transient story drift ratios larger than 4.5%, which corresponds to a structural collapse condition per LATBSDC, 2014). This is consistent with the envelopes of beam plastic rotation condition, as shown in Figures 7.18 and 7.19. The dark-red bars from floor levels 6 to 9 in those two figures indicate that around 60% of beam-to-column connections completely lost their moment capacities. The column splices in floor levels 5, 7, and 9 also suffered partial or complete fracture during the dynamic analyses; some floors had more than 70% of the column splices partially or completely fracture, as shown in Figures 7.21 and 7.22.

To illustrate the behavior of the structure during the simulation of column splice fracture, column response histories are shown for one of the four exterior corner columns (one of the Group 1 columns shown in Figure 7.23). To assist future discussions, columns are grouped into six different groups according to their member sizes, cross-sectional shapes and tributary areas, as shown in Figure 7.23.

Figure 7.24 shows typical column axial force and bending moment response time histories of a corner column on the 7^{th} floor that contains a column splice during BSE-1E motion number 1. The column splice section completely fractures at around 8.6 sec. This is the only column splice failure in this story that occurred before the simulation stopped for this record. As shown in Figure 7.20, the column splice fractures as it goes into net tension. While uplift occurs there is no moment capacity at the splice location. However, moments at the splice develop again as compression occurs after the splice reseats. There are substantial transient oscillations of moment (and shear) as the splice opens and then reseats. It is very important to recognize that the fiber-based numerical model of the splice fracture used in these analyses continues to transfer shear force across the splice and does not permit the two parts of the column above and below the splice to offset laterally. This might be thought to represent a retrofit condition where a detail to prevent lateral movement of the columns at the splice is installed but the tension capacity is not enhanced allowing fracture. Without this restraint of lateral offset, convergence problems increased.

Similar splice failures are shown in the response history plots for the other two ground motions; see Figures 7.25 and 7.26. In particular, in Figure 7.25, it is noticed that uplift at a ruptured splice occurs for more than a second.

Table 7.3 Ground motion records selected for detail comparison.

Hazard Level (ID)	Earthquake (NGA #; Year)	Magnitude	Distance (km)	Duration (sec)
BSE-1E (1)	Loma Prieta (NGA 776; 1989)	6.9	27.9	60
BSE-1E (11)	Cape Mendocino (NGA 3744; 1992)	7.0	12.2	28.6
BSE-1E (18)	El Mayor-Cucapah (NGA 5832; 2010)	7.2	26.6	130
BSE-2E (1)	Loma Prieta (NGA 776; 1989)	6.9	27.9	60
BSE-2E (10)	Cape Mendocino (NGA 3744; 1992)	7.0	12.2	28.6
BSE-2E (15)	El Mayor-Cucapah (NGA 5832; 2010)	7.2	26.6	130

In addition to rupture of column splices under this set of BSE-1E ground motions, column yielding is also observed in some story levels; see column P-M-M interaction diagrams in Figures 7.27, 7.28, and 7.29. P/P_y ratios far greater than 0.5 are observed during the dynamic analyses. Note that compression loads have a negative sign in these plots.

Figures 7.30, 7.31, and 7.32 show three typical hysteresis loops of beam ends moment-rotation relationships under three selected ground motions. The hysteretic loops reflect a range of behavior. The loops show that the simulated mechanical behavior of connections follows the ASCE 41-13 general modeling requirements for steel beam-to-column connections. In Figures 7.31 and 7.32, it is clear that the connections exhibit limited ductility (consistent with ASCE 41 recommendations, and complete fracture occurs at this seismic hazard level only after a very limited number of cycles.

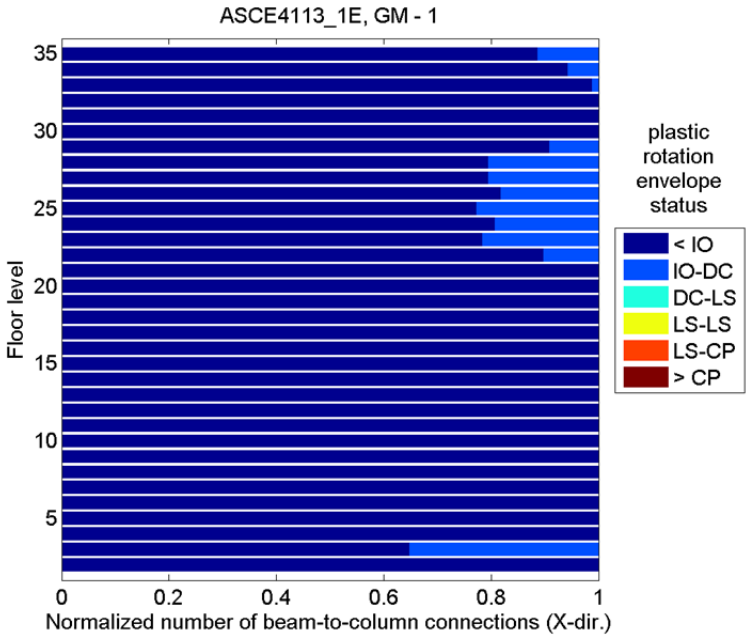

(a)

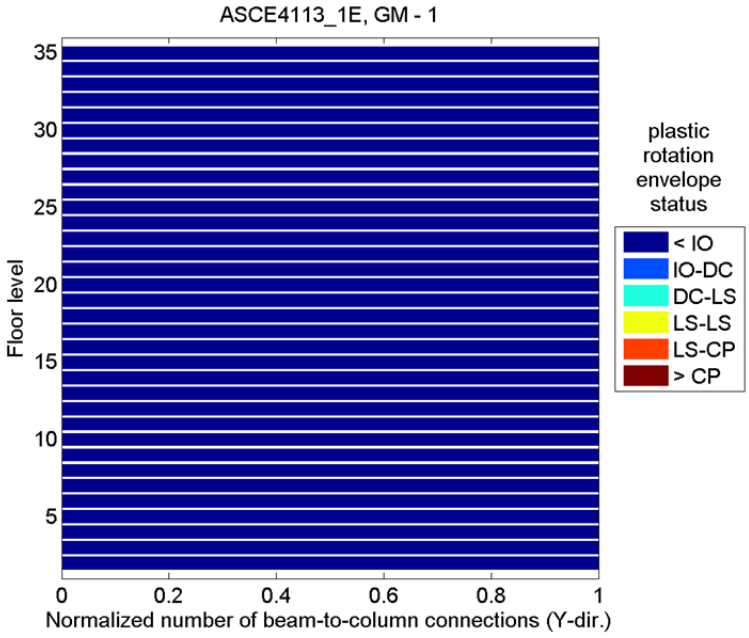

(b)

Figure 7.17 **Beam end plastic rotation envelope status of Model 1d* under ground motion number 1 of BSE-1E hazard-level ground motions: (a) *X*-direction and (b) *Y*-direction.**

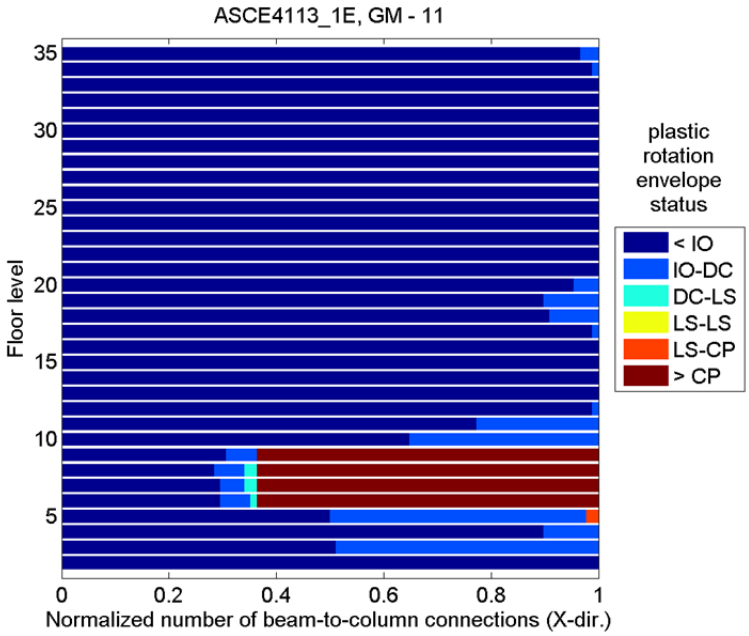

(a)

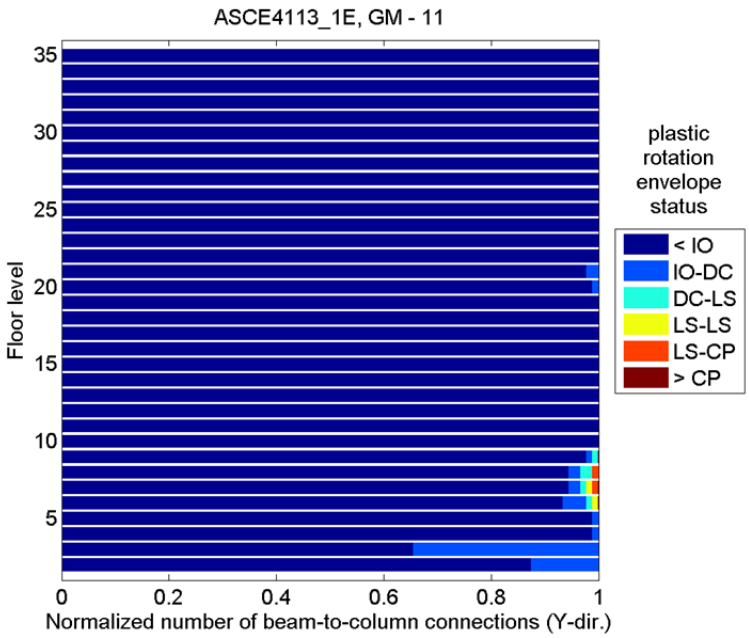

(b)

Figure 7.18 **Beam end plastic rotation envelope status of Model 1d* under ground motion number 11 of BSE-1E hazard-level ground motions: (a) *X*-direction and (b) *Y*-direction.**

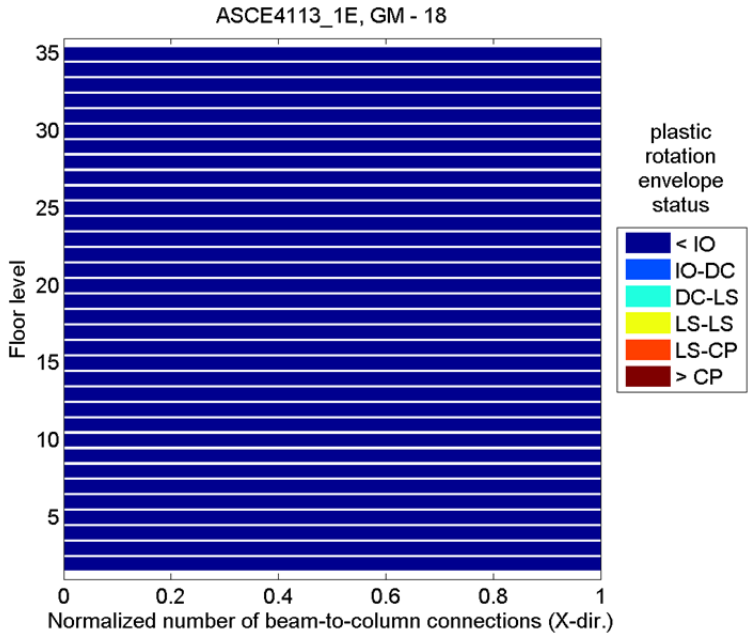

(a)

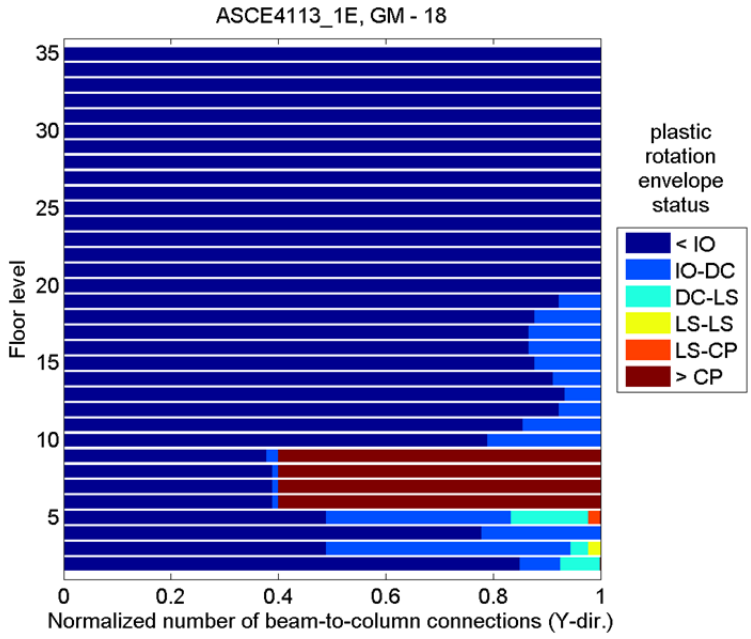

(b)

Figure 7.19 **Beam end plastic rotation envelope status of Model 1d* under ground motion number 18 of BSE-1E hazard-level ground motions: (a) X-direction and (b) Y-direction.**

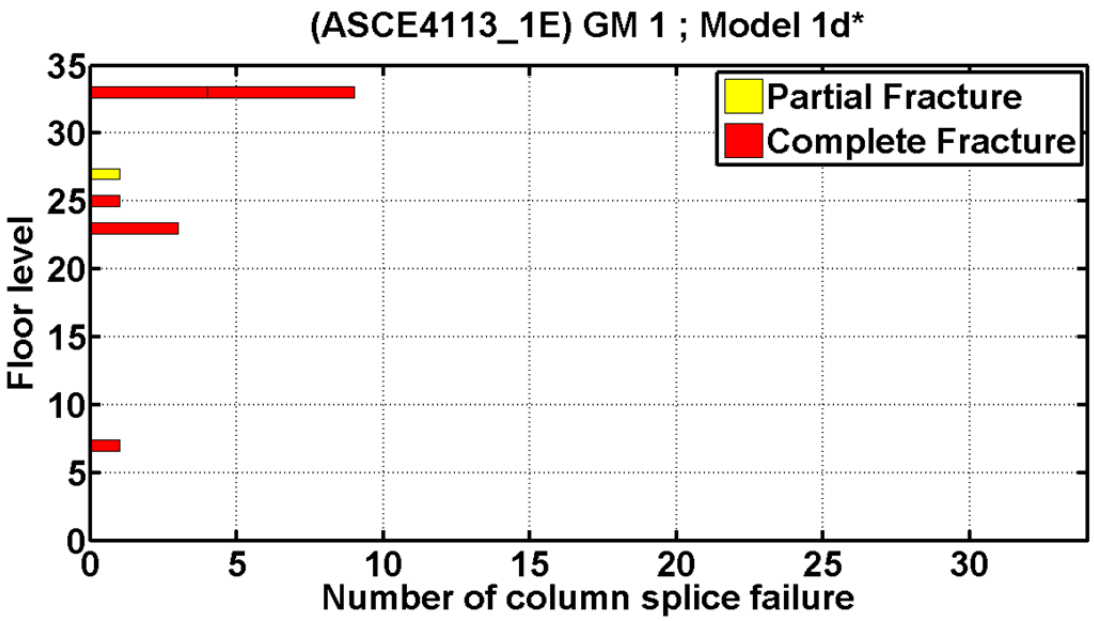

Figure 7.20 Number of column splice failure in each floor level of Model 1d* under ground motion number 1 of BSE-1E hazard-level ground motions.

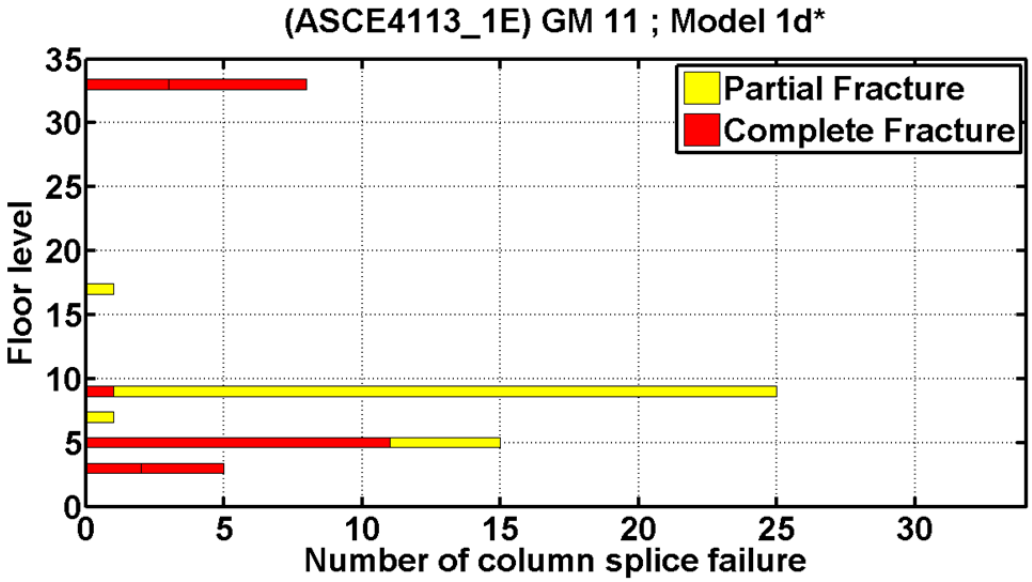

Figure 7.21 Number of column splice failure in each floor level of Model 1d* under ground motion number 11 of BSE-1E hazard-level ground motions.

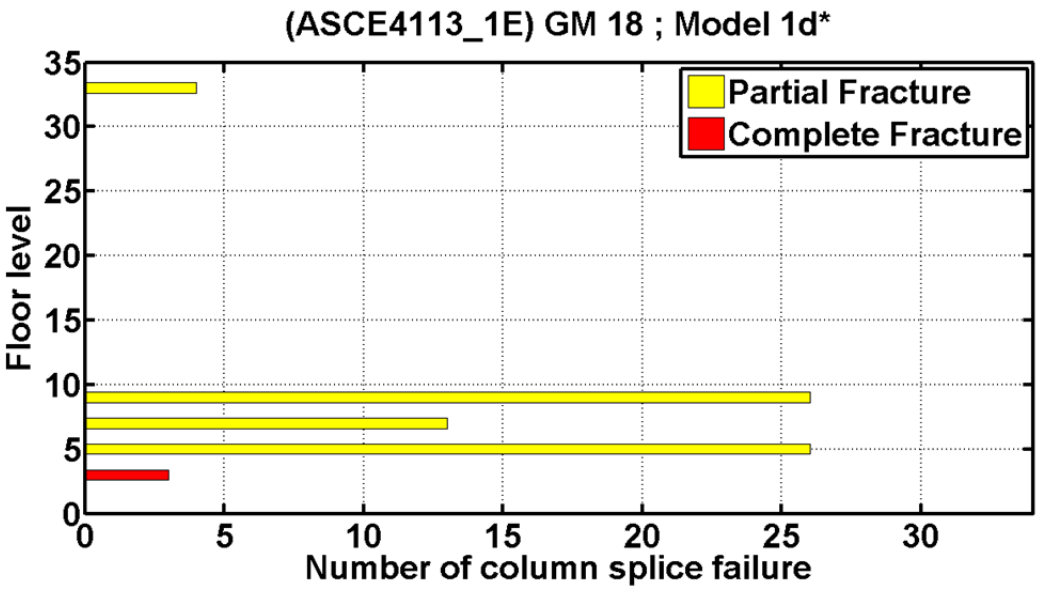

Figure 7.22 Number of column splice failure in each floor level of Model 1d* under ground motion number 18 of BSE-1E hazard-level ground motions.

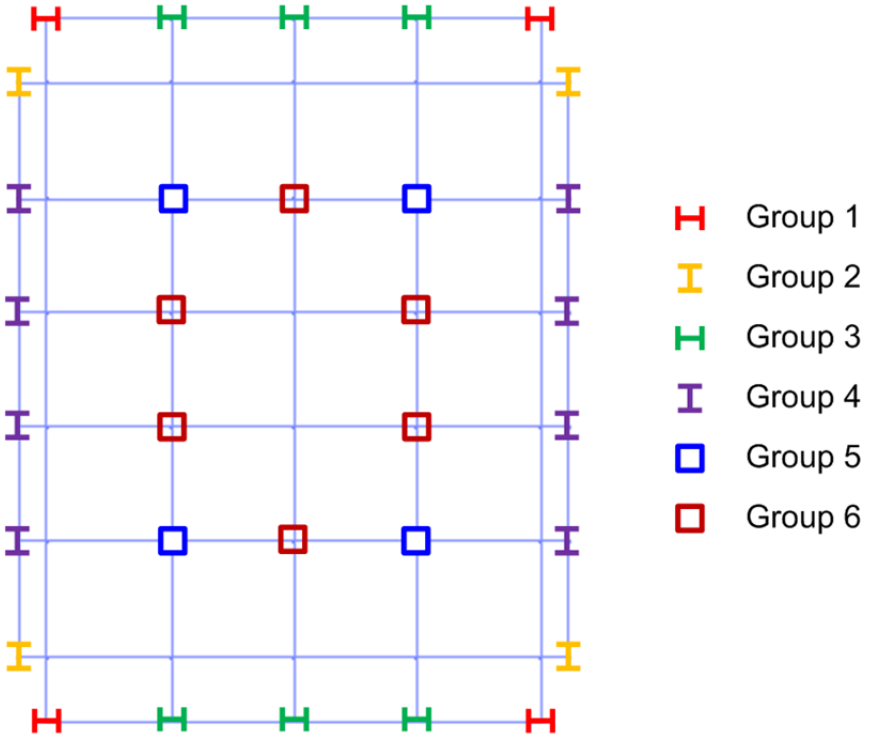

Figure 7.23 Illustration of column lines grouping.

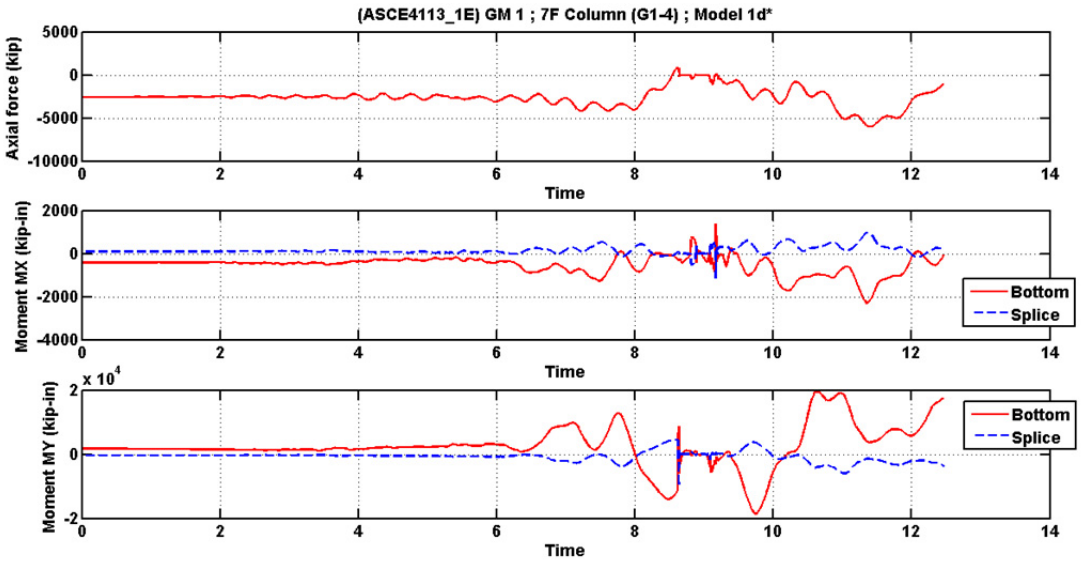

Figure 7.24 Axial force, bending moments response histories of a corner column in the 7th floor of Model 1d* under ground motion number 1 of BSE-1E hazard-level ground motions.

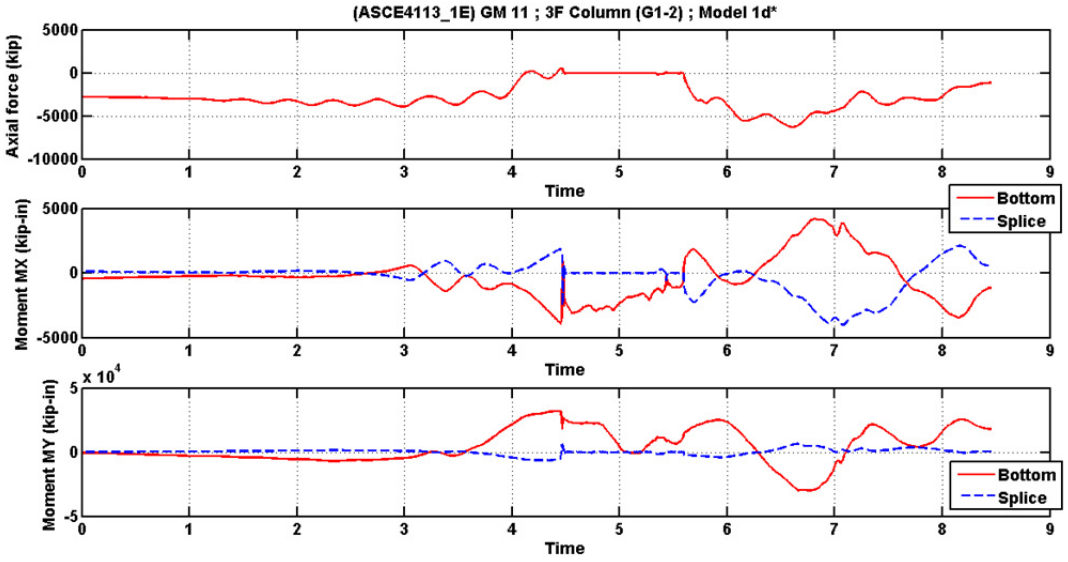

Figure 7.25 Axial force, bending moments response histories of a corner column in the 3rd floor of Model 1d* under ground motion number 11 of BSE-1E hazard-level ground motions.

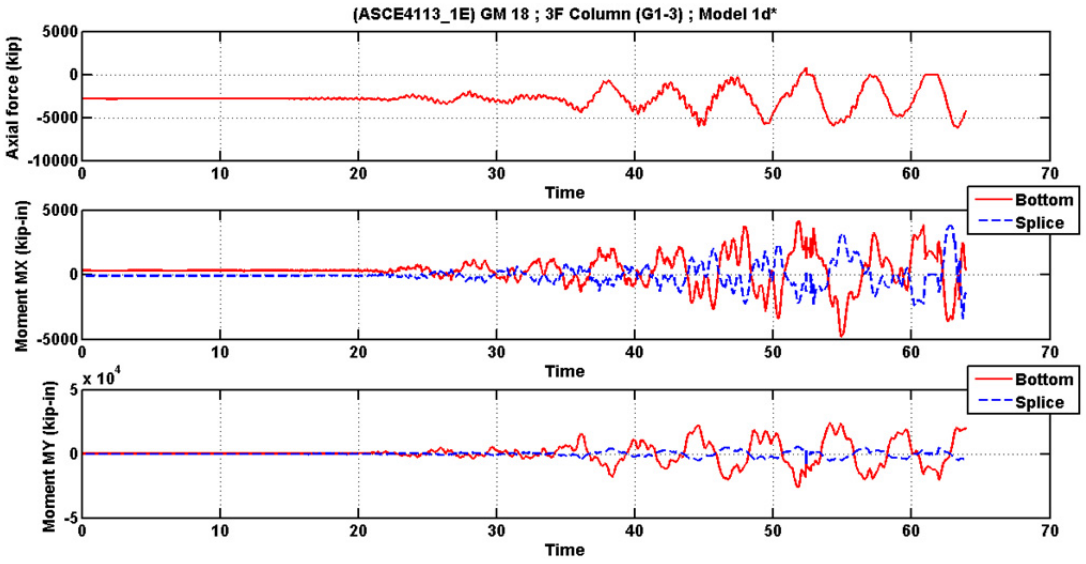

Figure 7.26 Axial force, bending moments response histories of a corner column in the 3rd floor of Model 1d* under ground motion number 18 of BSE-1E hazard-level ground motions.

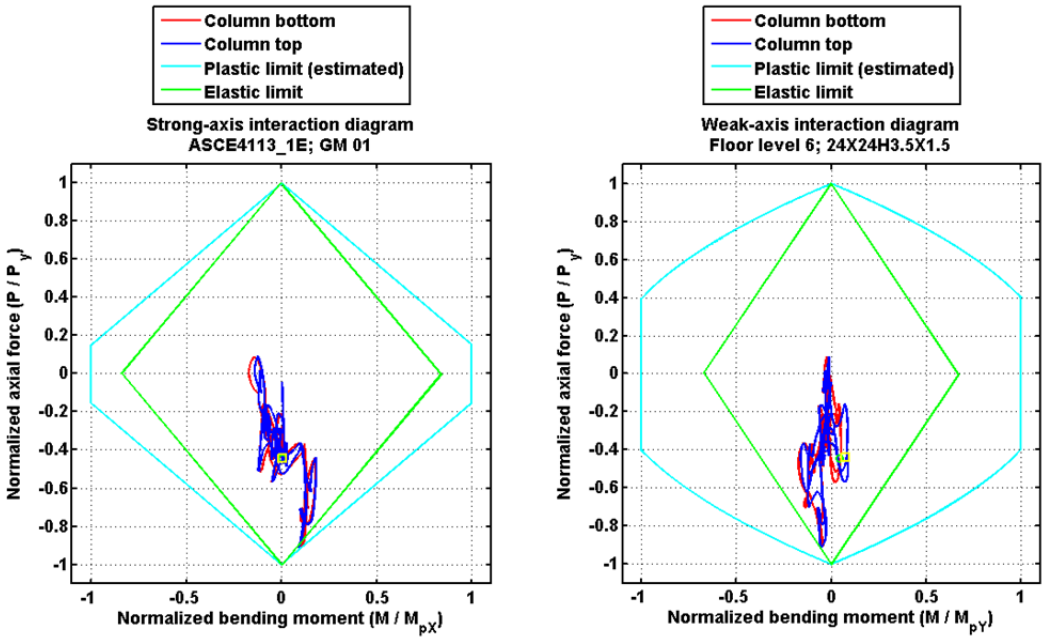

Figure 7.27 The P-M-M interaction diagrams of a corner column (group 5) in the 6th floor of Model 1d* under ground motion number 1 of BSE-1E hazard level ground motions.

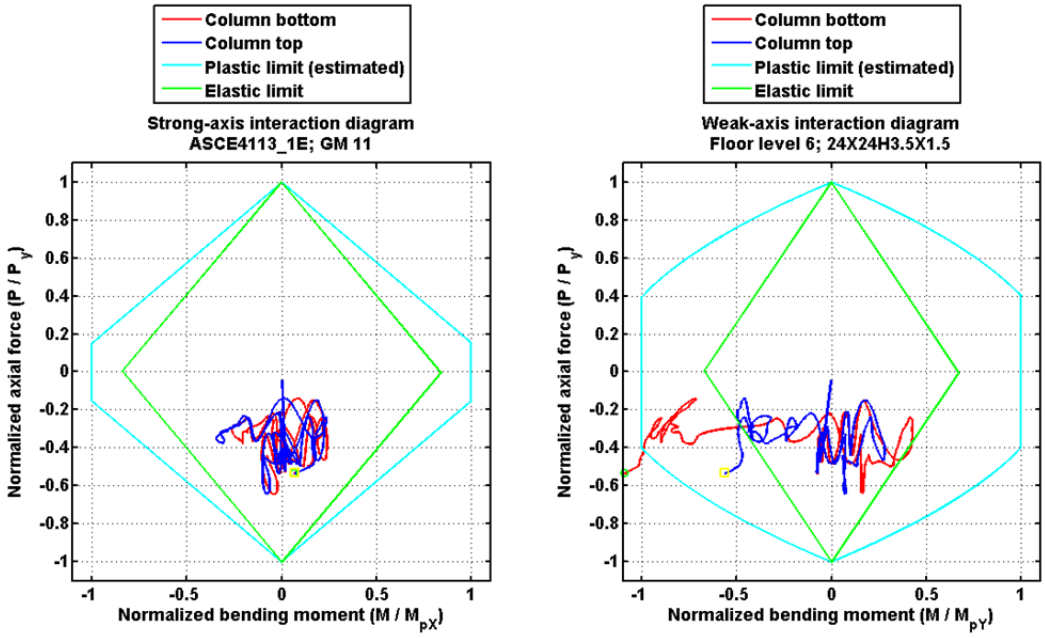

Figure 7.28 The P-M-M interaction diagrams of a corner column (group 5) in the 6th floor of Model 1d* under ground motion number 11 of BSE-1E hazard level ground motions.

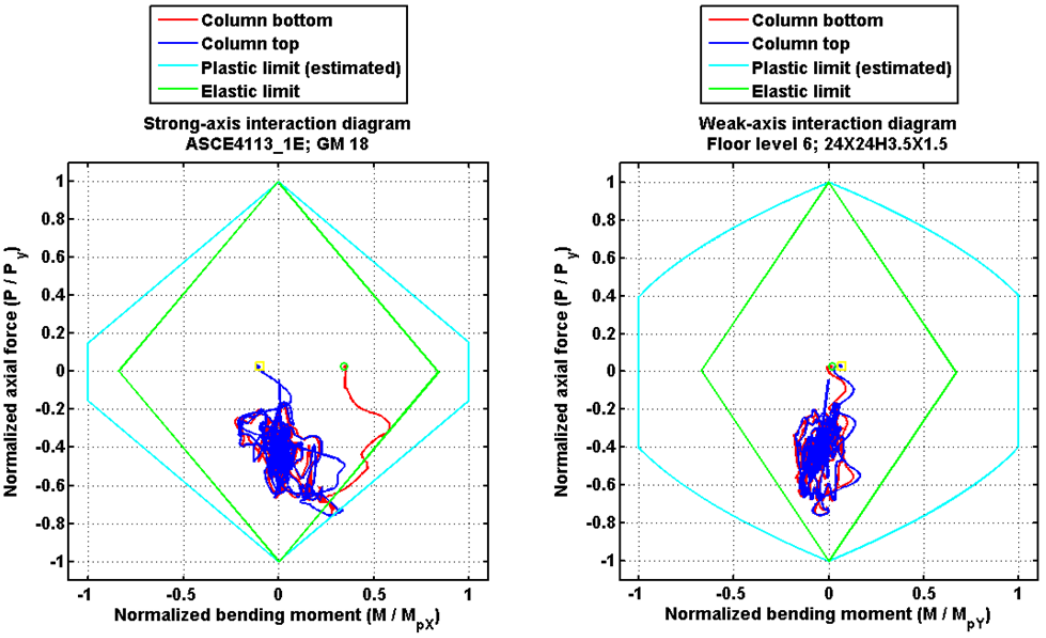

Figure 7.29 The P-M-M interaction diagrams of a corner column (group 5) in the 6th floor of Model 1d* under ground motion number 18 of BSE-1E hazard-level ground motions.

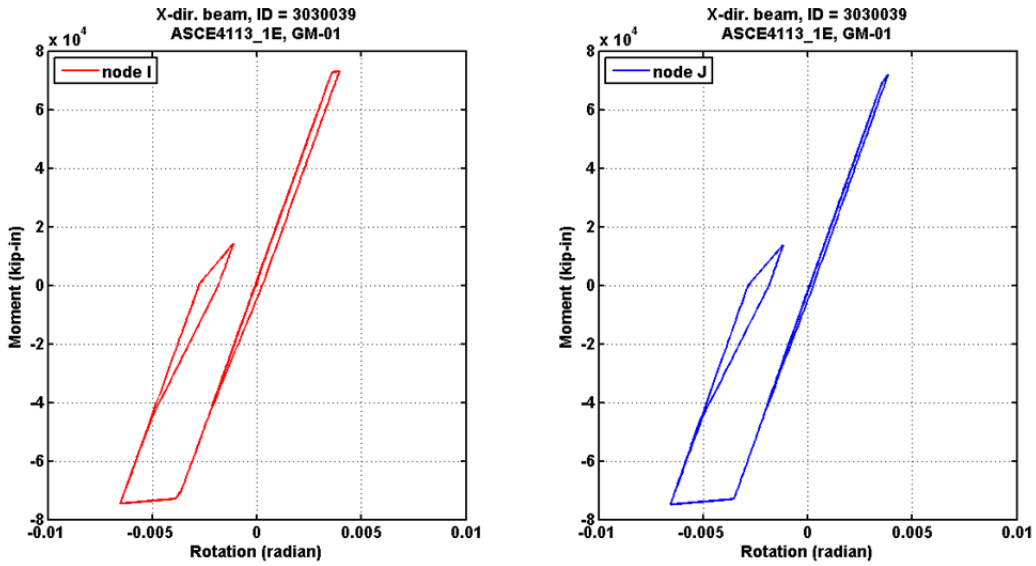

Figure 7.30 Hysteresis loops of an *X*-direction beam in the 3rd floor of Model 1d* under ground motion number 1 of BSE-1E hazard-level ground motions.

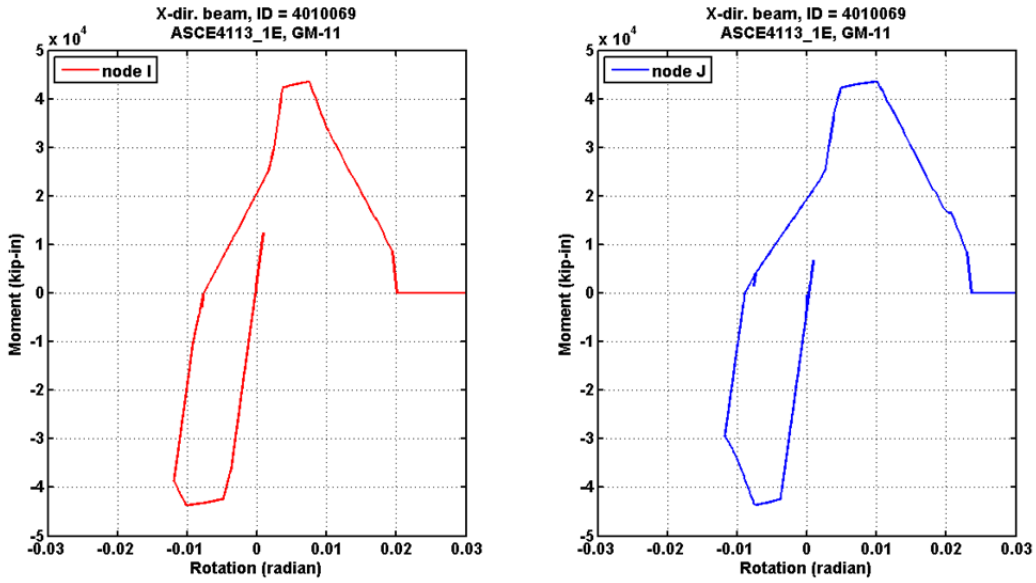

Figure 7.31 Hysteresis loops of an *X*-direction beam in the 6th floor of Model 1d* under ground motion number 11 of BSE-1E hazard-level ground motions.

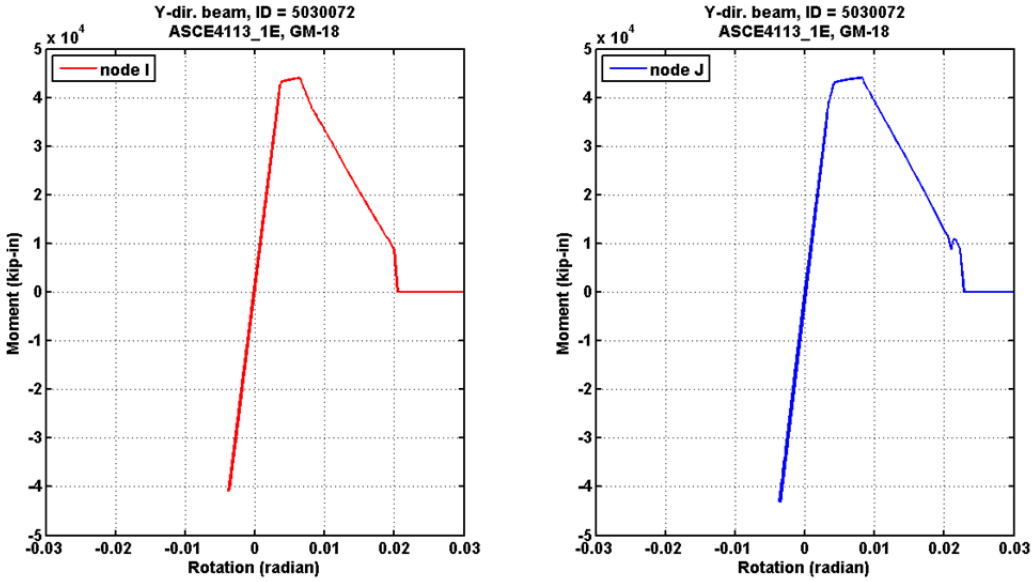

Figure 7.32 **Hysteresis loops of a *Y*-direction beam in the 7th floor of Model 1d* under ground motion number 18 of BSE-1E hazard-level ground motions.**

7.4.3 Dynamic Responses under BSE-2E Hazard-Level Ground Motions

7.4.3.1 General Responses

Figure 7.33 shows the peak story drift distribution over the height of Model 1d* for the case-study building under the BSE-2E hazard level events. Similar to the responses presented in Section 7.4.2, the results displayed in Figure 7.33 only include simulation cases where the analysis terminated normally. Under the BSE-2E hazard-level ground motions, there are only seven normal termination cases; thus, thirteen cases failed to converge. In all of the "failed-to-converge" cases, column splice failures occurred earlier than when the beam-to-column connections began to lose their capacities (more than 80% loss of their moment capacities). The large number of failed connections and especially splices caused computational instability issues that led to premature termination of many of the analyses.

Median peak drifts of the seven normally terminated cases were less than 10%. However, the computed peak story drift ratio was still as large as 28% (which triggers the simulation termination) under BSE-2E events. This value is significantly larger than the peak 4.5% drift limit permitted in several criteria (e.g., LATBSDC [2014]). The results also show a tendency towards weak-story behavior in the bottom third of the structure. The story shear envelope in Figure 7.34 shows that the median base shear force demand of BSE-2E level events is slightly larger than 15,000 kips, or five times the minimum design base shear considered at the time of the building's design.

The median peak beam end total rotation demands for BSE-2E events were as large as 10.3%; see Figure 7.35. Similar to the story drift responses, the beam end rotation demands had a tendency to concentrate in the bottom one-third of the building. In terms of percentage of beam-to-column connections at a floor level that completely lost their moment capacities (per ASCE 41-13 standard), the enveloped median percentage was about 30% under BSE-2E events; see

Figure 7.36. Moreover, the beam-end failure percentage was as high as 38% under a particular ground motion, and most peak values can be seen to occur below floor level 15. The peak median residual story drift ratio was about 9.5%, as shown in Figure 7.37, for the seven records that terminated normally. Large dispersions of residual drift ratios were also observed for the ground motions at this hazard-level; the actual residual drift would be larger if non-converged cases were included.

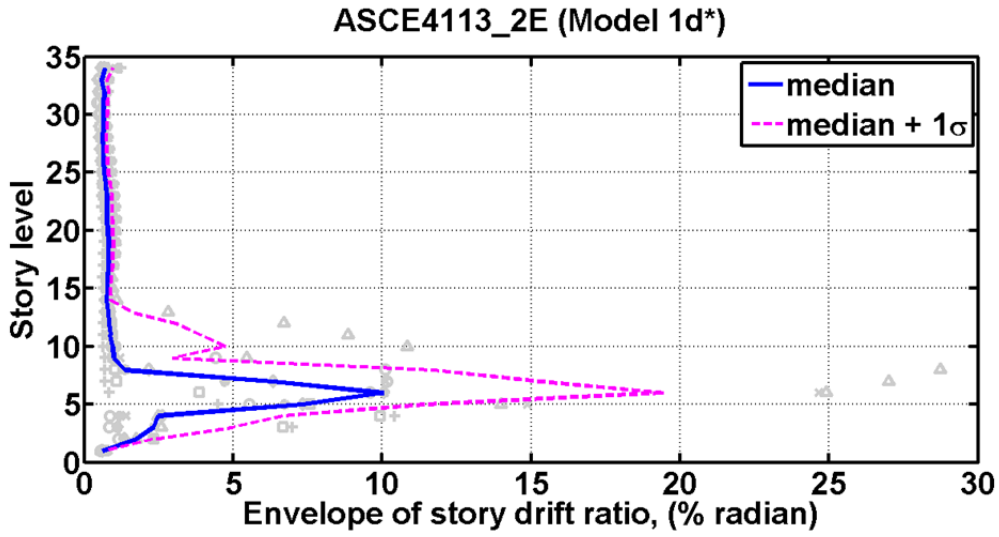

Figure 7.33 **Story drift envelope of Model 1d* under BSE-2E hazard-level ground motions.**

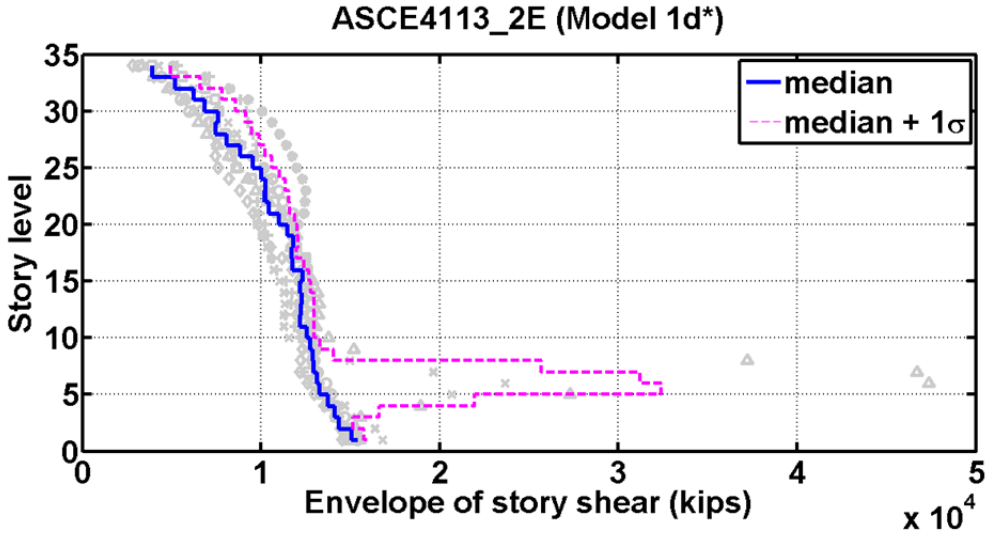

Figure 7.34 **Story shear envelope of Model 1d* under BSE-2E hazard-level ground motions.**

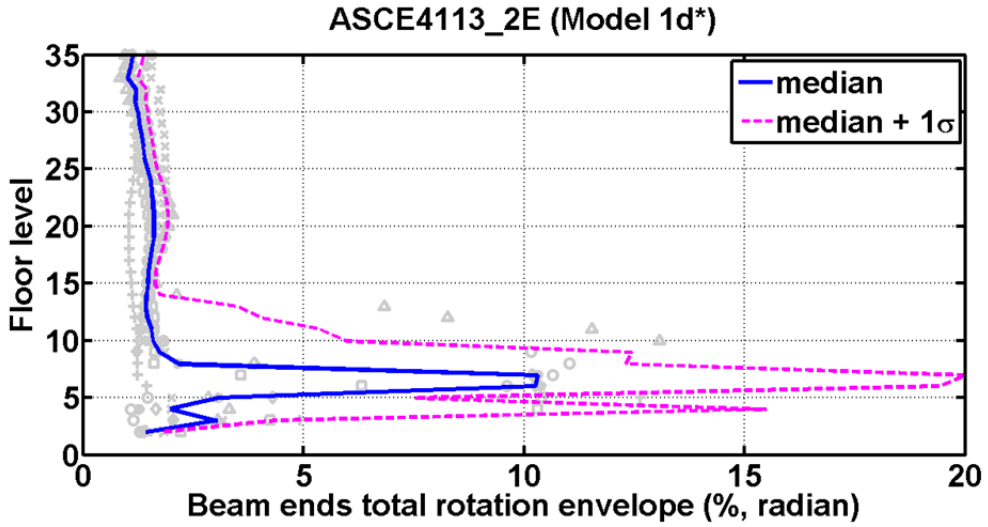

Figure 7.35 Beam ends total rotation envelope of Model 1d* under BSE-2E hazard-level ground motions.

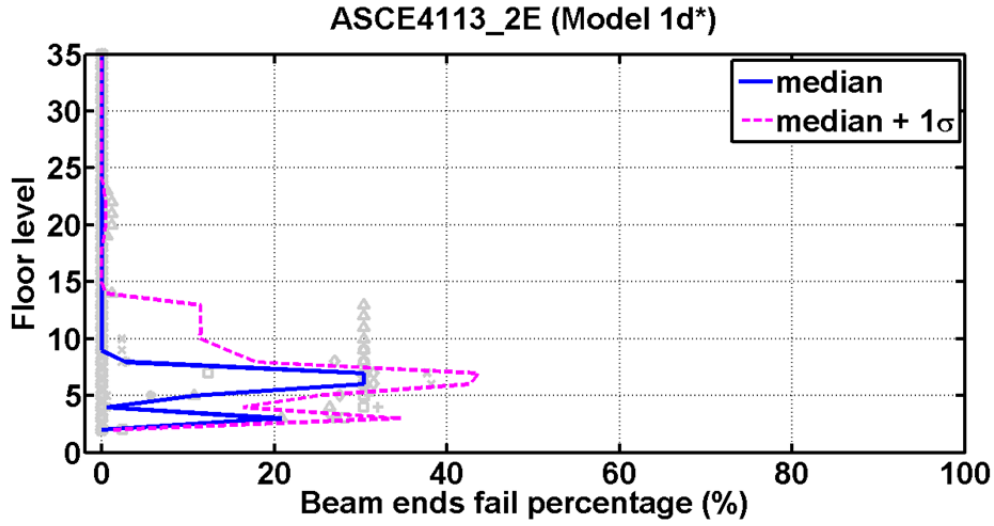

Figure 7.36 Beam ends failure percentage of Model 1d* under BSE-2E hazard-level ground motions.

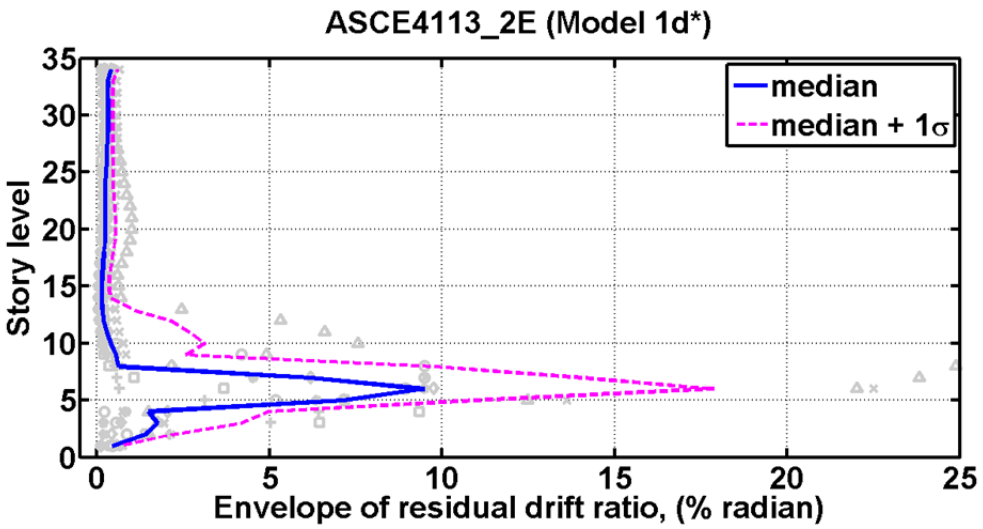

Figure 7.37 **Residual drift envelope of Model 1d* under BSE-2E hazard-level ground motions.**

7.4.3.2 Responses under Selected Ground Motions

Dynamic responses under three particular ground motions from the BSE-2E hazard level set are examined. Figures 7.38, 7.39, and 7.40 show *X*-direction and *Y*-direction beam end plastic rotation envelopes for ground motion numbers 1, 10, and 15 (see Table 7.3). As shown in Figures 7.38–7.40 and the target performance levels shown in Table 4.1, beam ends plastic rotation responses of the case-study building under these three particular ground motions do not satisfy the "limited safety" performance level. Note that under BSE-2E ground motion 1, the simulation terminated early at 14.6 sec, instead of running through the entire ground motion duration of 60 sec; this was believed to be due to numerical instability issues caused by column splice failures.

Complete fracture of column splices was predicted in several floor levels, as shown in Figure 7.41. The numerical simulations predicted transient story drift ratios (corresponding to failure to achieve collapse prevention limit state) larger than 4.5% per LATBSDC [2014] for BSE-2E ground motion numbers 10 and 15. Again, this is consistent with the envelopes of beam end plastic rotation condition shown in Figures 7.39, and 7.40. The dark-red bars from floor level 3 to 7 in those two figures indicate that more than 60% of beam-to-column connections in several floor levels complete lost their capacities.

Column splices in floor levels 3, 5, and 7 also suffered partial or complete fracture during the dynamic analyses; some floors had more than 50% of the column splices fracture; see Figures 7.42 and 7.43. The column splice failure percentages in some floor levels reached up to 74% (25/34). Figures 7.44, 7.45, and 7.46 show typical column axial forces and bending moment response histories of corner columns (group 1 columns, see Figure 7.23) in the 3rd story that contains column splices. Note that the column splice section completely fractured before the normal termination of the numerical analysis.

The column P-M-M interaction diagrams shown in Figures 7.47, 7.48, and 7.49 for a corner column in the 6th floor indicate that plastic hinges formed at column both ends; high axial force ratios ($P/P_y > 0.5$) were observed.

Figures 7.50, 7.51, and 7.52 show three typical hysteresis loops of beam ends moment-rotation relationships for three particular locations under three selected ground motions. Again, the loops show the simulated mechanical behavior of connections follows the ASCE 41-13 general modeling requirements for steel beam-to-column connections.

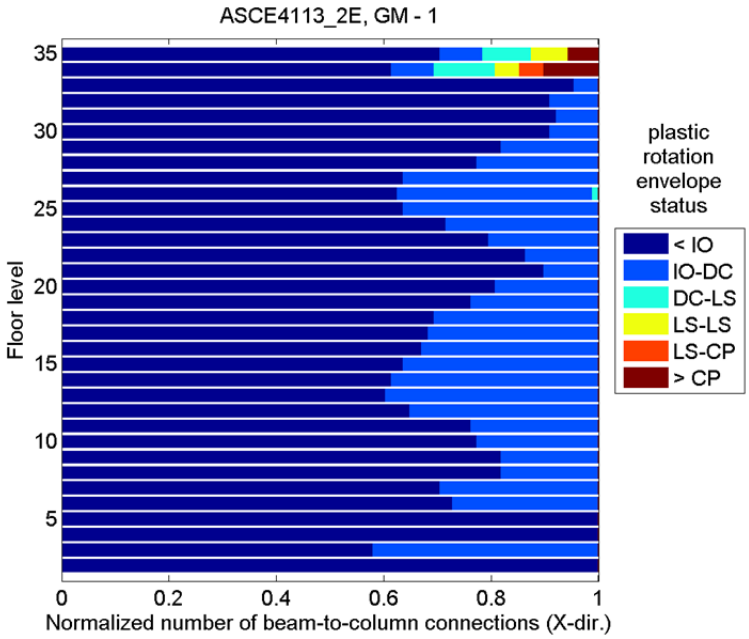

(a)

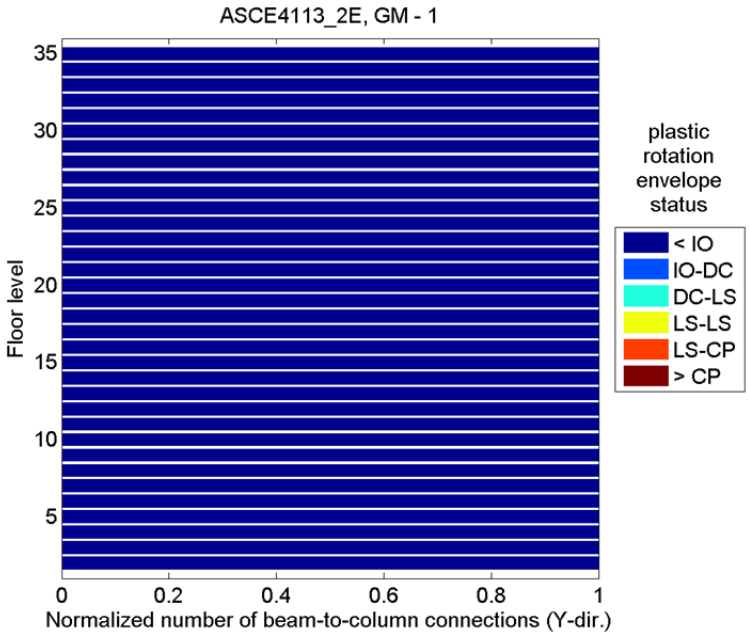

(b)

Figure 7.38 **Beam end plastic rotation envelope status of Model 1d* under ground motion number 1 of BSE-2E hazard-level ground motions: (a) *X*-direction and (b) *Y*-Direction.**

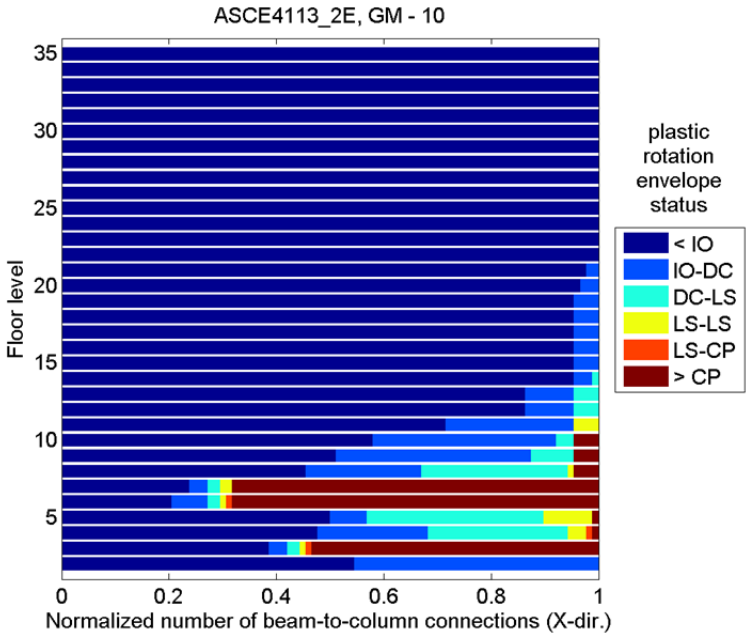

(a)

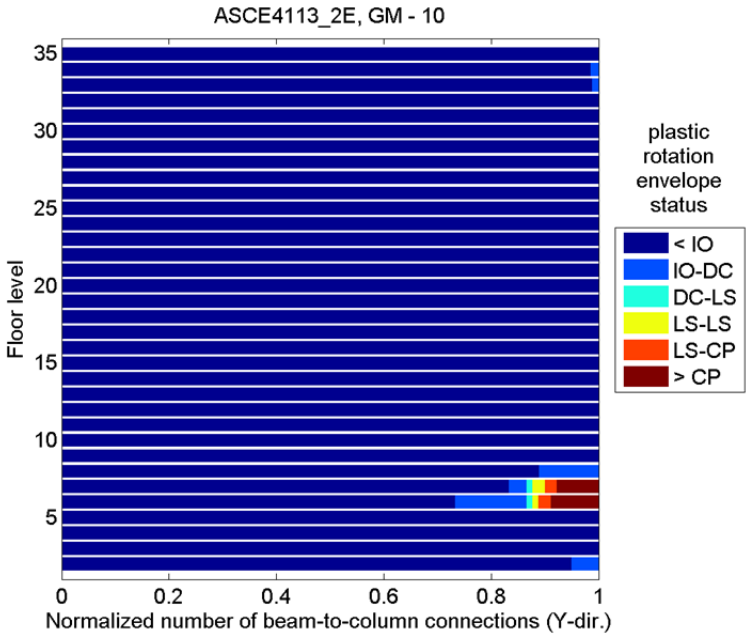

(b)

Figure 7.39 **Beam end plastic rotation envelope status of Model 1d* under ground motion number 10 of BSE-2E hazard-level ground motions: (a) *X*-direction and (b) *Y*-direction.**

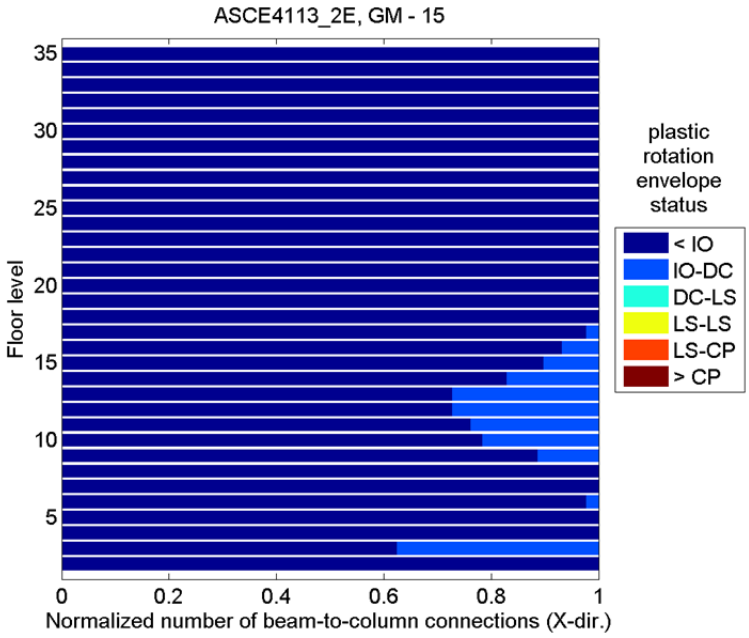

(a)

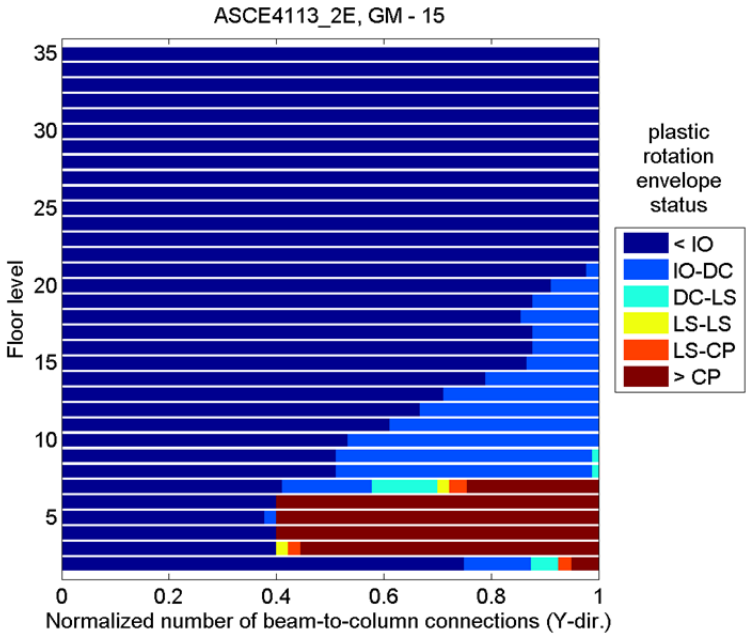

(b)

Figure 7.40 **Beam end plastic rotation envelope status of Model 1d* under ground motion number 15 of BSE-2E hazard-level ground motions: (a) *X*-direction and (b) *Y*-direction.**

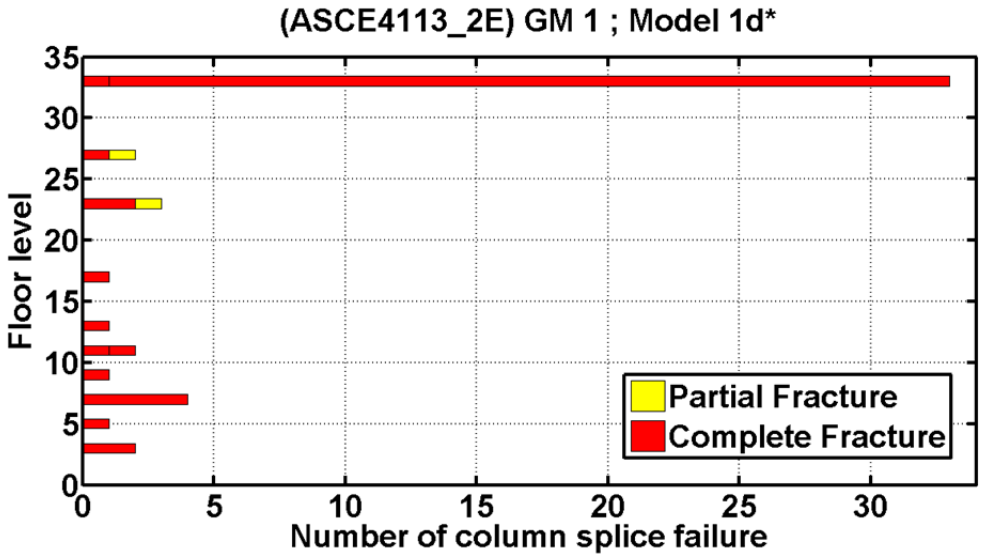

Figure 7.41 Number of column splice failures in each floor level of Model 1d* under ground motion number 1 of BSE-2E hazard-level ground motions.

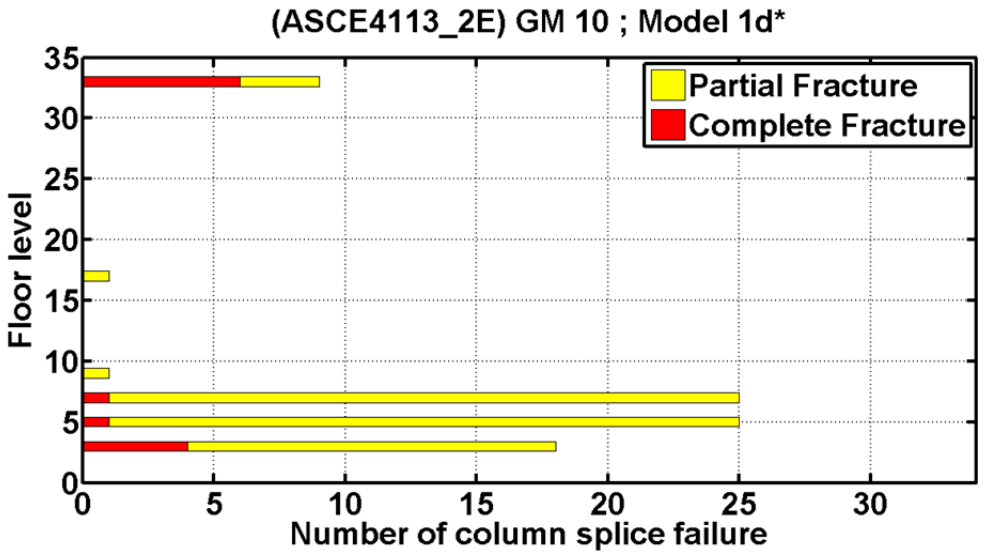

Figure 7.42 Number of column splice failures in each floor level of Model 1d* under ground motion number 10 of BSE-2E hazard-level ground motions.

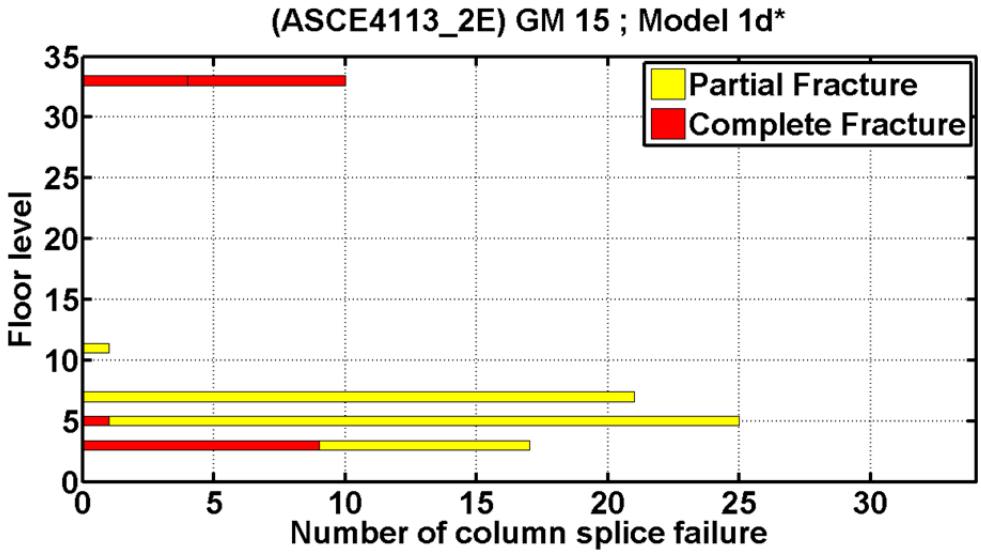

Figure 7.43 Number of column splice failures in each floor level of Model 1d* under ground motion number 15 of BSE-2E hazard-level ground motions.

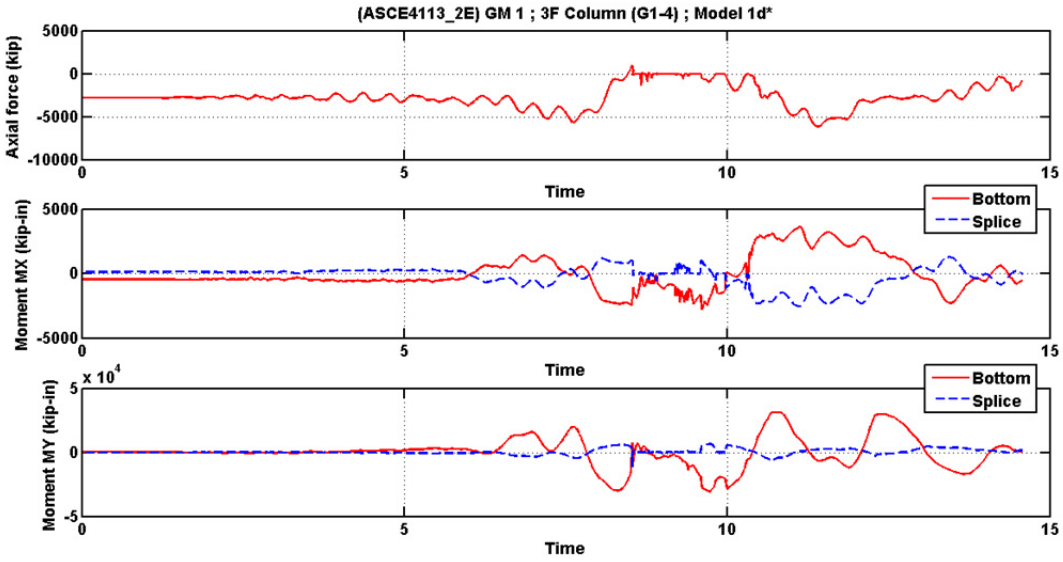

Figure 7.44 Axial force, and bending moments response histories of a corner column in the 3rd floor of Model 1d* under ground motion number 1 of BSE-2E hazard-level ground motions.

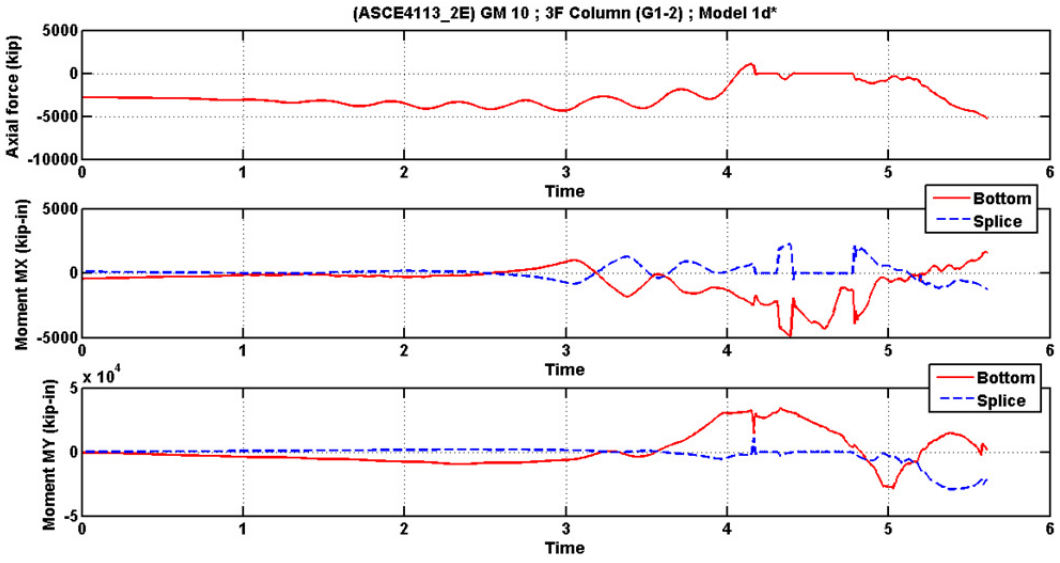

Figure 7.45 Axial force and bending moments response histories of a corner column in the 3rd floor of Model 1d* under ground motion number 10 of BSE-2E hazard-level ground motions.

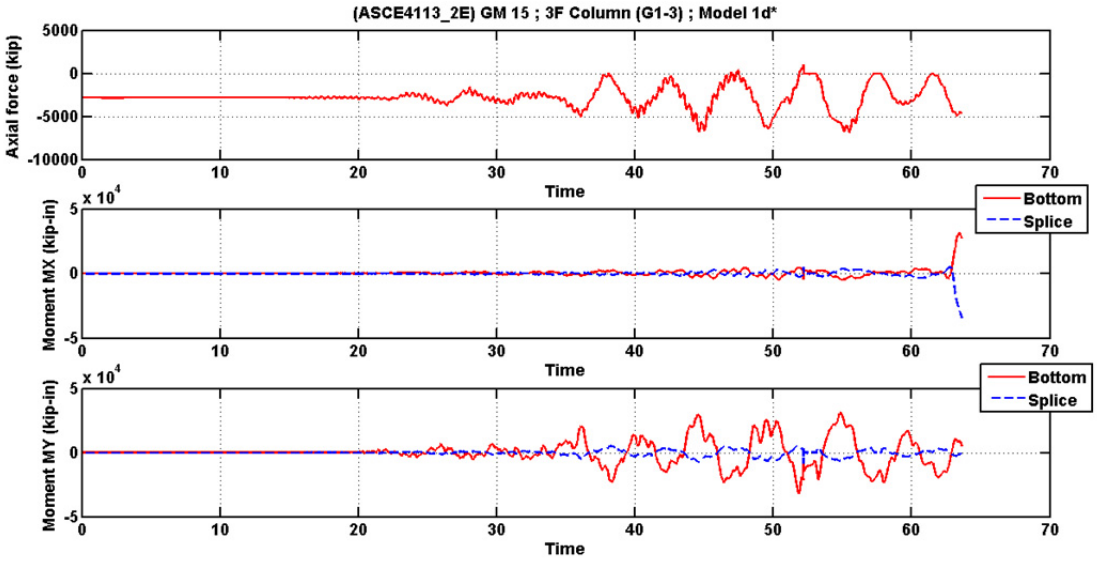

Figure 7.46 Axial force and bending moments response histories of a corner column in the 3rd floor of Model 1d* under ground motion number 15 of BSE-2E hazard-level ground motions.

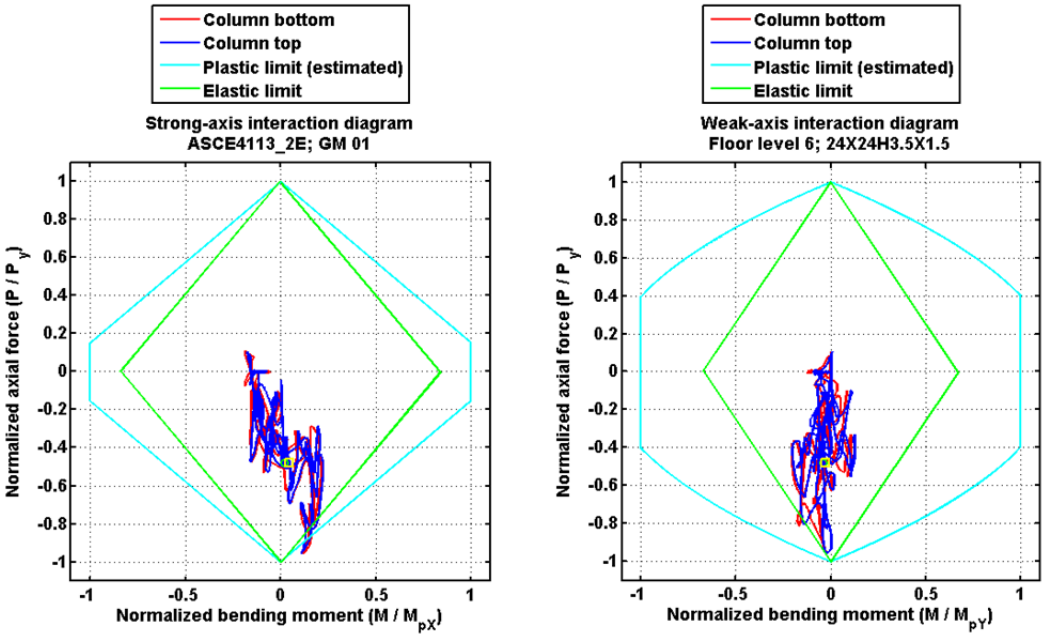

Figure 7.47 ***P-Mx-My*** **interaction diagrams of a corner column (group 5) in the 6th floor of Model 1d* under ground motion number 1 of BSE-2E hazard-level ground motions.**

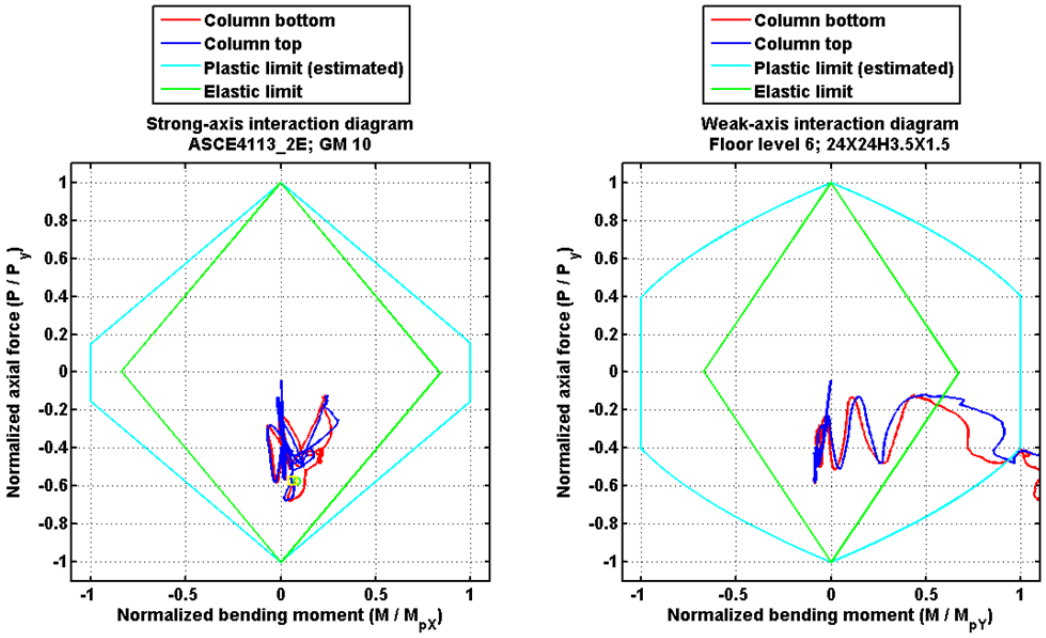

Figure 7.48 ***P-Mx-My*** **interaction diagrams of a corner column (group 5) in the 6th floor of Model 1d* under ground motion number 10 of BSE-2E hazard-level ground motions.**

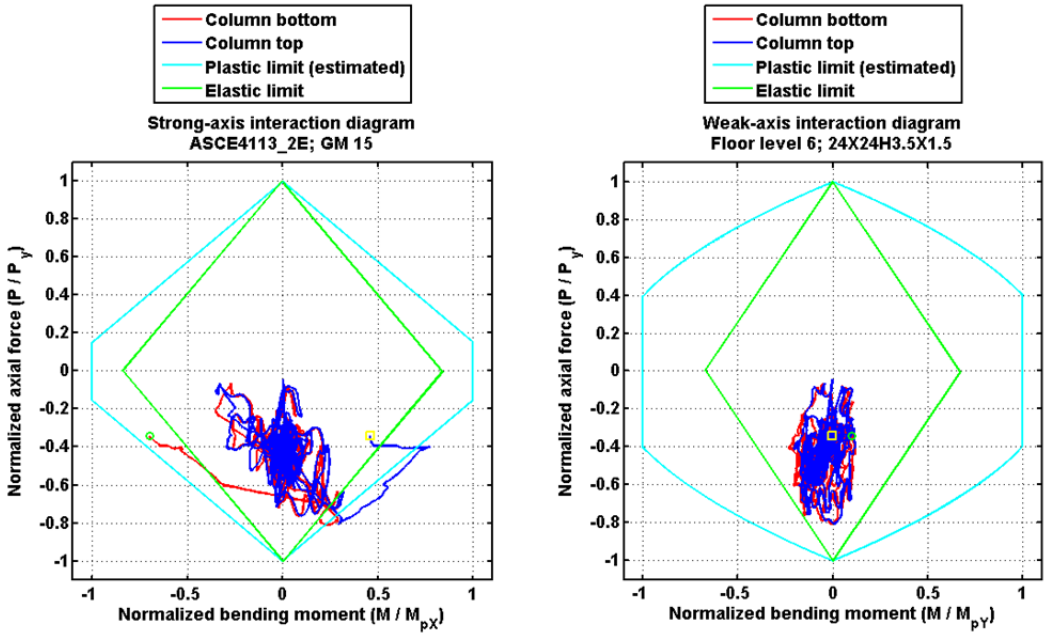

Figure 7.49 ***P-M_x-M_y*** **interaction diagrams of a corner column (group 5) in the 6th floor of Model 1d* under ground motion number 15 of BSE-2E hazard-level ground motions.**

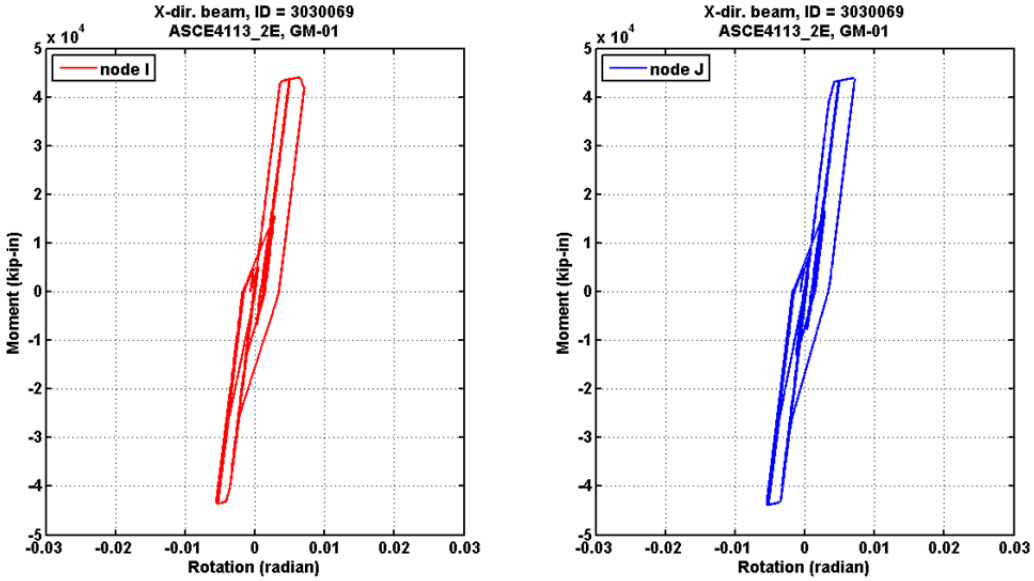

Figure 7.50 **Hysteresis loops of an *X*-direction beam in the 6th floor of Model 1d* under ground motion number 1 of BSE-2E hazard-level ground motions.**

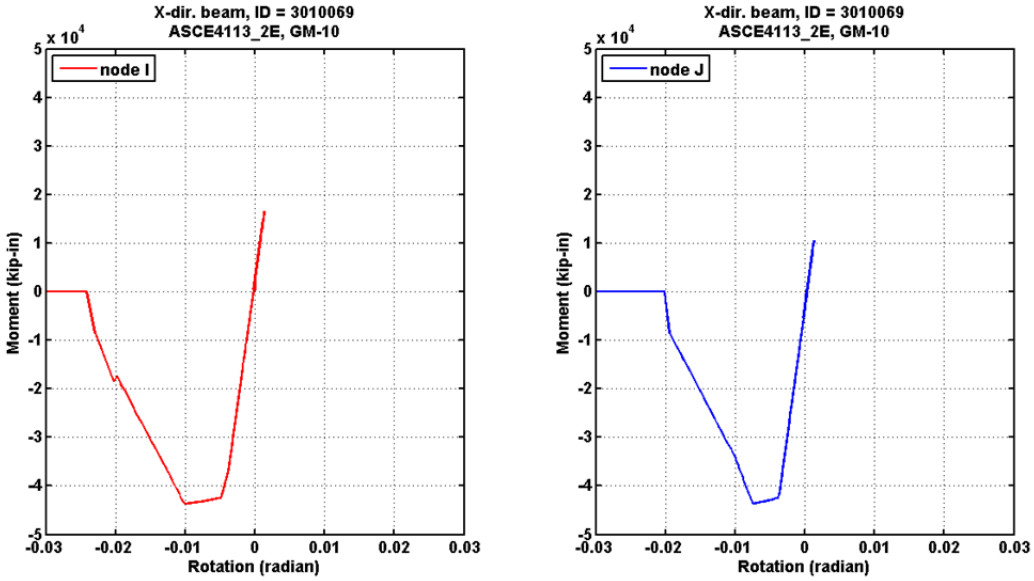

Figure 7.51 Hysteresis loops of an *X*-direction beam in the 6th floor of Model 1d* under ground motion number 10 of BSE-2E hazard-level ground motions.

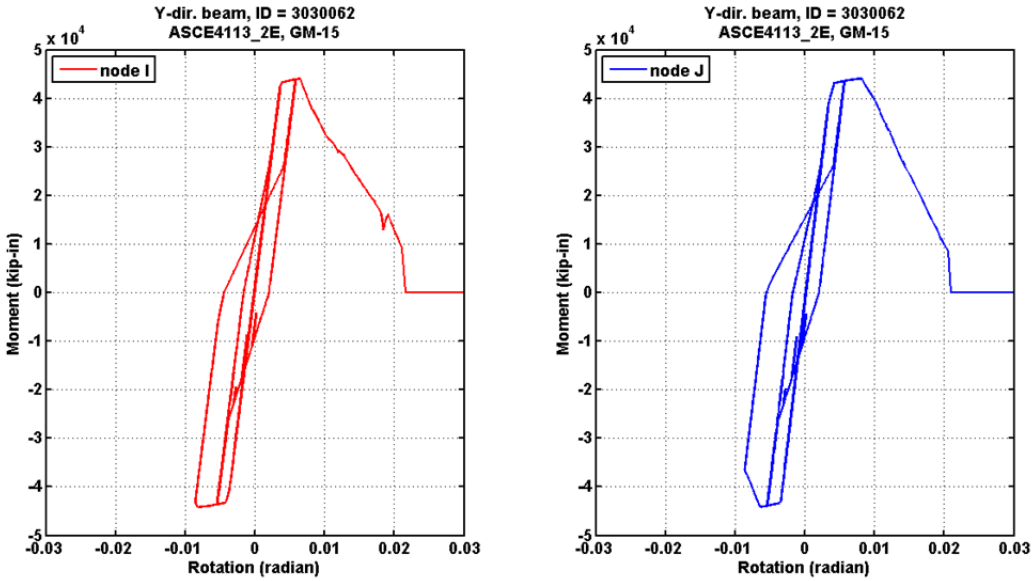

Figure 7.52 Hysteresis loops of a *Y*-direction beam in the 6th floor of Model 1d* under ground motion number 15 of BSE-2E hazard-level ground motions.

7.4.4 Dynamic Response under Events with a 50% Probability of Exceedance in 30 Years (43-year Mean Return Period) Hazard-Level Ground Motions

It is useful to understand the severity of earthquake excitation that would initiate fracture of connections and splices, or other undesirable behavior. To assess this, a historic distant event recorded at a nearby site was previously examined in Section 7.4.1. This section examines responses to a set of service-level earthquakes having a 50% probability of exceedance in 30 years.

Figure 7.53 displays the story-drift envelope over the height of the case-study building (Model 1d*) under the 43-year mean return period hazard level events. Responses from all 20 ground motions were obtained and included in this plot. The peak median drift is 0.51%. This maximum occurred at the mezzanine level. Most story levels have median drift ratios around 0.37%. Compared with the story-drift envelope when the building is subjected to the Loma Prieta earthquake (see Figure 7.10), these results are larger, except at the roof level. The story-shear envelope (Figure 7.54) shows that the median base shear force demand for the 43-year mean return period events was slightly larger than 8600 kips. By comparing the base shear force envelope with static pushover results (Figures 7.3 and 7.4), the case-study building is expected to remain essentially elastic under most of these service level ground motions, although in some local cases structural elements moved into the inelastic range.

The median peak beam end total rotation demand under this hazard level was 0.73% (Figure 7.55) and occurs in the upper one-half of the building. None of the beam-to-column connections at any floor levels lost their moment capacities completely under this hazard level. No residual story drifts observed under this hazard-level ground motions.

No column splice failures were observed under these hazard-level ground motions, and the median compression axial force demand-to-capacity ratio envelopes of exterior and interior corner columns (group 1 and group 5) were all less than about 0.65; see Figures 7.56 and 7.57. Note that column tension forces (and these were relatively small) were only observed in some ground motions near the base or roof levels. Higher than normal axial compression stress was observed in some of the columns. Group 1 columns had median axial compression force demand-to-capacity ratios greater than 50% between floor levels 2 and 15, while the group 5 columns had high median axial compression force demand-to-capacity ratios between floor levels 3 and 21.

For the capacity term used in computing the *D*/*C* ratios, the column tension and compression capacities were calculated in accordance with AISC 360-10 specification and ASCE 41-13 standard. For odd numbered stories where column splices occur, the tension capacities of column splices were calculated using Equation 7.1. For even numbered stories, the tension capacity of a column was computed according to the Equation 9-8 in the ASCE 41-13 standard.

$$P_{CL} = \varphi \cdot A_{\text{net}} \cdot F_{\text{allowable}} \tag{7.1}$$

where P_{CL} is the lower-bound column splice tension capacity, strength reduction factor $\phi = 1.0$, A_{net} is the net section area of partial joint penetration (PJP) welds at the column splice region, and $F_{\text{allowable}}$ is the estimate allowable stress in the PJP welds derived from Equation (6.1).

Demand-to-capacity ratios under gravity loads are also shown in the same figure; see Figures 7.56 and 7.57. Bending components of demand and capacity were not considered in computing these simple *D*/*C* parameters.

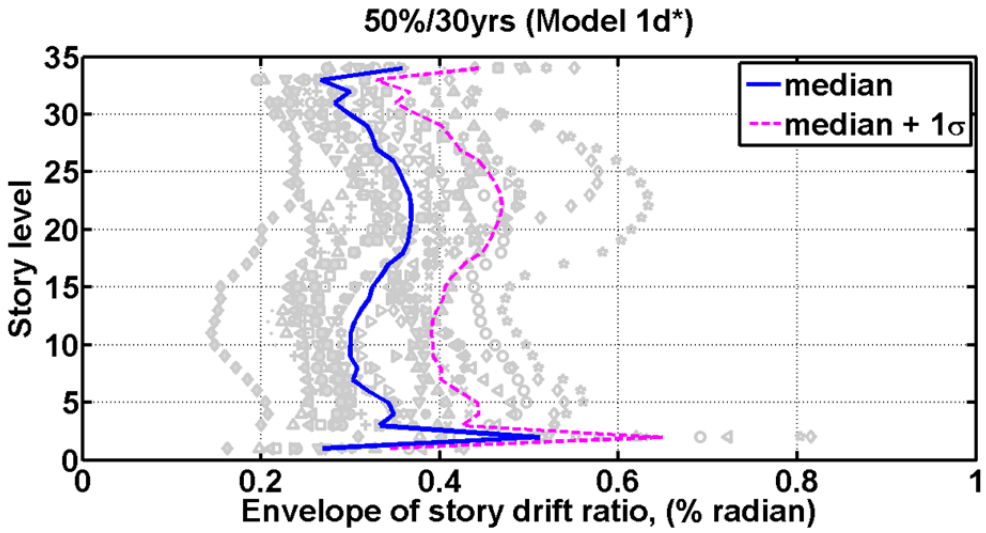

Figure 7.53 **Story drift envelope of Model 1d* under 50%/30yrs hazard-level ground motions.**

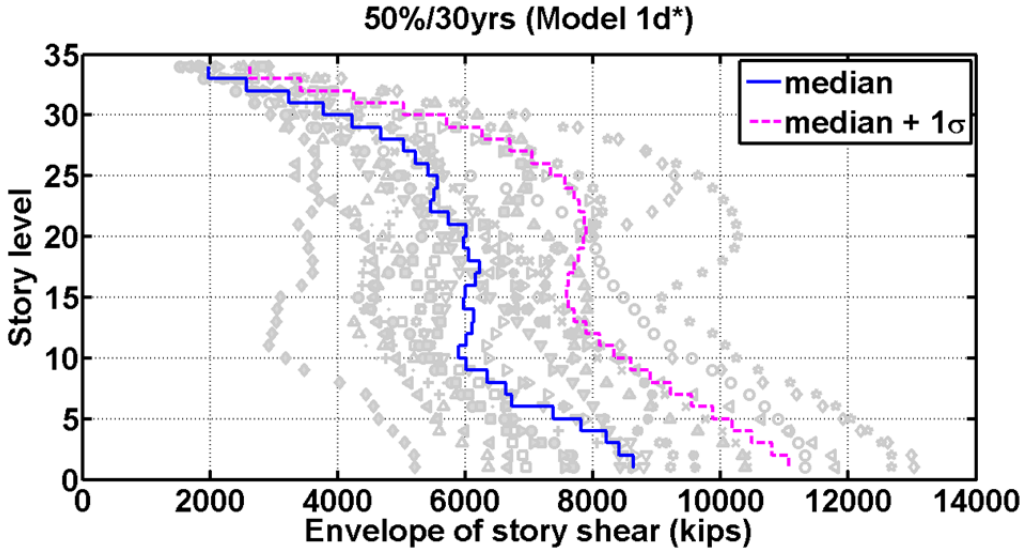

Figure 7.54 **Story shear envelope of Model 1d* under 50%/30yrs hazard level ground motions.**

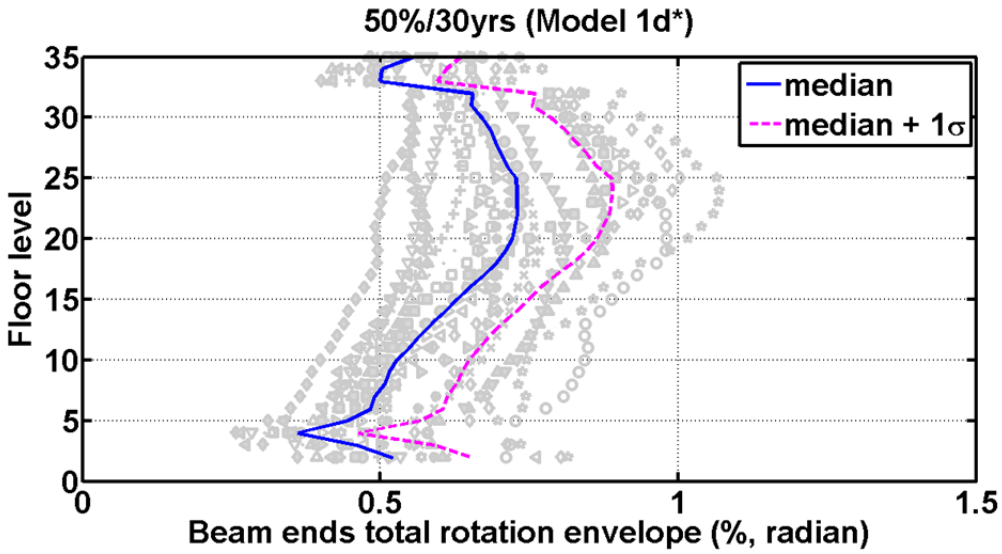

Figure 7.55 Beam ends total rotation envelope of Model 1d* under 50%/30yrs hazard-level ground motions.

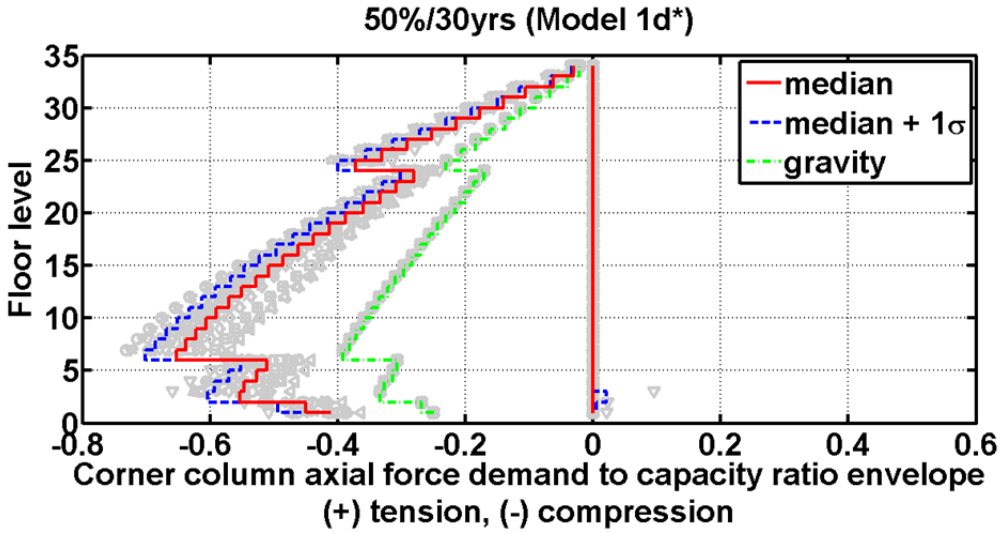

Figure 7.56 Exterior corner column (group 1) axial force demand to capacity ratio envelope of Model 1d* under 50%/30yrs hazard-level ground motions.

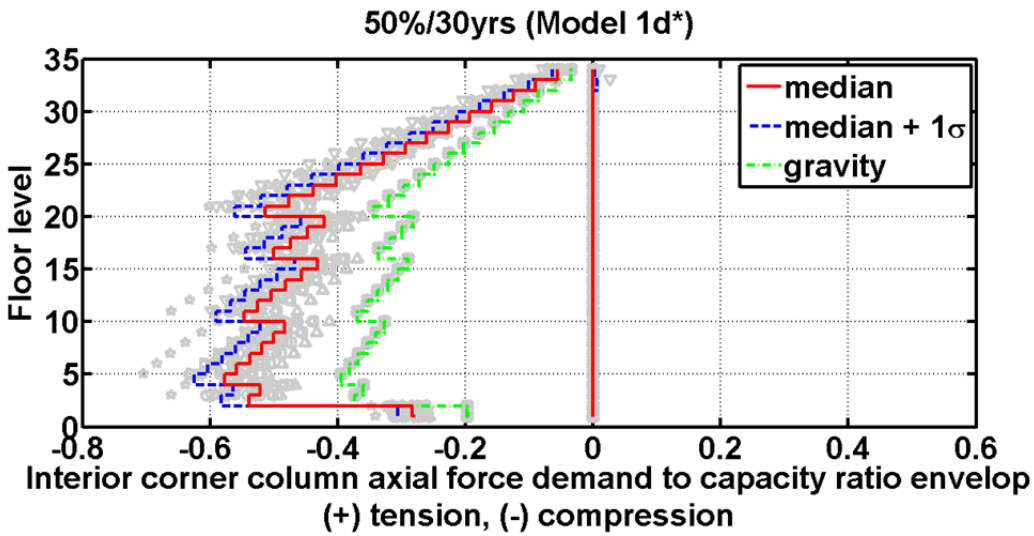

Figure 7.57 **Interior corner column (group 5) axial force demand to capacity ratio envelope of Model 1d* under 50%/30yrs hazard-level ground motions.**

7.5 NONLINEAR DYNAMIC ANALYSIS OF MODEL 1C (THE "BASELINE" MODEL)

From the dynamic analysis results shown in the previous section, it is clear that the current building condition (represented by Model 1d* in this study) without any seismic upgrades or modifications cannot meet the BPOE as defined in ASCE 41-13. As mentioned in Chapter 4, removal of heavy claddings might be a simple and relatively inexpensive way to lower the seismic demands on an existing building. Thus, it is beneficial to examine the dynamic responses of the case-study building in a scenario where the heavy claddings are removed.

Results for Model 1d* suggest that a significant number of column fractures are likely even if the heavy cladding is removed. Because the analytical models used in this study to simulate the brittle fracture of column splices are approximate, and lead to numerical instability when multiple column splices in the structure fracture, the confidence that can be placed in the results of this model may be limited. While more accurate column splice failure models should be developed and validated by tests, a pragmatic engineer evaluating the building might elect to simply upgrade problematic the easily accessible partial penetration column splice welds and make them complete joint penetration welds as part of any retrofit. Thus, Model 1c was developed and used as the "baseline" retrofit model in this study. Model 1c includes removal of the cladding from the building model, and a retrofit of all column splices to prevent premature tensile fracture at the splice locations. This feasible retrofit strategy is examined in this section.

Similar to the analyses performed on Model 1d* in Section 7.4, the dynamic responses of the baseline Model 1c was subjected to one historic low level earthquake record, which was then followed by the nonlinear dynamic analyses performed in OpenSees using BSE-1E and BSE-2E hazard level ground motions, as well as the service level events. Each hazard level contained 20 ground motion records, and each record contained three components (i.e. two horizontal components plus one vertical component, $2h+v$).

Note that only the dynamic analysis results of Model 1c (the baseline model mentioned in Chapter 4) are presented in this section. Complete analysis results for other models (such as Model 1a and Model 1d), and a comparison of cases with and without the vertical component of ground motion are discussed in Section 7.6.

7.5.1 Dynamic Responses under CSMIP Station 58480, 1989 Loma Prieta Earthquake

The baseline model (Model 1c) is first subjected to an actual ground motion recorded at CSMIP [2015] station 58480 near the case-study building site during the 1989 Loma Prieta earthquake (see Figure 7.7). Since very little yielding and no column splice fractures was predicted for this event, comparison of results for Models 1d* and 1c provides direct insight into the effect of the cladding on the dynamic properties and response of the structure during low-level excitations.

Figure 7.58 shows the roof displacement response histories (relative to the ground) and roof displacement orbits. The peak roof displacement is slightly larger than 9 in. in the *Y*-direction, while the peak displacement is less than 4 in. in the *X*-direction. Again, this is well within the elastic range of the building suggested from the static pushover curves presented previously. No permanent roof displacement was observed at the end of the simulation. The responses after 60 sec., shown in the plot, are free-vibration responses with artificially increased damping.

The amplification factor of peak acceleration was about 2.2 at the roof level (0.38*g*/0.17*g*) as shown in Figure 7.59. The peak story drift ratio along the height of the building was around 0.44% (see Figure 7.60), which is less than the typical 0.005 limit often considered acceptable for immediate occupancy. As shown in Figure 7.61, the peak base shear force (maximum of both directions) was 5752 kips, indicating that the building essentially remained elastic during this earthquake as evidenced by comparing the base shear force and the peak roof displacement with the static pushover results in Figures 7.5 and 7.6.

The removal of claddings reduced the modal periods of case-study building (Section 7.2.1). As a result, the story-drift envelope was reduced, and the story-shear force demands were reduced as well; compare Figures 7.10 and 7.11 with Figures 7.60 and 7.61. Significant reduction of the peak story drift occurred at the mezzanine level. However, the peak roof displacements were not necessarily reduced in the *X*- and *Y*-directions; compare Figures 7.8 and 7.58; the peak roof accelerations in both *X*- and *Y*-directions increase (as seen by comparing Figures 7.9 and 7.59).

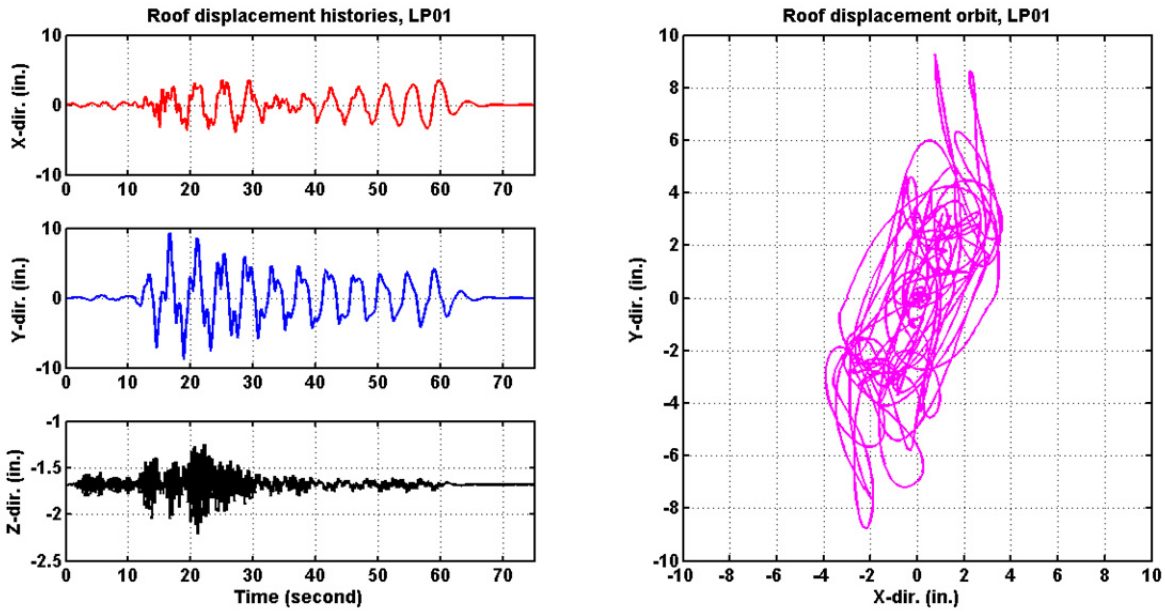

Figure 7.58 Roof displacement histories and orbital responses to the actual recorded ground motion (Model 1c)

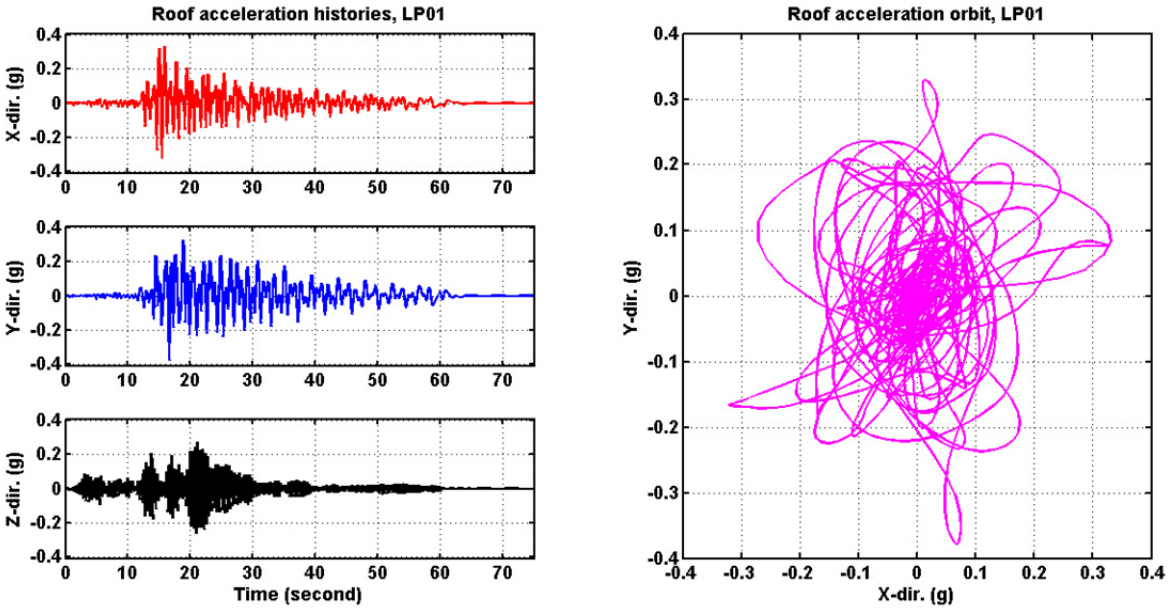

Figure 7.59 Roof absolute acceleration histories and orbits of the case-study building subjected to the actual recorded ground motion (Model 1c).

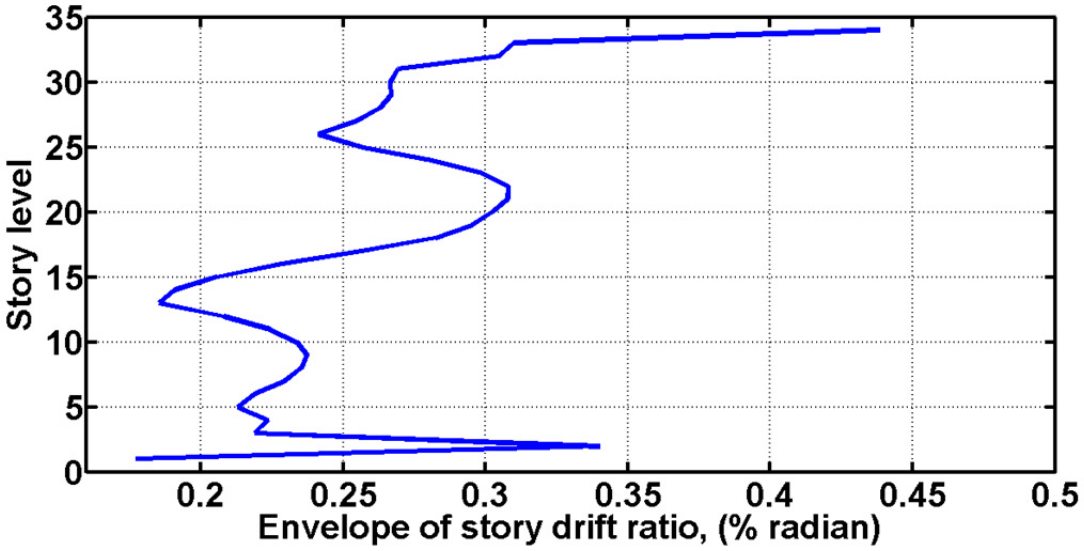

Figure 7.60 Story drift ratio envelope under an actual recorded ground motion (Model 1c).

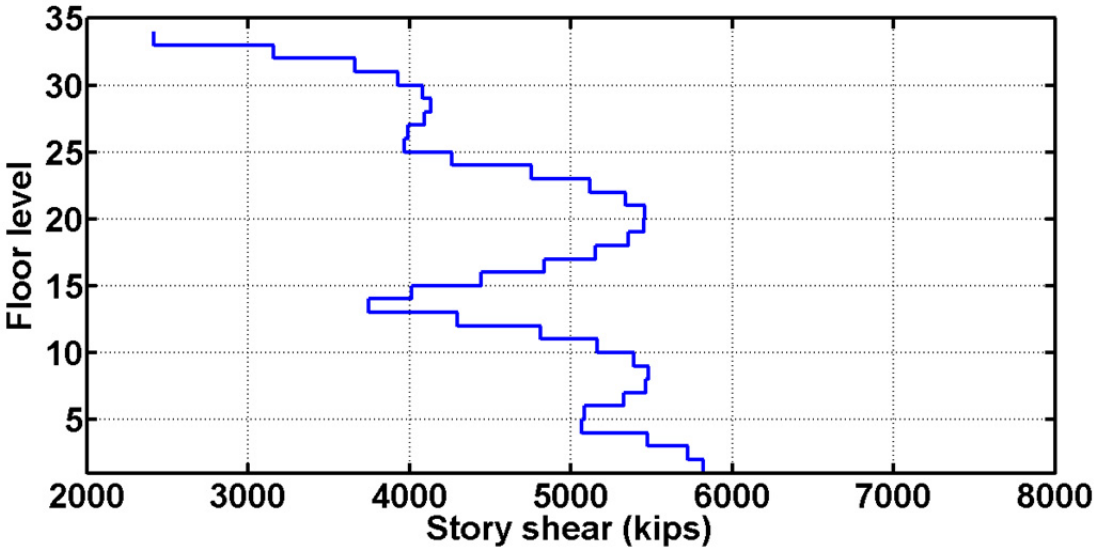

Figure 7.61 Story shear force envelope under an actual recorded ground motion (Model 1c).

7.5.2 Dynamic Responses under BSE-1E Hazard-Level Ground Motions

Figure 7.62 presents the story drift envelope distribution over the height of Model 1c under BSE-1E hazard level events (all 20 simulation cases converged and are included in the plot). Median peak story drifts were all less than 1.2%. However, the maximum peak story drift ratio was as large as 46% under the BSE-1E events, which was significantly larger than the peak 4.5% drift limit included in several criteria (e.g., LATBSDC [2014]). Note that Figure 7.62 only shows the story drift up to 2.5% radian, though some drift values are greater. The results still show a tendency towards weak story behavior in the bottom third of the structure. The story-shear envelope (Figure 7.63) shows that the median base shear force demand of BSE-1E level events was about 15,000 kips. Median peak beam end total rotation demand for the BSE-1E level events was as large as 1.2% (Figure 7.64), thus failing to conform to the ASCE 41 performance criteria for this level of excitation. Similar to the story drift responses, the beam end rotation demands had a tendency to concentrate in the bottom one-third of the building. In terms of the percentage of failed beam-to-column connections at a floor level, the median percentage was zero under BSE-1E events (Figure 7.65). However, some ground motions generated failures as high as 38% in a given floor. The median residual story-drift envelope under BSE-1E hazard-level earthquakes was essentially zero (for a peak residual story drift is 0.05%), and the residual story-drift envelope had large dispersion (as large as a 10% story drift ratio) between floor level 5 and 10; see Figure 7.66). Note that the 10% story drift ratio was set as a limit to terminate the analyses; consequently, the actual median and dispersion values for residual drift are expected to be larger than those shown in the figure.

The envelopes of column axial force demand-to-capacity ratio of four exterior corner columns (group 1, see Figure 7.23) are shown in Figure 7.67. As before, the tension capacity is shown as a positive value. In this model, the PJP splice welds were fixed, thereby the tension demand-to-capacity ratio improves substantially, as evidenced by the small peak value (i.e., median values for exterior columns less than 0.2). Following the simplified formula based on fracture mechanics from [Stillmaker et al. 2016] increases the tension capacity of the spice region by a factor of 9–10. Therefore, without the retrofit of the splices, it is likely that column splice fracture would still occur in the event of a BSE-1E level earthquake. With regard to column compression forces, the peak median value for an external column approaches 0.8 at floor 6. As before, the D/C ratios calculated in the figures do not include contributions from bi-axial bending.

In terms of interior columns, both tension and compression demands are smaller than for the exterior columns because of the absence of overturning moment effects. However, the compression demands due to gravity are larger for interior columns because of the larger tributary area supported by these columns. This increased gravity load leads to a decrease of peak tension demands. The peak median compression force demand-to-capacity ratio was less than 0.7 (indicated on negative side of figure) under BSE-1E hazard-level ground motions; nonetheless, about two-thirds of floor levels exceed a value of 0.5, which would diminish the column bending capacities, rending them quite vulnerable to flexural yielding due to P-M interaction effects.

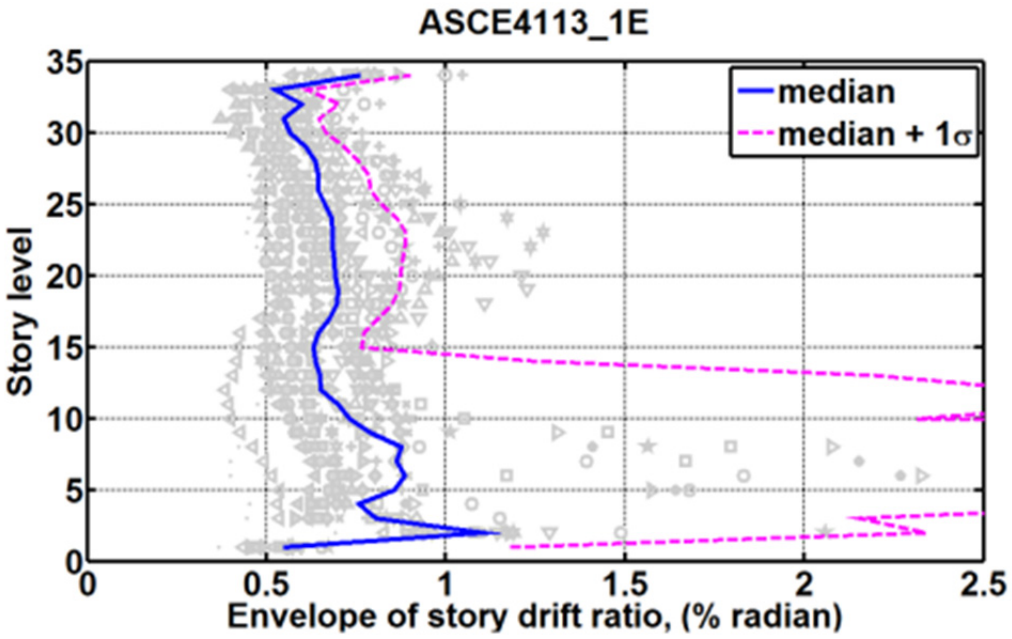

Figure 7.62 Story drift envelope of Model 1c under BSE-1E hazard level events.

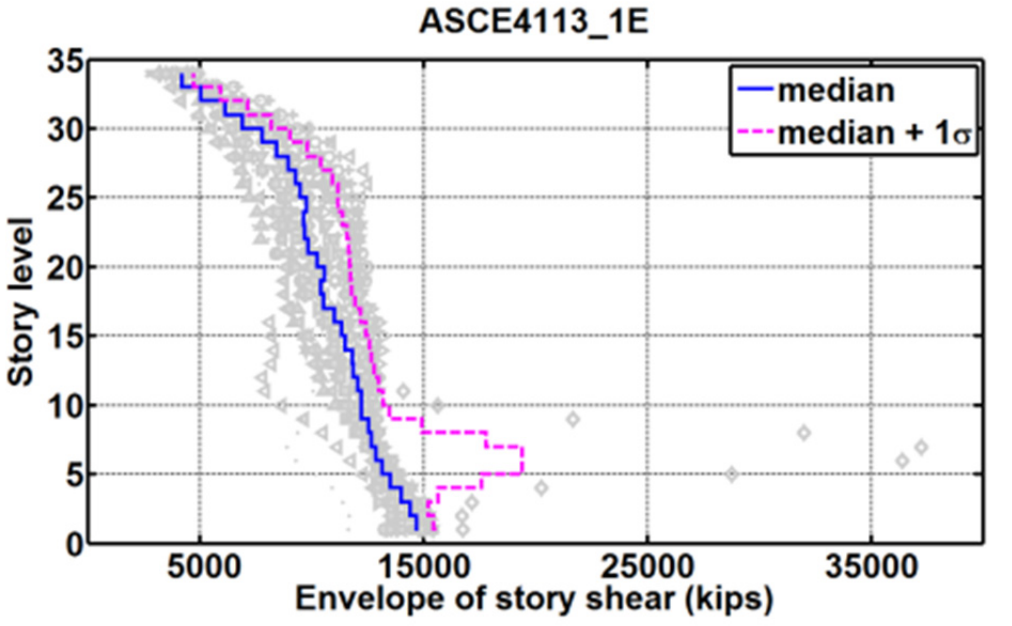

Figure 7.63 Story shear envelope of Model 1c under BSE-1E hazard level events.

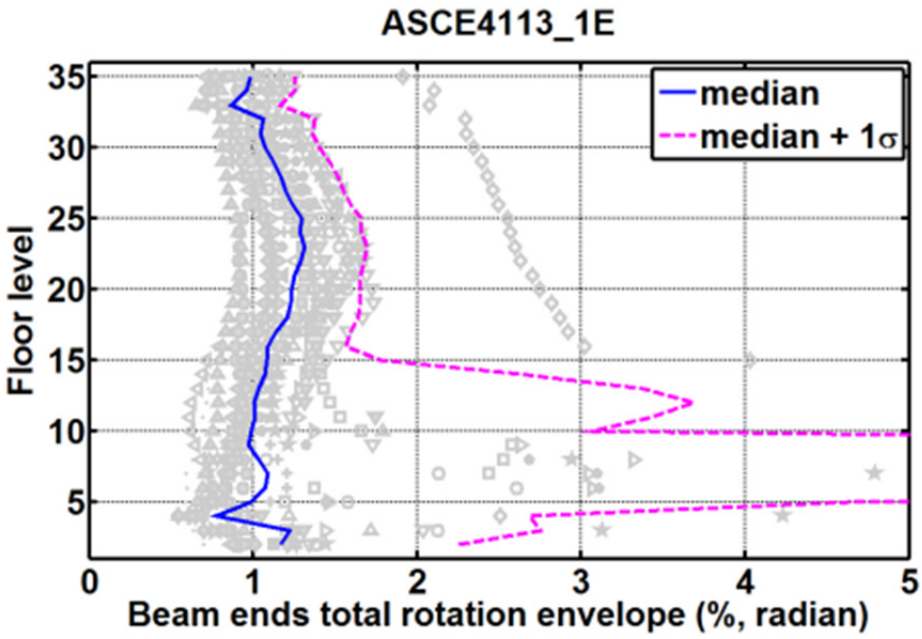

Figure 7.64 Beam ends total rotation envelope of Model 1c under BSE-1E hazard level events.

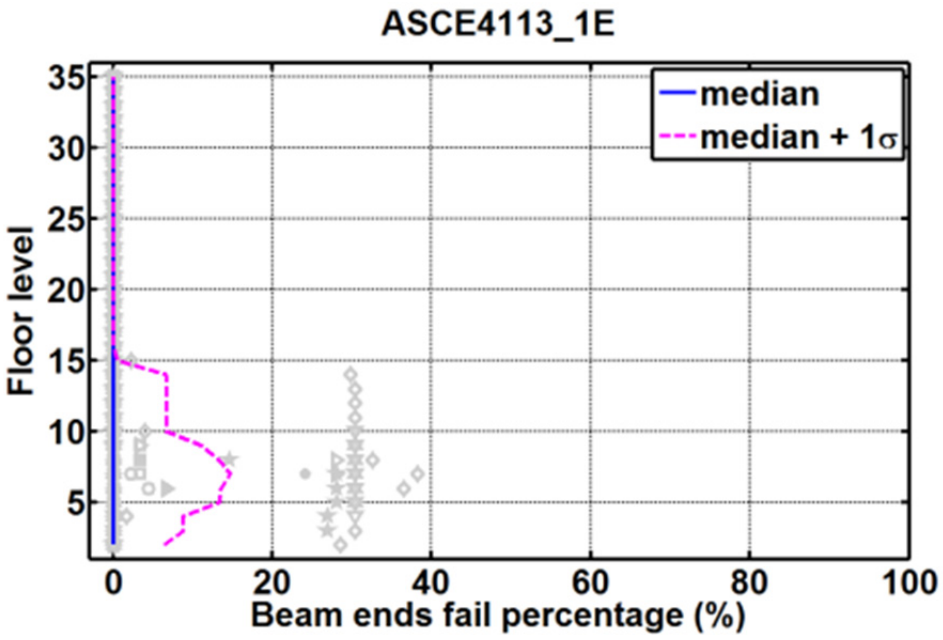

Figure 7.65 Beam ends failure percentage of Model 1c under BSE-1E hazard level events.

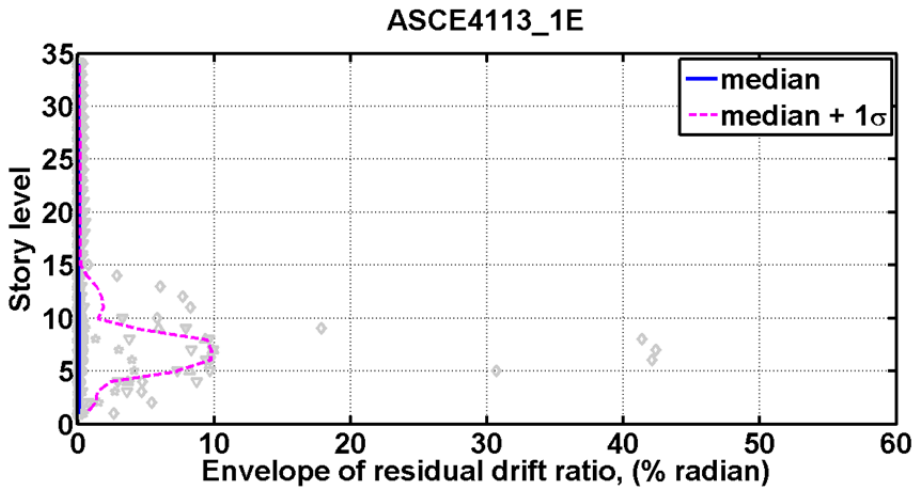

Figure 7.66 Residual drift envelope of Model 1c under BSE-1E hazard level events.

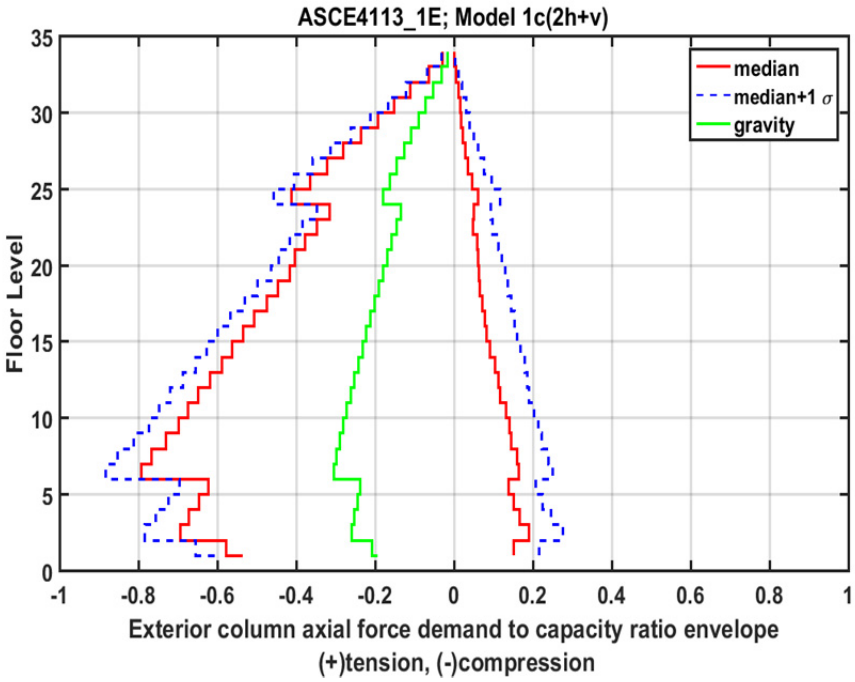

Figure 7.67 Column axial force demand to capacity ratios of exterior corner columns (group 1 columns; Model 1c; BSE-1E).

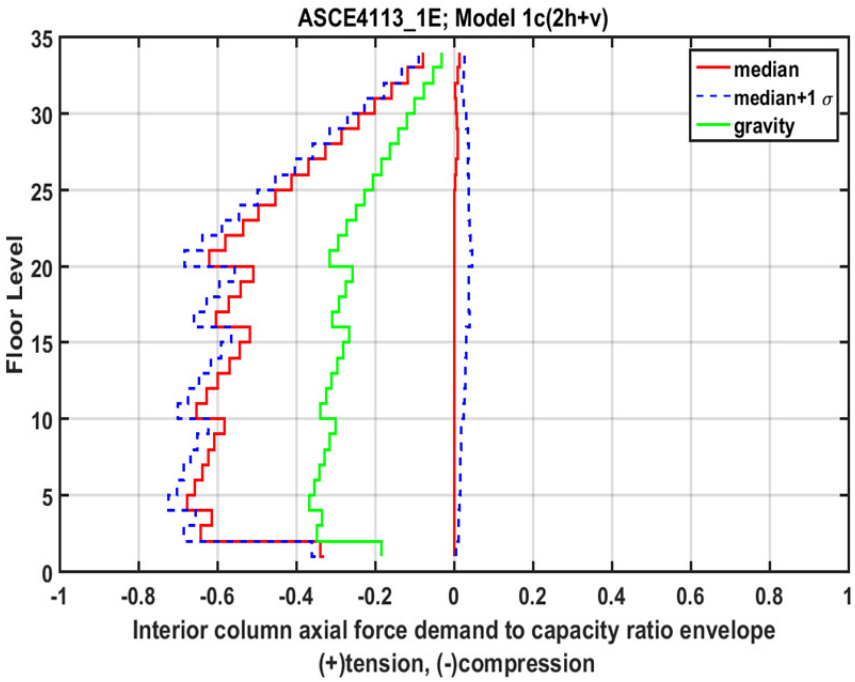

Figure 7.68 **Column axial force demand to capacity ratios of interior corner columns (group 5 columns; Model 1c; BSE-1E).**

7.5.3 Dynamic Responses under BSE-2E Hazard-Level Ground Motions

Figure 7.69 presents the peak story drift envelope distribution over the height of Model 1c under BSE-2E hazard level events. Median peak drift responses of 20 ground motion records were as large as 7.0%. The peak story drift ratio was as large as 55% under some of the BSE-2E events, which is significantly larger than the peak 4.5% drift limit included in several criteria (e.g., LATBSDC [2014]). Note that Figure 7.69 only shows the story drift up to 7.5% radians. The results show a tendency towards weak-story behavior in the bottom one-third of the structure. The story-shear envelope (Figure 7.70) shows that the median base shear force demand of BSE-2E level events was slightly larger than 15,000 kips. Median peak beam end total rotation demands for BSE-2E events were as large as 9% (Figure 7.71), thus failing to conform to the ASCE 41 performance criteria. Similar to the story-drift responses, the beam end rotation demands had a tendency to concentrate in the bottom one third of the building. In terms of percentage of beam-to-column connections at a floor level that completely lost their moment capacities (per ASCE 41-13), the median percentage was as high as 30% under BSE-2E events; see Figure 7.72. Moreover, the beam end failure percentage was as high as 70% for a particular ground motion, with most peak values being concentrated below floor level 15.

The peak median residual story drift ratio was about 6.3% at story level 7; see Figure 7.76. Note that this value is larger than the 1.5% maximum residual drift ratio allowed per the LATBSDC consensus document [2014]. Large dispersions of residual drift ratios were also observed.

Similar to the results discussed in Section 7.5.2, large column tensile force demands are anticipated. Demand-to-capacity ratios (Figure 7.74 and Figure 7.75) at column splice locations

were computed with the upgraded strength (assuming the splice regions are fixed). The tensile D/C values for exterior columns are much larger than interior ones, with enveloped median value around 0.28. As mentioned in Section 7.5.2, there would be a significant reduction (about 90% reduction) of tension capacity if the vulnerable PJP welds were not remediated. For compression, the peak median compression force demand to capacity ratio is very close to 0.9 the D/C ratios in compression exceed 0.5 on many floors under the BSE-2E hazard-level ground motions for both exterior and interior columns. The calculation of demand-to-capacity ratio here does not include the contributions from bi-axial bending.

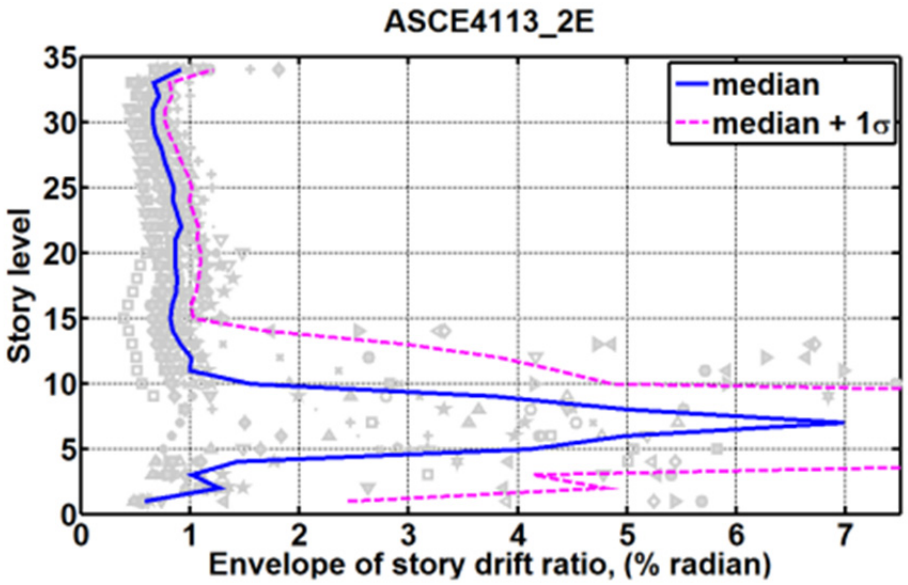

Figure 7.69 **Story drift envelope of Model 1c under BSE-2E hazard level events.**

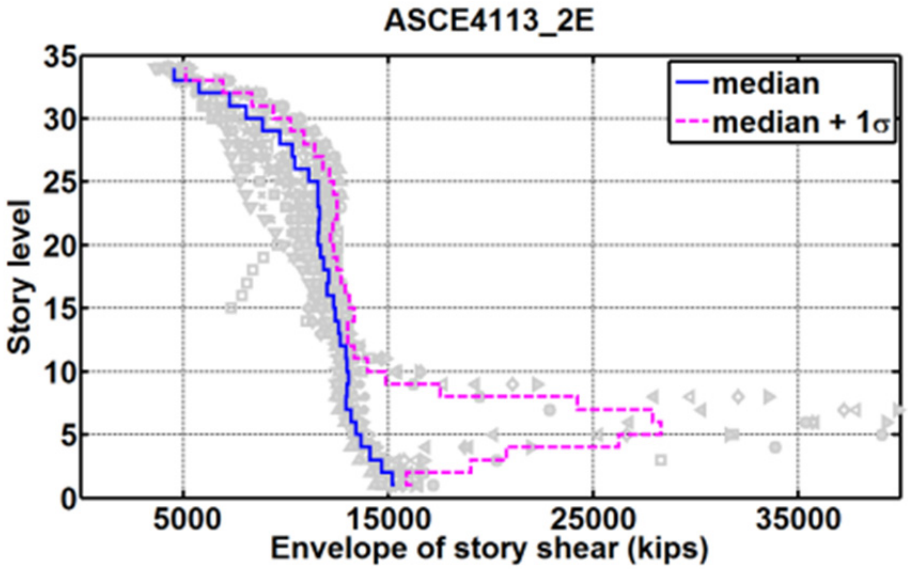

Figure 7.70 **Story shear envelope of Model 1c under BSE-2E hazard level events.**

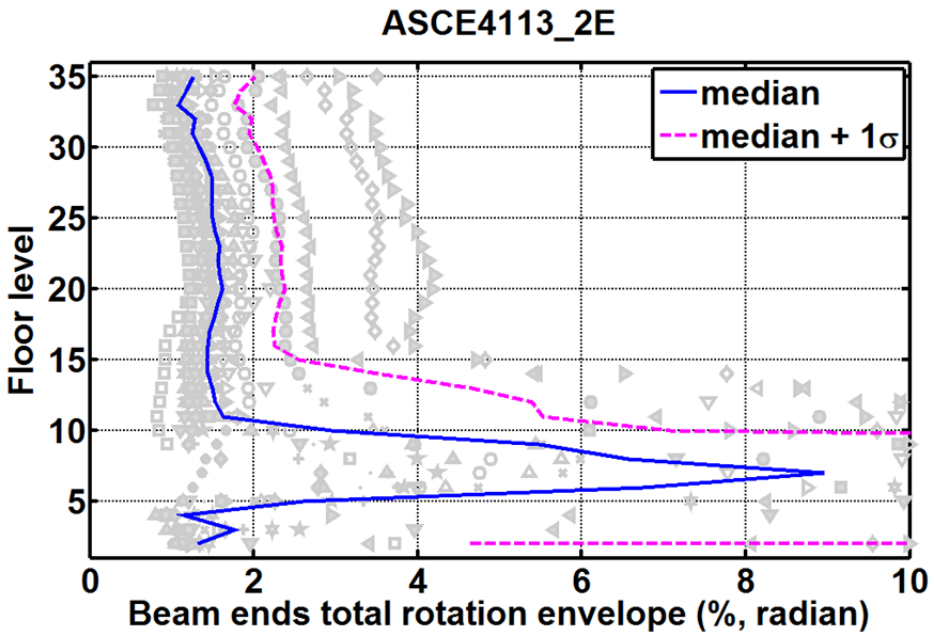

Figure 7.71 Beam ends total rotation envelope of Model 1c under BSE-2E hazard level events.

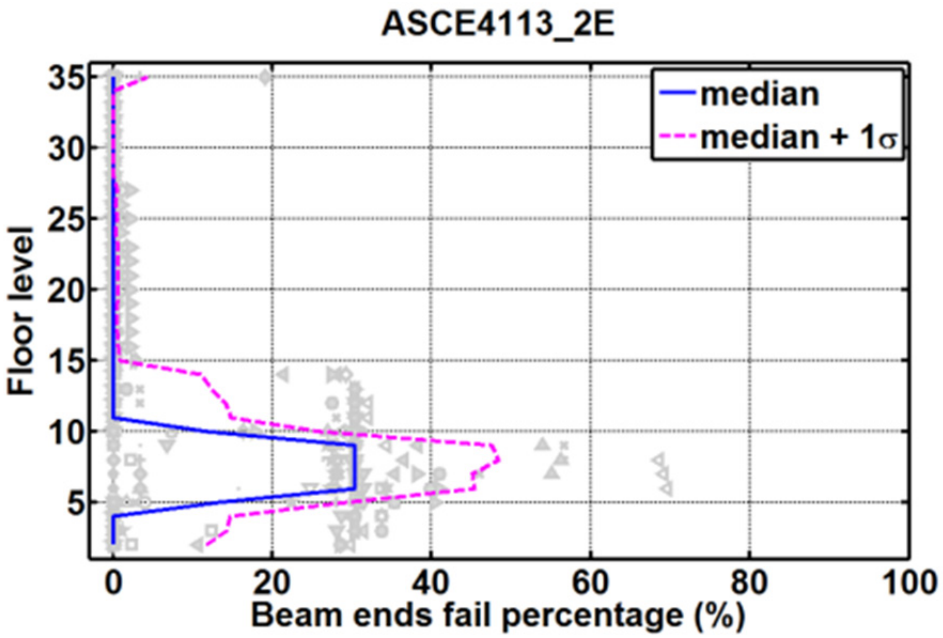

Figure 7.72 Beam ends failure percentage of Model 1c under BSE-2E hazard level events.

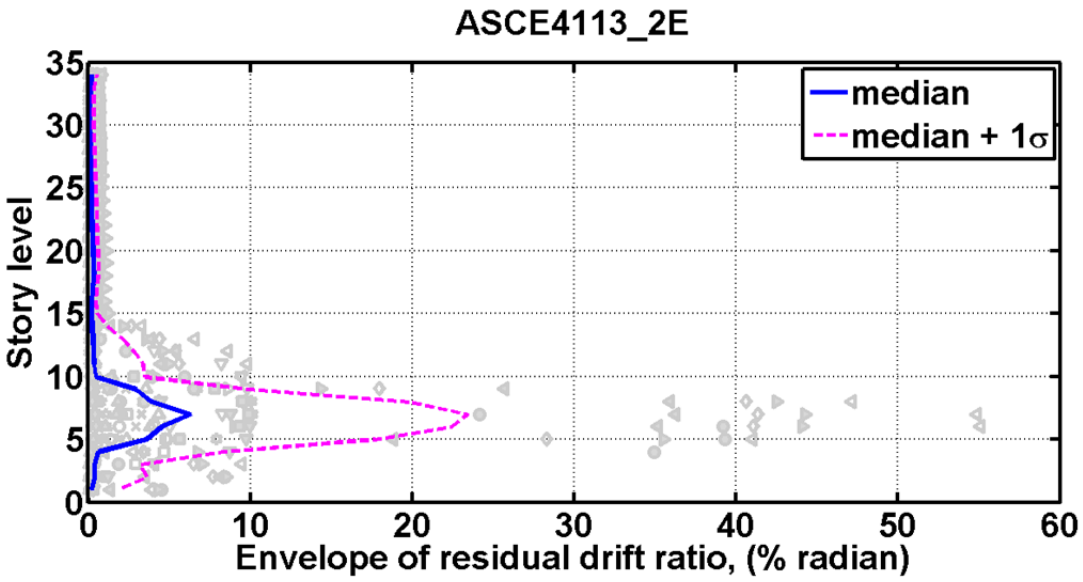

Figure 7.73 Residual drift envelope of Model 1c under BSE-2E hazard level events.

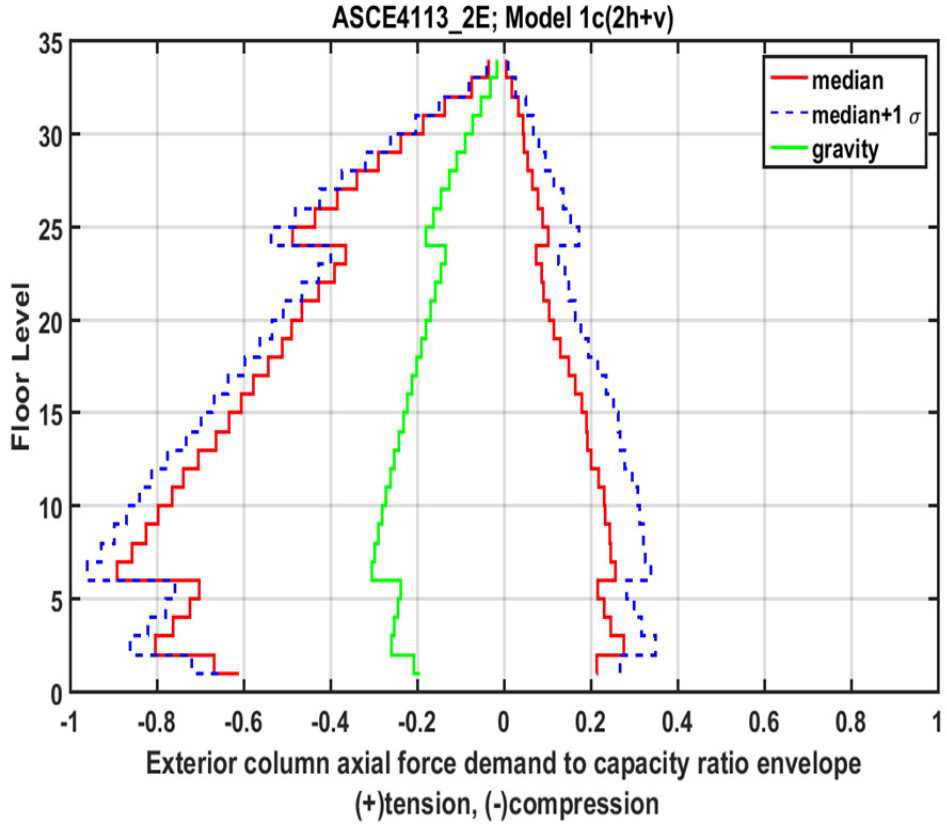

Figure 7.74 Column axial force demand to capacity ratios of exterior corner columns (group 1 columns; Model 1c; BSE-2E).

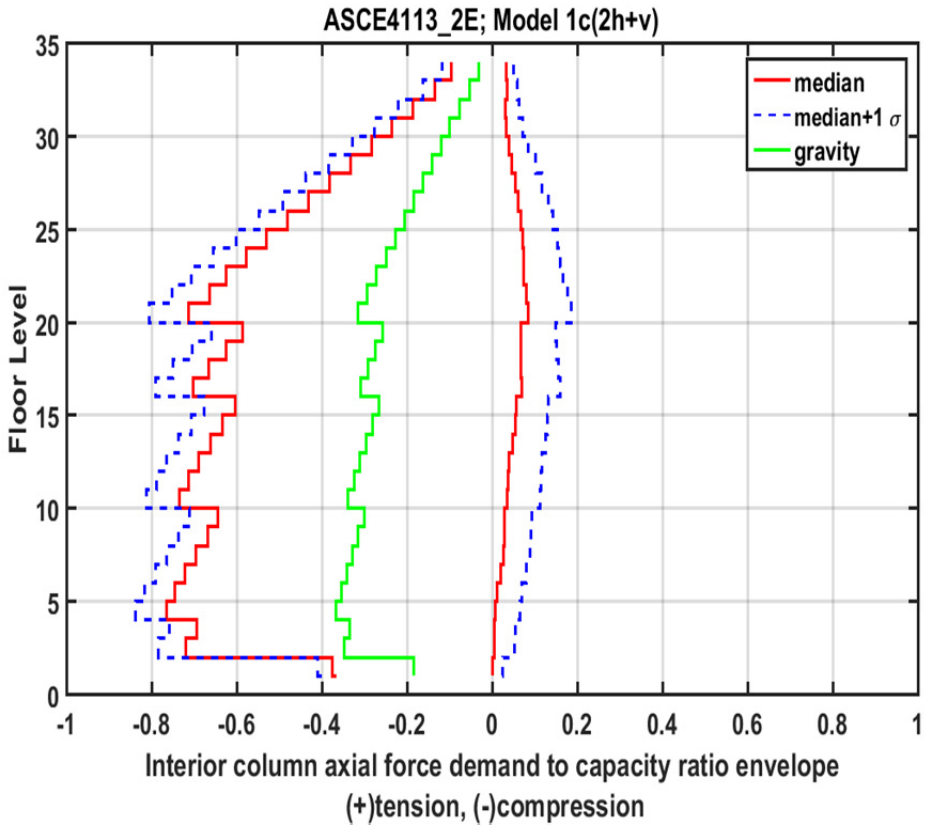

Figure 7.75 **Column axial force demand to capacity ratios of interior corner columns (group 5 columns; Model 1c; BSE-2E).**

7.5.4 Dynamic Responses under Events with 50% Probability of Exceedance in 30 Years (43-Year Mean Return Period)

Nonlinear dynamic analyses were also performed on Model 1c using the 43-years mean return period ground motions. Figure 7.76 presents the story-drift distribution over the height of case-study building under these service level events. The peak median story drift ratio was 0.47% at the mezzanine level, and most floor levels had median drift ratios around 0.3%. Figure 7.77 shows that the median base shear force demand was around 8,000 kips. The median peak beam end total rotation demand for this hazard was 0.68% (Figure 7.78) and occurred in the upper half of the building. No connection failures or permanent story drifts were observed. The median story drifts of Model 1c were about 92% of the median dynamic responses of Model 1d*. This is proportional to the period ratio for Model 1d* and Model 1c. Since the structure is essentially elastic for these records, one of the main differences between Model 1c and Model 1d* is the cladding weight. Assuming that the displacement is proportional to period, and period is proportional to a structures mass, one would expect a change in response of $\sqrt{(1-15\%)} \approx 0.92$, consistent with the change observed.

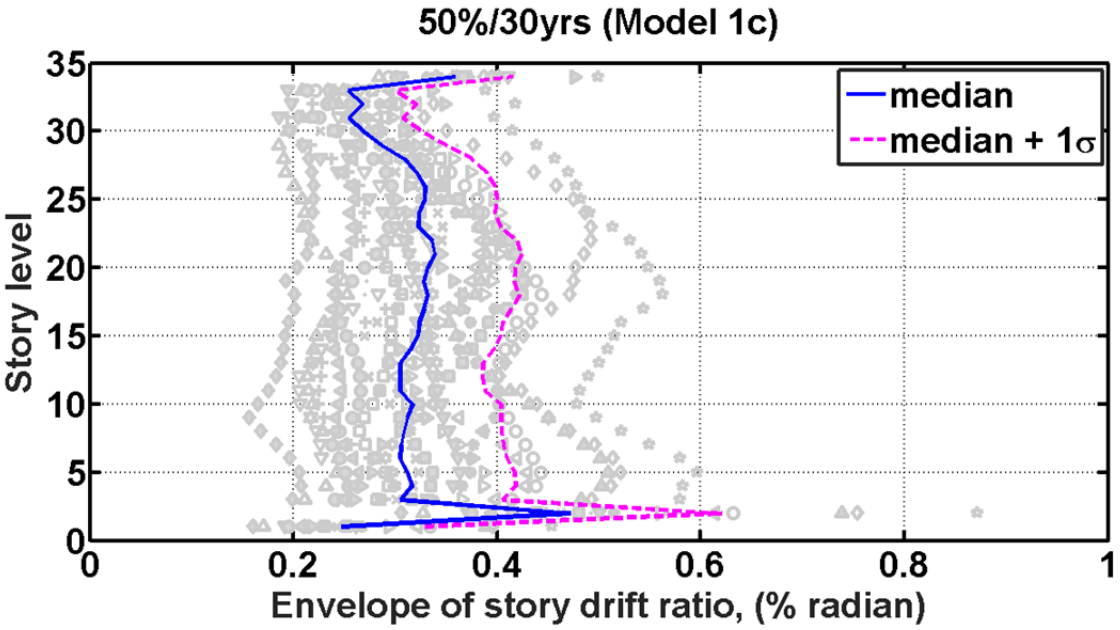

Figure 7.76 Story-drift envelope of Model 1c under 50%/30yrs hazard-level ground motions.

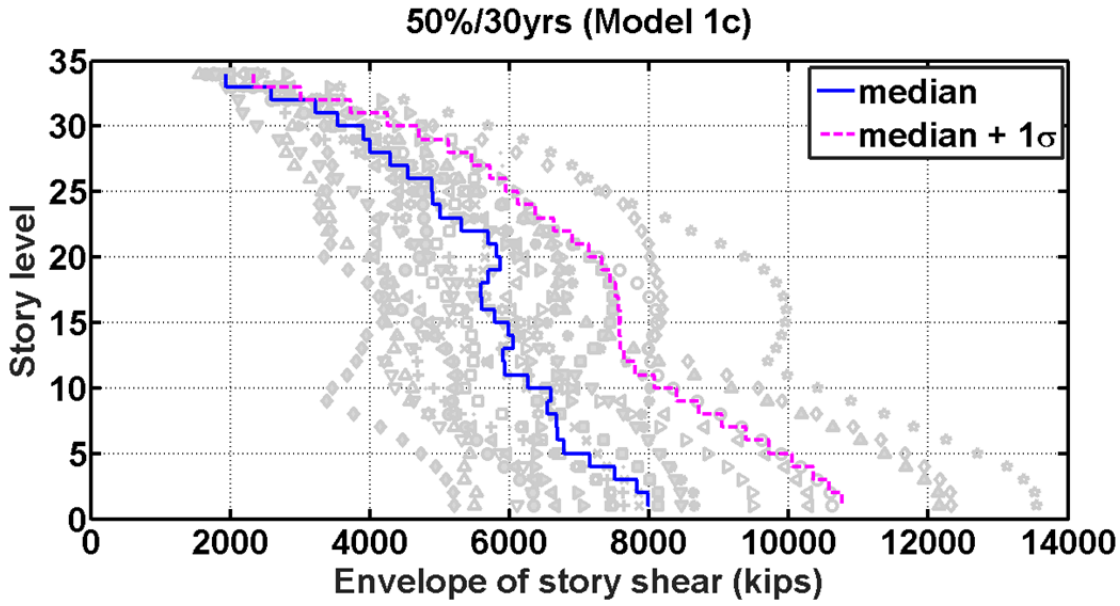

Figure 7.77 Story shear envelope of Model 1c under 50%/30yrs hazard level ground motions.

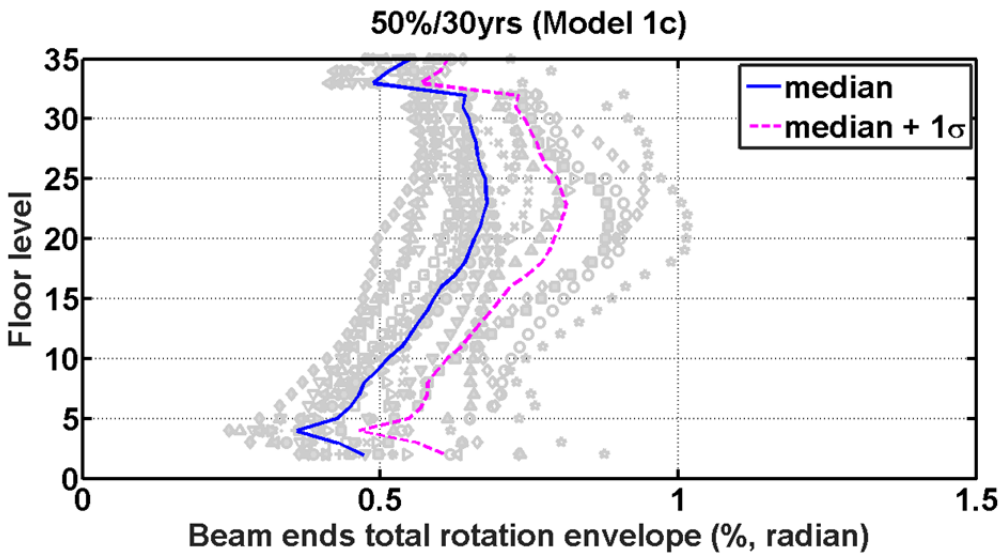

Figure 7.78 **Beam ends total rotation envelope of Model 1c under 50%/30yrs hazard-level ground motions.**

7.6 EFFECT OF VERTICAL COMPONENT OF GROUND-MOTION

The ASCE 41-13 evaluation procedure does not require consideration of the vertical component of ground shaking. Results of dynamic analysis of Model 1c are compared in this section to assess the importance of the vertical component of excitation on the performance of tall buildings. Specifically, cases with and without the vertical component of ground motion are compared. In this section, a few selected ground motions from the BSE-1E and BSE-2E ground motion sets are compared. However, Appendix F (electronic file) contains a comprehensive comparison for all 20 ground motions at the BSE-1E and BSE-2E hazard levels. Table 7.3 lists six ground motion records selected from BSE-1E and BSE-2E hazard level ground-motion sets. All of the selected ground motions were recorded in California.

From the roof displacement histories, orbital plots, and base shear versus roof displacement hysteresis loops shown in Figures 7.79–7.96, it appears that the vertical component of excitation has little effect on global response at the BSE-1E level, but can have a significant effect for some records at the BSE-2E level of excitation. However, the vertical motion does not have a consistent consequence. That is, in some cases it may increase response (compare the blue solid line and red dashed line in Figure 7.97), but in another case it may do the opposite (see the red dashed line in Figure 7.82). Under BSE-2E hazard level events, the presence of vertical motion typically results in larger residual roof displacements (see the blue solid line in Figures 7.88 and 7.98), and it may amplify the displacement trend of a building during collapse as shown in Figure 7.99 (note the blue solid line).

Another important aspect investigated was the axial force in the columns. Vertical excitation might affect the axial demands in columns significantly if the magnitude of excitation is large. As before, column demand versus capacity ratio plot for a group of corner columns (Group 1 in Figure 7.23) are presented to investigate the effects of the vertical excitations; see Figure 7.100 and Figure 7.101. The red solid line and blue dash line are median values of response under two-

horizontal excitations only and three-component excitations, respectively. Under smaller earthquakes, the discrepancy between two cases is negligible, with only a slight increase for the cases where vertical excitation was included. When the earthquake becomes larger, the difference becomes larger for two scenarios (Figure 7.101). For cases where vertical excitations were included, there is a 10%-20% increase of the peak demand to capacity ratios. In general, the vertical excitation increased the tension and compression demands, rendering the columns more vulnerable to failure.

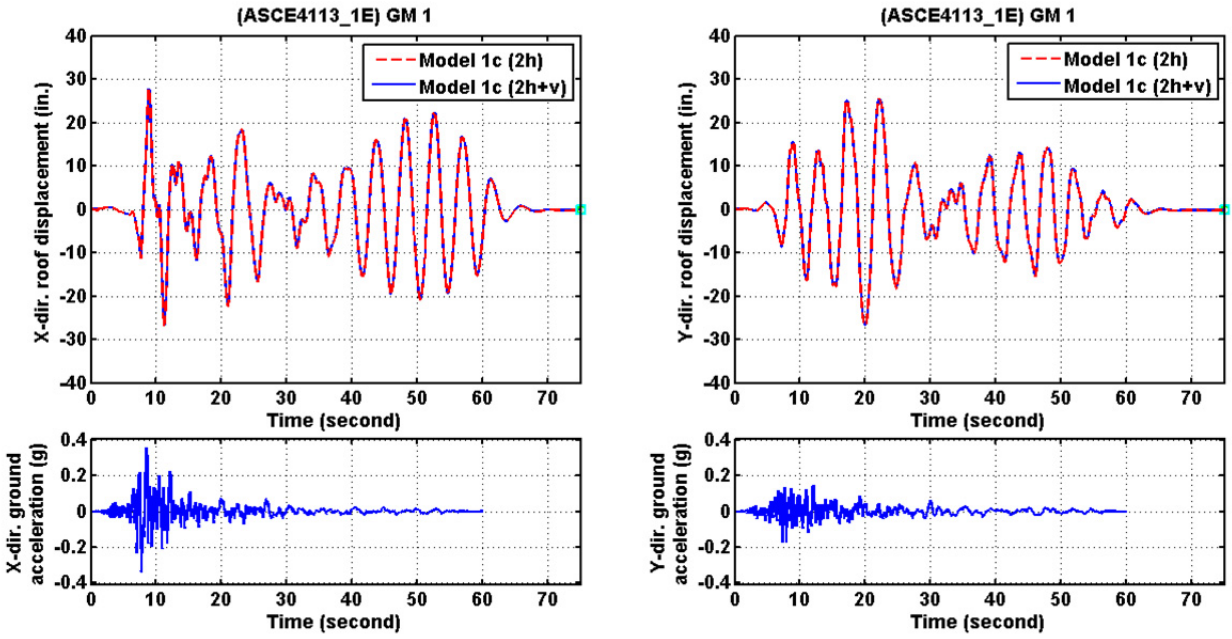

Figure 7.79 Roof displacement histories under BSE-1E level ground motion number 1 with and without vertical component motions (Model 1c).

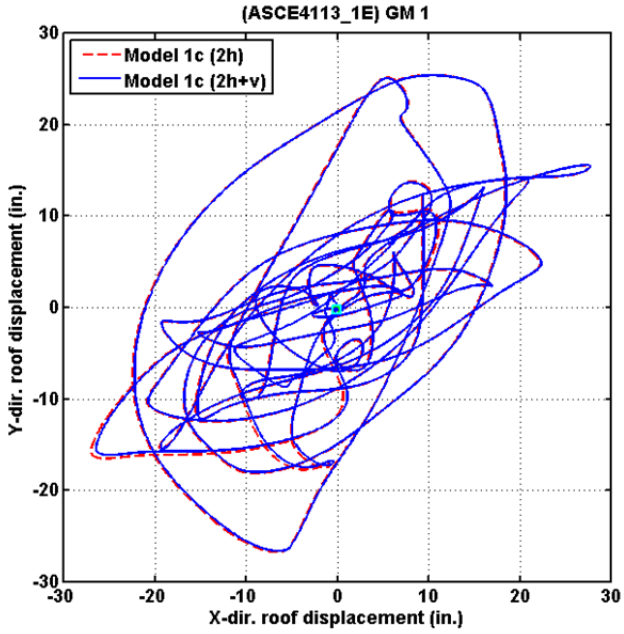

Figure 7.80 Roof displacement orbits under BSE-1E level ground motion number 1 with and without vertical component motions (Model 1c).

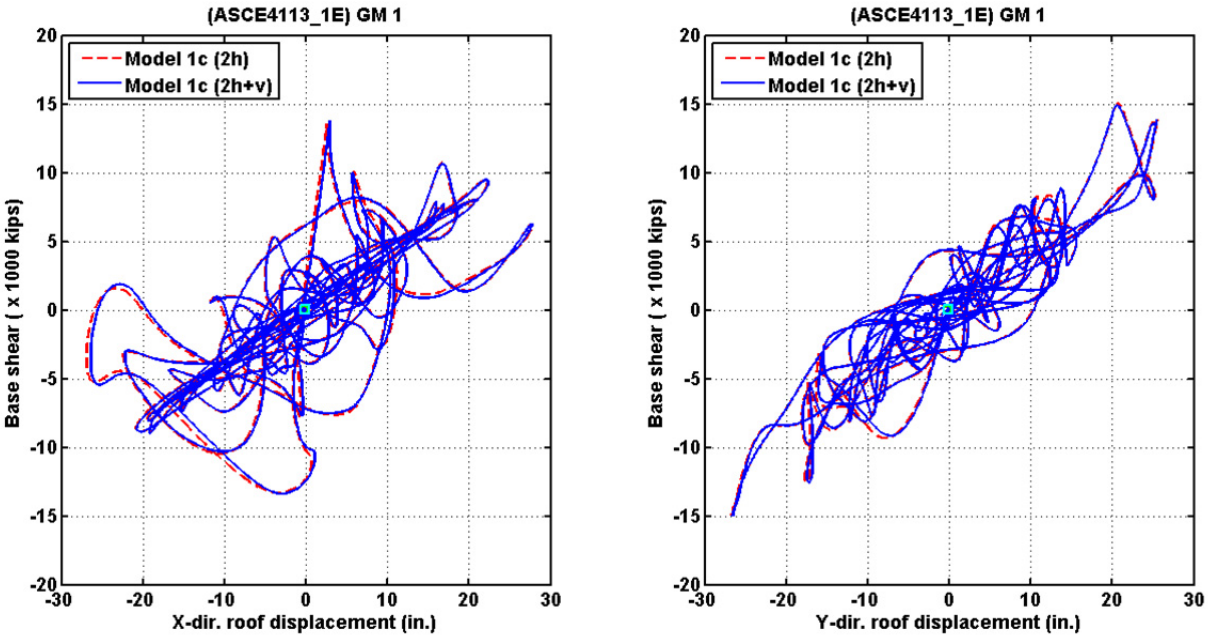

Figure 7.81 Base shear versus roof displacement relationships under BSE-1E level ground motion number 1 with and without vertical component motions (Model 1c).

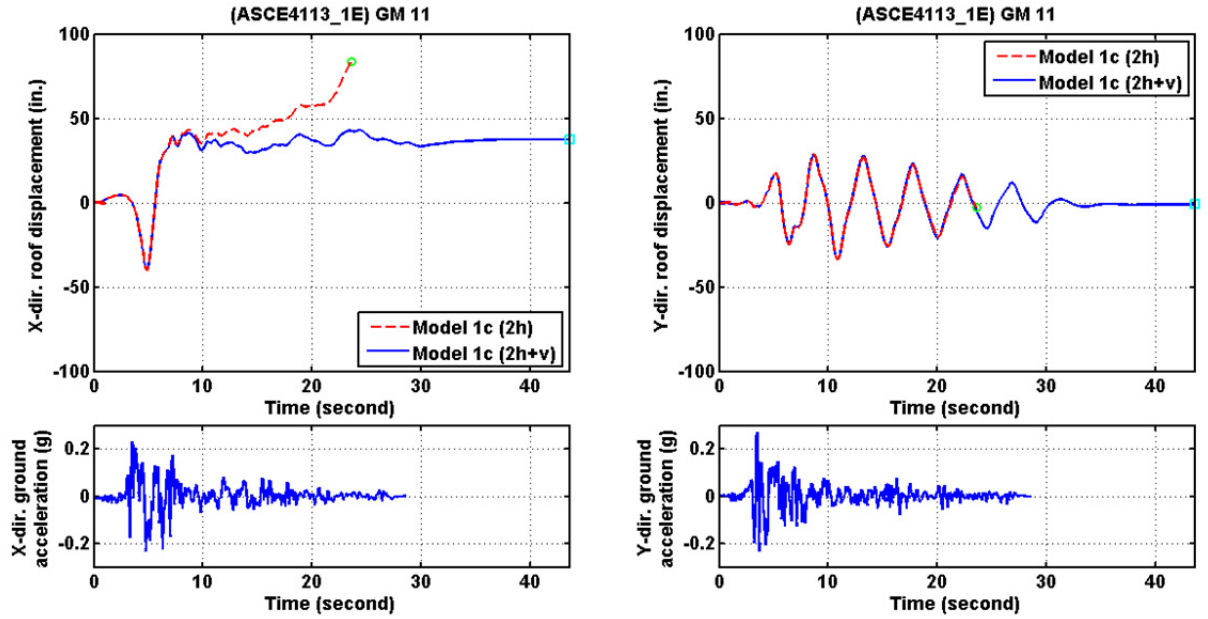

Figure 7.82 Roof displacement histories under BSE-1E level ground motion number 11 with and without vertical component motions (Model 1c).

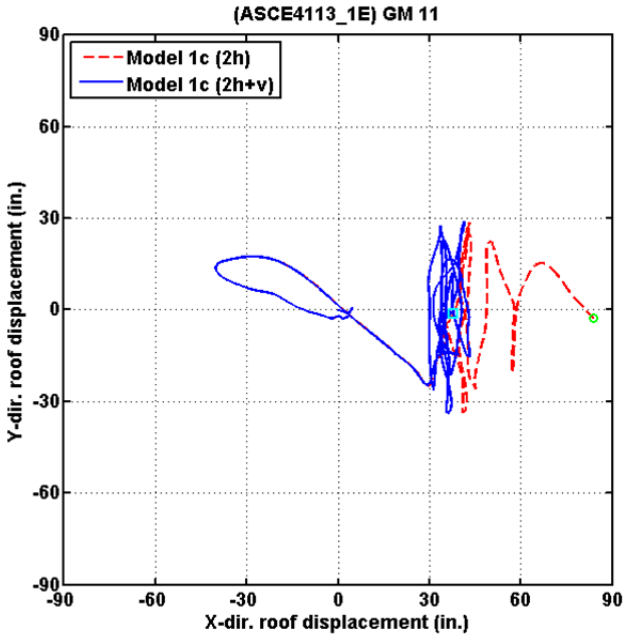

Figure 7.83 Roof displacement orbits under BSE-1E level ground motion number 11 with and without vertical component motions (Model 1c).

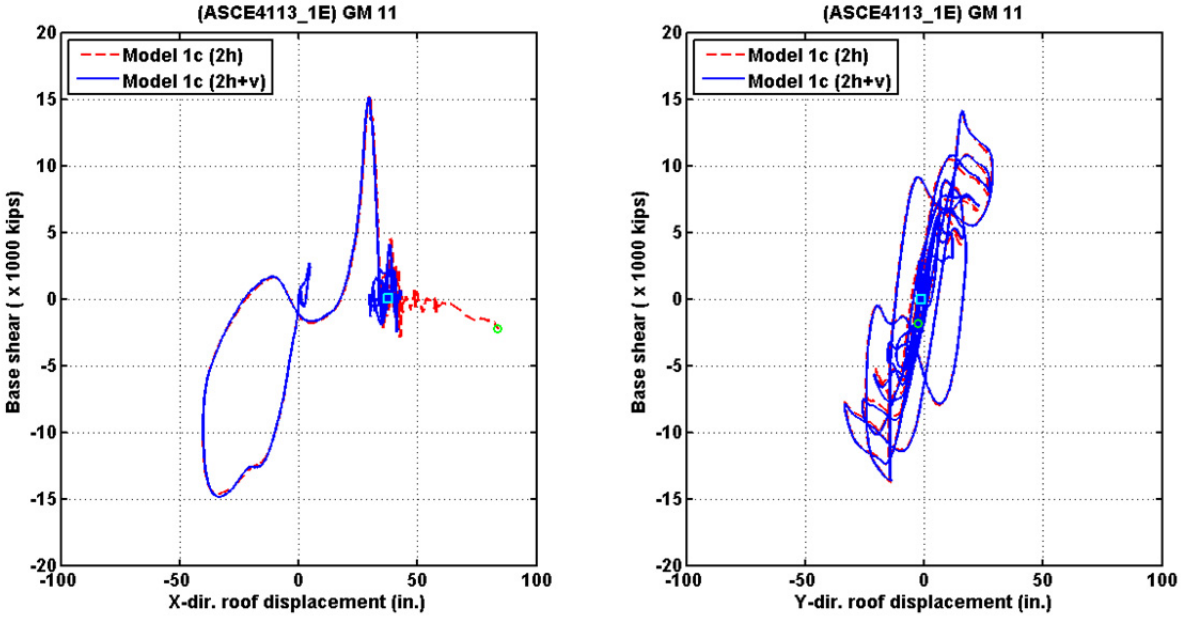

Figure 7.84 Base shear versus roof displacement relationships under BSE-1E level ground motion number 11 with and without vertical component motions (Model 1c).

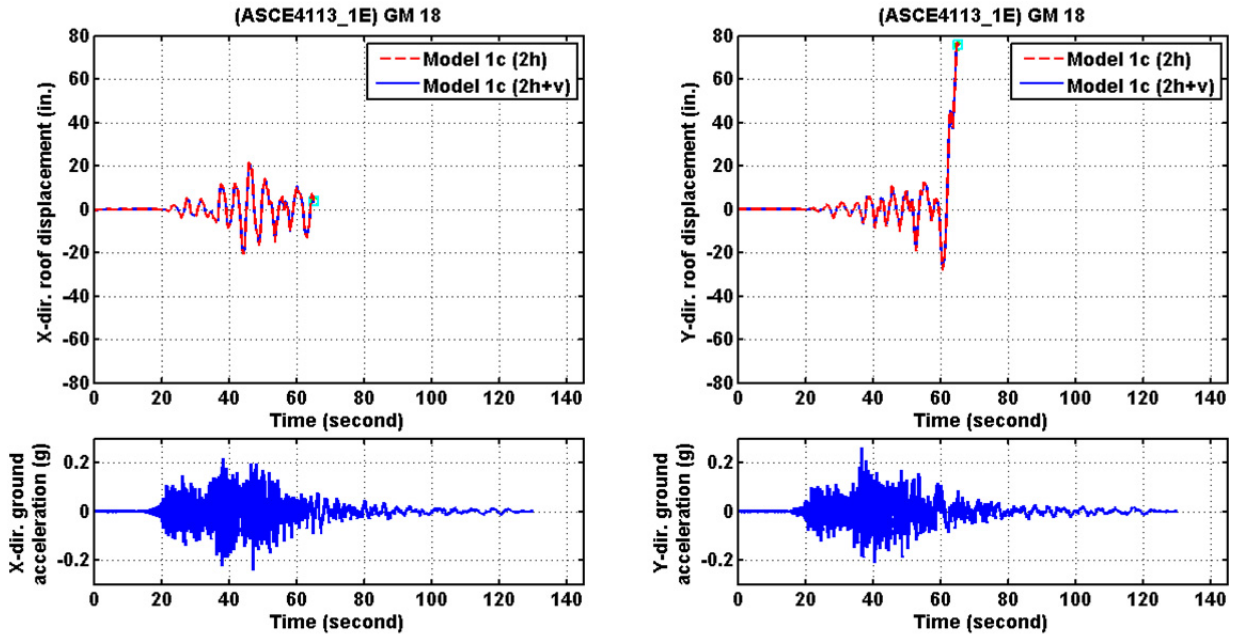

Figure 7.85 Roof displacement histories under BSE-1E level ground motion number 18 with and without vertical component motions (Model 1c).

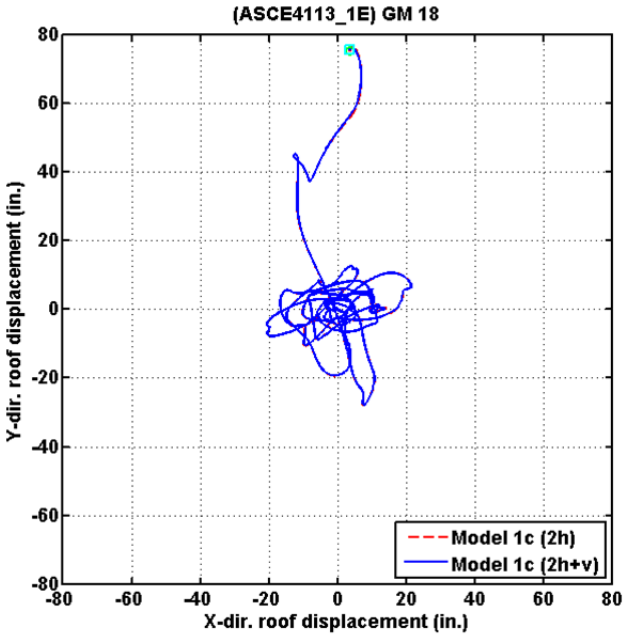

Figure 7.86 Roof displacement orbits under BSE-1E level ground motion number 18 with and without vertical component motions (Model 1c).

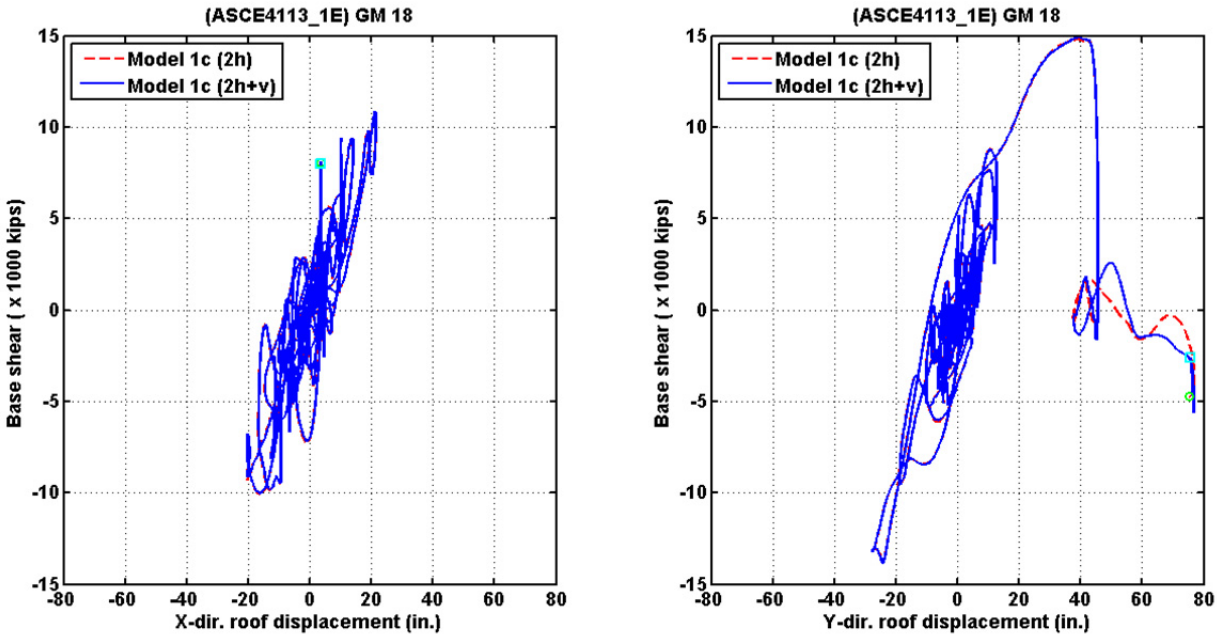

Figure 7.87 Base shear versus roof displacement relationships under BSE-1E level ground motion number 18 with and without vertical component motions (Model 1c).

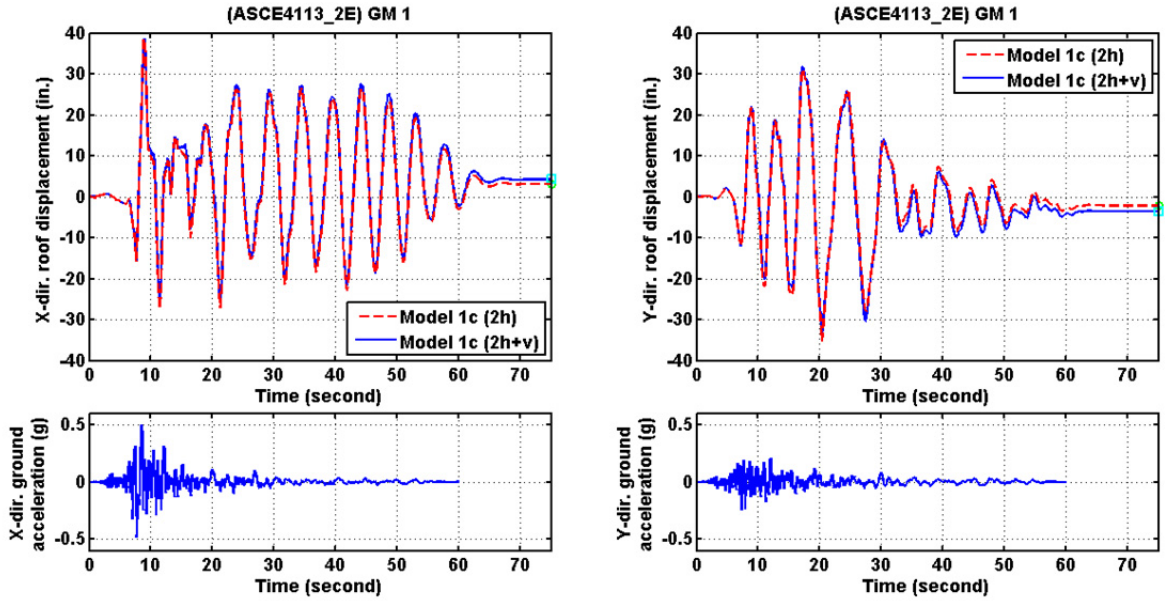

Figure 7.88 Roof displacement histories under BSE-2E level ground motion number 1 with and without vertical component motions (Model 1c).

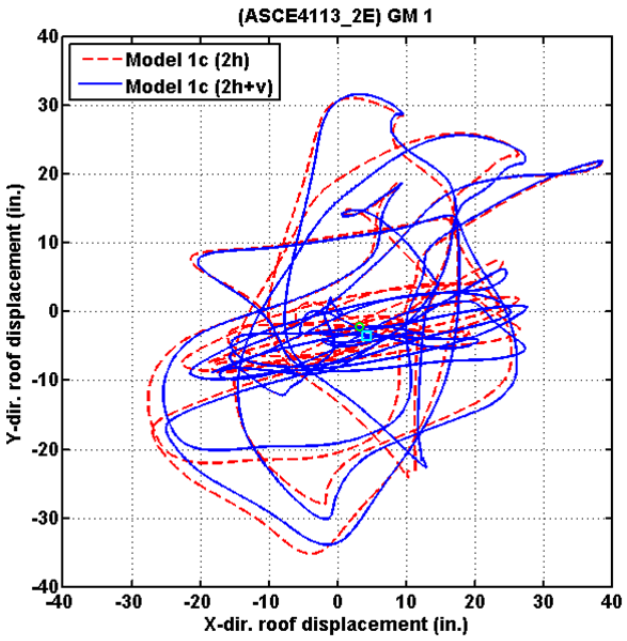

Figure 7.89 Roof displacement orbits under BSE-2E level ground motion number 1 with and without vertical component motions (Model 1c).

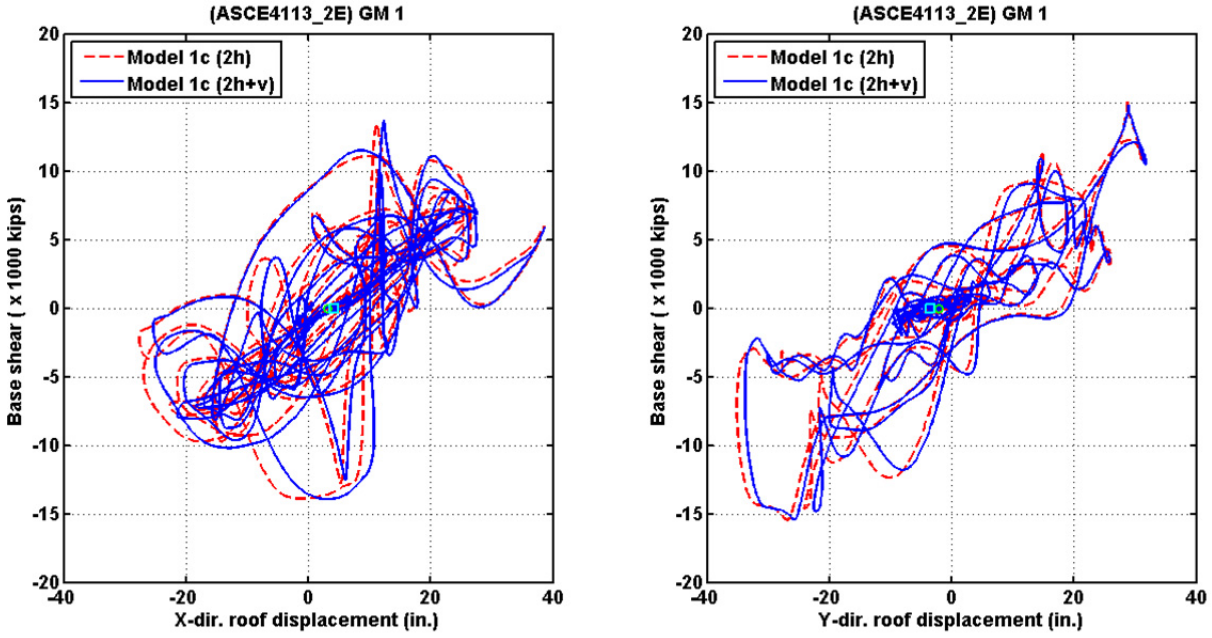

Figure 7.90 Base shear versus roof displacement relationships under BSE-2E level ground motion number 1 with and without vertical component motions (Model 1c).

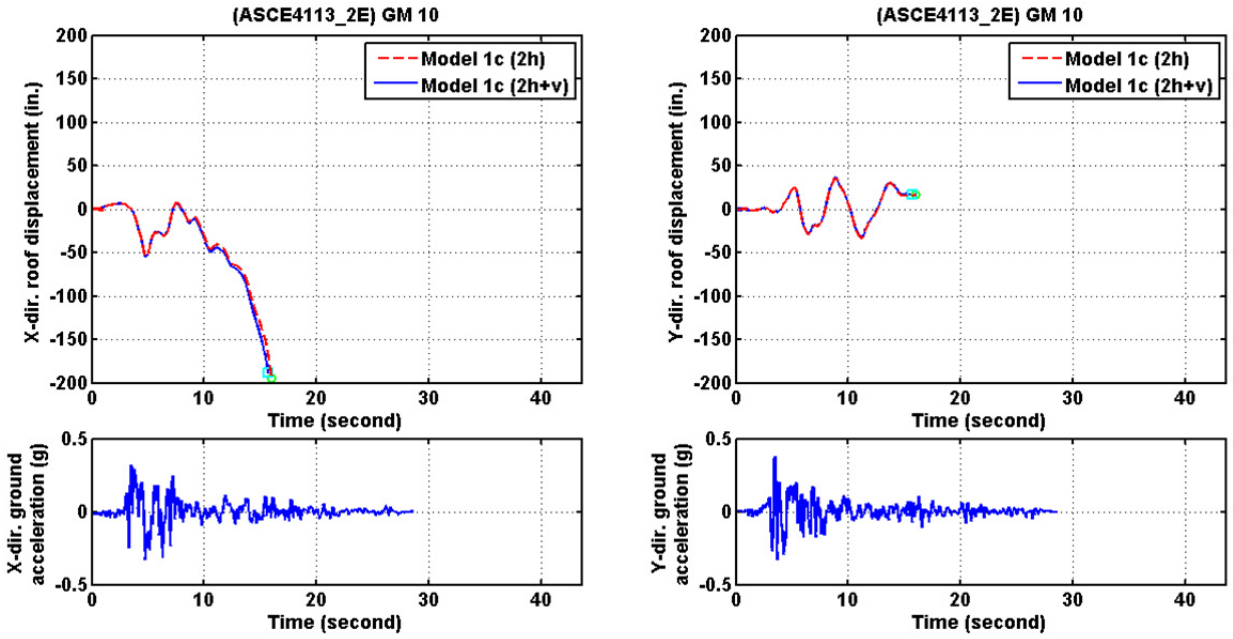

Figure 7.91 Roof displacement histories under BSE-2E level ground motion number 10 with and without vertical component motions (Model 1c).

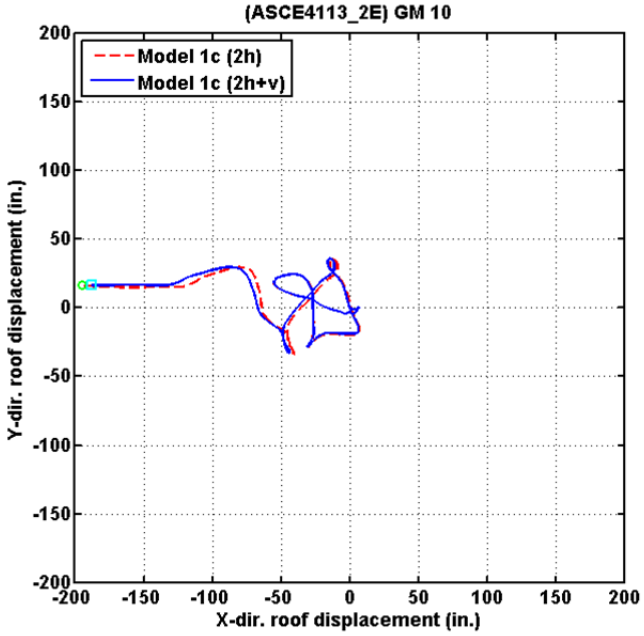

Figure 7.92 Roof displacement orbits under BSE-2E level ground motion number 10 with and without vertical component motions (Model 1c).

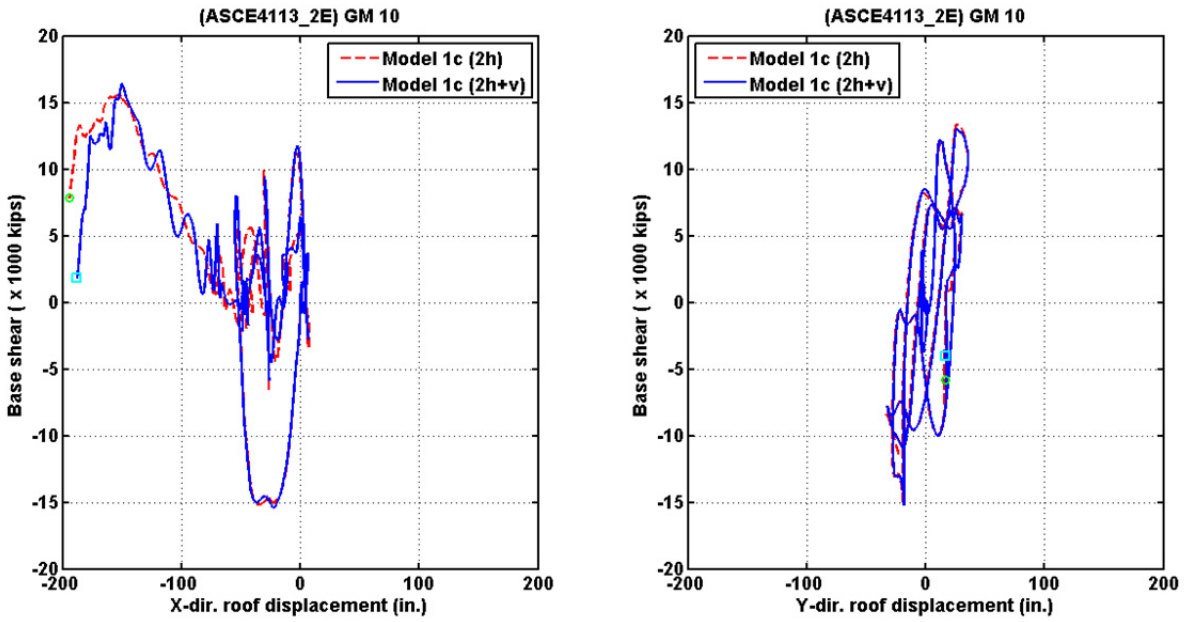

Figure 7.93 Base shear versus roof displacement relationships under BSE-2E level ground motion number 10 with and without vertical component motions (Model 1c).

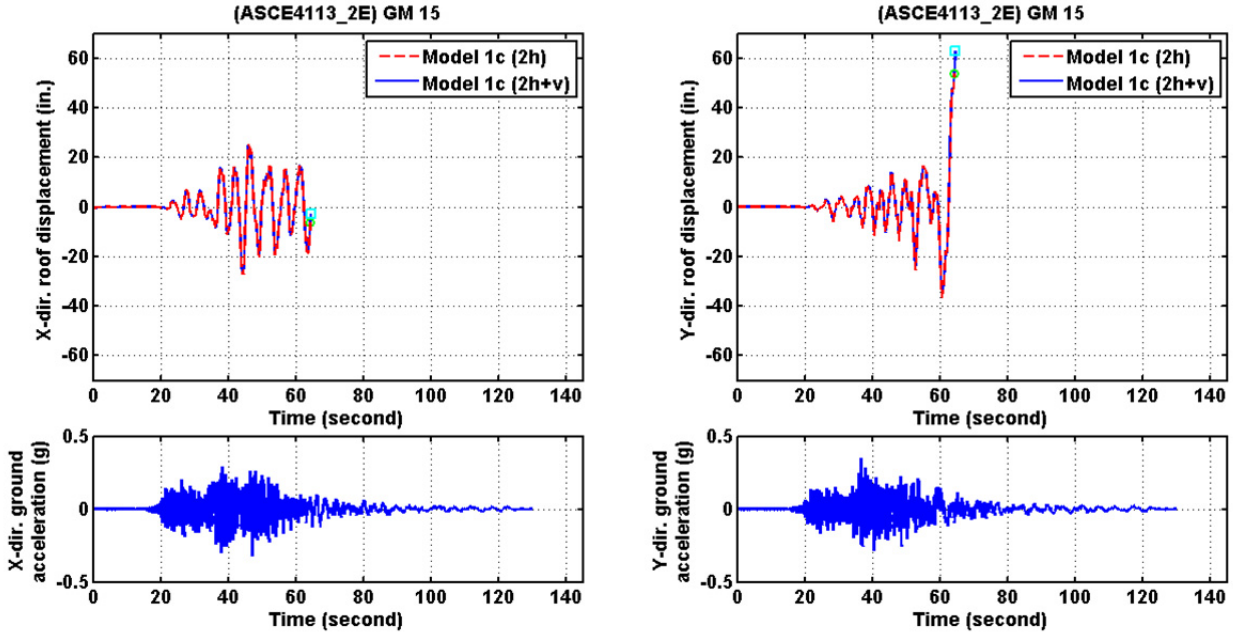

Figure 7.94 Roof displacement histories under BSE-2E level ground motion number 15 with and without vertical component motions (Model 1c).

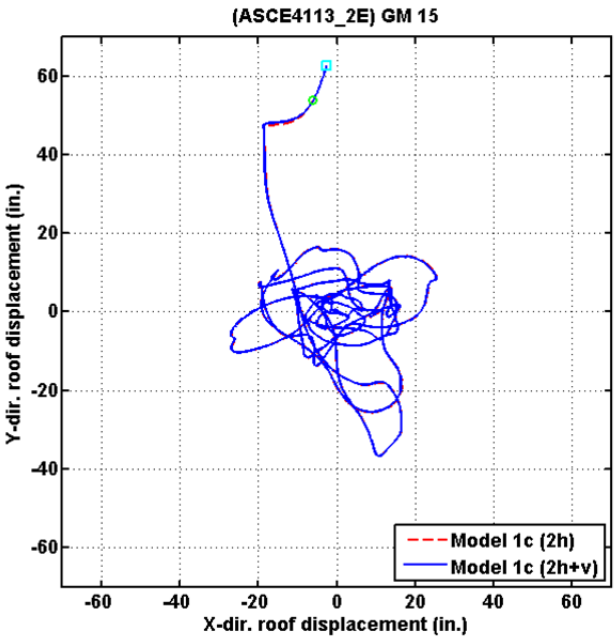

Figure 7.95 Roof displacement orbits under BSE-2E level ground motion number 15 with and without vertical component motions (Model 1c).

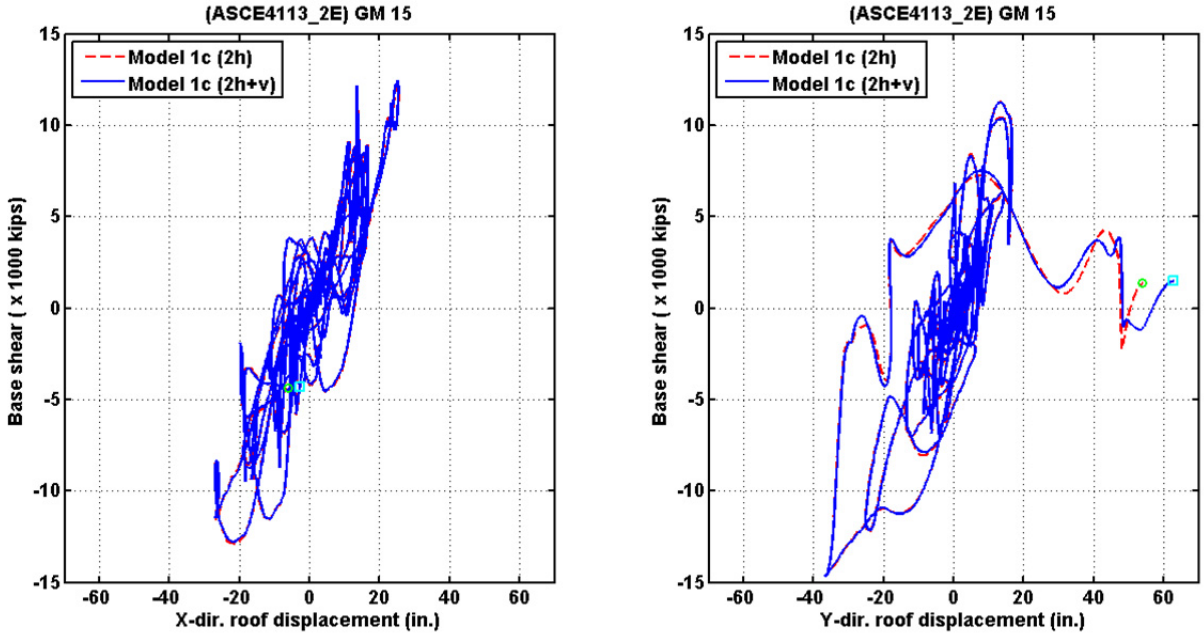

Figure 7.96 Base shear versus roof displacement relationships under BSE-2E level ground motion number 15 with and without vertical component motions (Model 1c).

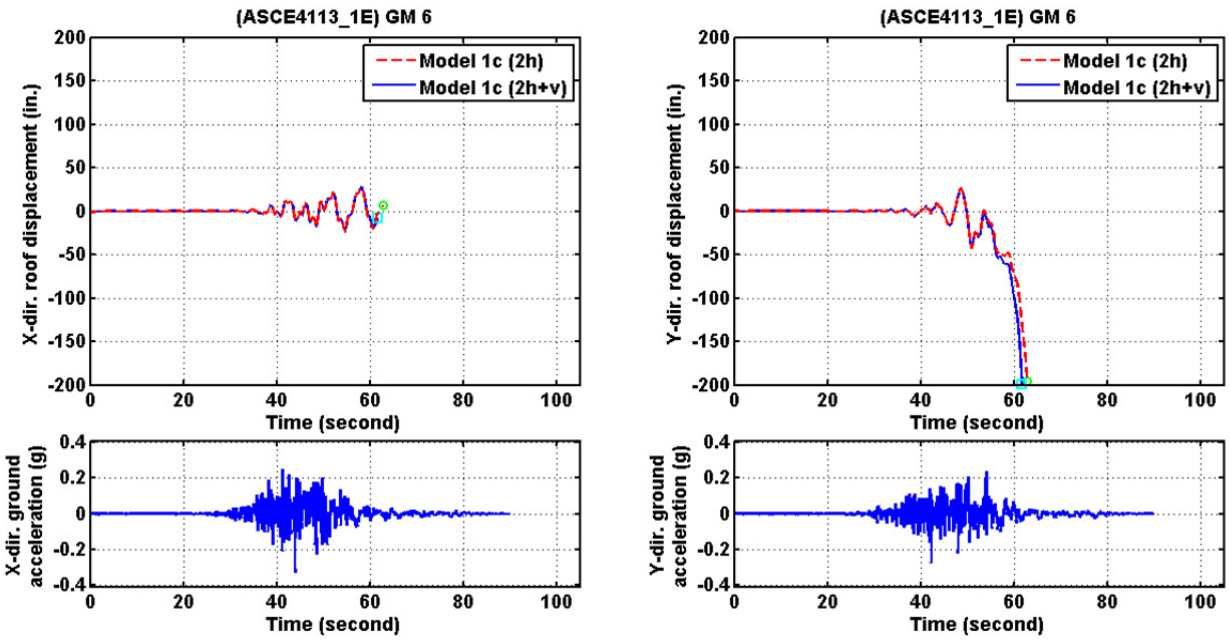

Figure 7.97 Roof displacement histories under BSE-1E level ground motion number 6 with and without vertical component motions (Model 1c).

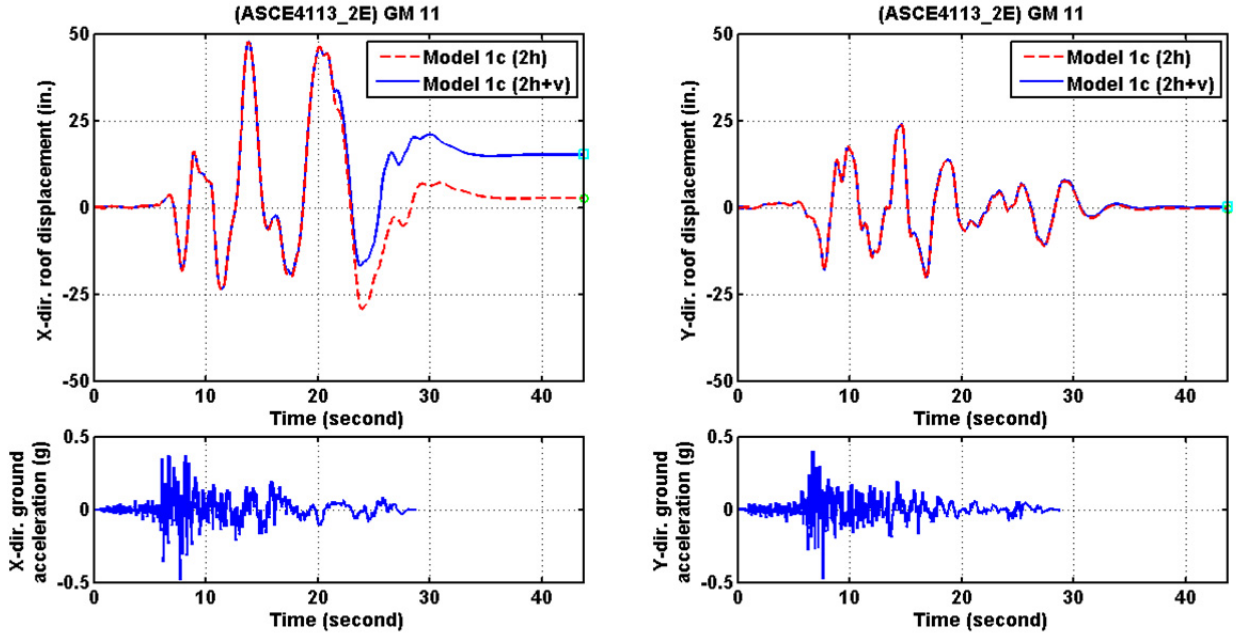

Figure 7.98 Roof displacement histories under BSE-2E level ground motion number 11 with and without vertical component motions (Model 1c).

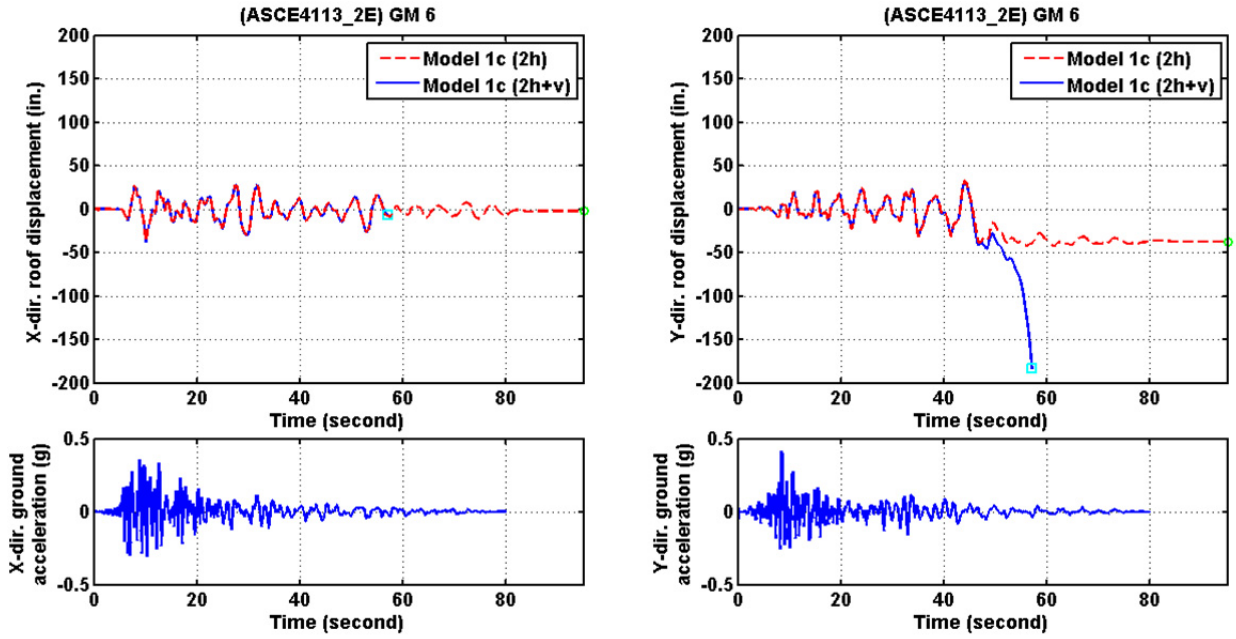

Figure 7.99 Roof displacement histories under BSE-2E level ground motion number 6 with and without vertical component motions (Model 1c).

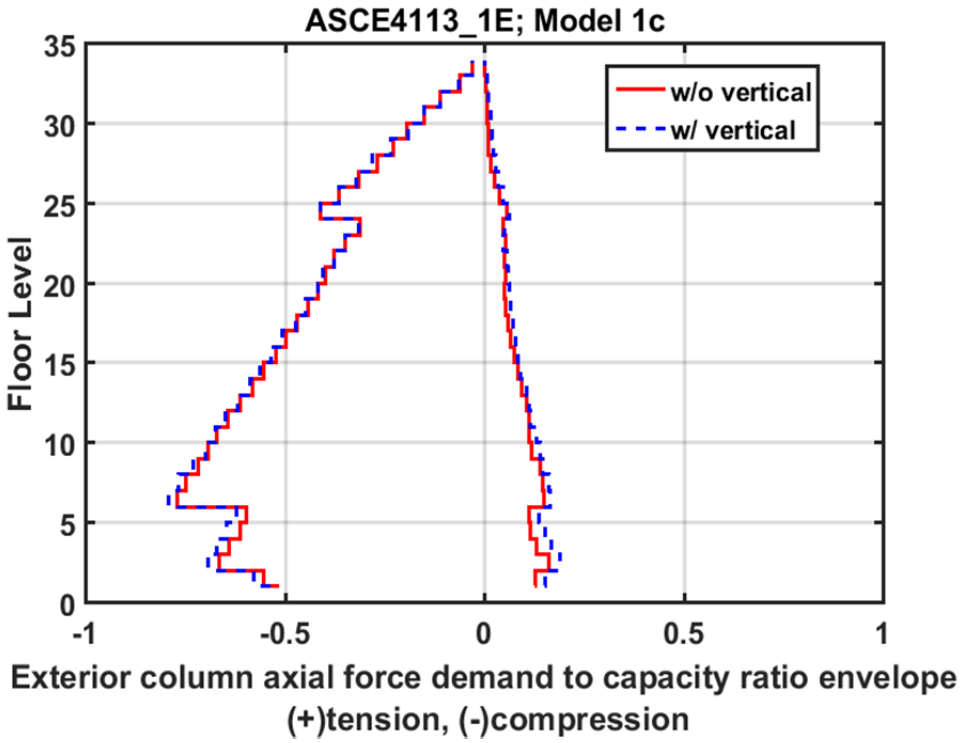

Figure 7.100 Column axial force demand to capacity ratios of exterior corner columns (group 1 columns; Model 1c; BSE-1E).

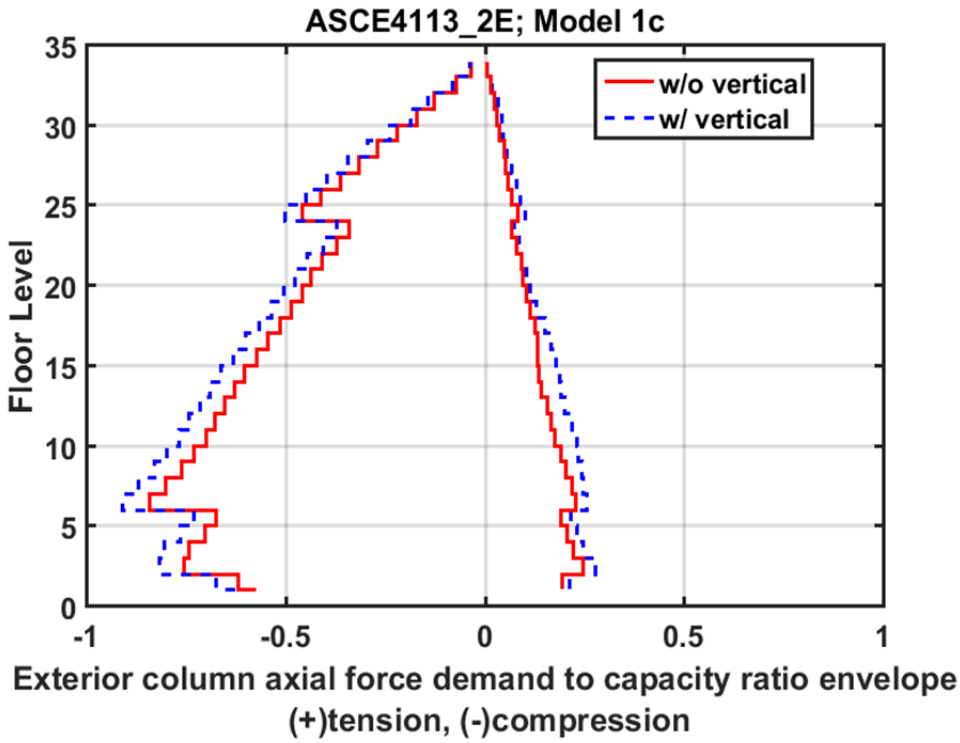

Figure 7.101 **Column axial force demand to capacity ratios of exterior corner columns (group 1 columns; Model 1c; BSE-2E).**

7.7 EFFECTS OF MECHANICAL BEHAVIOR OF BEAM-TO-COLUMN CONNECTIONS

Clearly, the response of case-study building is dependent to a great extent on the limited ductility and possible rapid deterioration and fracture of beam-to-column connections and column splices. To facilitate understanding of this behavior on the building's response, this section compares the dynamic results from different numerical models exhibiting different connection behavior. In this case, three models that have had the cladding removed are compared. Examined cases include: (1) both beam-to-column and column splice deterioration are modeled (Model 1d); (2) only beam-to-column deterioration is included (Model 1c); and (3) where all beam-to-column and column splice details have been locally retrofitted to avoid deterioration due to local buckling or fracture (Model 1a). Both BSE-1E and BSE-2E ground-motion datasets are considered. However, only the ground motions in Table 7.3 are presented in this section; Appendix G (electronic file) contains a comprehensive set of plots for all 40 records.

From the roof displacement histories, orbital plots, and base shear versus roof displacement hysteresis loops shown in Figures 7.102–7.119, it is obvious that the mechanical behavior of connections have a significant effect on the dynamic response. In general, the response of the baseline model with the column splice retrofits behaves similarly to the model without column splice retrofits until the point at which many column splices fail. Although the

column retrofits are seen generally to extend the life of the structure, in most cases this is only momentarily. Thus, column splice retrofit, while beneficial, does not seem an adequate strategy by itself, especially for the BSE-2E excitations.

Also, there is evidence of significant effective period lengthening for the models with connection or splice deterioration and fracture (Models 1d and 1c), as evidenced by comparing the roof displacement response histories with those for the fully ductile model (Model 1a); In particular, see Figures 7.102, 7.105, 7.111, and 7.114. The baseline model (Model 1c) also tends to have larger permanent roof displacements; see Figures 7.106, 7.109, 7.112, 7.115, and 7.118. Worth noting is that the peak roof displacements that occur after member fracturing and deterioration has occurred (as evidenced by significant period shifting in the response histories) were smaller in the baseline model (Model 1c) than for the fully ductile model (Model 1a); see Figures 7.102 and 7.111. In some cases, Model 1c hit the 10% story drift limit for normal termination, while the fully ductile model did not; see Figures 7.108, 7.114, and 7.117.

The peak base shear forces were not sensitive to the mechanical properties of connections; see Figures 7.104, 7.107, 7.110, 7.113, 7.116, and 7.119. Figures 7.120 to 7.121 show the median peak story drift ratios and median peak residual drift ratios between different models. Obviously the fully ductile model exhibits significant improvement in terms of the peak drift ratios and exhibits far better behaviors than the other models. Thus fixing all brittle beam-to-column connections could be considered as a feasible retrofit solution. From a practical point of view, however, it might be prohibitively expensive to fix all pre-Northridge connections in the existing building. Alternative cost-effective strategies will be explored in Chapter 8.

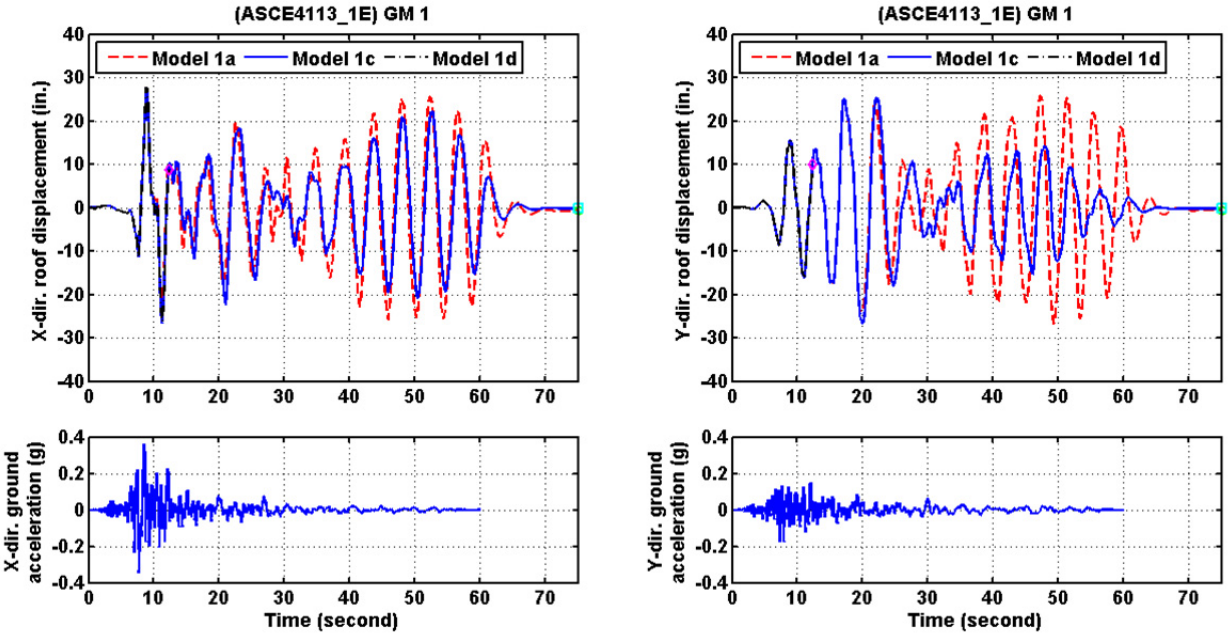

Figure 7.102 **Roof displacement histories under BSE-1E level ground motion number 1 of Model 1a, Model 1c, and Model 1d.**

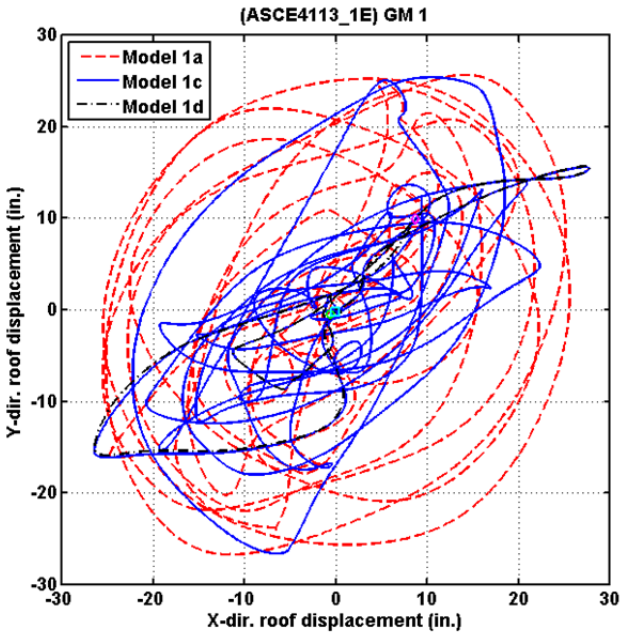

Figure 7.103 Roof displacement orbits under BSE-1E level ground motion number 1 for Model 1a, Model 1c, and Model 1d.

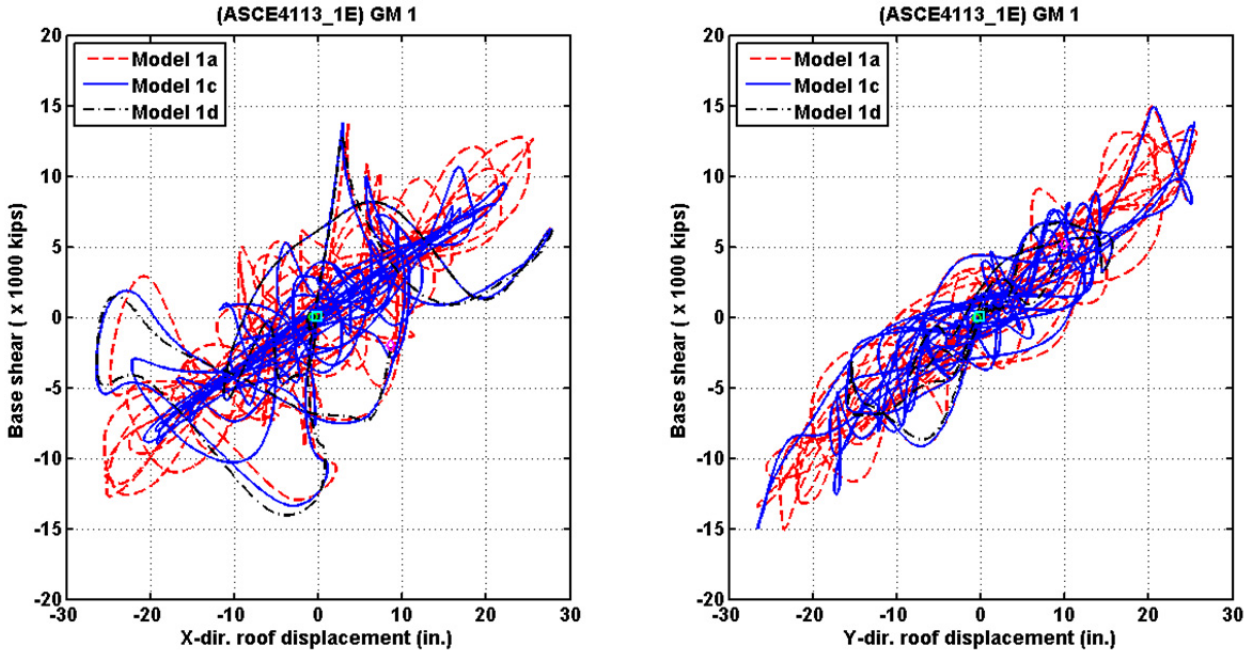

Figure 7.104 Base shear versus roof displacement relationships under BSE-1E level ground motion number 1 for Model 1a, Model 1c, and Model 1d.

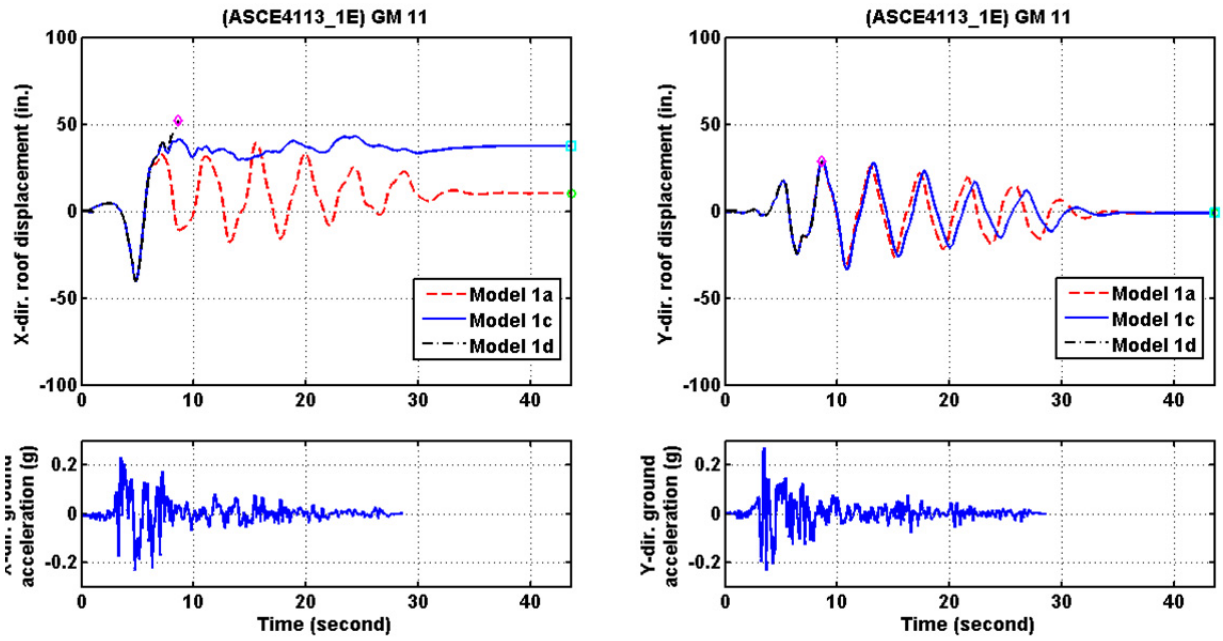

Figure 7.105 Roof displacement histories under BSE-1E level ground motion number 11 for Model 1a, Model 1c, and Model 1d.

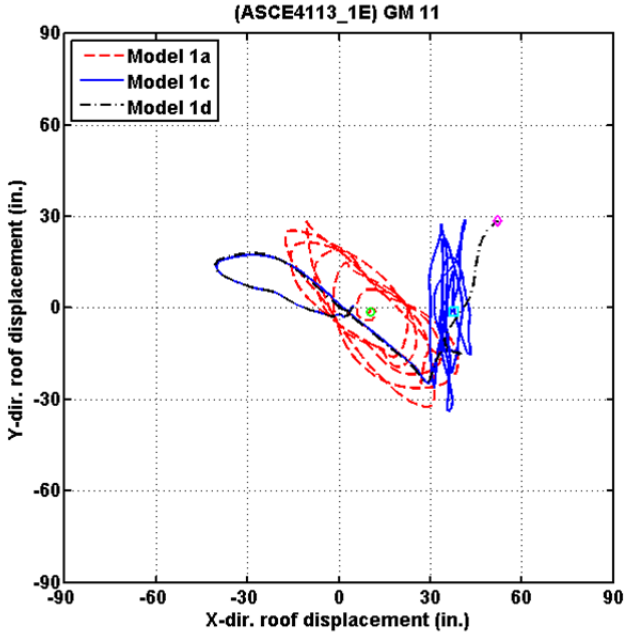

Figure 7.106 Roof displacement orbits under BSE-1E level ground motion number 11 for Model 1a, Model 1c, and Model 1d.

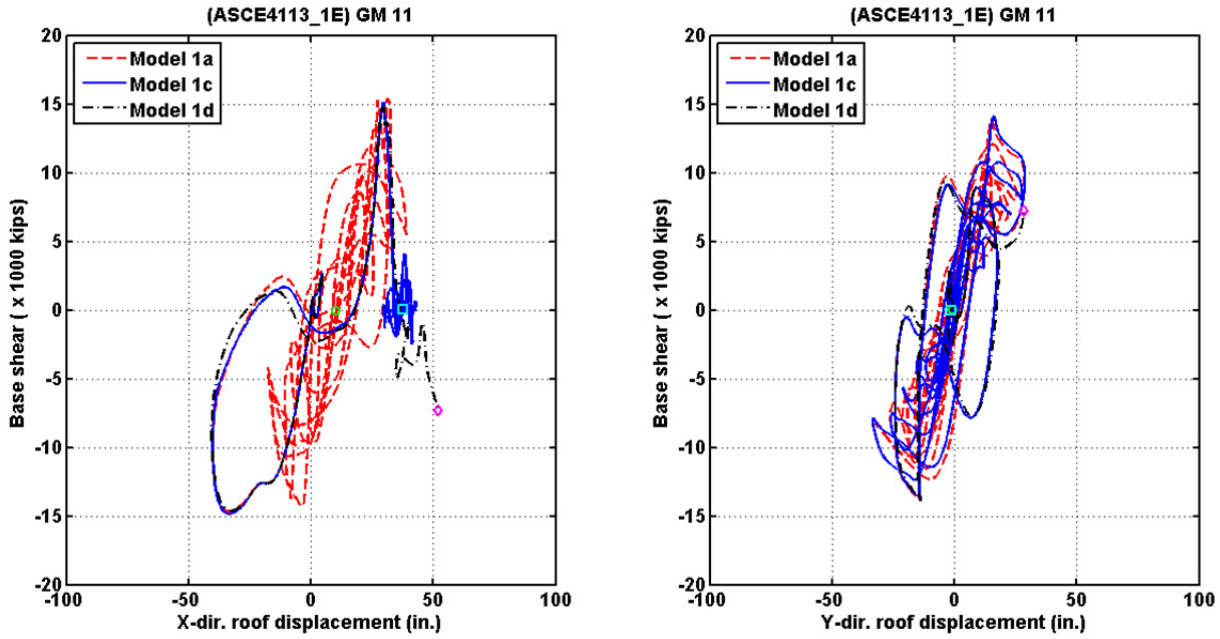

Figure 7.107 Base shear versus roof displacement relationships under BSE-1E level ground motion number 11 for Model 1a, Model 1c, and Model 1d.

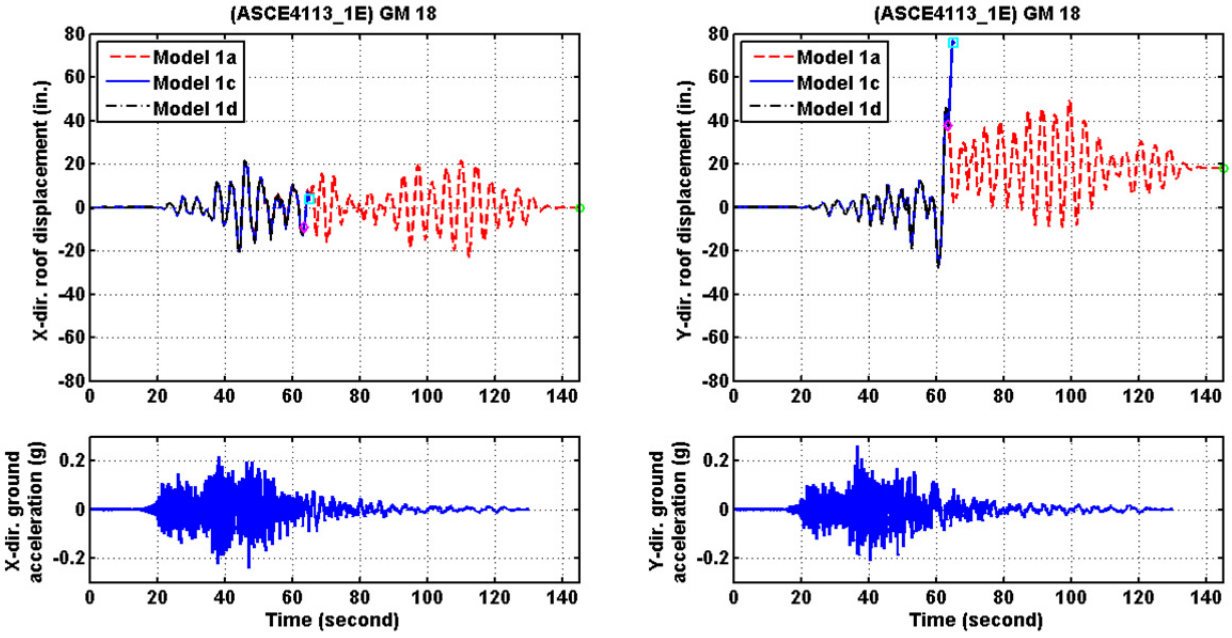

Figure 7.108 Roof displacement histories under BSE-1E level ground motion number 18 for Model 1a, Model 1c, and Model 1d.

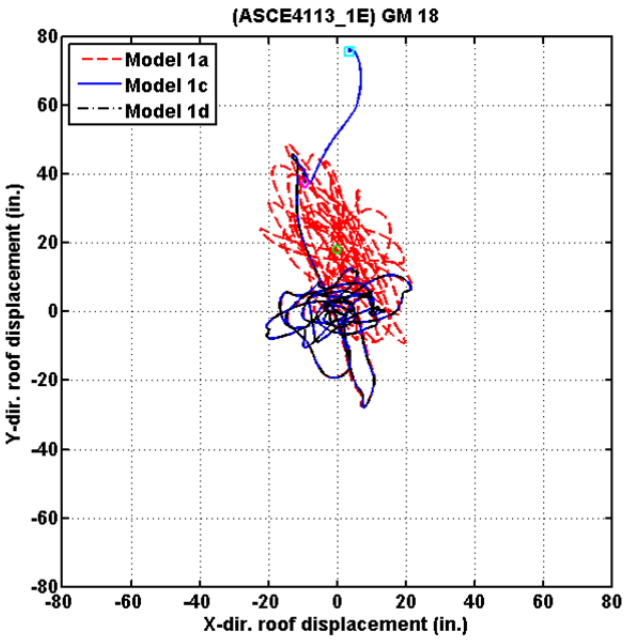

Figure 7.109 Roof displacement orbits under BSE-1E level ground motion number 18 for Model 1a, Model 1c, and Model 1d.

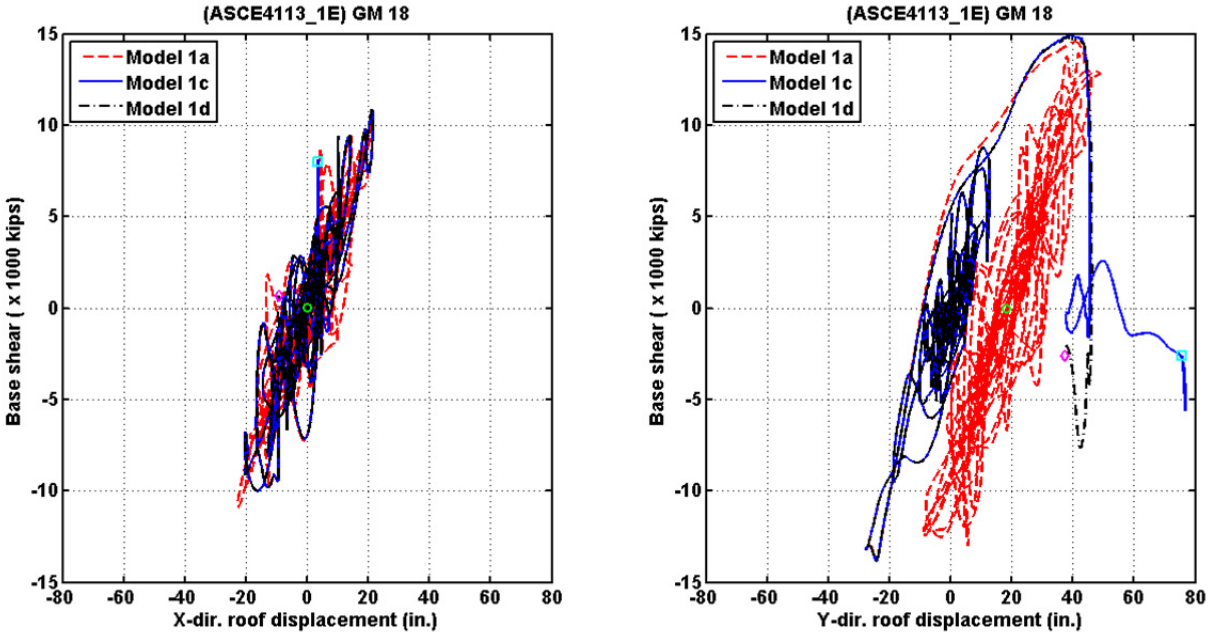

Figure 7.110 Base shear versus roof displacement relationships under BSE-1E level ground motion number 18 for Model 1a, Model 1c, and Model 1d.

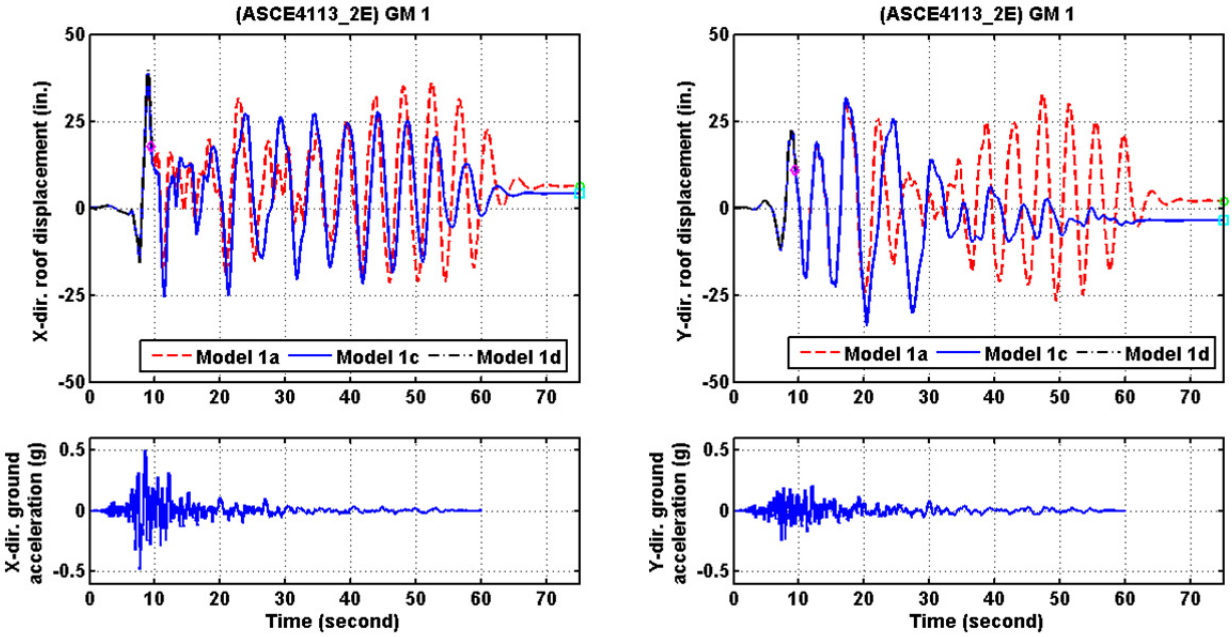

Figure 7.111 Roof displacement histories under BSE-2E level ground motion number 1 for Model 1a, Model 1c, and Model 1d.

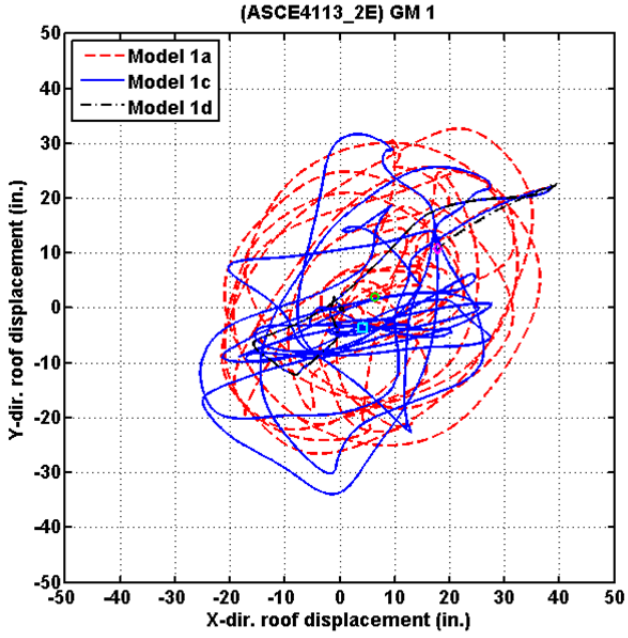

Figure 7.112 Roof displacement orbits under BSE-2E level ground motion number 1 for Model 1a, Model 1c, and Model 1d.

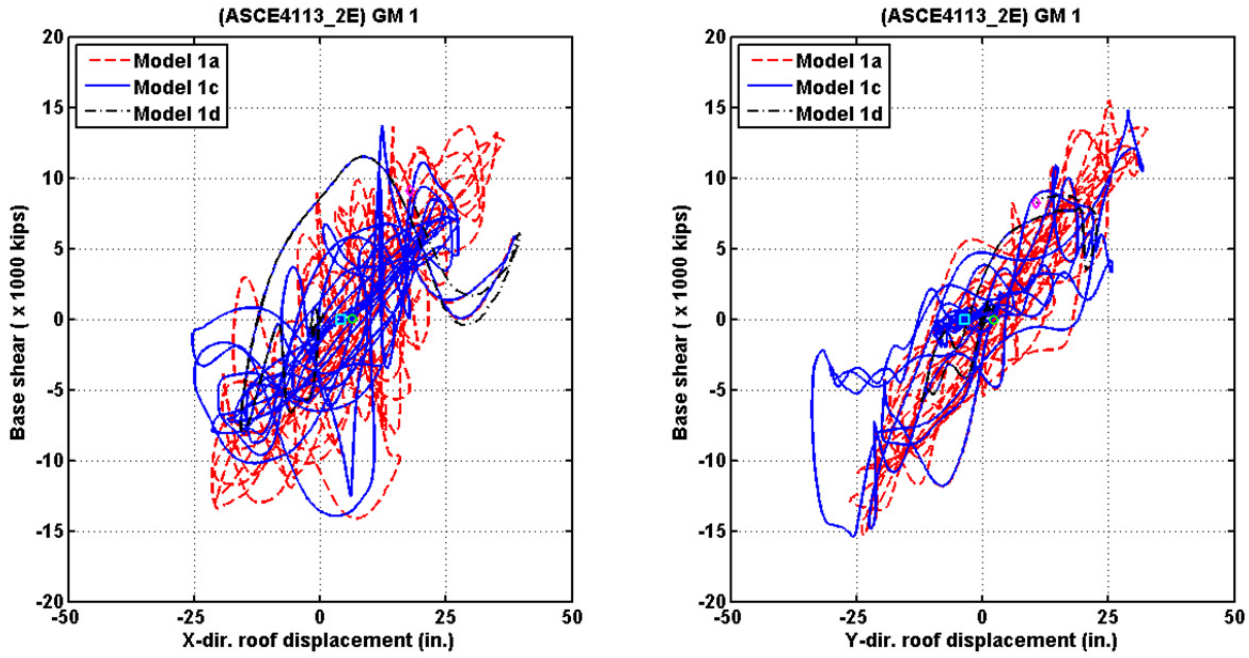

Figure 7.113 Base shear versus roof displacement relationships under BSE-2E level ground motion number 1 for Model 1a, Model 1c, and Model 1d.

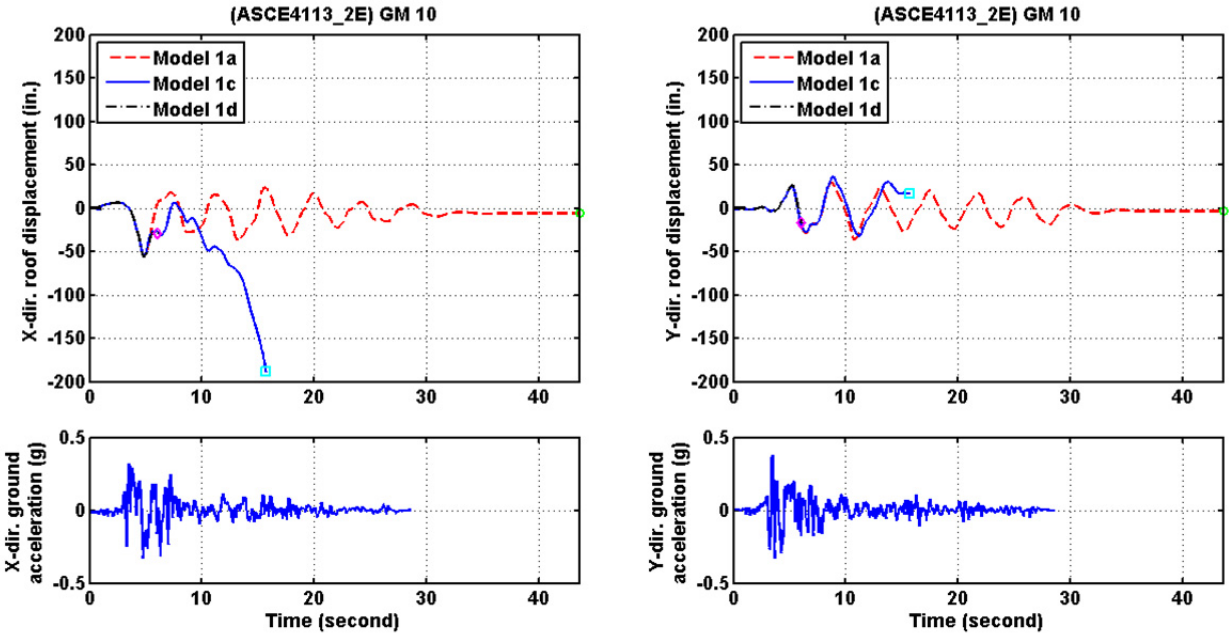

Figure 7.114 Roof displacement histories under BSE-2E level ground motion number 10 for Model 1a, Model 1c, and Model 1d.

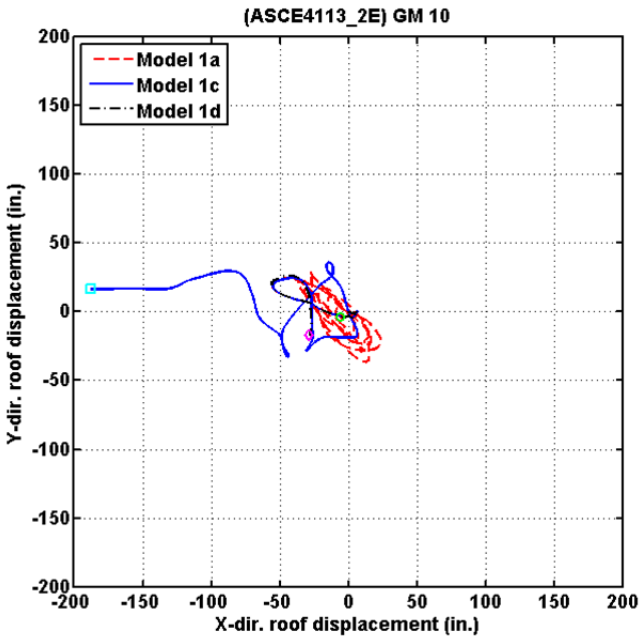

Figure 7.115 Roof displacement orbits under BSE-2E level ground motion number 10 for Model 1a, Model 1c, and Model 1d.

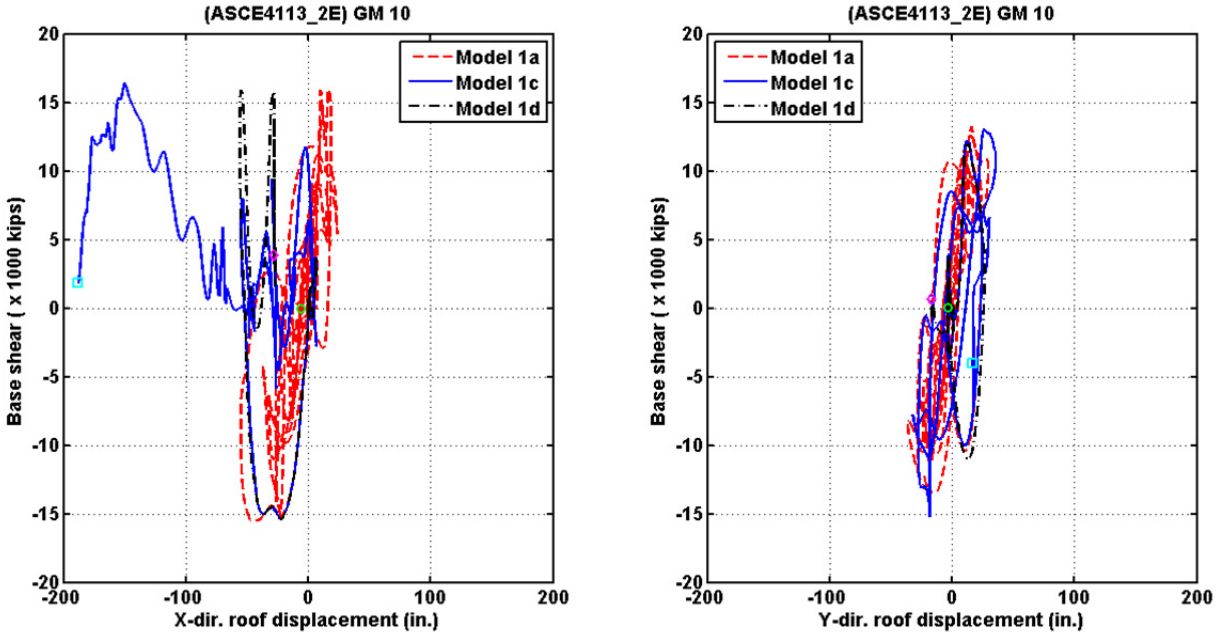

Figure 7.116 Base shear versus roof displacement relationships under BSE-2E level ground motion number 10 for Model 1a, Model 1c, and Model 1d.

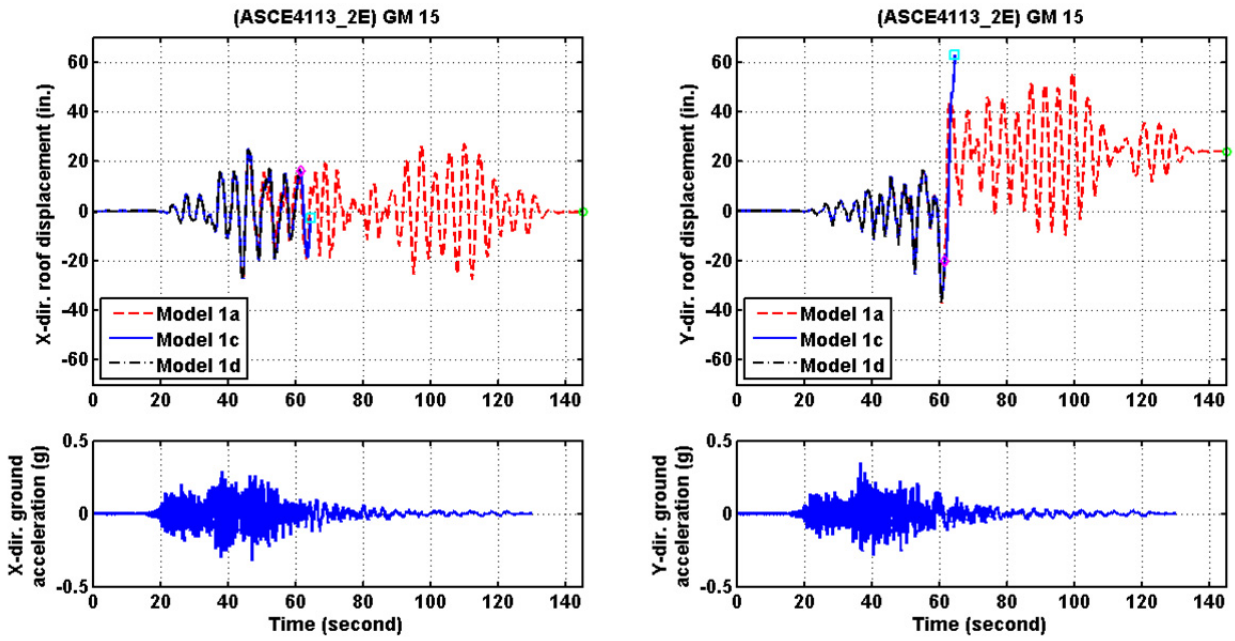

Figure 7.117 Roof displacement histories under BSE-2E level ground motion number 15 for Model 1a, Model 1c, and Model 1d.

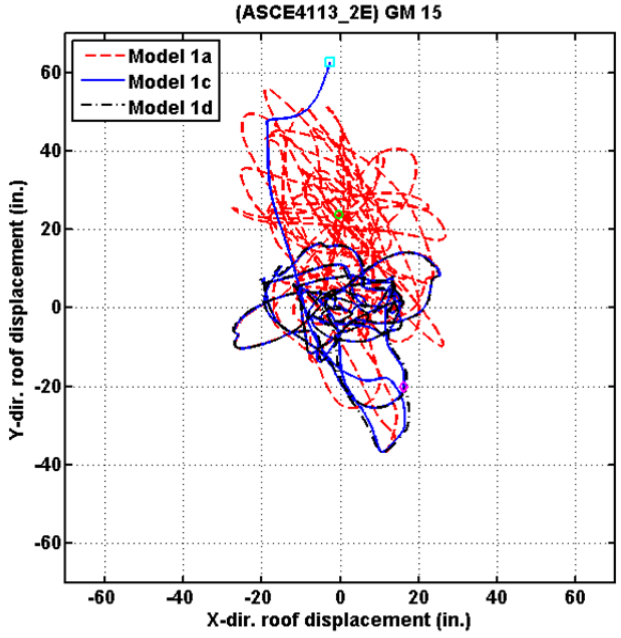

Figure 7.118 Roof displacement orbits under BSE-2E level ground motion number 15 for Model 1a, Model 1c, and Model 1d.

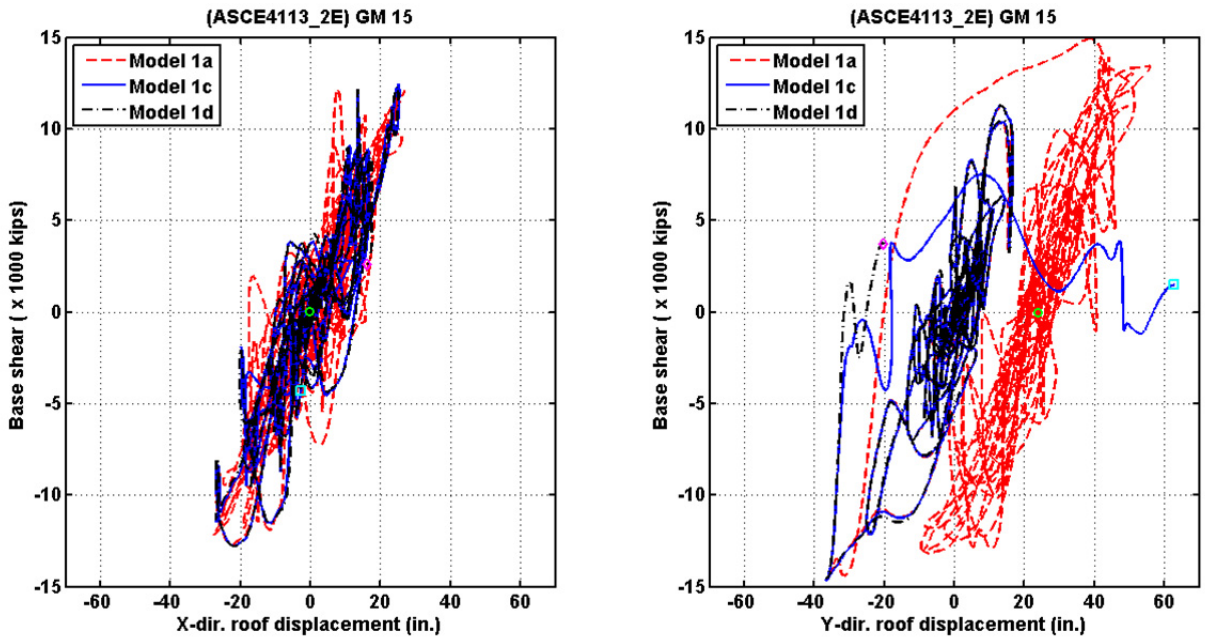

Figure 7.119 Base shear versus roof displacement relationships under BSE-2E level ground motion number 15 for Model 1a, Model 1c, and Model 1d.

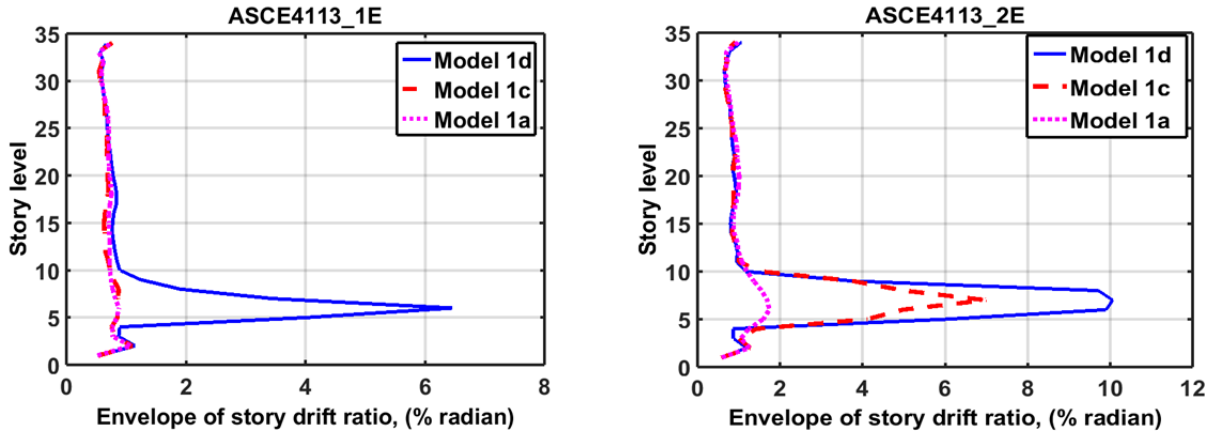

(a). BSE-1E (b). BSE-2E

Figure 7.120 Median story drift ratios of Model 1a, Model 1c, and Model 1d.

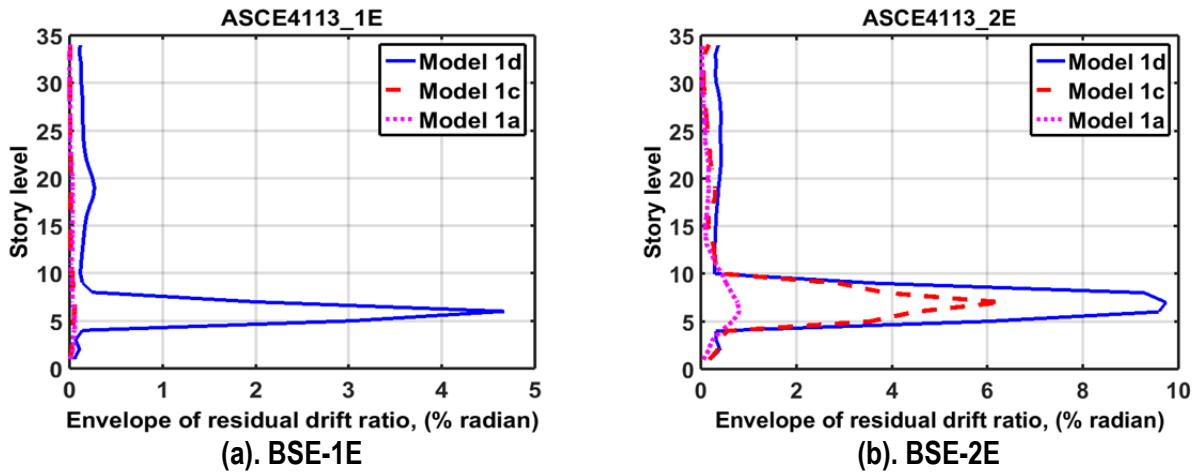

Figure 7.121 Median residual story drift ratios of Model 1a, Model 1c, and Model 1d. (BSE-1E)

7.8 EFFECT OF CLADDING WEIGHT ON GLOBAL DYNAMIC REPONSES

This section determines the effect of cladding weight on global dynamic response by comparing the results between Model 1d* and Model 1d. As discussed in Section 7.2, the full removal of the cladding weight reduces the modal periods roughly in proportion to the square root of the mass reduction. The effect of cladding weight was also examined in Sections 7.31 (static nonlinear pushover analyses) and Section 7.5 (comparison of Models 1d* and 1c).

In general, for small earthquakes—such as the 43-year mean return period earthquakes—the removal of claddings reduces both median story drift and median story shear force demands; see Section 7.2. The reduction is proportional to the period shifting rate since the case-study building is essentially elastic under small intensity earthquakes.

For BSE-1E hazard-level earthquakes, although the removal of cladding (represented by Model 1d) effectively reduced the maximum median peak drift ratio from 9.5% to 6.5%, as shown by comparing Figures 7.12 and 7.122, the tendency to form a weak story remains. For BSE-2E hazard-level earthquakes, the removal of claddings did not reduce the maximum peak drift ratio; see Figures 7.33 and 7.123. Although it is clear that removal of cladding weight does improve the performance of the case-study building up to a certain intensity of ground shaking, it does not completely remedy the failure of column splices nor the development of a weak story mechanism.

That said, removing heavy cladding in addition to retrofitting beam-to-column connections and column splices within the lateral force-resisting system (Model 1a) *can* effectively reduce the drift demands; for example, see Figures 7.20 and 7.21. The plastic rotation demand envelope may still fail to satisfy the target performance level under BSE-1E and BSE-2E hazard-level ground motions (see Figures 7.126 and 7.127), but the addition of supplemental damping to the system might be able to address this issue, as examined in Chapter 8.

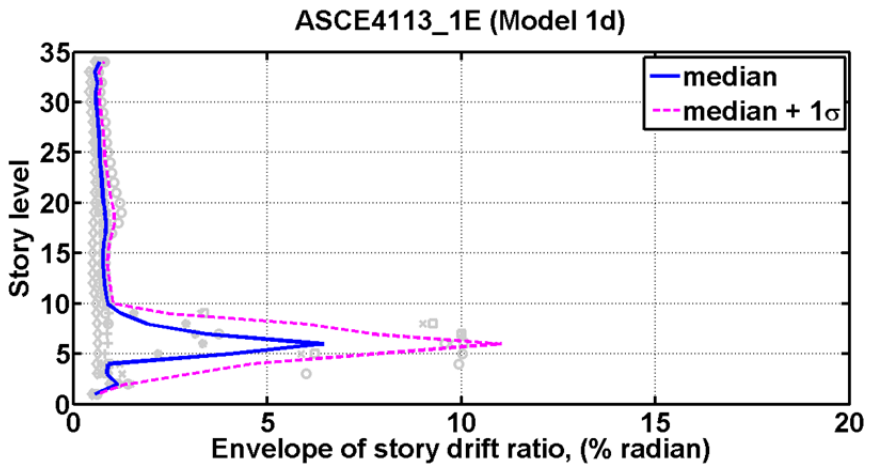

Figure 7.122 Story drift envelope of Model 1d under BSE-1E hazard-level ground motions (only includes responses from six normal termination cases).

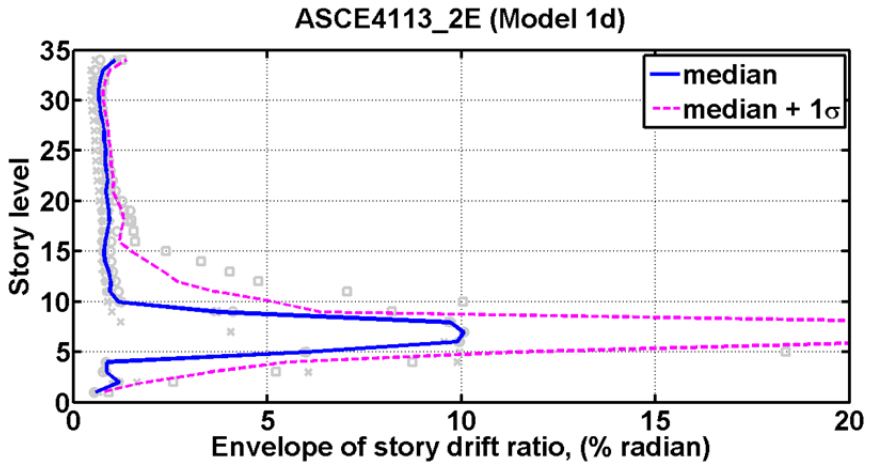

Figure 7.123 Story drift envelope of Model 1d under BSE-2E hazard-level ground motions (only includes responses from five normal termination cases).

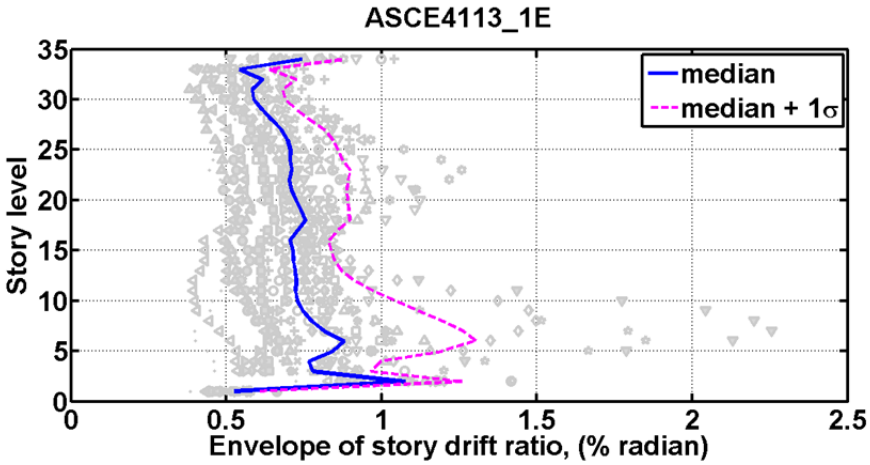

Figure 7.124 Story drift envelope of Model 1a under BSE-1E hazard-level ground motions.

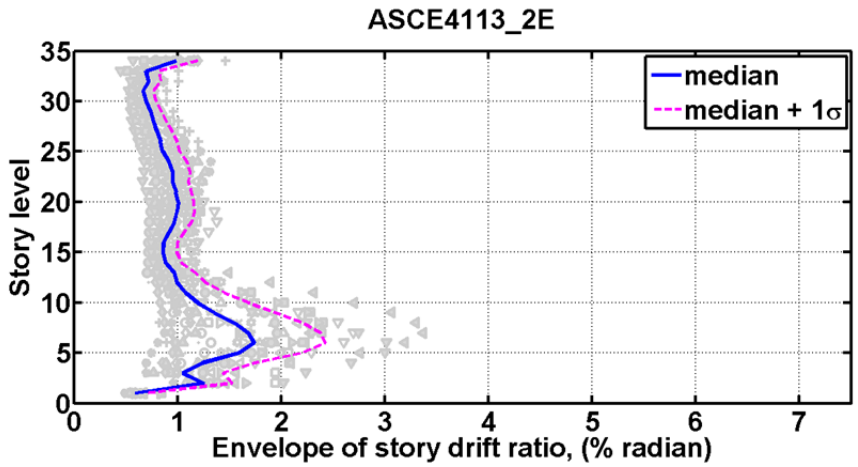

Figure 7.125 Story drift envelope of Model 1a under BSE-2E hazard-level ground motions.

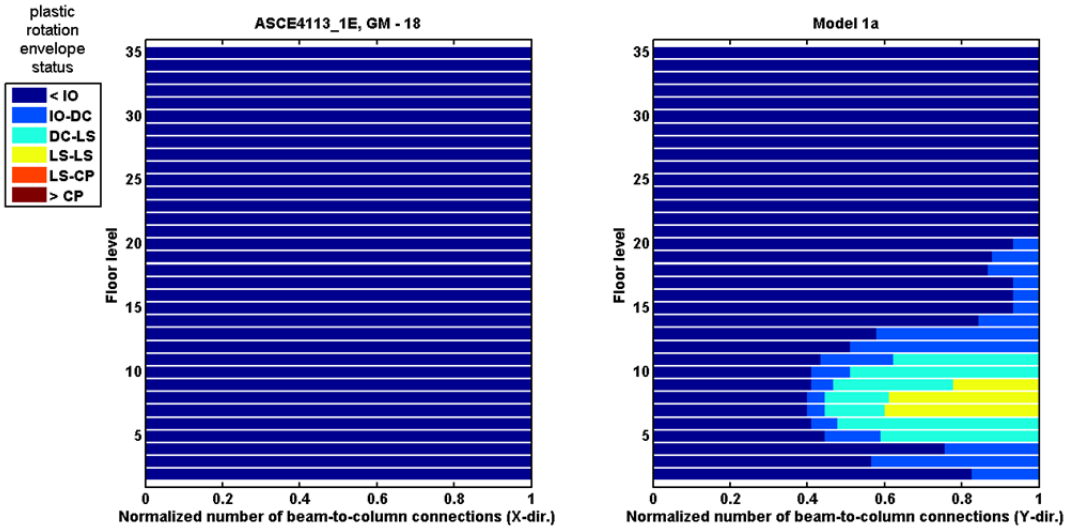

Figure 7.126 Beam end plastic rotation envelope status of Model 1a under ground motion number 18 of BSE-1E hazard-level ground motions.

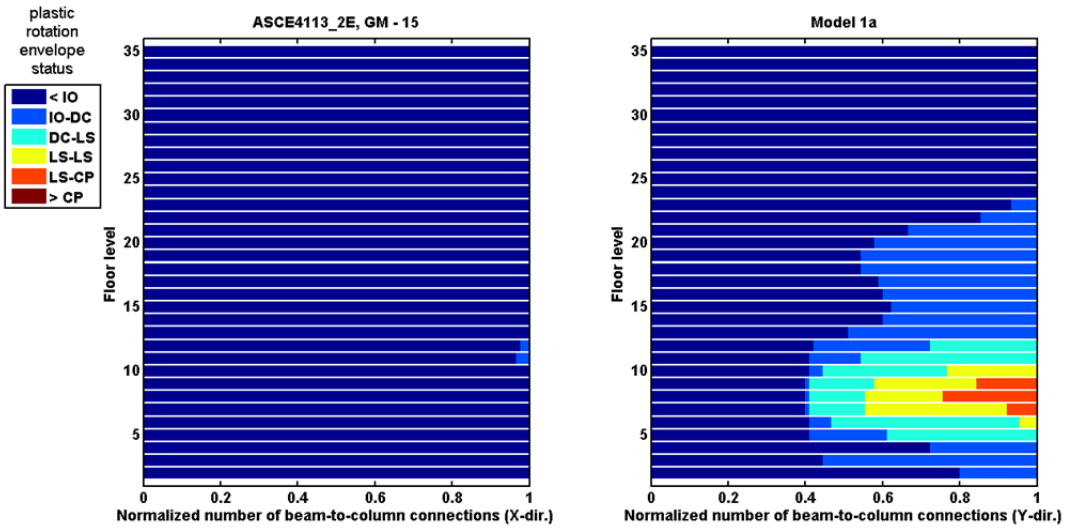

Figure 7.127 Beam end plastic rotation envelope status of Model 1a under ground motion number 15 of BSE-2E hazard-level ground motions.

7.9 EFFECTS OF MULTIPLE EARTHQUAKES

Typically, when a building is subjected to a major earthquake, it must sustain a series of events including foreshocks, the main shock, and aftershocks, as well as subsequent but nearby earthquakes. Typically, researchers and engineers are more interested in building response under the main shock; however, several field investigations have reported the collapse of buildings under repeated shakings. Recent examples are the Christchurch, New Zealand, earthquakes in 2011 and 2012. The effects of earthquake sequences on the global response of case-study building are discussed below. Two hypothetical earthquake sequences were selected, and the dynamic responses of Model 1d* (representing the building's as-built condition) are presented.

As shown in Figures 7.128 and 7.129, earthquake sequences were selected to represent two scenarios; (1) a foreshock followed by a main shock; and (2) a main shock followed by an aftershock. The first earthquake sequence combines one BSE-1E ground motion (GM-02) and one BSE-2E ground motion (GM-01). The second earthquake sequence combines one BSE-1E ground motion (GM-02) and one 2/3-scaled BSE-1E ground motion (GM-01). A 15-sec silence (shown in figures as a green line) is introduced between two ground motion records, as shown in Figures 7.128 and 7.129.

Figure 7.130–7.137 display the dynamic response of the case-study building under the earthquake sequences. The first scenario where a main shock follows a small foreshock indicated that a foreshock is likely to increase drift demands in lower stories, while at the same time reduce the drift demands in upper stories, making the soft-story trend even worse; see Figure 7.130 and 7.131 for the drift ratio and residual drift ratio envelopes. In those figures, the blue solid line and red solid line are the main shock or foreshock only, and the pink dashed line is result under the sequential earthquake scenario. For the case where an aftershock event takes place shows that the peak drift ratio might not be further increased by an aftershock, while the residual drift ratio demands could be amplified; see Figure 7.134 and 7.135. Significant *P*-Δ effects can be seen

through the slope of base shear versus roof displacement plot shown in Figure 7.133 under Scenario 1 earthquake sequences (the foreshock followed by the main shock sequence).

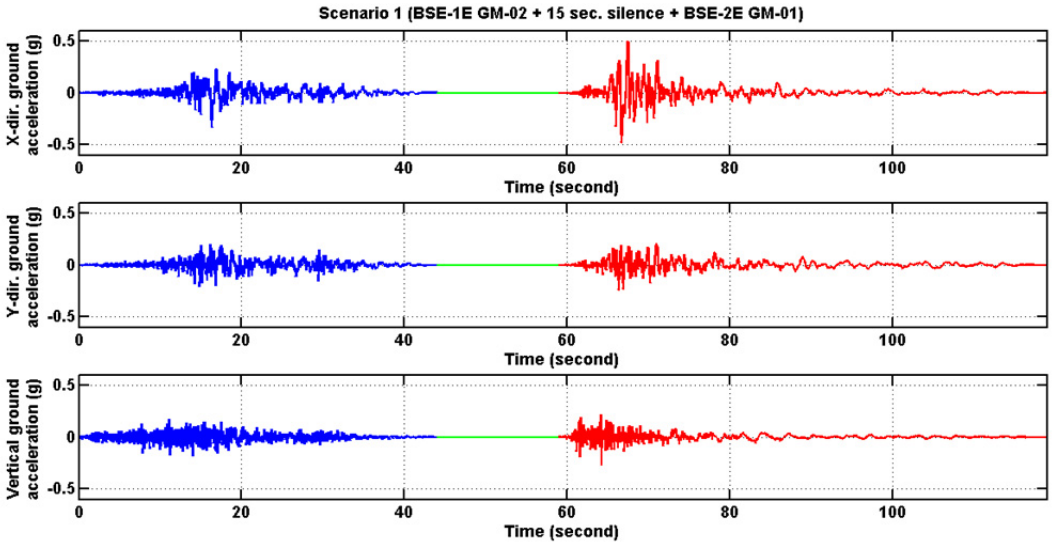

Figure 7.128 Scenario 1 earthquake sequence.

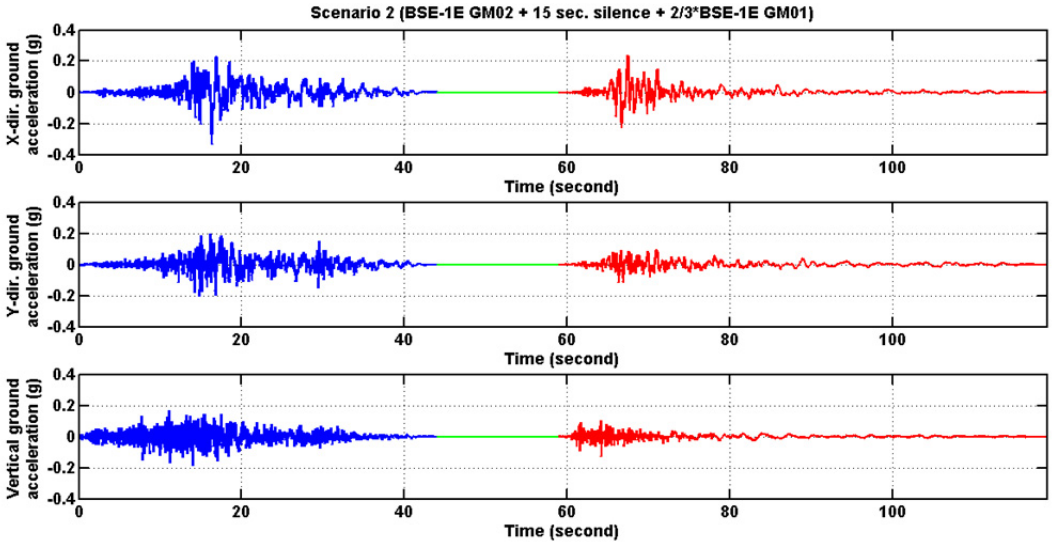

Figure 7.129 Scenario 2 earthquake sequence.

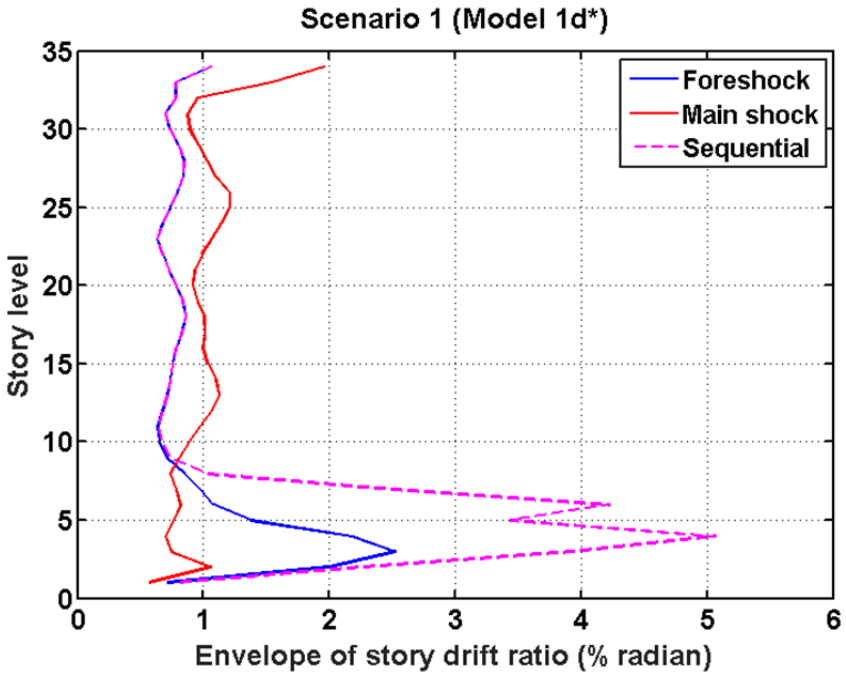

Figure 7.130 Story drift envelope of Model 1d* under Scenario 1 earthquake sequence, and each record individually.

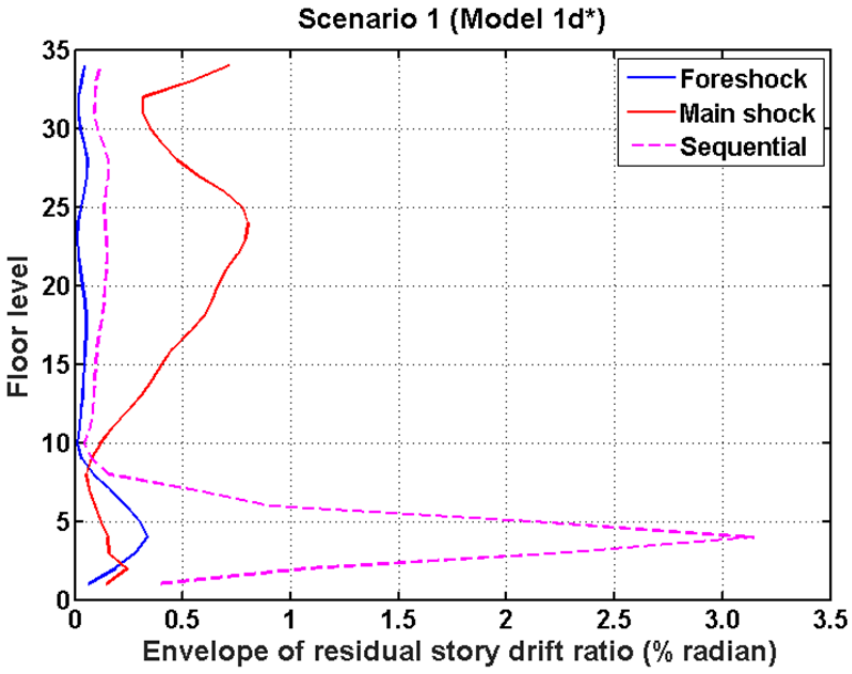

Figure 7.131 Residual drift envelope of Model 1d* under Scenario 1 earthquake sequence, and each record individually.

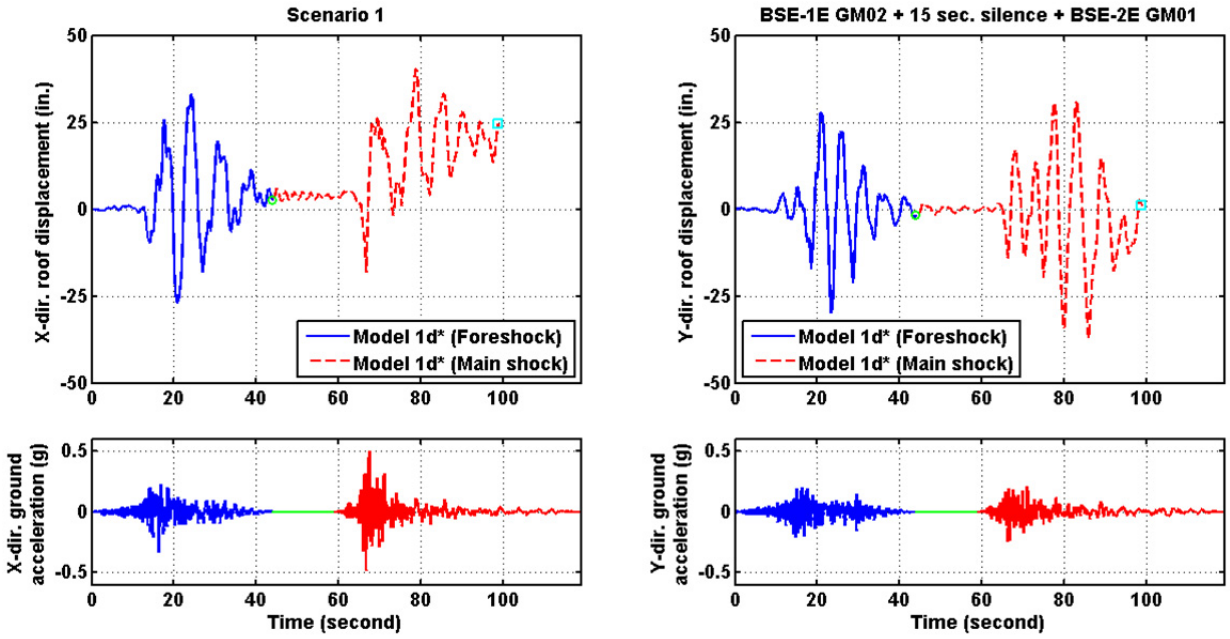

Figure 7.132 Roof displacement histories under Scenario 1 earthquake sequence (Model 1d*).

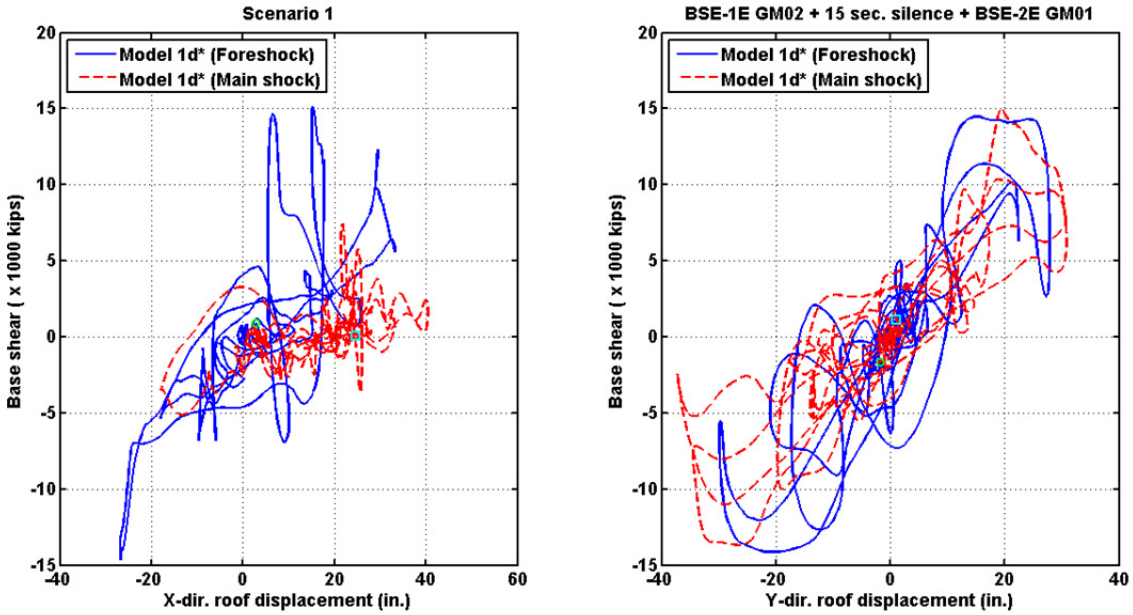

Figure 7.133 Base shear versus roof displacement relationships under Scenario 1 earthquake sequence (Model 1d*).

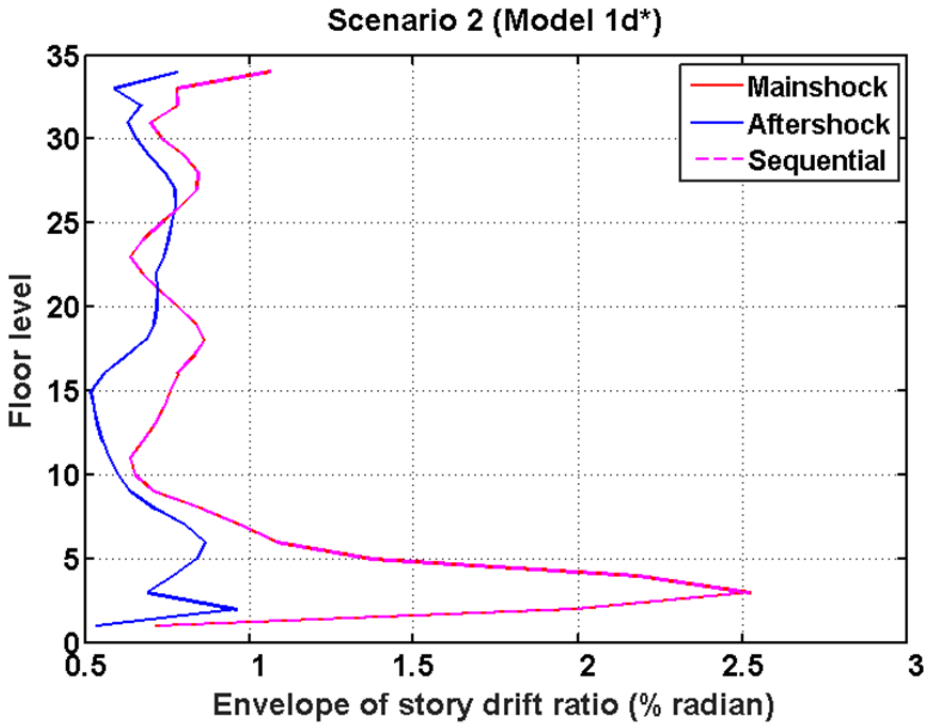

Figure 7.134 Story drift envelope of Model 1d* under Scenario 2 earthquake sequence, and individual earthquake records.

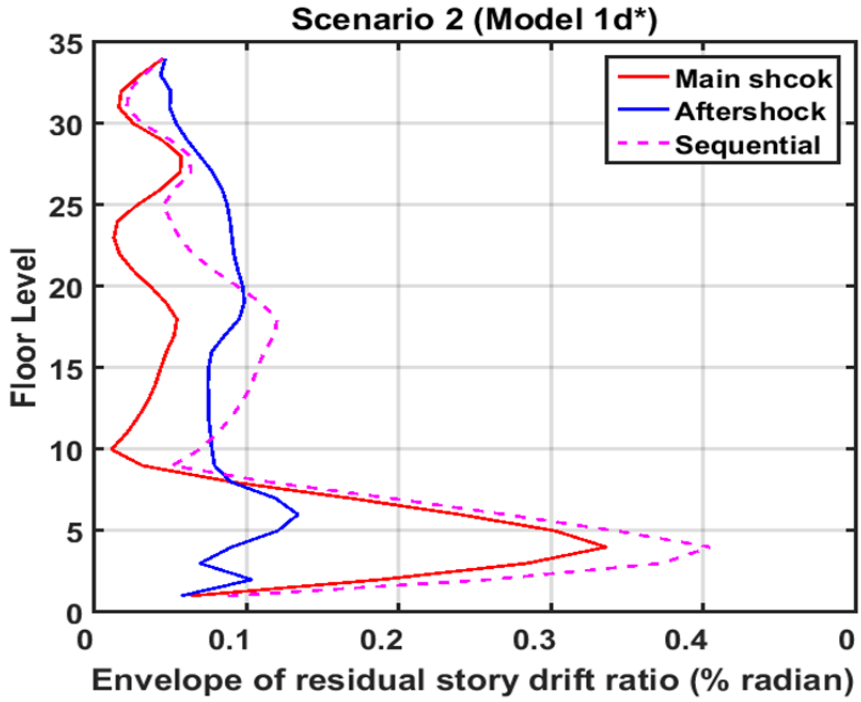

Figure 7.135 Residual drift envelope of Model 1d* under Scenario 2 earthquake sequence, and individual earthquake records.

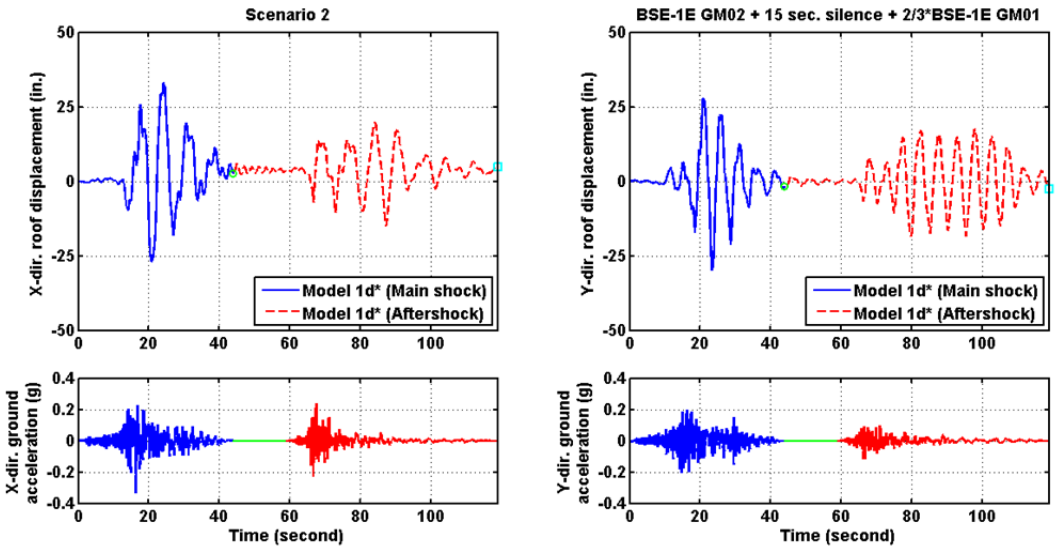

Figure 7.136 **Roof displacement histories under Scenario 2 earthquake sequence (Model 1d*).**

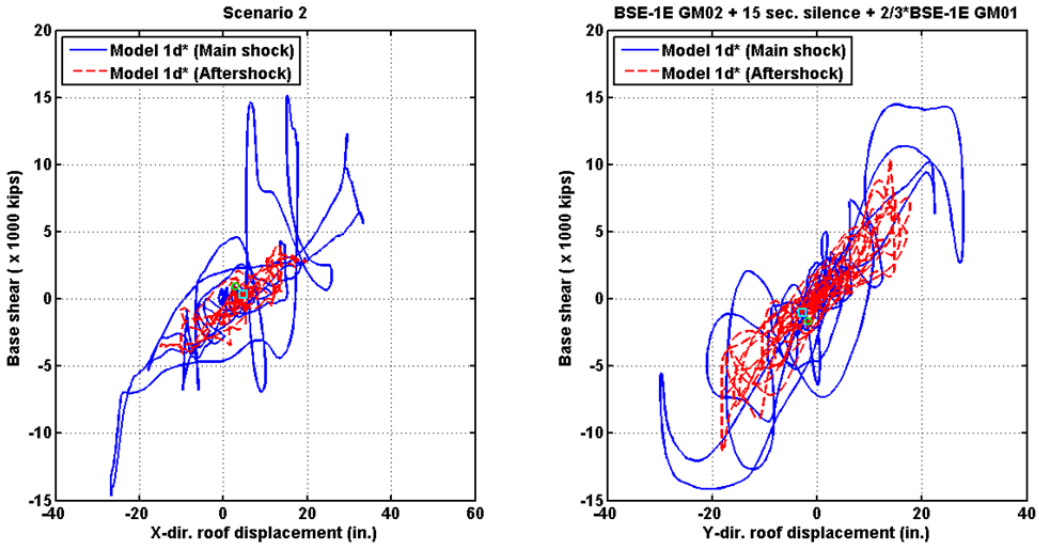

Figure 7.137 **Base shear versus roof displacement relationships under Scenario 2 earthquake sequence (Model 1d*).**

7.10 FEMA 351 PROCEDURE (GLOBAL COLLAPSE EVALUATION)

As mentioned in Chapter 2, the evaluation guidelines in FEMA 351 provide a probabilistic approach to evaluate the seismic performance of existing buildings. It establishes the confidence levels to achieve immediate occupancy (IO) and collapse prevention (CP) performance levels by checking the global drift, local drift, and the column force demands in both compression and tension states. With the results of nonlinear dynamic analysis performed for the case-study

buildings, it is relatively straightforward to calculate the confidence levels against two discrete structural performance levels (IO and CP) under BSE-1E and BSE-2E hazard levels. Following the FEMA 351 procedure, it is possible to derive the global drift limits to achieve the minimum recommended confidence levels—50% for IO and 90% for CP—for any given hazard-level earthquakes as listed in Table 7.4.

Using the four different mathematical models in this study (Model 1d*, Model 1d, Model 1c, and Model 1a), it is possible to predict confidence levels to achieve IO and CP. Here, four earthquake scenarios will be considered: one recorded nearby event and 50%/30yrs, BSE-1E and BSE-2E hazard-level datasets as listed in Table 7.5. For Model 1d* and Model 1d, more than half of the numerical simulations failed to converge at either BSE-1E or BSE-2E events due to column splice tension fractures. Most likely this indicates that the structure would experience global instability even if the peak deformation is still small. Nonetheless, these results were excluded in the following analysis; the resulting confidence levels presented will be unrealistically high.

As shown in Table 7.5, the case-study building basically satisfies the minimum confidence levels to achieve IO and CP under the 43-years mean return period events or the actual recorded Loma Prieta earthquake. Nevertheless, none of the models satisfy the 50% minimum confidence level needed to achieve an IO performance level under BSE-1E or BSE-2E events according to FEMA 351. Note that column-splice failure occurs in every single simulation under both BSE-1E and BSE-2E hazard-level ground motions; see Table 7.6.

Despite the remediation strategies incorporated in Model 1d (removal of heavy claddings), Model 1c (removal of claddings plus retrofitting all column splices), and Model 1a (removal of claddings and fixing all pre-Northridge beam-to-column connections and column splices), the building still failed to meet the minimum 90% confidence level requirement to achieve collapse prevention per FEMA 351 global performance evaluation procedure under both BSE-1E and BSE-2E hazard-level events. Even Model 1a, the case-study building with fully ductile connections and without heavy cladding did not satisfy the minimum confidence level to achieve collapse prevention performance level under BSE-2E hazard-level ground motions; see Table 7.5. This represents the best structural achievement possible for the case-study building without the strategic intervention in terms of additional damping.

Table 7.4 Global drift limits satisfying minimum confidence level for immediate occupancy and collapse prevention performance levels per FEMA 351

Performance level	Immediate occupancy (IO)	Collapse prevention (CP)
Min. confidence level (%)	50	90
β_{UT}	0.2	0.55
λ	1.06	0.78
γ_a	1.04	1.1
γ	1.6	1.8
C	0.01	0.06
ϕ	0.85	0.6
Global drift angle limit, D (%)	**0.54**	**1.41**

Table 7.5 Confidence levels for global responses (FEMA 351 evaluation).

Model types	Model 1d*		Model 1d		Model 1c		Model 1a	
	Confidence levels (%) to achieve immediate occupancy (IO) or collapse prevention (CP)							
Hazard levels	**IO**	**CP**	**IO**	**CP**	**IO**	**CP**	**IO**	**CP**
Loma Prieta	74.2	99.9	-	-	85.6	99.9	-	-
50% / 30yrs	61.5	99.9	-	-	76.3	99.9	-	-
BSE-1E	**0.0****	1.48**	**0.0****	4.96**	**0.0**	94.3	**0.03**	96.3
BSE-2E	**0.0****	0.73**	**0.0****	0.64**	**0.0**	**5.2**	**0.0**	**81.7**

**Note: cases encounter numerical instability are excluded in the analysis.

Table 7.6 Percentage of simulation cases having column splice failure in any story.

Model types	Model 1d*	Model 1d
Hazard levels	**Percentage (%)**	
BSE-1E	100	100
BSE-2E	100	100

7.11 RISK CATEGORY III VERSUS RISK CATEGORY II

As mentioned in Section 4.2, Risk Category III was initially selected for evaluating the case-study building, even though many tall office buildings are assumed to belong to Risk Category II. One factor that affects the assignment of risk is the occupancy of building. Table 7.7 illustrates how the basic BPOE changes as the risk category changes. Basically, the BPOE of a Risk Category III building can be regarded as enhanced performance objectives for a Risk Category II building. Risk category assignment may be quite relevant when designing and evaluating retrofits.

Table 7.7 BPOE for Risk Category II and Risk Category III buildings per ASCE 41-13.

		Performance level				
		Immediate occupancy (IO)	**Damage control (DC)**	**Life safety (LS)**	**Limited safety (LS)**	**Collapse prevention (CP)**
Seismic hazard level	**BSE-1E (20%/50yrs, MRP = 225 yrs)**		Risk category III	Risk category II	Limited objectives	
	BSE-2E (5%/50yrs, MRP = 975 yrs)		Enhanced objectives		Risk category III	Risk category II

7.12 CONCLUDING REMARKS

The case-study building performed well under a set of 20 ground motions at the 43-year mean return period hazard level as well as for a recorded Loma Prieta earthquake motion. The building models remained essentially elastic, and median peak story drift ratios were less than 0.005; see Table 7.8. Based on the FEMA 351 evaluation procedure (Table 7.5) for the global collapse evaluation, it can achieve an IO performance level.

However, the original (current at the time of this writing) condition of the case-study building (represented by Model 1d*) failed to satisfy the basic performance objectives based on the ASCE 41-13 standard. A high probability of column splice brittle failures under BSE-1E and BSE-2E hazard-level ground motions was determined. Even considering several seismic upgrade strategies, such as removal of heavy claddings (Model 1d), removal of claddings plus retrofitting all column splices (Model 1c), or removal of claddings and fixing all pre-Northridge beam-to-column connections and column splices (Model 1a), the performance of case-study building still did not satisfy the target performance objectives of ASCE 41-13. To achieve that level of performance, the case-study building requires additional seismic upgrade schemes.

Although not required by the ASCE 41-13 standard, the effect of the vertical component of ground motions on dynamic response is a factor that should be considered; see Section 7.6. The vertical component of excitation can have some beneficial or detrimental effect on global response, but it has a definite effect on column axial loads (10% to 20% increase in compression D/C ratios). Thus, the vertical component of ground motions should be considered for existing tall buildings, such as the case-study building, where very high compression stresses are likely in columns, and tension stresses at critical locations such as base plates and column splices are of particular concern.

This study also revealed that the ultimate building response is quite sensitive to the dynamic characteristics of the ground motions considered in the evaluations. Thus, selection of the ground motions is a critical aspect of seismic performance evaluation.

Mechanical behavior of beam-to-column connections had a very significant effect on the dynamic response of the case-study building, both in terms of effects on the global and local responses, and in terms of the ability of current modeling techniques to account for response of systems where many members and connections deteriorate significantly, up to and including complete failure. These behavior effects are evident in the nonlinear static pushover analyses shown for the building, where sudden “cliff edge” behavior was apparent in the models that mimicked the tendency for members and connections to deteriorate and fail. Generally, the ductile connections will reduce the transient story drift demands, but permanent story drift demands may be high; see Table 7.8.

One simple way to look at the global collapse potential of the case-study building is to review the percentages of simulated cases (that do not suffer numerical convergence problems) that have large transient story drift ratios or large permanent story drift ratios. For example, for new tall buildings the maximum permitted transient story drift is 4.5%, and the maximum permitted residual story drift is 1.5% [LATBSDC 2014].

Table 7.9 summarizes the percentages of total simulation cases (i.e., 20 ground motions) that have peak transient or residual story drift responses larger than the maximum permitted drift ratios for four selected models (Model 1d*, Model 1d, Model 1c, and Model 1a) subjected to

BSE-1E and BSE-2E hazard-level ground motions. Model 1d* and Model 1d had significant numerical issues, where more than half of simulations became numerically unstable after a significant number of column splices failed. As these results are considered unreliable, they have been excluded in these quantitative calculations. However, the inability of the numerical models to track behavior may be a strong indicator of unacceptable structural response.

From the summary of global responses shown in Table 7.9, it is clear that the current condition (Model 1d*) of the case-study building has a high probability of global collapse under BSE-1E and BSE-2E hazard-level ground motions. Even if the current condition of the building is considered to have fully ductile connections everywhere and the absence of heavy cladding material (i.e., Model 1a), the permanent residual story drifts under BSE-2E ground motions remain highly problematic.

Table 7.8 Summary of global drift responses.

Model types	Model 1d*		Model 1d		Model 1c		Model 1a	
	Median peak transient story drift ratio (TSD) and median peak residual story drift ratio (RSD) (%)							
Hazard levels	**TSD**	**RSD**	**TSD**	**RSD**	**TSD**	**RSD**	**TSD**	**RSD**
Loma Prieta (1 ground motion)	0.48	0	-	-	0.44	0	-	-
50% / 30yrs (20 ground motions)	0.51	0	-	-	0.47	0	-	-
BSE-1E (20 ground motions)	9.5**	9.1**	6.7**	2.2**	1.2	0.05	1.07	0.06
BSE-2E (20 ground motions)	10.0**	9.5**	10.1**	7.4**	7.0	6.3	1.74	0.8

**Note: cases encounter numerical instability are excluded in the analysis.

Table 7.9 Summary of global responses.

Model types	Model 1d*		Model 1d		Model 1c		Model 1a	
	Percentage of simulation cases having peak transient story drift ratio larger than 4.5% (CT) or peak residual story drift ratio larger than 1.5% (CR) in any stories							
Hazard levels	**CT**	**CR**	**CT**	**CR**	**CT**	**CR**	**CT**	**CR**
BSE-1E	63.6**	63.6**	83.3**	50**	25	25	0	0
BSE-2E	100****	100**	100**	100**	70	75	0	20

**Note: cases encounter numerical instability are excluded in the analysis.

Presented in Section 7.7, dynamic analyses performed on Model 1d that explicitly considered the column splices failure to determine the effects of mechanical properties on system response. As shown in Figure 7.105 (black dashed-dot line), the mechanical behavior of column splices can affect the overall system behavior. Because the current numerical model for column splice failure has significant limitations, the dynamic analyses results of baseline model (Model 1c) are considered to be more reliable than those of Model 1d* or Model 1d. However, the results for Models 1d and 1d* indicate the tendency for many splices to fail in the building, leading to large uncertainties in estimating safety and other performance related parameters. Also noted is that explicit modeling of column splices behavior is not required per the ASCE 41-13 standard, and such consideration where partial penetration welds are used for steel column splices should be required.

Removal of heavy cladding did improve the performance of the case-study building under BSE-1E hazard-level earthquakes or smaller earthquakes, but it had little effect under BSE-2E hazard-level earthquakes. In particular, the significant tendency of the building to form a weak-story region in the bottom one-third of the building was not remedied.

Two particular earthquake scenarios representing one combination of a foreshock and a main shock (Scenario 1), and one combination of a main shock and an aftershock (Scenario 2) demonstrate the effect of multiple earthquakes on the dynamic response of the case-study building. Cumulative deformations and damage were observed under these earthquake sequences. Further study is required to assess if these findings extrapolate with ground motion characteristics or if the sequence investigated had particular effects on the building's dynamic response.

From a more probabilistic point of view that incorporated in ASCE 41-13, the current condition of the case-study building (Model 1d*) failed to conform to the minimum 90% confidence level requirement to achieve collapse prevention per FEMA 351 global performance evaluation procedure under both BSE-1E and BSE-2E hazard-level events; see Table 7.5. Even when the heavy cladding was removed, with fully ductile beam-to-column connections, and fully ductile column splices (Model 1a), the building still could not conform to the minimum 90% confidence level to achieve collapse prevention under BSE-2E hazard-level ground motions.

Five major seismic deficiencies were identified during the Tier 3 evaluation procedure of the case-study building:

- Even for an ideally ductile model of the building, the strength of the building was inadequate to limit inelastic deformations to an acceptable level for current guidelines;
- The building had a tendency to form weak-story regions in the lower one-third of the building;
- Pre-Northridge beam-to-column connection details resulted in a high percentage of connection failure under BES-2E events (see Figure 7.72); and
- The PJP column splice weld detail posed great danger to the seismic integrity of the building.

- The columns demand-to-capacity ratios were excessive in both tension and compression at the bottom one-third of the building, thus leading to column yielding or rupture.

These issues were all detected and found to be problematic in the detailed dynamic analyses.

As shown in previous sections, the computed response of the case-study building did not satisfy the target performance objectives: neither a damage control state under BSE-1E hazard or a limited safety state under BSE-2E hazard was achieved. Reduced (or limited) performance objectives could be satisfied, but considering the high probability of connection failures and their consequences, the focus of this study now shifts to retrofit scenarios that anticipate mitigation of significant post-earthquake repairs.

8 Seismic Upgrading Strategies

8.1 RECOMMENDED RETROFIT SCHEMES

A number of different approaches are possible for the seismic retrofit of a tall building. One approach is to increase the inelastic deformation capacity of existing connections. However, as described in Chapter 4.3, Model 1a with ideally ductile beam-to-column connections and ductile column splices that were able to develop the full yielding capacity very large story drift demands still occurred between levels 5 and 10. Furthermore, substantial residual displacements predictions question the viability of this retrofit scheme that focuses on only increasing the systems ductility capacity to meet performance objectives. Even if the analytical results suggested acceptable seismic response, the large number of beam-to-column connections needing retrofit would likely make this approach economically prohibitive. Thus, an approach that reduces story-drift deformation demands, beam end rotational demands, and the tendency of the structure to form a weak-story mechanism should be explored.

The deficiencies identified from Tier 1 screening (Chapter 7.1), such as the lack of column attachment to the foundation and the fragility of the columns, pose significant challenges to stiffen the building through the addition of strong, centralized bracing or wall elements. Retrofit schemes such as adding distributed velocity- or displacement-dependent bracing devices to the current lateral force-resisting frames or implementing mid-level isolation systems are a possible solution. By distributing these elements, or selecting improved installation configurations, the accumulation of axial forces in columns might be avoided.

To provide the required lateral stiffness and energy dissipation needed to reduce lateral displacements while not increasing demands on the structure is challenging. Common approaches in the U.S. consider the addition of buckling restrained braces, FVDs, or viscous wall dampers. Because of the vulnerability of the columns in compression and tension, the use of FVDs is explored in some detail in this chapter. In this approach, the FVDs result in a peak force resistance that is out of phase with the forces acting in the structural elements of an elastically responding system, which may limit drifts without creating excessive demands on the columns and beams.

Several other alternatives that might be considered include reducing the force demands on the system by reducing the weight of the structure. For instance, the heavy cladding used on the building could be replaced with a much lighter curtain wall system as discussed in Chapter 7. Similarly, adding an isolation system to the building is another possible solution. For example, an isolation plane might be introduced above the mezzanine level, with the lowest levels of the building being reinforced to mitigate structural irregularities at these levels and to provide

resistance to the local P-Δ moments induced by the isolation system. Given that this option introduces substantial changes in the architectural components, elevators, stairs, utilities, and structure near its base, the focus in this study was placed on the use of FVDs. Figure 8.1 illustrate some of the above-mentioned strategies in engineering practice.

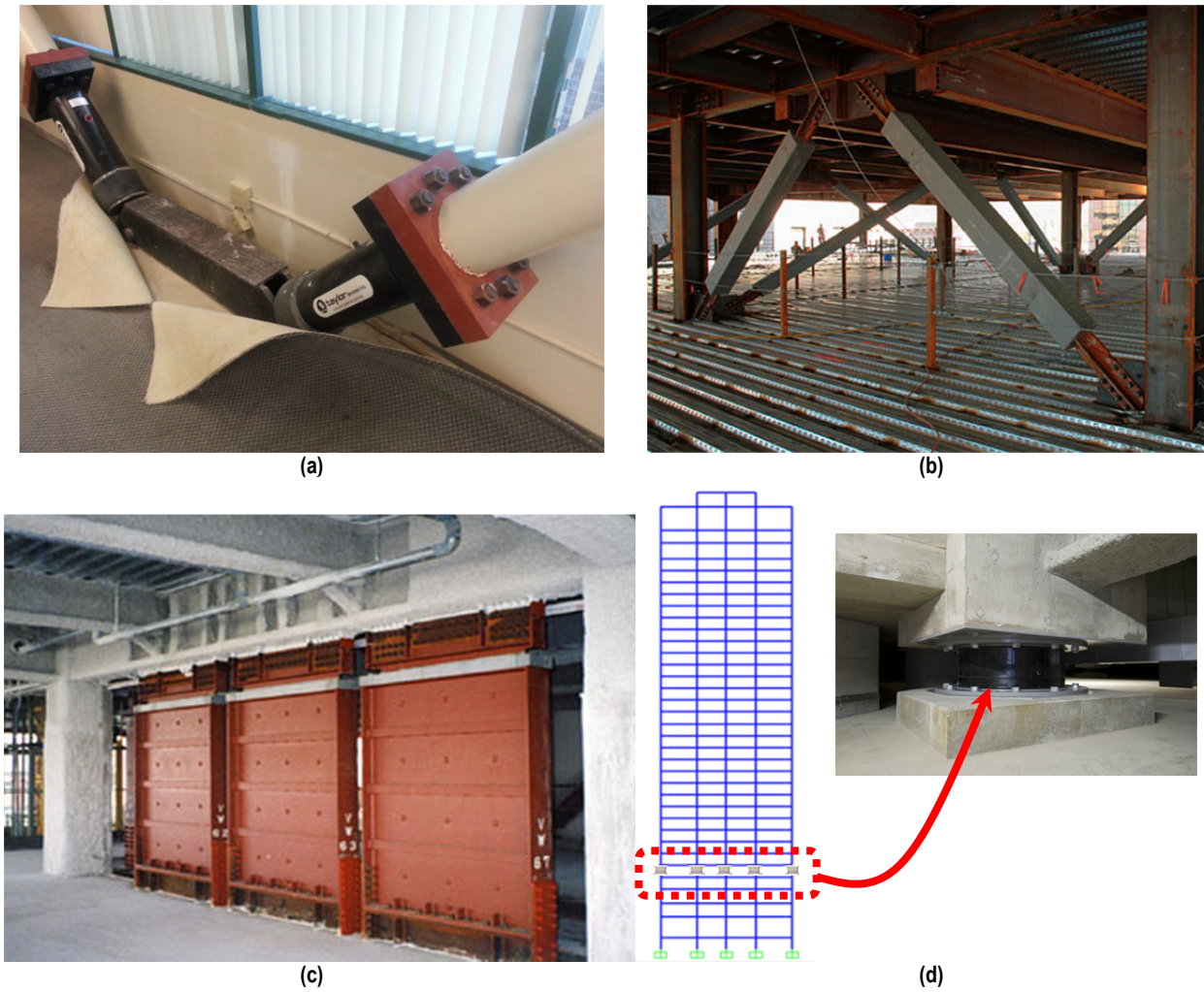

Figure 8.1 **Illustration of supplemental energy dissipation devices: (a) fluid viscous dampers; (b) buckling restrained braces; (c) viscous damping walls; and (d) mid-level isolation.**

8.2 INTRODUCTION OF FLUID VISCOUS DAMPERS

A FVD is a velocity-dependent energy-dissipation device. Assuming that the damper would be operating under the cutting-off frequency, where the storage stiffness of FVD is not significant, the ideal force output of a FVD can be expressed as:

$$F_D = C|v|^a \operatorname{sign}(v) \tag{8.1}$$

where F_D is the damper force, C is the damping constant, v is the relative velocity between two ends of damper element, α is the exponent within the range of 0 and 1 (α >1 is usually not considered in typical engineering practice), and sign (v) takes the sign of the relative velocity. The relationship between damper force and relative velocity, and damper force versus relative displacement are shown in Figure 8.2, which assumes that the same amount of energy is dissipated under a sine wave excitation. The damping constant C and displacement amplitude are kept constant for all the cases. Nonlinear dampers with damping exponents smaller than 1.0 produce larger damper forces at smaller velocities and also suppress the peak damper force. When $\alpha = 0$, the damper becomes a Coulomb friction damper; when $\alpha = 1$, it becomes a regular linear viscous damper.

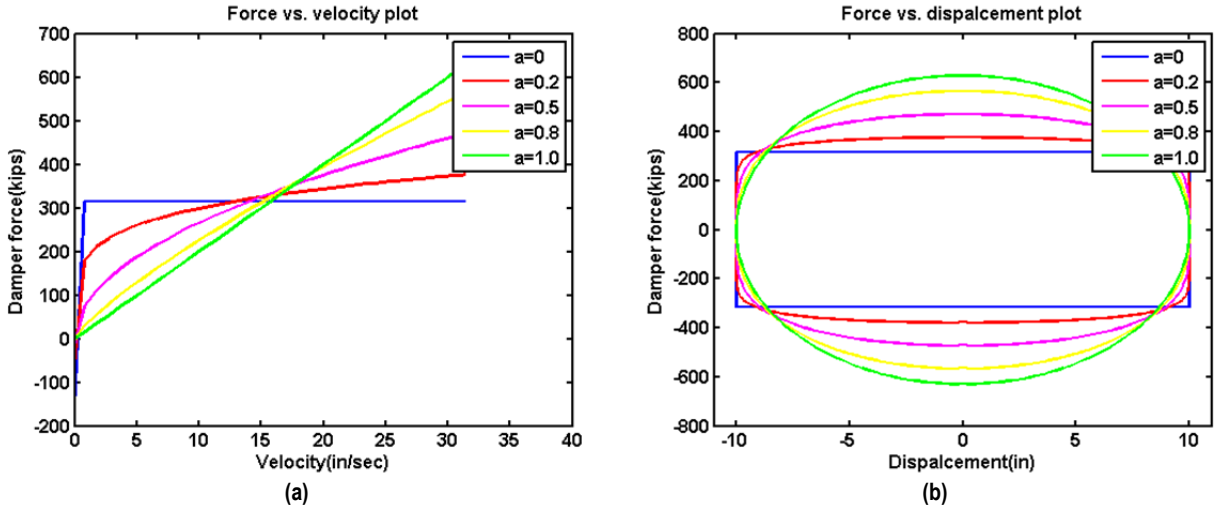

Figure 8.2 **Characteristic damper properties with different α values: (a) force versus velocity and (b) force versus displacement.**

Equation (8.1) represents the force due to the viscosity of the damper, which is 90° out of phase with the motion. With such a velocity-dependent property, a FVD is capable of dissipating energy at small displacements. Another advantage that distinguishes a FVD system from other protective systems for elastic structural response lies in its out-of-phase action with structural members that are in-phase with displacement amplitudes; the peak damper force tends to avoid occurring concurrently with peak forces in other elastic elements. Therefore, for structures that are relatively stiff and within the elastic range, adding FVDs could provide a way to reduce the structural responses without significantly increasing the total maximum forces in columns and beams. Numerical and experimental investigations have both shown merits of such devices [Reinhorn et al. 1995; Symans and Constantinou 1998]. According to a list provided by Taylor Device Inc. [2015a, b, c], there are more than 610 buildings and bridges all over the world, including newly constructed and existed structures that have used Taylor fluid dampers from 1984 to 2015. Among those applications, more than 57 buildings taller than 20 stories used FVDs to control structural response under seismic or/and wind load. The application of FVD increased significantly following the 1994 Northridge earthquake and 1995 Kobe earthquake, when large numbers of structures thought to be highly seismic resistant turned out to be damaged severely by those seismic events. As a result, engineers quickly discovered that FVDs were an ideal solution to accommodate the ever-increasing seismic design requirements [Miyamoto and Scholl. 1996; Taylor and Katz 2004]. Post-earthquake observations after recent major

earthquakes (e.g., 2011 Tohoku, Japan, and 2003 Colima, Mexico) have shown that incorporating viscous dampers not only meets the life-safety requirements, but have also proved to be effective at controlling damage [EERI 2012; Takewaki et al. 2013].

Design of FVDs involves several key steps, including selecting effective damper locations within architectural constraints, evaluating effective damping ratios needed, and optimizing designing parameters such as the damping constant and damping exponent, α. Among these, sizing dampers (mainly constant C) plays a crucial role; as such, its selection is the major research focus in this retrofit study.

Considerable research in the 1990s resulted in at least five code-oriented procedures for designing passive energy-dissipation systems [Ramirez et al. 2001]. Guidelines and codes such as ASCE 41-13 and ASCE 7-10 provide methods to account for the supplemental damping effects of these devices by modifying the design spectrum. In this way, general damper characteristics can be selected to achieve basic performance goals. However, they do not prescribe specific methods for optimally placing dampers in a building, and the location of dampers can have a significant impact on both structural behaviour and the cost of damper-based retrofits.

A wide variety of methods have been suggested to identify optimal damper location. The most commonly adopted optimization methods are generally divided into three categories:

(1) *Gradient based methods*: Typical algorithms for linear structures includes the method of feasible directions [Balling and Pister 1983], the steepest direction search algorithm using transfer function [Takewaki 2000], Rosen's gradient projection method [Singh and Moreschi 2001], and gradient of eigenvalue method [Lee et al. 2004]. Later work by Levy and Levan. [2006] extended applications to nonlinear structural behaviour; their algorithm targeted an optimal design where dampers were assigned only to stories where a performance index exceeded a predetermined allowable value. This category of methods usually requires programming and differentiability of the optimization space.

(2) *Genetic algorithm*: Typical work includes that of Singh and Moreschi [2002], Lavan and Dargush [2009], and Apostolakis and Dargush [2010]. The main advantage of this type of algorithm is its wide applicability, with no restrictions on linearity of the structure. Moreover, it allows discrete design variables and is aimed at global optimal rather than local optimal values; however, extensive computation is required.

(3) *Control theory-based algorithm*: Examples of this approach include Gluck et al. [1996] and Yang et al. [2002]. Those methods have the advantage of reducing computational efforts since they do not require the computation of structural responses from dynamic analysis. Zhang and Soong [1992] developed a sequential search algorithm based on the concept of controllability. Later, a simplified sequential search algorithm was proposed [Garcia and Soong 2002] was proposed that essentially achieved all the advantages of the conventional sequential method but was less complicated. Yet such algorithms are formulated within the framework of linear matrix inequalities, and thus their applicability is limited. A criticism of such a method also lies in the lack of performance-based design criteria within the methods [Whittle et al. 2012].

Most of the aforementioned methods focus on FVDs in low- to median-rise buildings. Intensive computation is needed to optimize the distribution of dampers and their properties even

for low- to median-rise structures. Whittle et al. [2012] compared two conventional design methods and three advanced optimization methods, and showed that even for computationally efficient optimization algorithms, the total computation time required for a ten-story building was 10–50 times that for a conventional design. For a taller building with complex 3D, nonlinear dynamic behavior, typical optimization algorithms are not expected to be computationally efficient. Moreover, an automated process without conducting dynamic analysis would perhaps hide the underlying causal dependencies between damper properties and placement, and system performance. This chapter outlines a step-by-step FVD preliminary design procedure, with particular emphasis placed on the story-wise damper placement method. Three conventional damper placement schemes are proposed, and their advantages and limitations are examined. An improved design is proposed based on performance-related and cost-related factors. Finally, factors affecting the damper design, such as the damper supporting brace stiffness and damper locations in one frame, are discussed.

8.3 ANALYSIS METHOD

In ASCE 41-13 [ASCE 2014], four possible analysis methods are allowed: Linear Static Procedure (LSP), Linear Dynamic Procedure (LDP), Nonlinear Static Procedure (NSP), and Nonlinear Dynamic Procedure (NDP). For retrofitted structures that are likely to enter the inelastic range, the most appropriate method would be a NDP. With the introduction of concentrated damping forces at the FVD's point of attachment, their effects on adjacent structural elements should be explicitly simulated with damper elements rather than an equivalent global damping ratio. This renders static analysis methods inappropriate. Another justification for NDP is that for cases where dampers are not assigned at all story levels, other analysis procedures can lead to inaccuracies in calculating the demand on structural members [ASCE 2014]. Therefore, NDP was chosen to examine the structural behavior with supplemental damping devices. The FVD elements were modeled as a spring and dashpot in series (Maxwell element) supplementing the as-built building model at selected damper locations.

For the feasibility study, the retrofit design focused primarily on a hazard level corresponding to the Basic Safety Earthquake, Level 2 for existing buildings (BSE-2E) prescribed in ASCE 41-13. The intent of the retrofit was to reduce the concentration of drifts in the lower levels (stories 5–10) and to reduce the overall drifts of the structure to a level where brittle fracture of the beam-to-column connections were reduced in number so as to not jeopardize the overall stability of the structure under the BSE-2E hazard level. Previous analysis showed that column splices need to be repaired in multiple places to ensure structural stability. Removing the heavy concrete cladding helped reduce the drift demands and provided space for installation of supplemental dampers. Therefore, a "two-stage" retrofit plan was proposed. In stage-1 plan, strategies were used to fix the brittle column splices and remove the exterior concrete cladding, which is denoted as the "as-built" ("Model 1c" in Chapter 4.3). In the stage-2 plan, the fluid viscous dampers were introduced.

8.3.1 Ground-Motion Selection

To streamline the analysis process during these preliminary feasibility studies, only three records were used. However, as stipulated by ASCE 41-13, the largest response value computed for the parameter of interest was used to assess the performance of the system. Ground motions were

selected based their pseudo-acceleration response spectra's match to the target spectrum at the fundamental period of the as-built structure, as shown in Figure 8.3. For the BSE-2E hazard, the ground motions selected correspond to two recordings from the 1989 Loma Prieta earthquake (South and Pine Streets in Hollister and Hollister City Hall) and the Fortuna Blvd. station from the 1992 Cape Mendocino earthquake.

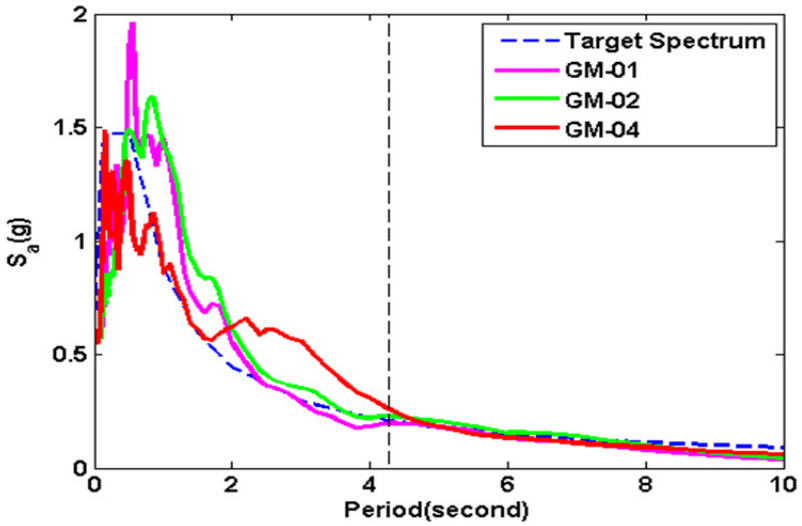

Figure 8.3 Response spectra of selected ground motions and target spectrum.

8.4 PRELIMINARY DESIGN PROCEDURE

8.4.1 Architectural Constraints

Figure 8.4 shows the plan and elevation views of the building. In the plan view of a typical floor, the black boxes indicate column locations and the crossed boxes indicate openings. The interior frames are usually adjacent to stairs and elevator locations. Locating dampers there would interfere with office space and egress; it would also likely result in a more disruptive retrofit approach than having only limited numbers of elements added to the building's exterior. Therefore, the perimeter frames were initially selected as the ideal place to add dampers. The dampers were distributed across each frame, as seen in Figure 8.4, to minimize accumulation of damper forces in adjacent columns. Additional discussion about damper locations will be addressed in Section 8.6.4. The odd number of bays in the longitudinal direction of the building resulted in a skewed distribution of dampers. In this feasibility study, the difficulty associated with the installation of dampers on the perimeter of the building associated with the architectural features were not considered.

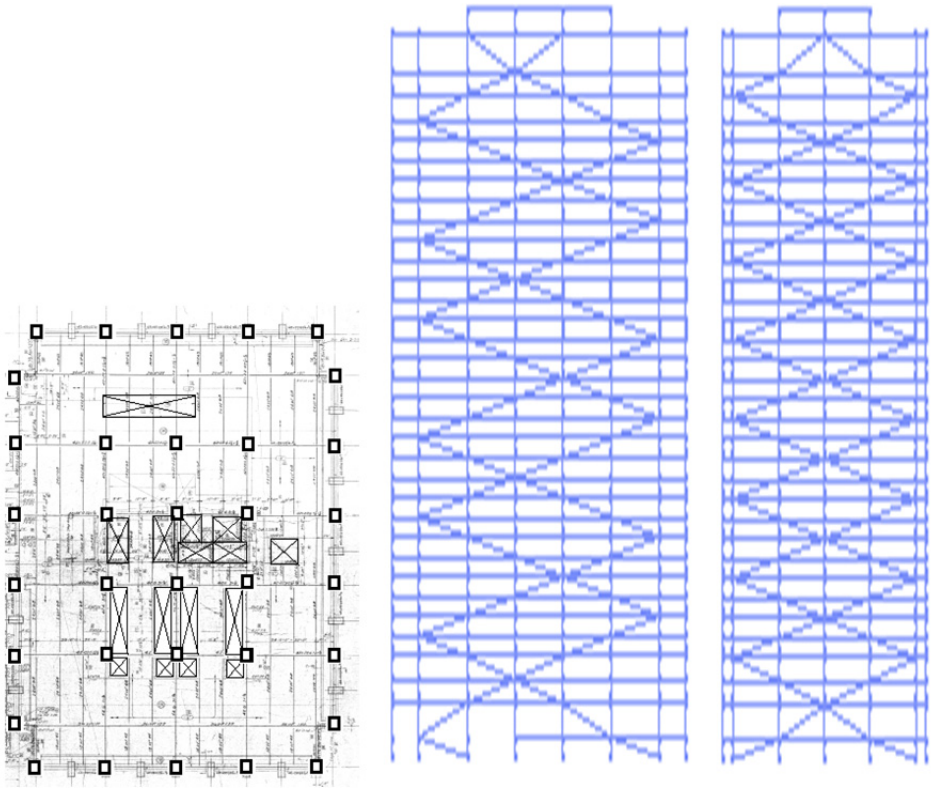

Figure 8.4 **Plan view and exterior elevations of the case-study building with trial placement of damper.**

8.4.2 Effective Damping Ratio

Estimating the overall effective damping needed (including the intrinsic damping and supplemental damping from the FVDs) to reduce the overall drifts and drift concentrations to acceptable levels is a crucial step in selecting the appropriate number and size of dampers. For this preliminary study, a simple and direct approach was used. Several guidelines and codes provide damping coefficients to modify the design response spectrum to account for damping values other than 5%. The values are typically derived based on responses of simple structural systems to a limited selection of ground motions, not including records on soft-soil sites and from near-fault sites [Ramirez et al. 2001].

This study used a spectrum modification approach developed by Rezaeian et al. [2012], which uses a damping scale factor (DSF) to adjust the 5% damped spectral ordinates to damping ratio ranges between 0.5–30%. The factors from Rezaeian's study are based on analyses using the entire NGA-W2 earthquake record set. In this procedure, the target acceptance criterion was based on the roof drift at which the as-built structure suddenly collapses. This was implemented simply by examining Figures 7.2 and 7.3. For the model considered (Model 1c), the roof displacement in the *X*- and *Y*-directions at which the structure exhibits a complete loss of capacity was identified. The value was identified as 38 in. in the *X*-direction and 32 in. in the *Y*-direction. Then, ASCE 41-13 (2014) was applied to assess the expected roof displacement for the BSE-1E and BSE-2E excitation using Equation 7-28 in the standard:

$$\delta_{t\,5\%}=C_0C_1C_2S_aT_e^2/4\pi^2g$$

where:

C_0 = modification factor for transforming from SDOF to MDOF, 1.3;

C_1 = modification factor for elastic analysis, 1.0;

C_2 = modification factor for pinched hysteresis shape, degraded stiffness, and deteriorated strength, 1.0; and

T_e = fundamental period, sec.

This results in an estimated roof displacement in the *X*-direction of 48 in. at the BSE-2E hazard level; therefore, a DSF of (38/48=) 0.79 is needed in this direction. The value of required damping to achieve this DSF was estimated from the regression analysis equation proposed by Rezaeian et al. [2012]:

$$\ln(DSF) = b_0 + b_1 \ln(\beta) + b_2 \left[\ln(\beta)\right]^2 + \left\{b_3 + b_4 \ln(\beta) + b_5 \left[\ln(\beta)\right]^2\right\} M + \left\{b_6 + b_7 \ln(\beta) + b_8 \left[\ln(\beta)\right]^2\right\} \ln(R_{RUP} + 1)$$

where the regression coefficients b_i can be found in Table 4.1 of their report.

Following this procedure, an effective damping ratio of 10% and 15% for the *X*-direction and *Y*-direction, respectively, were required for BSE-2E hazard level. For comparison, damping tables contained in ASCE 7-10 suggest 12% and 18% effective damping for the same BSE-2E hazard-level target roof displacement for the *X*- and *Y*-directions, respectively. The procedure selected the performance target from the pushover curve of the specific building and considered the two horizontal directions separately; in addition, it used an improved DSF that considers variations of magnitude, source-to-site distance, and local site conditions. The validity of this method will be demonstrated later using the results of nonlinear dynamic analyses of retrofitted building models.

8.4.3 Initial Placement Method

The effective damping ratio relates to the damping constants *C* of the FVDs, which is a parameter related to the damper force by Equation (8.2). The set of *C* values were calculated based on the strain energy method in ASCE 41-13, considering both linear dampers and nonlinear dampers:

$$\xi_{\text{eff}} = \xi_0 + \frac{\sum_j \lambda C_j \phi_{ij}^{1+\alpha} \cos^{1+\alpha}\theta}{2\pi A^{1-\alpha} \omega^{2-\alpha} \sum_j m_i \phi_i^2} \tag{8.2}$$

For the results presented herein, the structure's first-mode frequency and mode shape were used in conjunction with the desired effective damping ratio to identify the *C* coefficients for nonlinear FVDs (here with α = 0.35). The damping exponent α was selected based on a parametric study to find optimized damping nonlinearity. Further details are provided in Section 8.6.1.

Besides the optimization algorithms, some quick and intuitive ways to locate dampers are more popular in engineering design. Soong and Dargush [1997] suggested a uniform distribution of viscoelastic dampers design for the original World Trade Center, though it might not be very effective especially in the top floors. Because dampers on upper stories are less effective at reducing drift than those in the lower stories, Hwang [2008] proposed that C values be sized such that the damper force be proportional to story–shear forces. Another possible approach is stiffness proportional placement, requiring larger dampers at stiffer stories. This generates a stiffness proportional Rayleigh-type damping, without coupling of different modes. Therefore, three conventional distributions of C over the height of the building were considered:

(I) Uniform damping constant;

(II) Damper force proportional to story–shear demand; and

(III) Damping constant proportional to story stiffness.

The in-line brace used to drive the brace was given stiffness equal to twice the story stiffness to ensure the effectiveness of viscous dampers. Issues related to the cost effective supporting bracing stiffness are discussed in Section 8.6.3. The braces were arranged as a single diagonal across a bay. The configuration over the height of the structure is shown in Figure 8.4.

Figure 8.5 sketches the conceptual consequence of distributing damping constant C on story force. Scheme II and Scheme III are similar, yet the results indicated smaller damper sizes (C values) for stories 5–9 for Scheme II, and for story 2 (mezzanine level) for Scheme III.

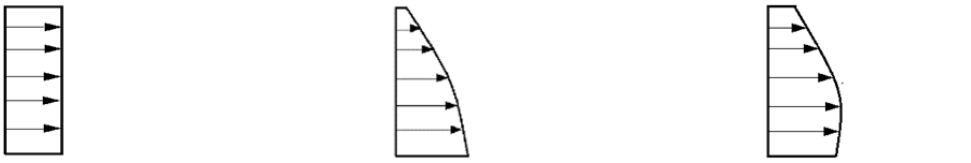

Figure 8.5 Conventional schemes for distributing damper constant along building height.

8.4.4 Results

8.4.4.1 Structural Responses

Peak story drift, floor displacement, and floor acceleration envelopes were examined to check the effectiveness of the three proposed damping systems. As required by ASCE 41-13, the maximum value for the three time-history analyses was used to compare the different systems. Each direction was evaluated separately, considering different damping ratio used; only X-direction responses are presented here. Responses in the Y-direction show a similar trend.

Figures 8.6 and 8.7 show the envelopes of maximum story displacement and maximum story drift. All three design schemes help reduced the story drift ratio by about 20–30%, and by a much larger amount in stories 5 through 9. Scheme II was the least effective, which was most likely due to the small damping constants assigned in this range. Schemes I and III were more effective, with Scheme III being slightly more effective in reducing the peak story drift ratio. A comparison of the drift ratio distribution in different cases demonstrates that a reduction of drift

ratio in floors 5–9 would be likely to increase the drift ratio in the mezzanine level, indicating that the dampers would change the modal properties of the building and thus the higher mode participation. For the most effective scheme in terms of reducing drift ratio (Scheme III), the maximum peak story drift is about 1.1%, which is acceptable under the BSE-2E hazard-level earthquake [LATBSDC 2014; ASCE 2014]. Figure 8.6 also shows that the peak maximum roof displacement is about 38 in. for all three cases, validating the method to calculate the effective damping ratio (Section 8.4.2).

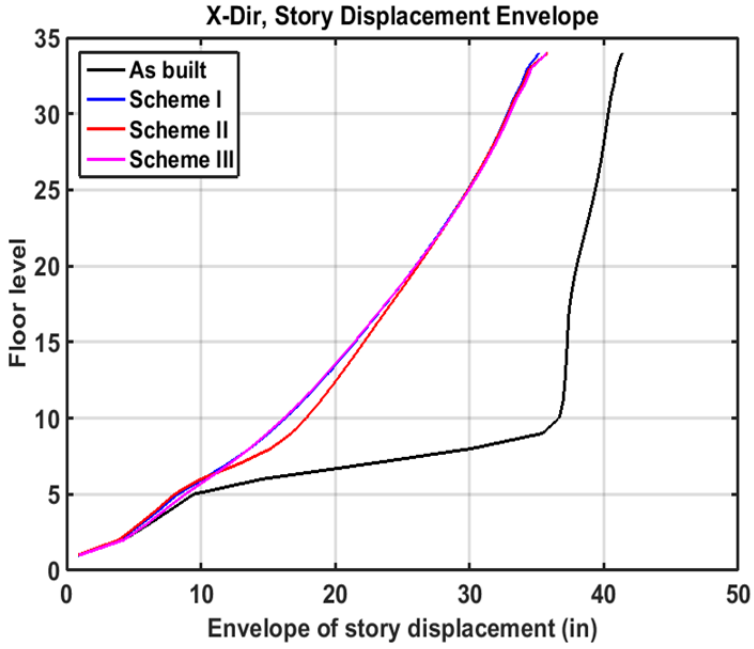

Figure 8.6 **Peak story drift displacement in *X*-direction (BSE-2E).**

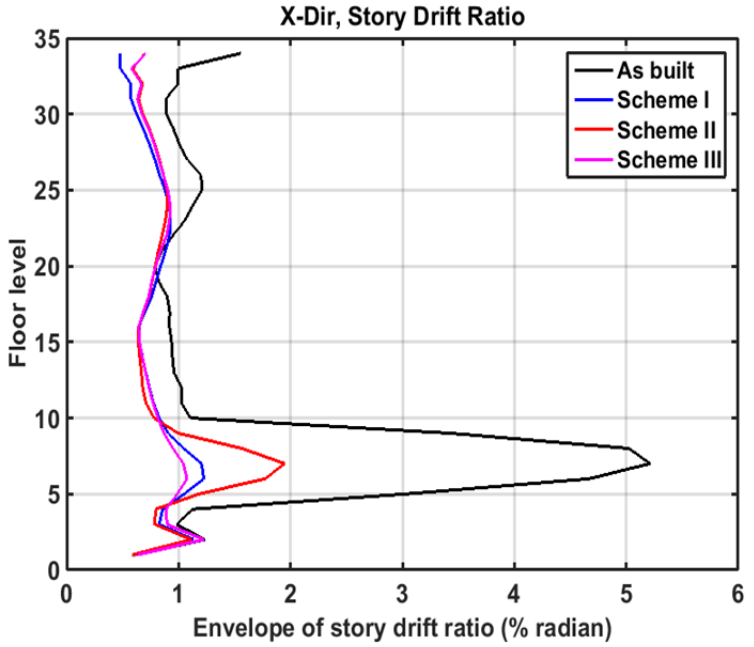

Figure 8.7 **Peak story drift ratio in *X*-direction (BSE-2E).**

One of the relevant improvements resulting from the suppression of weak stories was the reduction of beam-to-column connection failures; see Figure 8.8. In terms of the percentage of beam-to-column connection failures at a floor level, the maximum percentage was reduced from 58% to less than 2% (Scheme III). Connection failure corresponded with beam end rotation demands larger than the collapse prevention criteria per ASCE 41. Such a reduction significantly reduced the number of connections that required retrofitting, thus reducing repair costs.

Figure 8.9 shows the maximum peak floor acceleration (total accelerations) envelope. The FVDs reduced the floor accelerations by about 30–40% throughout the stories. The peak value, which occurs at the roof level, was reduced from almost 0.9*g* to about 0.5*g*. Another benefit of introducing FVDs is that it results in a faster decay of structural vibrations at the end of the earthquake, as indicated by the acceleration time history in Figure 8.10 for Scheme III evaluated at floor 26. The reduction of both story drifts and floor accelerations could help reduce both structural and non-structural damage, and the fear and discomfort of occupants.

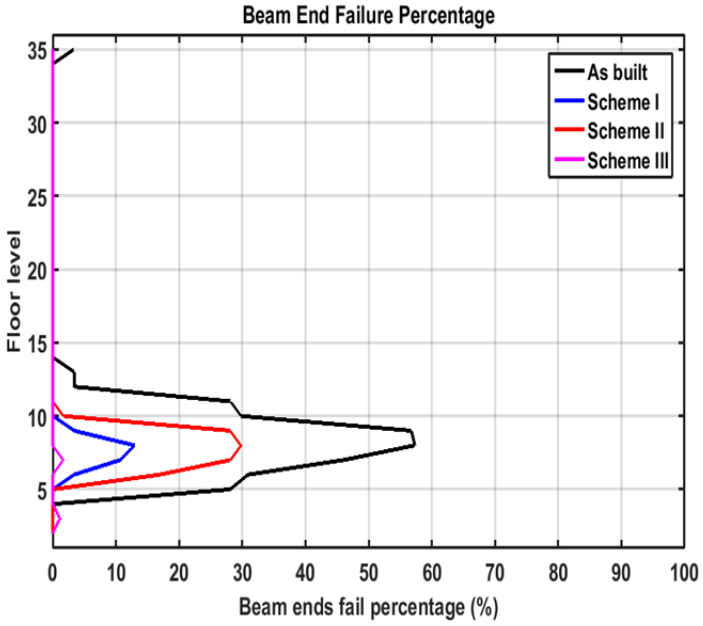

Figure 8.8 Beam-to-column connection failures (BSE-2E).

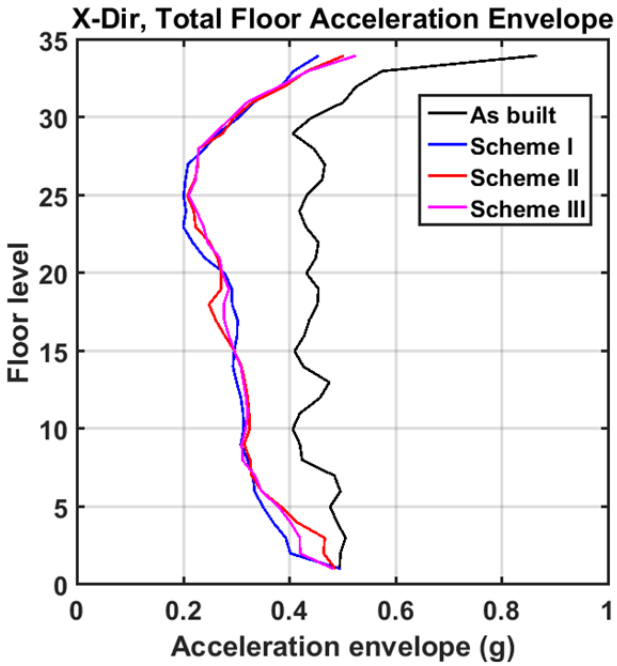

Figure 8.9 **Peak floor total accelerations in *X*-direction (BSE-2E).**

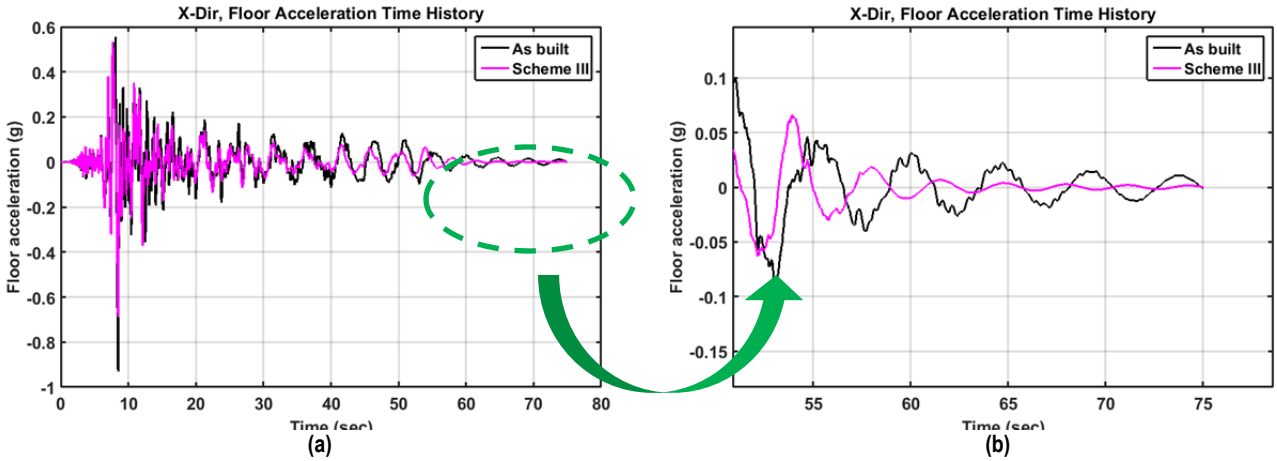

Figure 8.10 **Story-26 acceleration time history (Scheme III): (a) acceleration time history for the 26th floor in the *X*-direction; and (b) zoomed in view at the free vibration period.**

8.4.4.2 Damper Responses

Damper responses need to be determined in order to assess potential costs of incorporating dampers. The hysteresis loop of the maximum-loaded damper element is plotted in Figure 8.11(b), and the damper force demand envelopes are shown in Figure 8.11(a). The peak damper forces are generally in *Y*-direction since the damping demands are much larger in this direction.

All cases give fairly large damper forces, with the maxima ranging from 1240 kips to 1470 kips at the lower stories. Note that Scheme III, which produced the most effective reduction

in story drift and about the same acceleration as the other damped cases, has a smaller damping force demand (1240 kips).

Such large dampers are possible to fabricate; see Taylor Device Inc. [2010a, b, c]. Table 8.1 is an excerpt from a list provided by Taylor Device Inc., showing variable damper sizes with different force capacities, strokes, and weights, and current designs within the manufacturing scope. However, large dampers with capacities up to 1300 kips used in engineering practice [Taylor and Katz 2004] might require installing a mega brace system, which would increase the cost of installation. Thus, alternative strategies include using two dampers per driver (for example, installed in parallel), more damped bays at selected stories, or utilizing toggle-brace mechanisms to magnify the effective force of a damping device [Constantinou et al. 2001].

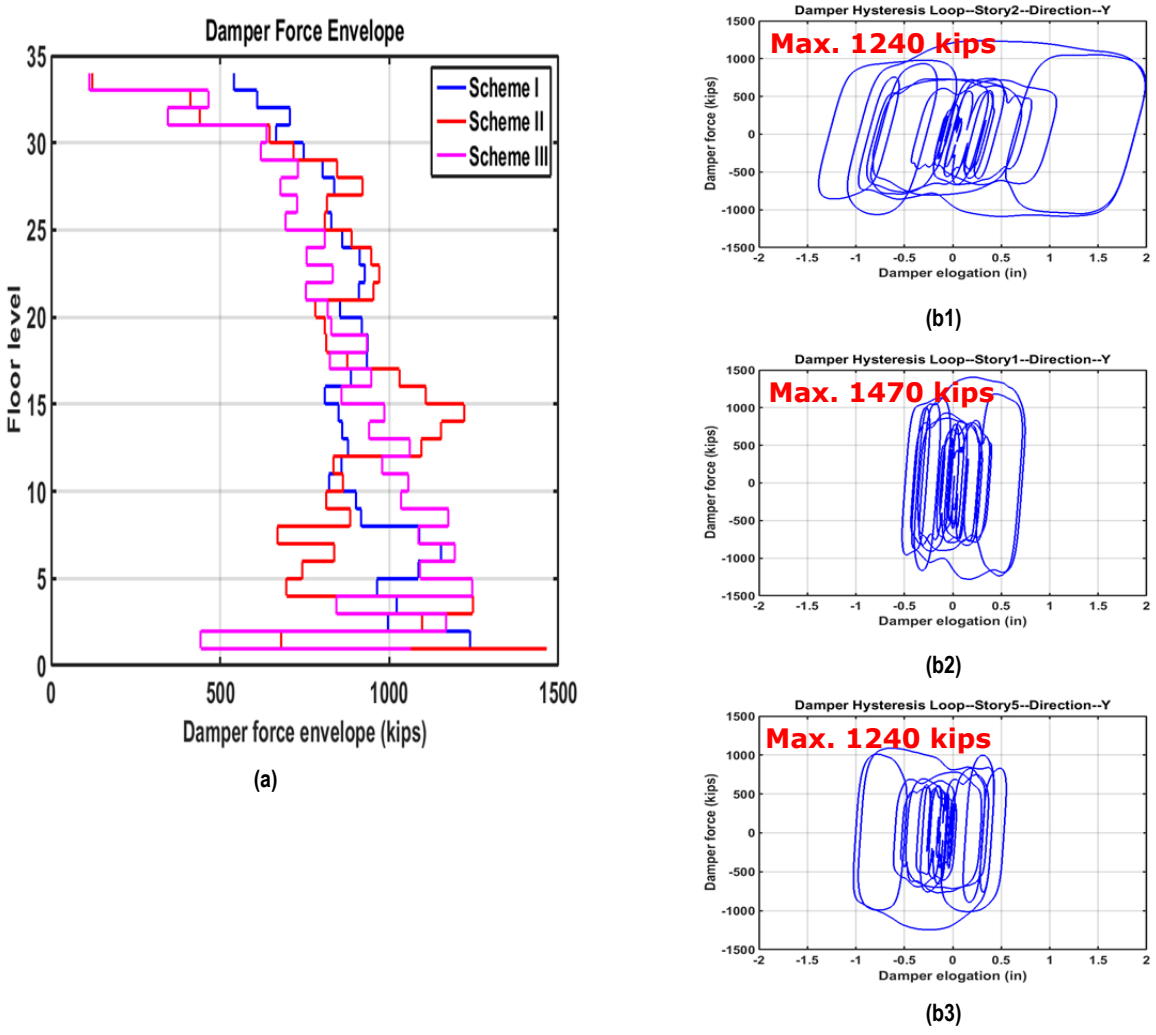

Figure 8.11 **Damper responses: (a) peak damper force; (b1) Scheme I; (b2) Scheme II; and (b3) Scheme III.**

Table 8.1 Available damper sizes (Taylor Device Inc.).

Force (kips)	Stroke (in.)	Weight (lbs)
55	±3	90
110	±4	185
165	±4	300
220	±4	425
330	±4	600
440	±5	900
675	±5	1300
900	±5	2650
1450	±5	4100
1800	±5	5500

8.4.4.2 Column Axial Forces

Another primary concern associated with the addition of dampers is possible accumulation of axial forces in adjacent columns. This is especially true for base columns in tall buildings where the forces due to gravity and seismic loading are already large. Dampers might exacerbate this condition due to accumulation of forces transferred to the adjoining columns.

The compression and tension status of one group of corner columns [Group 1 identified in Figure 7.23] was evaluated, and the D/C ratio envelope is plotted in Figure 8.12 where tension is assumed to have a positive sign. In the model with FVDs, the column splices are fixed; thus, the tension capacities were estimated based on the gross section yielding following ASCE requirements, i.e., $P_t = A_g \times F_y$. On the compression side, the buckling of columns were considered to find the lower bound compression capacities: $P_c = A_g \times F_{cr}$. The green line plotted in the same figure indicates the demands due to gravity loads alone, which was about 30% of the total demands. The results indicate that the dampers put extra demands on the columns. The uplift issue was eliminated here since the column splices were assumed to have been retrofitted.

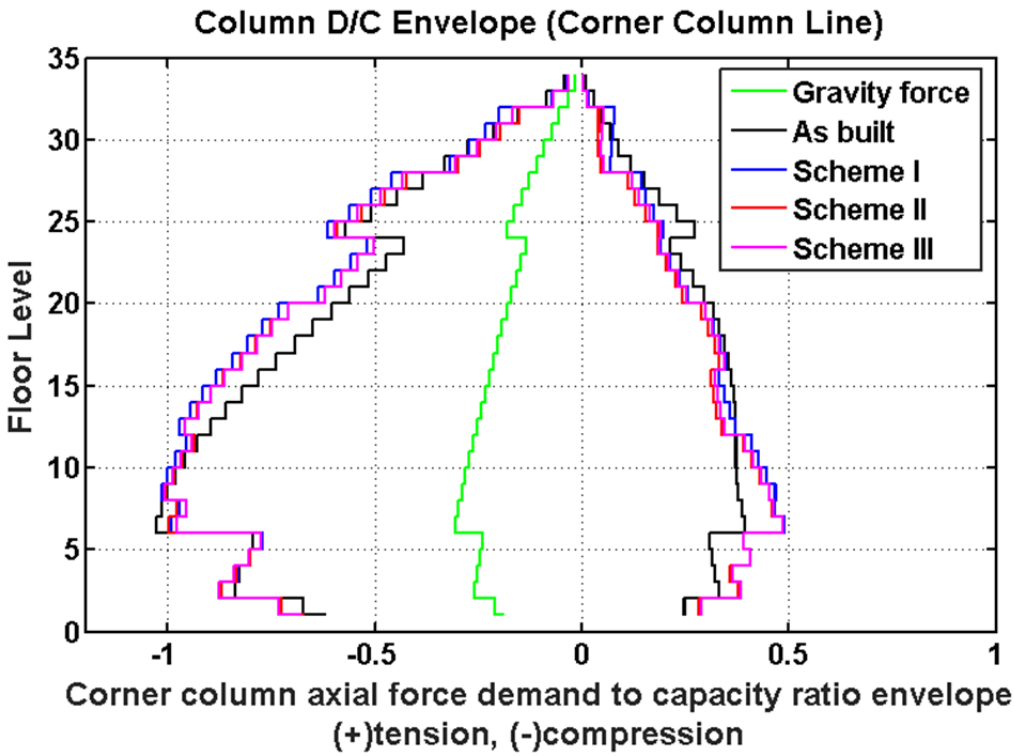

Figure 8.12 **Peak column compression D/C ratio (BSE-2E): column D/C ratio envelope, tension (+), and compression (-).**

8.4.4.3 Observations

A comparison of the three schemes studied demonstrates that uniformly sized dampers provided reasonable results; however, it required installing larger dampers than necessary in the upper stories and, in particular, led to large damping forces near the base of the structure. Scheme II, where dampers were sized in order to achieve damper force distribution proportional to story shear, failed to fully suppress the weak-story phenomenon in stories 5–9. Such a scheme sizes dampers based on the resulted story shear-force demands, which are highly dependent on the ground motion analyzed, number of elements failure, etc. The resulted distribution following this placement method gave a relatively small damping capacity in lower levels, indicating a weakness of this methodology. An alternative that might be more prudent is to size dampers based on target story-shear demands. Scheme (III), where the damping constant was proportional to story stiffness, provided the best results and introduced the smallest damper force demands; thus, it was selected as the candidate for further refinement design.

8.5 PHASE II: REFINEMENT

The results of the preliminary study showed that dampers were not equally effective in all stories. Thus, it was deemed more cost effective to concentrate dampers in only stories where the control effectiveness is greater. Also, under a given effective damping ratio, it would yield a better performance if a larger proportion of the damping were concentrated in the lower levels. Starting with Scheme III, an improved scheme was proposed to remove dampers from stories

where their effectiveness was limited. The scheme was further refined by re-sizing dampers at different story levels based on performance-related and cost-related indices. The objective was to reduce the cost of the dampers by limiting both the number of dampers and the peak damper forces, while still maintaining the desired structural response.

8.5.1 Strategic Damper Locations Based On Control Effectiveness

The control effectiveness of FVDs depends on properties of both dampers and frames. In general, locations with large horizontal deformations and thus larger axial deformation of dampers, are ideal locations for dampers since they maximize the energy dissipation capacity of dampers. This study considered an equivalent frame model [Kasai et al. 2013]. To evaluate the effectiveness of each story, two frame parameters were proposed: one representing the story stiffness of the frames alone and another for story stiffness with rigid braces.

8.5.1.1 Frame Parameters

Two models were constructed: one representing the as-built structure and the other one adopting artificial rigid elements placed in previously selected dampers locations. Two parameters were calculated for each story: K_N^i indicates the story stiffness without dampers, and K_R^i represents artificial rigid brace elements. Here the subscript "N" stands for the state N (no dampers), and "R" represents state R ("rigid" elements). The LSP was conducted for those two states by applying lateral forces following ASCE 7 [2010]:

$$F_x = \frac{w_x h_x^k}{\sum w_x h_x^k} V \tag{8.3}$$

A sketch of the frame models at two separate states (state N and state R) are illustrated in Figure 8.13. The key parameters for the study were the relative displacements and story forces at each state. These were obtained from static analysis; thus the story stiffness K_N^i and K_R^i be estimated with the following formula:

$$K_N^i = Q^i \Big/ \left(u_N^i - u_N^{i-1}\right) \qquad K_R^i = Q^i \Big/ \left(u_R^i - u_R^{i-1}\right) \tag{8.4}$$

Ideally, K_R^i would be larger than K_N^i at all levels since an increased story stiffness indicates that the supplemental components are capable of suppressing response. To quantify such control effectiveness, the ratio K_N^i / K_R^i was selected as a controlling parameter; the larger this value is, the more effective the control would be.

There is a wide range of this ratio for this particular building, ranging from 0.9 (floor 33) to 75 (floor 2), indicating ineffective control of adding supplemental devices in upper floors. The large value at the mezzanine level (floor 2) suggests an insufficient stiffness at this level, and other stiffening strategies might also be needed in conjunction with dampers in order to suppress the responses to a desired level. Kasai et al. [2008] have shown that $K_N^i / K_R^i \approx 2$ is acceptable for good passive control, and it is used herein as a basis to select damper locations. Detailed calculations are shown in Table 8.2, which identifies locations where the ratio is greater than 2 and thus dampers are retained. Locations where the ratio is less than 2 are considered to have less

passive control capabilities and dampers are removed. Following this adjustment, the number of dampers was reduced by about 37%, with more reduction in the *X*-direction.

Figure 8.14 shows the new configurations of damper elements in one frame. With the assumption that the damper sizes are the same as before (Scheme III), the reduction of damper numbers would result in a reduction of effective damping ratios: 7% in *X*-direction and 13% in *Y*-direction, respectively.

Table 8.2 Calculations of frame parameters.

Story, i	*X*-direction			*Y*-direction		
	K_N^i (k/in.)	K_R^i (k/in.)	K_R^i / K_N^i	K_N^i (k/in.)	K_R^i (k/in.)	K_R^i / K_N^i
1	19000.0	1226694.7	64.6	20332.0	237548.2	11.7
2	5847.4	439397.8	75.1	6248.2	464943.4	74.4
3	12570.9	107043.3	8.5	13447.8	294426.0	21.9
4	11208.0	34572.6	3.1	12241.7	103710.7	8.5
5	12619.8	53602.7	4.2	14108.7	45809.4	3.2
6	12160.5	73750.8	6.1	13896.0	44654.9	3.2
7	11855.3	52716.3	4.4	13703.8	69570.8	5.1
8	11624.6	28973.0	2.5	13536.2	63099.8	4.7
9	11391.1	34034.5	3.0	13322.0	52750.4	4.0
10	11233.6	40378.2	3.6	13131.4	41550.7	3.2
11	11160.5	33184.5	3.0	12954.7	56890.5	4.4
12	11111.3	23162.1	2.1	12809.9	49931.5	3.9
13	10994.6	24778.0	2.3	12640.9	41224.9	3.3
14	10879.1	28834.7	2.7	12499.5	39237.6	3.1
15	10752.8	25953.1	2.4	12347.8	31780.1	2.6
16	10568.0	19158.8	1.8	12146.6	28447.7	2.3
17	10058.4	19765.7	1.9	11589.1	33345.0	2.9
18	9592.3	22731.7	2.4	11069.8	32771.2	3.0
19	9428.0	20893.2	2.2	10872.8	29864.4	2.7
20	9313.4	16288.9	1.7	10724.0	26920.9	2.5
21	9079.9	16173.1	1.8	10430.0	30431.4	2.9
22	8847.6	18021.8	2.0	10152.0	26342.7	2.6
23	8627.8	16629.9	1.9	9953.7	24011.6	2.4
24	8433.1	13477.5	1.6	9790.6	22762.1	2.3
25	8222.8	12840.3	1.6	9615.4	20320.0	2.1
26	8005.7	13480.5	1.7	9431.6	17376.7	1.8
27	7710.2	12210.2	1.6	9185.8	17197.7	1.9
28	7395.5	9965.1	1.3	8906.0	16584.0	1.9
29	7041.1	8825.1	1.3	8566.4	14479.2	1.7
30	6608.4	8416.5	1.3	8139.6	12373.7	1.5
31	5929.0	6982.4	1.2	7421.6	10671.7	1.4
32	3466.5	3821.9	1.1	4477.1	5909.4	1.3
33	3514.9	3279.4	0.9	4619.5	5279.4	1.1
34	985.6	1004.2	1.0	1254.3	1512.6	1.2

Shaded boxes indicate locations where dampers are kept.

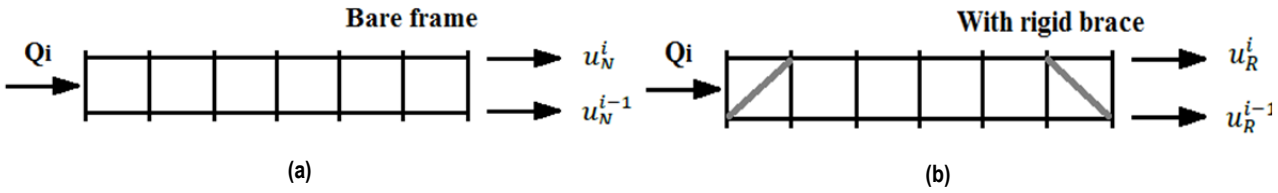

Figure 8.13 Sketch of frame models for each story: (a) state "*N*" and (b) state "*R*". [Kasai et al. 2013].

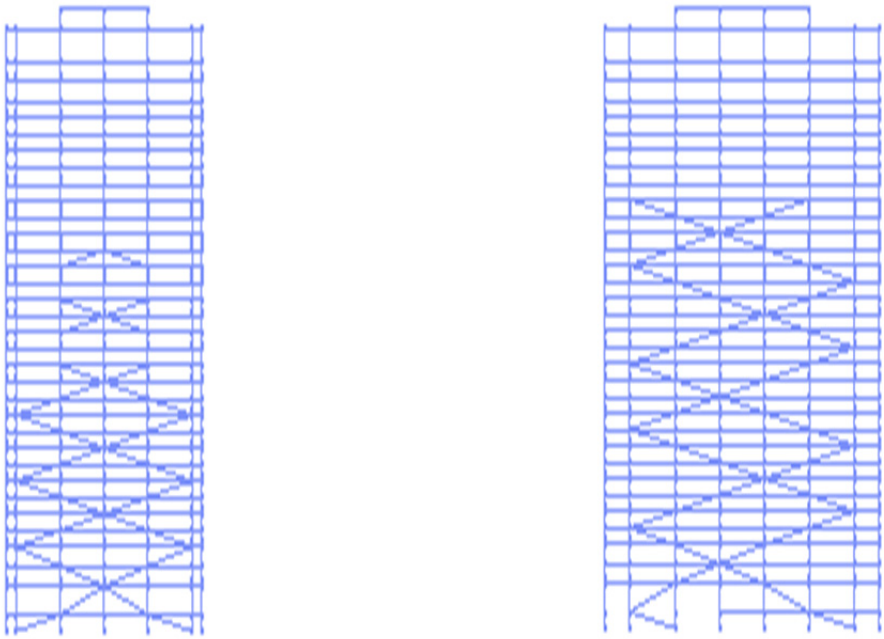

Figure 8.14 New configuration with reduced damper elements.

8.5.2 Resizing of Dampers Based on Performance- and Cost-Related Indices

Damper demands are different in various levels. The lower levels require large damping demands since more additional dissipated energy was required in those regions. Preliminary results indicate that a further increase of additional damping would be required at the lower stories if the IO objective was met at BSE-2E hazard-level earthquake. To determine quantitatively a proper damping distribution at different zones, a simplified optimization study was proposed to investigate the performance and cost at each story. The revised layout with fewer dampers (Section 8.5.1) was used as a basis, and nonlinear time history analysis was conducted. The performance-related and cost-related indices were then identified in order to assess quantitatively the structural responses and the additional cost of the dampers. Such a procedure could be used to evaluate control effectiveness associated with specific floor level or the whole system. As a result, a refined scheme with adjusted damping sizes (*C* values) was proposed and the improvement of such an optimizing procedure was checked.

8.5.2.1 Performance-Related Index

The control effectiveness of dampers at each floor are evaluated with the following EDPs: inter-story drift ratio, residual drift ratio, floor acceleration, and peak floor acceleration after 15 seconds of free vibration following the earthquake. Note that for the last EDP, peak floor acceleration after 15 sec of free vibration was an average value evaluated for the last cycle of responses. Different importance weights were assigned to each EDP, with their summation totaling 1.0. Response of the as-built and retrofitted scenarios were evaluated, and the performance index was defined to be 0.0 if the response of the as-built scenario was smaller than a predetermined allowable value. Otherwise, the performance index (PI) was defined as the ratio between the as-built EDP and the retrofitted value. Normalization of the PI for each EDP was performed by dividing the PI at each level by the maxima among all stories. This procedure is repeated for each EDP, and each index is multiplied with an importance weight to obtain a final PI, using the following equation:

$$PI(\%) = (w_1 \times PI_1 + w_2 \times PI_2 + w_3 \times PI_3 + w_4 \times PI_4) \times 100 \quad (8.5)$$

where PI_i , i = 1,…4 are the performance index for each EDP, and w_i, i = 1,…4, are the importance weights for each EDP.

The importance weights were selected based on engineering judgment by evaluating their effect on the overall response. In this study, those values are: w_1 = 0.3 for story drift ratio, w_2 = 0.2 for residual drift ratio, w_3 = 0.3 for peak floor acceleration, and w_4 = 0.2 for peak floor acceleration after 15 sec of free vibration. The *PI* is in the range of (0, 1); a larger value indicates better performance.

The maximum allowable values were selected considering both structural and non-structural aspects. For non-structural considerations, emphasis was placed on limiting the repair cost of the building. Simple cost analysis was conducted by Terzic et al. [2015] using the Performance Assessment Calculation Tool (PACT) for a three-story special moment-resisting frame (SMRF). Assuming that the SMRF undergoes uniform distribution of story drift, a relationship between repair costs of a SMRF system and the drift ratio was derived. In order to maintain the functionality of the building after a seismic event under aBSE-2E hazard-level event, a performance objective that limited the total repair cost within about 5% of the replacement cost of the building was selected; correspondingly, a 1% drift ratio limit was used as a maximum allowable value. Similarly, a value of 0.1% was selected for residual drift ratio. For the accelerations, a peak value of 0.5*g* was selected to limit the discomfort and fear of occupants, and a value of 0.001*g* was selected as the limit for peak acceleration after 15 sec of free vibration to suppress ongoing vibrations due to low inherent damping. These criteria could provide information directly relating EDPs to cost, providing both owners and engineers with better insight into each EDP.

8.5.2.2 Cost-Related Index

In order to achieve satisfactory structural responses without prohibitive expense, a cost-related index was proposed. Given that the construction fees would be highly dependent on the number of dampers used (cost of dampers, nonstructural elements' reallocation to accommodate dampers, installation fees, etc.), two parameters were incorporated in the cost-related index: the

peak damper force and the number of dampers. Following a similar procedure in the Section 8.5.2.1, the cost index (*CI*) is calculated as:

$$CI(\%) = (w_1 \times CI_1 + w_2 \times CI_2) \times 100 \tag{8.6}$$

where CI_i, I = 1,2 are ratios between the obtained demands and the maximum allowable values. They are normalized by the maxima of all stories. The maximum allowable peak damper force was selected as 1000 kips, and four dampers were selected as an allowable number of dampers per story in each direction. The importance weight w_i, I = 1,2, were selected to be 0.5 and 0.5, respectively, for each parameter. A smaller *CI* indicates less additional cost from dampers.

8.5.2.3 Index Investigation

To combine the effects of both structural performance and additional damper cost, a new index was proposed that subtracts the cost index from the performance index. The larger the new index, the more cost effective the dampers are in certain stories. The results indicate that the values are generally larger in weak stories and smaller in stories 10 and above. As a result, in the *X*-direction, a 30% increase of damping constants was introduced in stories 4–9, and a 20% reduction for stories above level 10. The other stories where dampers were retained were kept at the same size as before. Similarly, in the *Y*-direction, an increase of 20% in story damping constant was imposed in story 2 and stories 4–10. The smaller increase in the *Y*-direction was to avoid excessive damper forces considering the already large damper sizes in this direction. A check at further decreasing the number of floors installing dampers in *Y*-direction resulted in the formation of weak stories where dampers were removed. Thus, the dampers in the first 25 stories were retained, but a 20% reduction was imposed for stories 15–25.

Damping constants, *C*, used in the initial design (Section 8.4.3) were derived from theoretical values (proportional to story stiffness). This generated different *C* values for each story; however, this would limit the efficiency of systematic optimization. As such, a set of design *C* values were proposed to facilitate the optimization procedure; see Table 8.3.

Table 8.3 Allowable design *C* values.

C kip·(sec/in.)$^{0.35}$	150	225	300	375	450	525	600	675	750	825

8.5.3 Refined Placement Method

Following the procedure outlined in Sections 8.5.2 and 8.5.3, a new set of *C* values was generated, as indicated in Table 8.4. Note that there are no dampers above story 25. The damper configurations were the same as that in Section 8.5.1, as shown in Figure 8.14. The damping ratios were changed slightly from the preliminary scheme where dampers were placed in all story levels, as indicated at the end of Table 8.4. With the refined procedure, the total number of dampers was reduced from 272 to 172; dampers were installed in 18 stories in the *X*-direction and 25 stories in the *Y*-direction. The effective damping ratios were slightly smaller than before due to the refinement.

Table 8.4 Retrofit design comparison of *C* values.

Story, i	*X*-direction		*Y*-direction	
	Intial design kip·(sec/in.)$^{0.35}$	Refined design kip·(sec/in.)$^{0.35}$	Intial design kip·(sec/in.)$^{0.35}$	Refined design kip·(sec/in.)$^{0.35}$
1	454	450	766	750
2	135	150	211	300
3	490	525	739	750
4	360	525	519	600
5	520	675	818	825
6	492	675	748	825
7	502	675	810	825
8	459	600	737	825
9	474	600	803	825
10	447	450	715	825
11	465	375	792	750
12	450	375	704	675
13	465	375	770	675
14	449	375	682	675
15	464	375	739	600
16	442	0	678	525
17	429	0	704	525
18	389	300	590	525
19	404	300	660	525
20	391	0	590	450
21	380	0	625	450
22	340	300	528	450
23	347	0	572	450
24	330	0	519	450
25	338	0	572	450
26	323	0	510	0
27	328	0	557	0
28	315	0	504	0
29	323	0	552	0
30	317	0	497	0
31	322	0	546	0
32	163	0	244	0
33	262	0	348	0
34	45	0	62	0
Effective	**10%**	**8%**	**15%**	**13%**

8.5.3.1 Structural Response

The structural response and damper responses that were incorporated in the performance indices are examined. As before, the responses are the maxima from three time-history analysis set, and only responses in the *X*-direction are presented here for illustration.

Figures 8.15 and 8.16 show the story drift ratio and the story accelerations, respectively. Both retrofit designs resulted in substantially improved behavior from the as-built condition, with the refined case being slightly less effective. With the removal of dampers in upper stories, there is an observable increase of peak response for both drift ratio and acceleration. Note that the peak drift ratios in stories 2–3 increased slightly, as well as the residual drift ratio, which was most likely due to the decrease of total effective damping ratio. Such an increase might still be tolerable, given that the percentage of connection failures for both cases was small; see Figure 8.17.

On the other hand, there are observable increases in floor accelerations, especially at roof level, which has a peak value of about 0.7*g* for the refined damper scheme. The shape of the acceleration envelopes indicates that higher modes effects would still be large if dampers were removed from upper levels. Such accelerations are likely to cause discomfort and possibly fear of occupants during a large seismic event, thus future analysis could include small dampers in a few upper stories to get rid of "whipping effects." The difference of peak acceleration after 15-sec free vibration between initial design and refined design was insignificant, and thus became less of a concern.

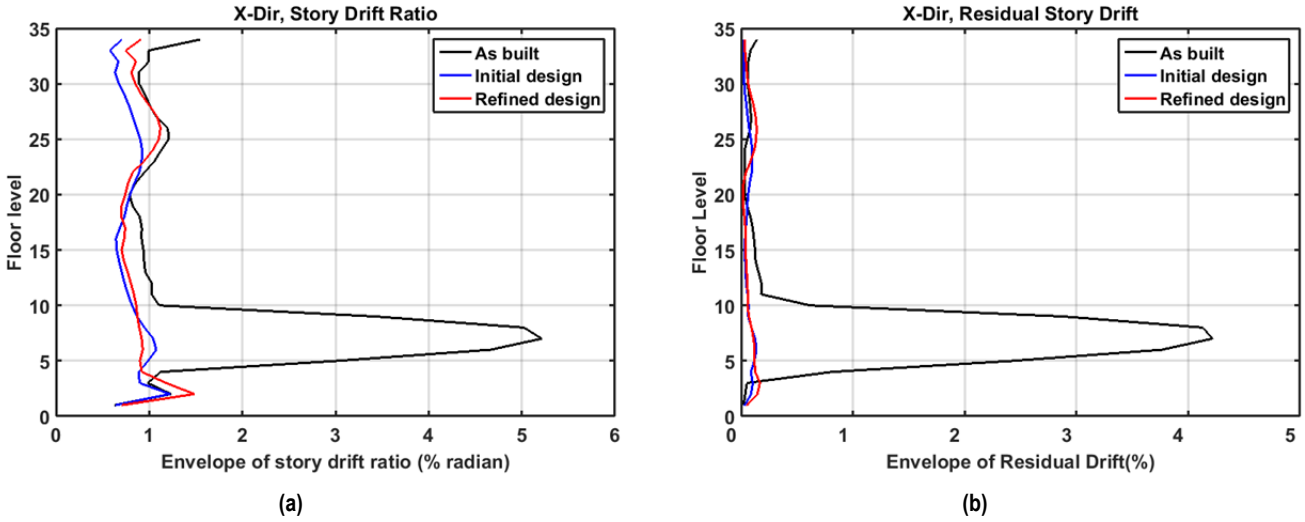

Figure 8.15 **Peak story drift ratio and residual drift ratio (*X*-direction): (a) peak story draft ratio and (b) residual story drift ratio.**

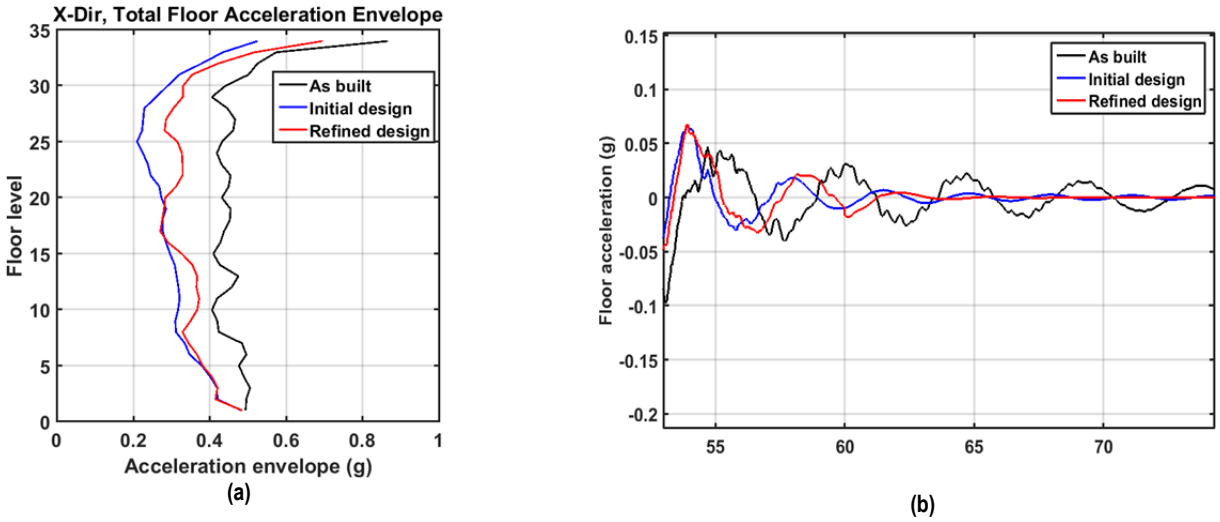

Figure 8.16 **Peak floor total acceleration and acceleration time history during free vibration (X-direction): (a) peak story acceleration and (b) acceleration history at free vibration period.**

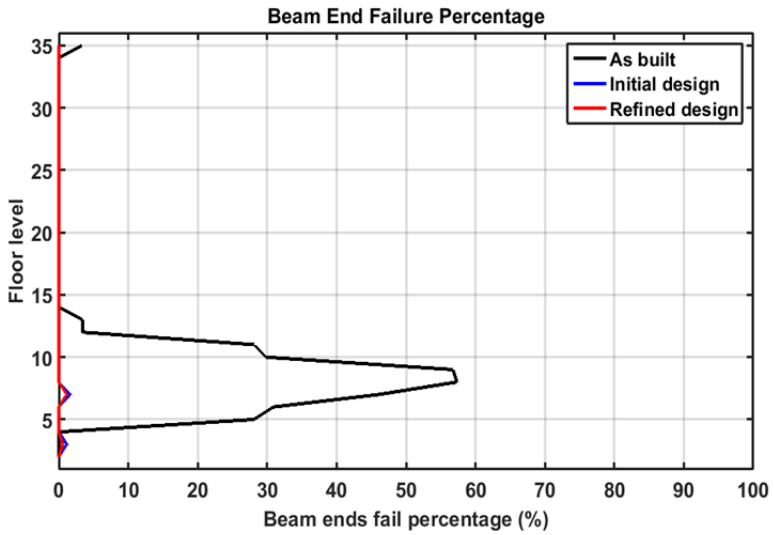

Figure 8.17 **Beam-to-column connection failure.**

8.5.3.2 Damper Responses

Peak damper responses were checked in both directions at each floor; see Figure 8.18. There was an increase of the peak forces in lower levels for the refined damper design, which was primarily in the *X*-direction. However, the decrease of damper force demand in upper levels could compensate for the increase in a few floors, and a significant reduction of damper demands were achieved by the removal of dampers in several floors.

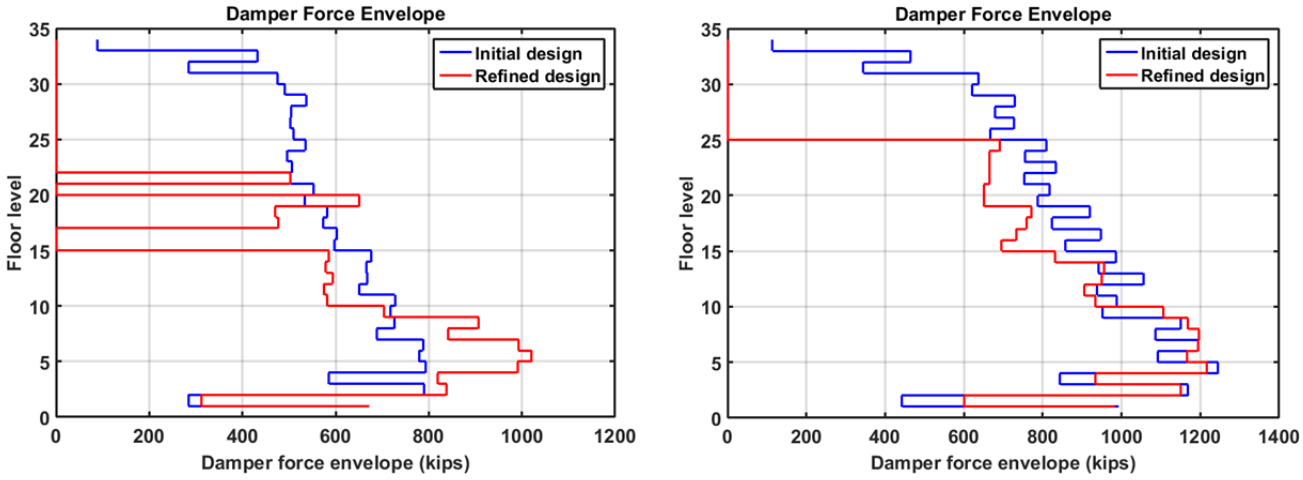

Figure 8.18 Peak damper forces: (a) *X*-direction and (b) *Y*-direction.

8.5.3.3 Column Axial Forces

The re-proportioning of damping in different stories modestly affected the peak column *D*/*C* ratio. Figure 8.19 plots the column tension and compression *D*/*C* ratio for the exterior column group (G1 in Figure 7.23) examined previously; see Section 8.4.4.2.

The refined design resulted in smaller compression and tension demands due to reduced damper sizes, bringing down the demands to the as-built case or even smaller. The reduction of column axial demands due to refinement is larger on the tension side, which brings down the peak results to be smaller than the as-built case. Since the PJP welds in the splice regions are assumed to be fixed, the tension expected is less of a concern. Nevertheless, the columns remain overloaded in compression, with peak values approaching or exceeding 1.0. Other strategies, such as strengthening the columns, adding exoskeleton system, etc., to be explored.

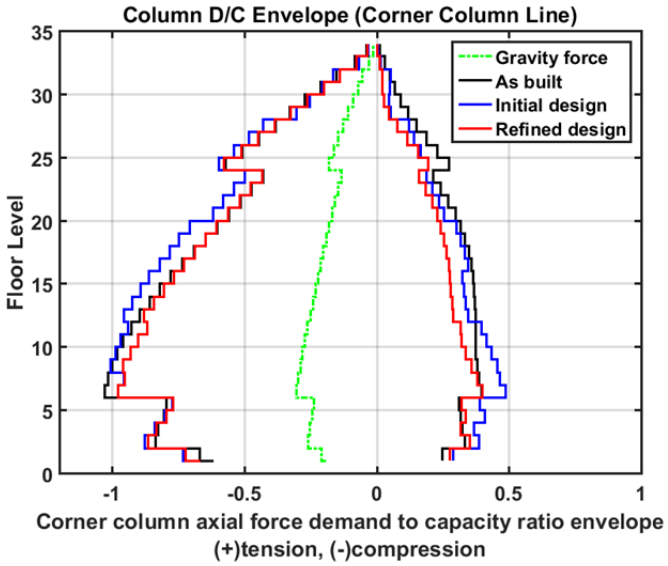

Figure 8.19 Column D/C ratio, tension (+), and compression (-).

8.5.3.4 Observation

The refined scheme proposed removing dampers in upper levels resulted in less control efficiency and re-proportioning damping constants along the building height. The structural performance was essentially maintained but with much reduced damper demands.

For completeness, a set of 20 nonlinear history analyses was conducted at both BSE-1E and BSE-2E hazard levels for the refined retrofit design. The envelopes in the following figures were the median value from 20 nonlinear time-history analysis (the solid lines). The dashed-lines indicating the median value plus one standard deviation (84th percentile) are also presented. The median values of the drift ratios and beam-to-column connection failures (in a total of two directions) showed a dramatic reduction from the as-built structure, demonstrating the efficiency of the proposed damper design. Meanwhile, the damper demands are much reduced from the preliminary design and are limited within a reasonable range at code-based hazard levels. Figure 8.22 shows the damper force demands evaluated at two BSE hazard levels. The peak damper forces (median values) are controlled within 1000 kips at BSE-1E hazard level and 1200 kips at BSE-2E hazard level. However, further refinement by reducing damper demands is desirable and a quantitative cost analysis needs to be conducted to demonstrate the cost feasibility.

Recall that the retrofit objective is to ensure structural stability at the BSE-2E hazard level, a quick check for the global collapse prevention potential is conducted for the retrofitted case, by assessing the percentage of simulation cases having peak transient story drift ratio and peak residual story drift ratio larger than permitted values by LATBSDC [2014]. Also probabilistic estimation of the confidence levels to achieve target performance objectives is conducted following the FEMA 351 procedure.

Table 8.5 is a summary of global responses based on the peak story drift ratio and permanent drift ratio. Under the BSE-1E hazard level, the retrofitted case could satisfy the requirements of both peak drift ratio and peak residual drift ratio for all cases. For the BSE-2E hazard level, a small percentage (10–15%) exceed the drift requirements suggested by the design guideline, but much improvement has been made from the case without dampers.

Table 8.6 summarizes the comparisons between the as-built structure and structure incorporating dampers in terms of their confidence to achieve the target performances. The uncertainty factor β_{UT}, confidence index parameter λ, demand variability factor γ_a, resistance factor ϕ, calculated demand for the structure D, and capacity of the structure C are listed in Table 7.4. As can be seen from Table 8.5, both structures have a high confidence of achieving the Collapse Prevention (CP) performance objective at the BSE-1E hazard; however when the earthquake hazard intensity becomes larger, under BSE-2E hazard-level excitations, the retrofitted building exhibits a much higher confidence level to achieve the CP performance objective. Recall that the retrofit objective is to ensure structural stability at the BSE-2E hazard level; such a high level of confidence (>85%) indicates a reasonable efficacy of the strategy to achieve the target performance. However, the retrofitted building has a very limited benefit of achieving an enhanced performance objective: only 4.3% confidence of achieving the Immediate Occupancy (IO) performance objective at the BSE-1E hazard level. Also note that this is larger than the confidence level estimated for a fully ductile building under the same hazard level. Therefore, installing dampers is more cost effective than fixing all the beam-to-column connections to have enhanced structural behavior.

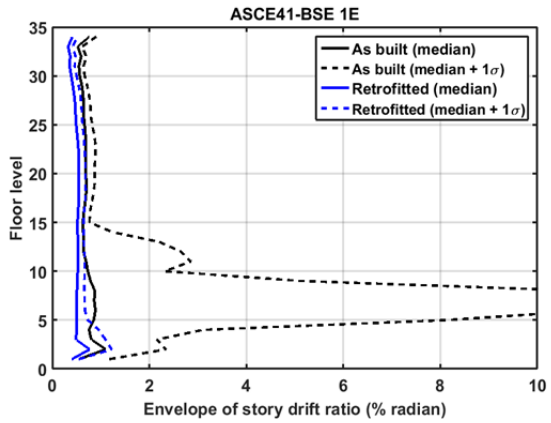

(a)

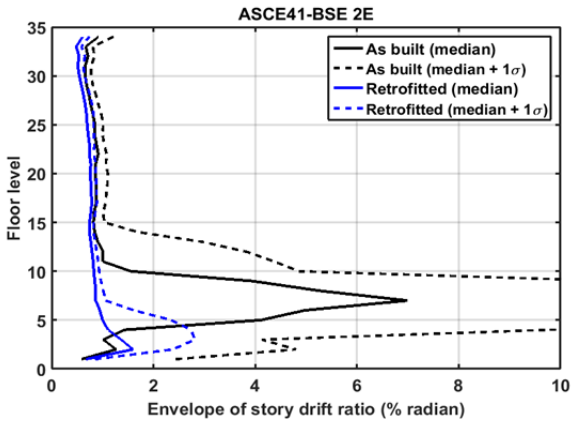

(b)

Figure 8.20 Peak drift ratio: (a) BSE 1E hazard level; and (b) BSE 2E hazard level.

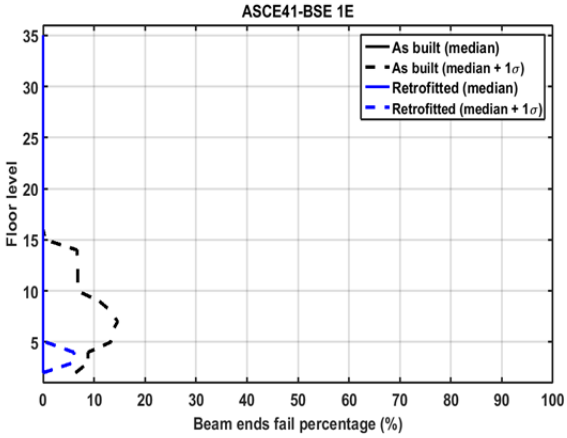

(a)

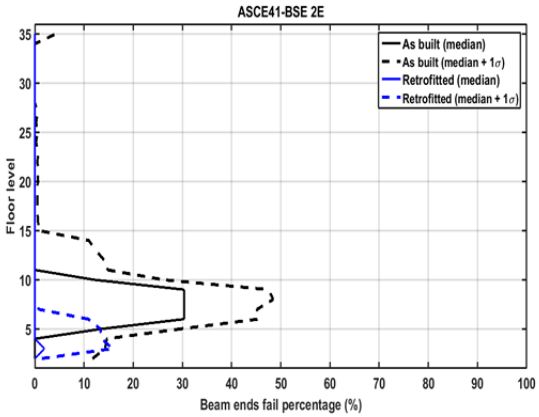

(b)

Figure 8.21 Beam-to-column connection failure: (a) BSE 1E hazard level; and (b) BSE 2E hazard level.

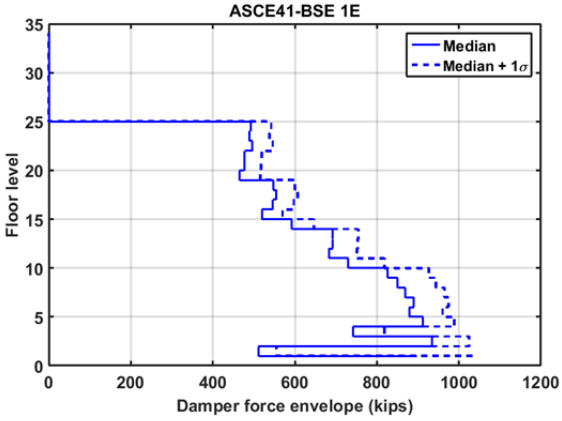

(a)

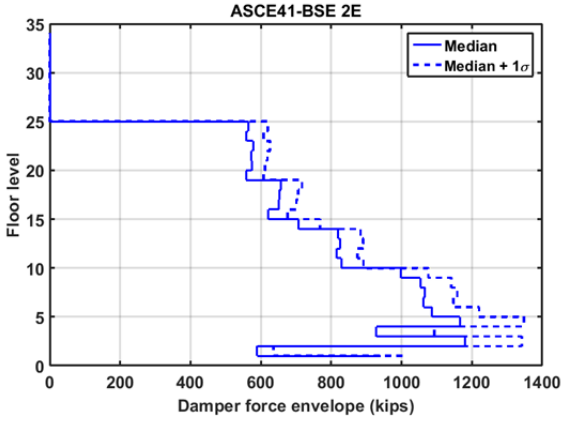

(b)

Figure 8.22 Damper force demands: (a) BSE 1E hazard level; and (b) BSE 2E hazard level.

Table 8.5 Summary of global response.

	As-built (stage-1)		With FVDs (stage-2)	
	CT	CR	CT	CR
BSE-1E	25	25	0	0
BSE-2E	70	70	10	10

Table 8.6 Confidence levels for global response (FEMA 351 evaluation).

	Immediate Occupancy			Collapse Prevention		
	Original (no retrofit)	As-built (stage-1)	With FVDs (stage-2)	Original (no retrofit)	As-built (stage-1)	With FVDs (stage-2)
BSE-1E	0.0	0.0	4.3%	1.48%	94.3%	99.3%
BSE-2E	0.0	0.0	0.0	0.73%	5.2%	85.9%

8.6 OTHER DESIGN ISSUES

8.6.1 Damping Nonlinearity

The two primary parameters involved in designing FVDs are the damping constants, C, and damping exponent, α; both are related to the damper force by the formula: $F_D = C|v|^a \operatorname{sign}(v)$. In previous studies, emphasis was placed on the calibration of C values along story height, while assuming damping exponent α to be a constant 0.35. The procedure to find an optimized α will be discussed next.

Damping coefficient α is closely related to the effectiveness of damper elements as well as their size. This value can be specified as a fixed number within the range of α = 0.15 to α = 2.0 for present damping technology [Taylor and Katz 2004]. Standard damper output in manufacturing is a linear FVD; optional output for nonlinear dampers with low-damping exponents are also possible [Taylor Device Inc. 2010c]. The schematic comparison shown in Figure 8.2 demonstrates that linear dampers are more effective in generating large damper forces and suppressing structural responses when the relative velocity is high, while nonlinear dampers perform better in the low-velocity range. However, large damper forces in linear dampers under moderate or major earthquakes could exceed the device capacity, thus jeopardizing the dampers and affect the energy dissipation capacity [Miyamoto et al. 2010].

There is a trade-off between ensuring the device capacity and maintaining the desired structural responses. Martinez-Rodriguez and Romero [2003] compared linear and nonlinear dampers in terms of their efficacy to upgrade a six-story steel structure; they concluded that, based on the two quantitative parameters that measured the overall structural performance and damper forces, a value for α that slightly smaller than unity would be optimum. Such a high

value (slightly smaller than 1) would still yield large damper forces for this structure if the desired structural response were to be achieved; therefore, a parametric study was conducted to find a better value specific to the selected high-rise building.

Damping exponents α = 0.2, 0.5, 0.8, and 1.0 were selected for the investigation, and the maximum value from three ground motions from the BSE-2E hazard level (see Section 8.3.1) was evaluated. Preliminary Scheme III, with damping constants "*C*" proportional to story stiffness and dampers installed in all stories, was used for this parametric study.

Figures 8.23 and 8.24 contain the resulting the drift ratio and floor accelerations, which indicate that the linear dampers are more effective in reducing floor accelerations, while the nonlinear dampers might be more helpful in reducing drift ratios; however, dampers with smaller damping exponents have smaller damper force demands (Figure 8.25). The peak damper force was reduced from 1700 kips for α = 1.0 to about 1100 kips for α = 0.2 evaluated in the *Y*-direction.

The column axial *D*/*C* ratios were also evaluated for the corner columns (Figure 8.26). In general, nonlinear fluid viscous dampers have an inconsequential influence the column axial *D*/*C*. Dampers with varying α values contribute similarly to the column demands on both tension and compression sides. Following the procedure outlined in Section 8.5.2, the overall effectiveness indices were derived; see Table 8.7. A larger value indicates a scheme's greater cost-effectiveness; thus, an α value in the range (0.2, 0.5) is desirable. Although it appears to be more attractive to use α = 0.5, a smaller value in between (0.2, 0.5) is more appropriate to limit the damper force demands.

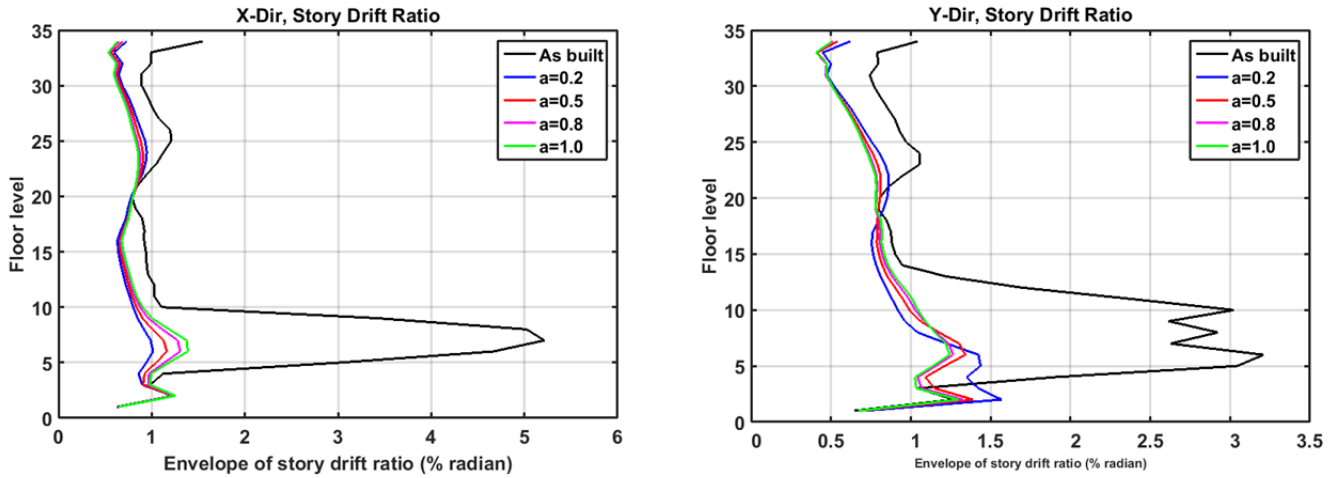

Figure 8.23 Peak drift ratio: (a) *X*-direction and (b) *Y*-direction.

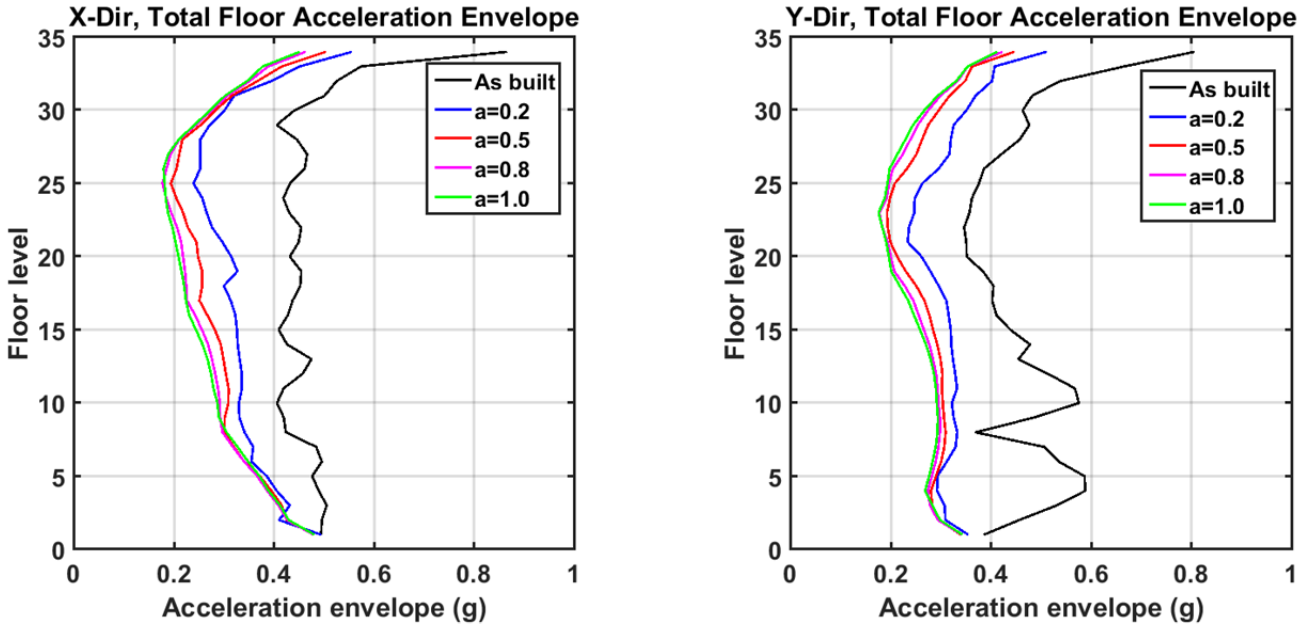

Figure 8.24 Peak floor acceleration: (a) *X*-direction and (b) *Y*-direction.

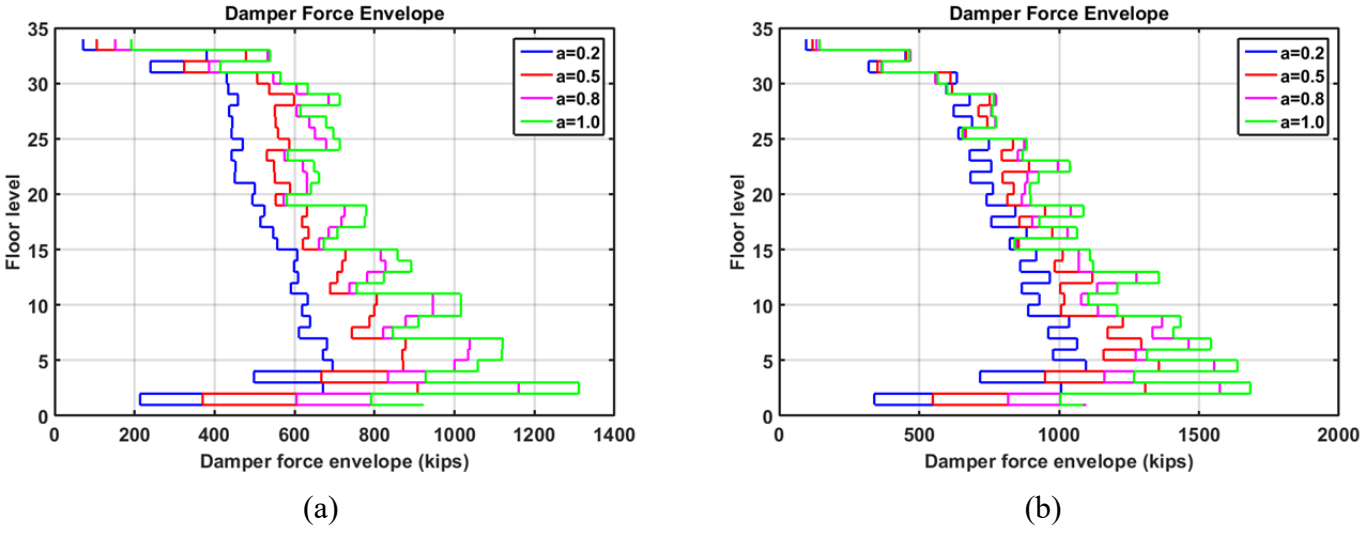

Figure 8.25 Peak damper forces: (a) *X*-direction and (b) *Y*-direction.

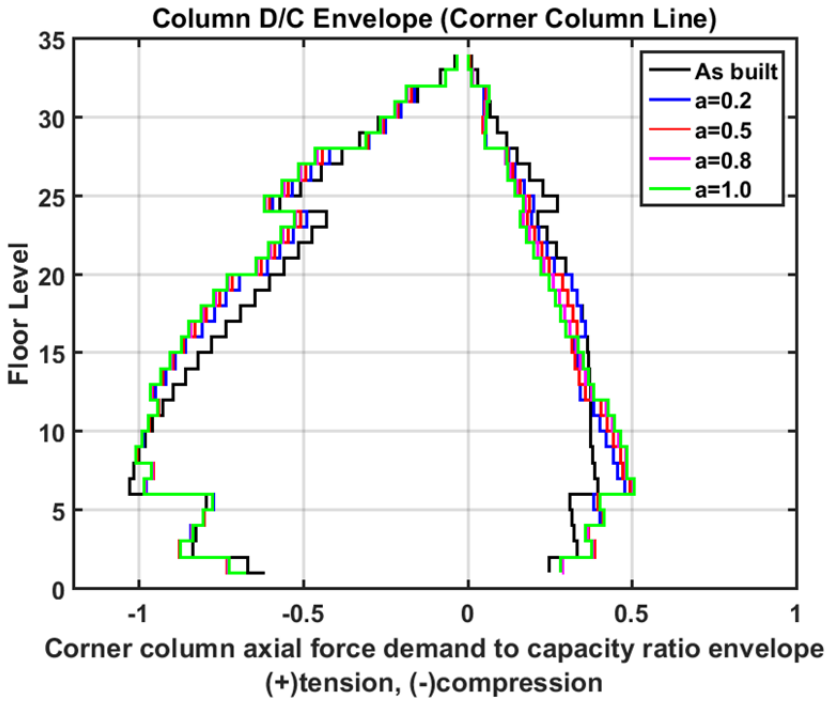

Figure 8.26 Column *D/C* ratio, tension (+), and compression (-).

Table 8.7 Cost effective index table.

α	0.2	0.5	0.8	1.0
Performance Index	6.3	8.9	6.7	4.4
Cost Index	0.9	1.1	1.4	1.5
Effective Index	5.4	7.8	5.3	2.9

* Shaded boxes indicate the selected range

8.6.2 Effective Damping Ratio

The procedure to calculate effective damping ratios was discussed in Section 8.4.2. A roof drift ratio corresponding to a point when the structure suddenly fractured (lost all its strength) was selected as the limiting value on which to base the calculation. The effective damping ratio was related to design parameters C and α based on the energy method, assuming the dampers would reach their full strokes. However, there are two limitations associated with this procedure: (1) the first-mode assumption might not be suitable in the case of the tall building under evaluation, and thus the roof displacement estimated from the ASCE spectra (5% damping) at the fundamental period might not be a good indication for the actual structural demand; and (2) it is unlikely that all dampers would be extended simultaneously to their full strokes. Therefore, the calculated effective damping ratio contained much uncertainty, and an extensive investigation was necessary to evaluate the effective damping ratio.

Four cases with the damper configuration of Scheme III (Section 8.4.3) were analysed, with total effective damping ratio as 50%, 100%, 150%, and 200% of the value based on the prior calculations. The required effective damping ratio was selected based on procedure outlined in Section 8.4.2.

Figures 8.27 and 8.28 showed the peak drift ratio and peak floor accelerations, respectively, in the two horizontal directions. These indicated that an increase of the effective damping ratio led to greater response reduction, with the effect being greatest in the weak-story region. An increase of additional damping also helped reduce the peak floor accelerations, with the effects being larger at middle levels and the roof level. Nevertheless, the incremental improvement was smaller as the effective damping ratio increased. The damper force envelope in both directions were also presented (Figure 8.29), and the values were approximately proportional to the effective damping ratio, indicating that in all cases the capacities of dampers were utilized to a similar extent.

Figure 8.31 shows the column demand to capacity ratios envelope. As expected, larger damper forces tend to contribute to larger column forces in both compression and tension. Such an increase is more obvious at lower stories on the tension side, where doubling the damper sizes increased the tension forces by about 30%.

As an overall evaluation, the previously defined effective damping ratios (10% in *X*-direction, and 15% in the *Y*-direction) were well-grounded considering their efficiency in reducing structural responses without incurring excessively large damper forces.

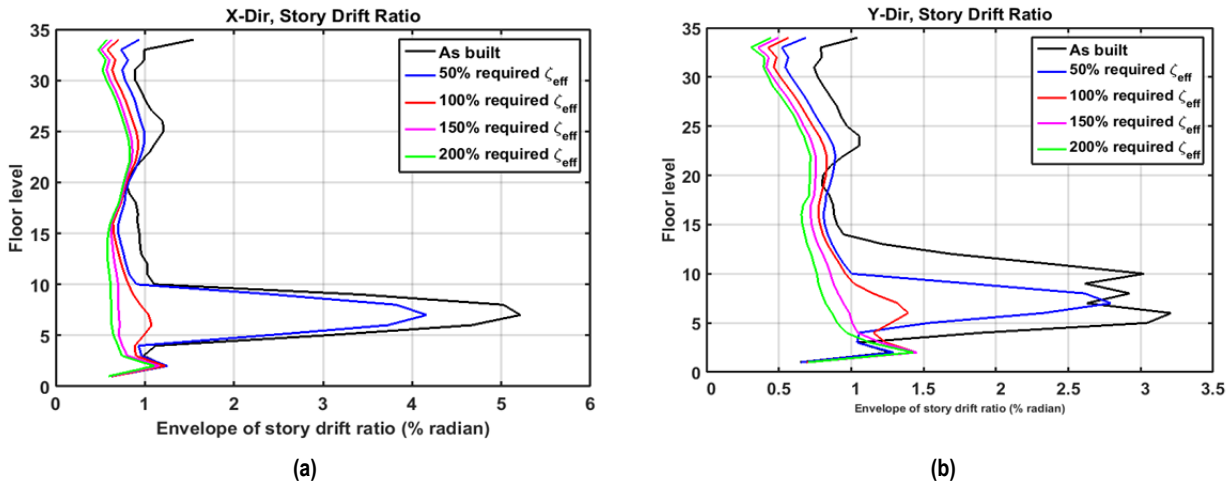

Figure 8.27 Peak drift ratio: (a) *X*-direction and (b) *Y*-direction.

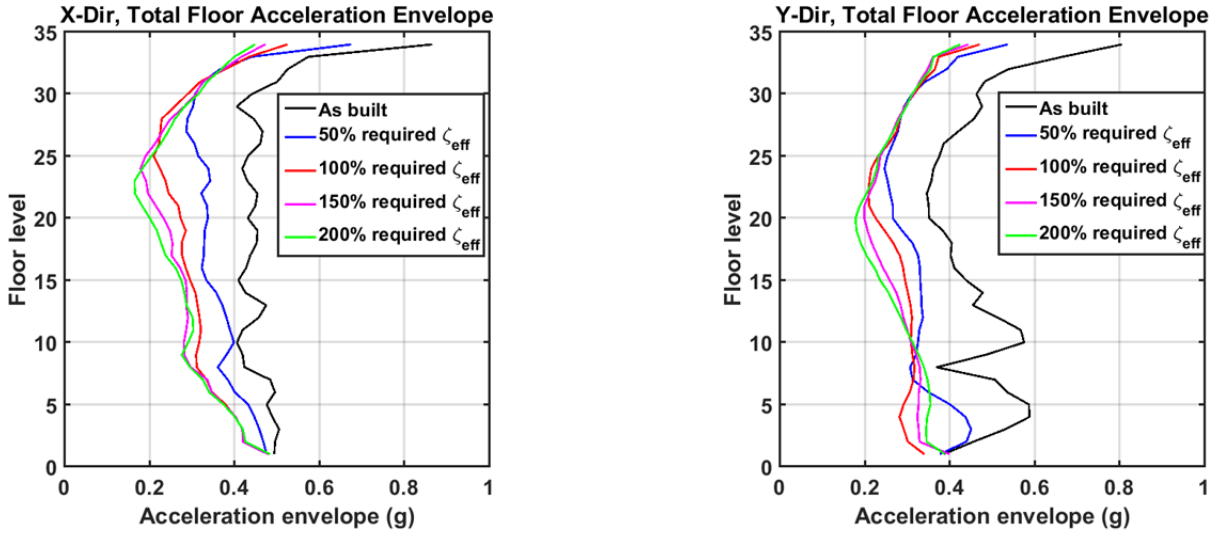

(a) (b)

Figure 8.28 Peak floor acceleration: (a) *X*-direction and (b) *Y*-direction.

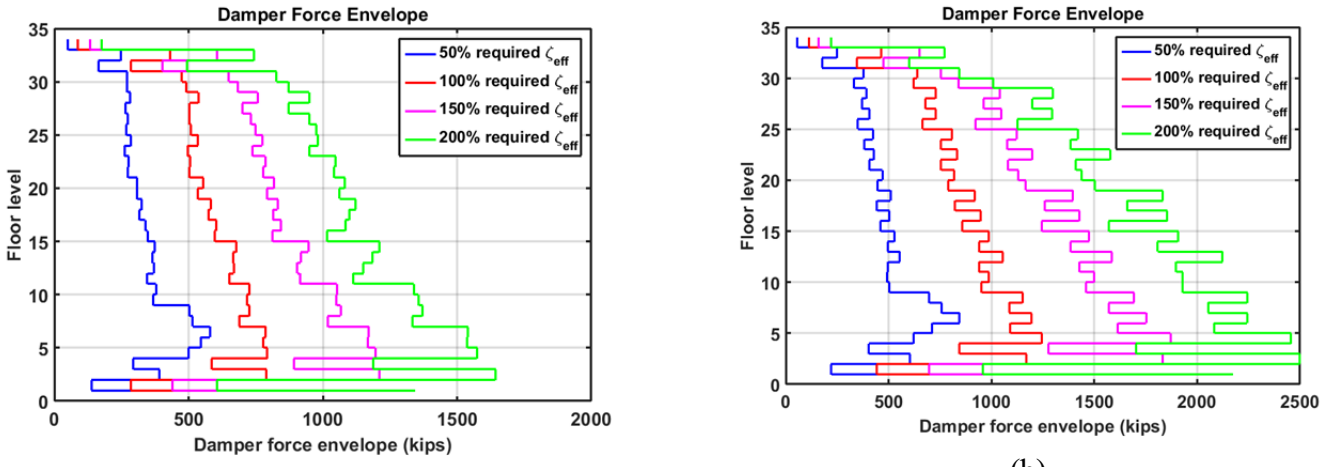

(a) (b)

Figure 8.29 Peak damper force: (a) *X*-direction and (b) *Y*-direction.

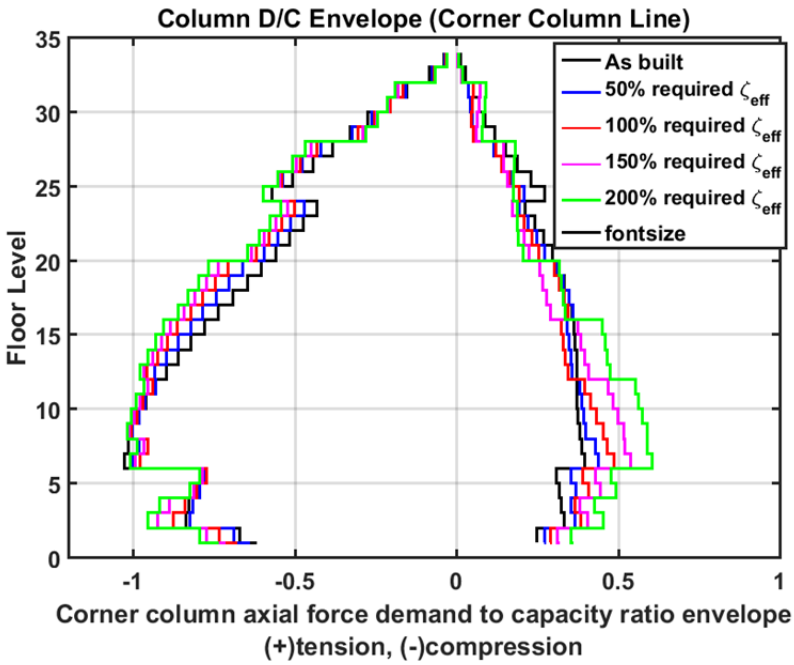

Figure 8.30 Column *D/C* ratio, tension (+), and compression (-).

8.6.3 Bracing Stiffness

Bracing stiffness for dampers is another factor to consider when in designing FVDs. A stiff supporting brace has a positive effect in reducing both S_d and S_a. Ideally, the damper supporting braces would be stiff enough to allow the velocity-dependent devices to perform out-of-phase with all other structural elements that are displacement-dependent. Nevertheless, in engineering practice, the braces may not be rigid enough to ensure the out-of-phase behaviors given the difficulty to construct very stiff braces and the high cost of constructing such braces. Therefore, the flexibility of braces should be included, which might inhibit damper deformation, diminish the damper effectiveness, and cause the peak damper responses to occur at a time closer to the time of peak story drift when other elements that are in-phase with structural drift reach the peak; however, brace stiffness need not be too large to achieve desired responses. Fu and Kasai [1998] suggested that brace stiffness at a magnitude of five times that of the frame is recommended based on the analysis of two non-dimensional parameters derived from a SDOF model with a linear FVD subjected to a sinusoidal wave.

Such a simplified mathematical model with a single DOF doesn't seem capable of accurately representing a complex tall building, and such stiff braces would be prohibitively expensive to construct. Chen and Chai [2011] used a gradient-based numerical procedure to determine the minimum brace stiffness and damper coefficients to meet the target response reduction, and concluded that brace stiffness equal to first story stiffness would be adequate in typical applications. Though it sounds plausible to relate the brace stiffness to a typical floor stiffness, it might not be prudent to extend such a method to an existing building, especially considering possible deficiencies associated with the existing building; a varying range of bracing stiffness related to multiple stories would provide more informative for design considerations. Given those limitations, the authors conducted a parametric study to find out the optimal bracing stiffness. First, a simplified SDOF frame model was designed using the same

software platform. With a given damping ratio, possible ranges of effective bracing stiffness were evaluated, and a reasonable range of bracing stiffness was selected. After narrowing down the range of the parameter, a systematic series of nonlinear dynamic history analyses was done for the tall building model, and an optimal stiffness value for the driving brace was selected.

Detailed results for selecting bracing stiffness of the tall building under study herein are discussed below. Five cases with various supporting brace stiffness values were selected, with values ranging from a very soft brace ($K_b = 0.5K_f$) to a very stiff one ($K_b = 5K_f$). Scheme III (with *C*-values proportional to story stiffness) was used for this study.

Observable improvement of peak drift ratios were exhibited in *Y*-direction, especially in the weak-story ranges with stiffer bracings; bracing stiffness was less sensitive in *X*-direction, as indicated in Figure 8.31. Further improvement was quite limited when $K_b = 2K_f$ or larger, and the results tended to stabilize after this threshold.

Figure 8.32 shows the damper hysteresis loops for multiple cases of a typical damper located on the 5th floor; the peak damper force demands were indicated as well. Comparison of these figures indicate that the hysteresis loop of the damper element with a larger bracing stiffness is closer to an ellipse, and that the dissipated energy together with the peak value would also be increased, demonstrating larger energy dissipation capacity.

A story force (including frame force and damper force) time history was studied to evaluate the efficiency of supporting brace in terms of maintaining the out-of-phase properties of FVDs; see Figure 8.33; the results for two extreme cases (very soft and very stiff bracing) are shown. Though not obvious, there is an observable difference between the two cases: the stiffer bracing forces the damper to act more out-of-phase with elastic structural members. Note that a stiffer bracing would result in a more rapid decay of structural response, as indicated by the smaller structural responses at the free-vibration phase. This further demonstrates the close link between bracing stiffness and the efficacy of the damper.

Clearly, optimal bracing stiffness is highly linked to the size of the dampers. For this case where the additional damping is in the range of 10–20%, using braces with $K_b = 2K_f$ would be optimal to ensure the effectiveness of dampers without further increasing the constructing fees.

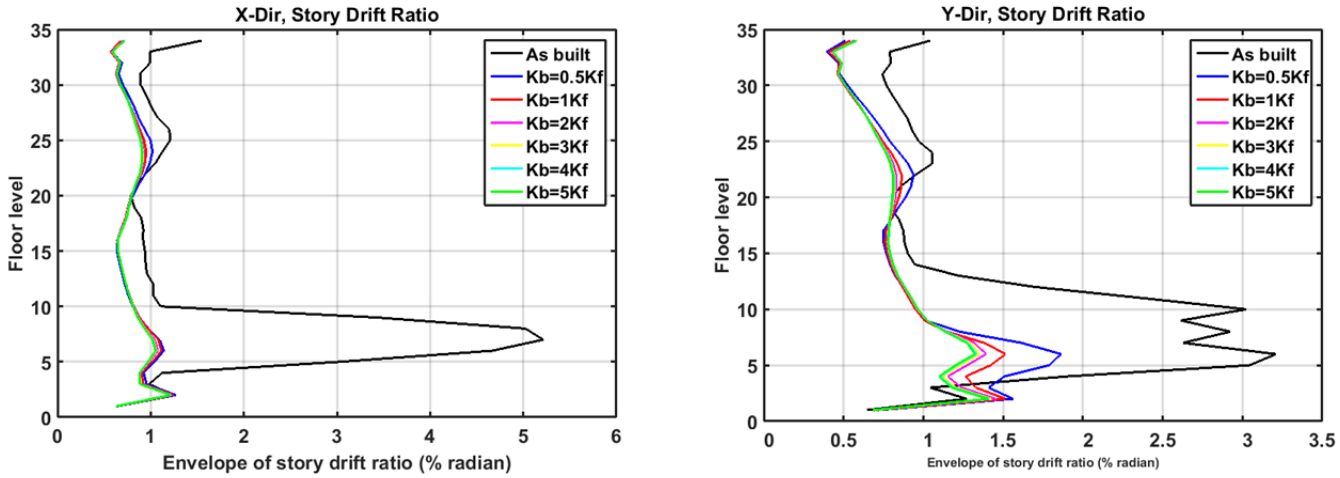

Figure 8.31 Peak drift ratio: (a) *X*-direction and (b) *Y*-direction.

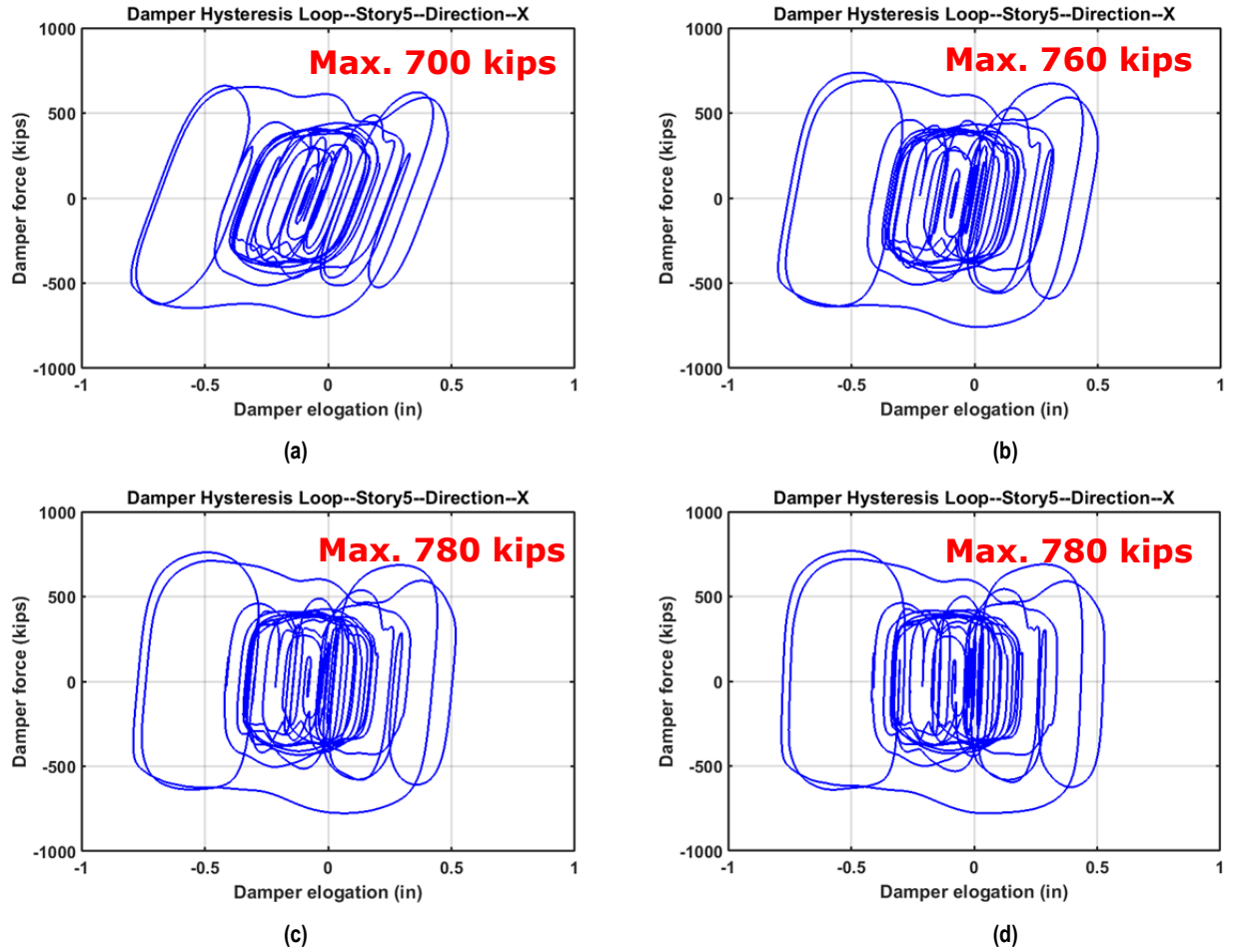

Figure 8.32 Typical damper response: (a) $K_b = 0.5K_f$; (b) $K_b = 5K_f$; (c) $K_b = 2K_f$; and (d) $K_b = 5K_f$.

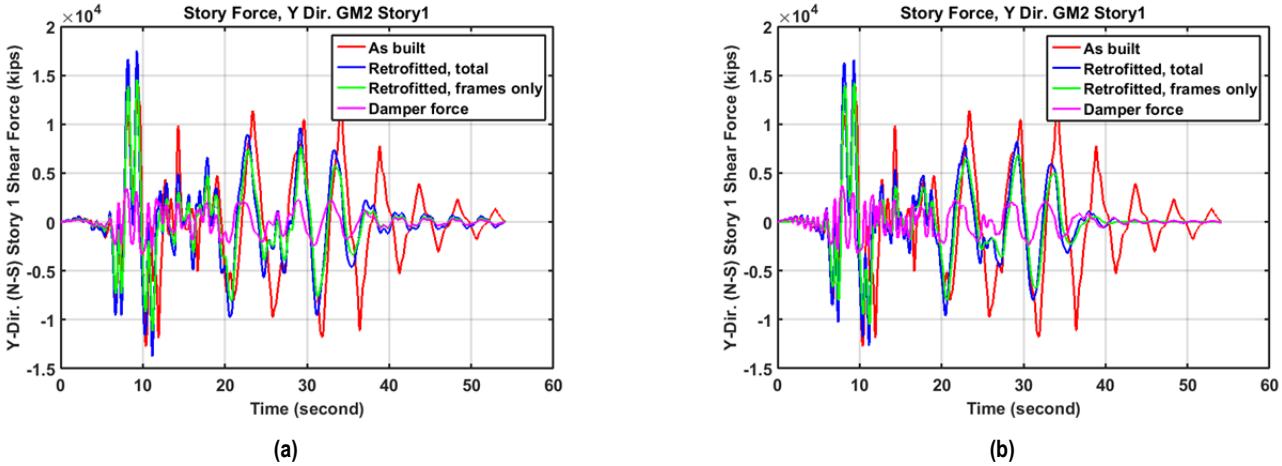

Figure 8.33 Story force time history: (a) K_b=0.5K_f and (b) K_b=5K_f.

8.6.4 Damper Locations

In the previous studies, the dampers were located at the outside frames in both directions and were distributed across bays. To understand better the influence of damper locations, another trial case was conducted where dampers were stacked above one another within single bays; its elevation are presented in Figure 8.34(b).

The advantage of putting dampers in multiple bays was significant: Figure 8.35 indicates that there was at least a 20 and 30% reduction of peak drift ratio in the weak-story zone for the *X*-direction and *Y*-direction, respectively. In general, larger damper force demands were required to ensure the efficacy for the more distributed damper configuration; see Figure 8.36. A discrepancy was observed at story 6–8 in the *Y*-direction, where the stacked damper configuration [case (b)] resulted in larger damper force; this was probably due to the much larger drift ratios demands at those stories, leading to increased elongation of dampers.

The scheme with dampers distributed in concentrated bays accumulates significant damper forces, which transfer to adjoining columns. If the structure experiences yielding at certain locations, an increase of the column axial forces would be significant. This is examined in Figure 8.37. The case (b) with dampers stacked one above another in limited bays resulted in an accumulation of damper forces, leading to a larger increase of demands than the distributed pattern for both compression and tension. As such, an approach to stack dampers in concentrated bays is determined to be inadvisable.

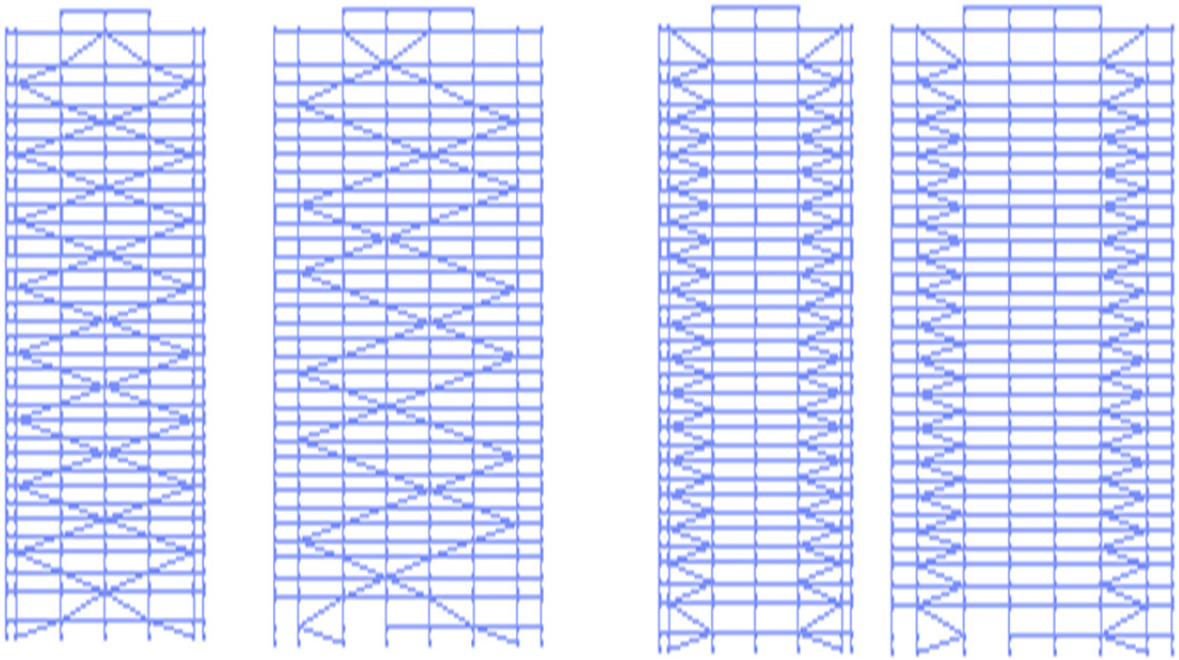

Figure 8.34 **Elevation views of two damper distribution cases: (a) distributed in multiple bays; and (b) stacked in corner bays.**

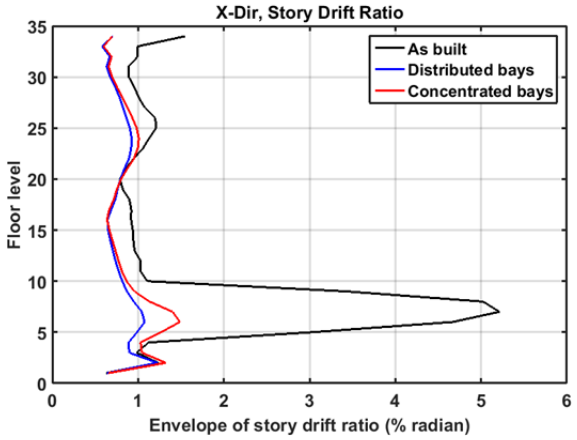

(a)

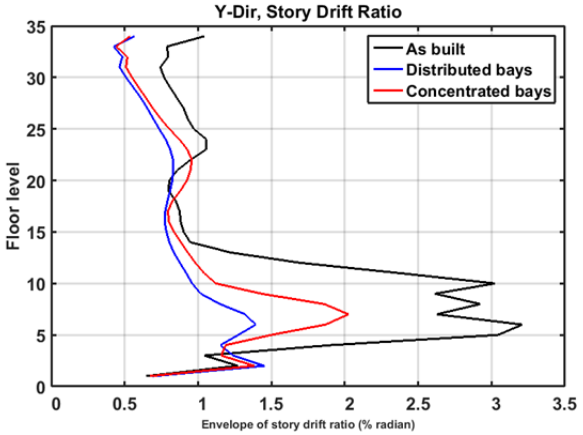

(b)

Figure 8.35 Peak story drift ratio: (a) *X*-direction and (b) *Y*-direction.

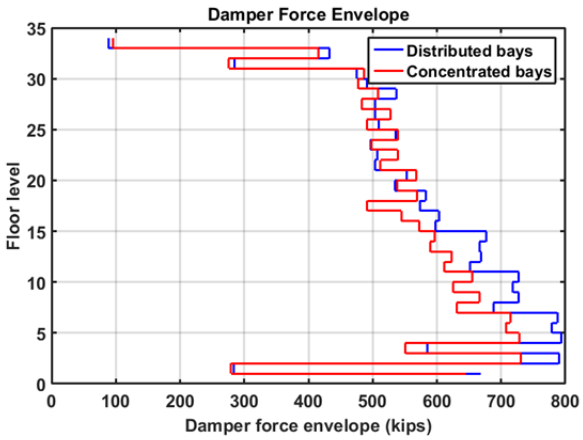

(a)

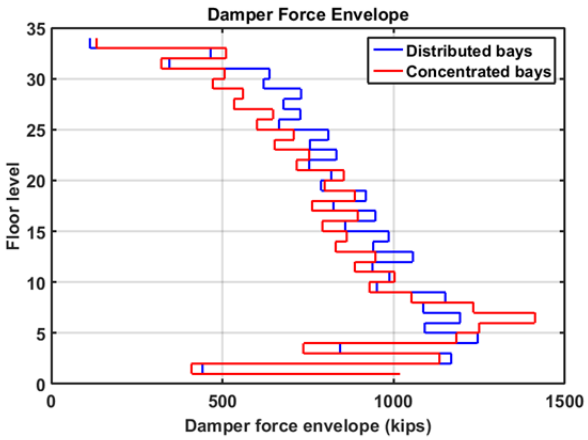

(b)

Figure 8.36 Peak damper forces: (a) *X*-direction and (b) *Y*-direction.

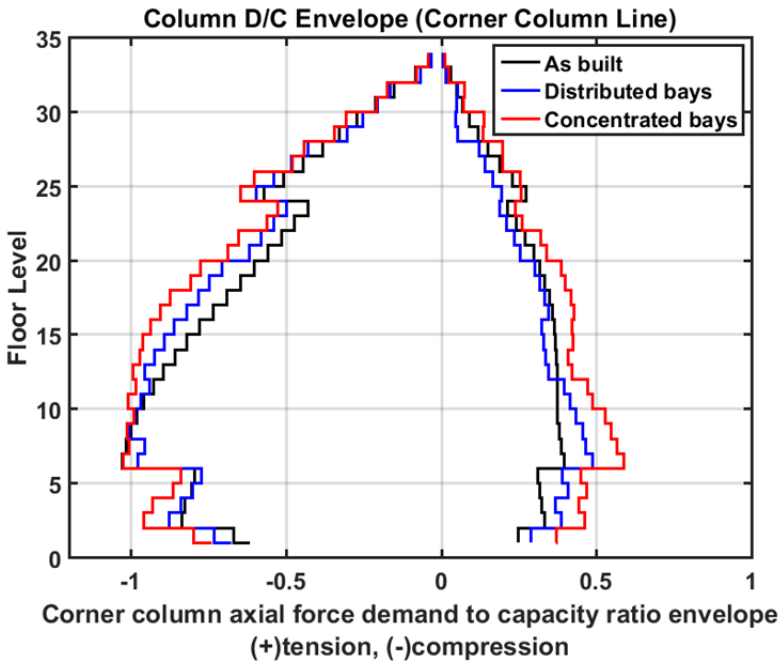

Figure 8.37 Peak column compression *D/C* ratio.

8.6.5 Model Sensitivity

Section 7.7 presented a thorough evaluation of models of interest, including a refined model (Model 1d), where brittle connection and brittle column splices were simulated, a model assuming all column splices were fixed (Model 1c), and an ideal model where all beam-to-column connection were assumed to be fully ductile (Model 1a). In the retrofit study so far, the "baseline model" was used to assess the contribution of dampers to this existing building; note that the baseline model (Model 1c) assumes that vulnerable column splices have been fixed, and heavy concrete cladding has been removed, but brittle beam-to-column connections have been retained.

The purpose of this study is to check the difference of dampers' efficacy between scenarios where structural elements are fixed and those are not; therefore, the above-mentioned models were re-visited with dampers incorporated. As before, the results were evaluated at BSE-2E hazard-level earthquakes, three ground-motion sets were selected, and the maximum responses were evaluated.

Figure 8.38 shows the drift ratio envelope for Model 1a and Model 1c. The solid lines are for the brittle case, including the as-built responses and retrofitted responses; the dashed lines are for the ductile case. A brief examination of the two black lines (as-built) indicates the significant differences between models with differing connection details. It is clear that there would be great benefit in retrofitting all the connections, which would lead to a reduction of the peak drift ratio in the weak-story zone. However, a comparison of the solid lines with dashed lines demonstrates that incorporating dampers would be much more effective than fixing all the connections in terms of reducing overall drift ratios. Note that the drift ratio envelope with dampers for both models are very close, validating the assumption that failures due to inadequate connection details were basically eliminated after retrofitting.

In terms of peak floor accelerations, retrofitting the connections was not able to control the responses, as evidenced by the increase of the accelerations at several floors; see Figure 8.39. Obviously, dampers are more beneficial in reducing the accelerations. The figure shows that the accelerations are reduced by about 30–40% in general, and some higher frequency content is also suppressed due to the dampers. Meanwhile, the damper force envelope (Figure 8.40) indicates a similar efficacy under both scenarios, which indicates that after installing dampers, no or few beam-to-column connections need to be retrofitted. Basically, a building with dampers would be much less dependent on the mechanical behavior of beam-to-column connections since the structural responses have been reduced to the extent that only a limited number of connections are likely to fail. Other differences, such as the shift of fundamental period and change of roof displacement orbits, were discussed in detail in Section 7.7.

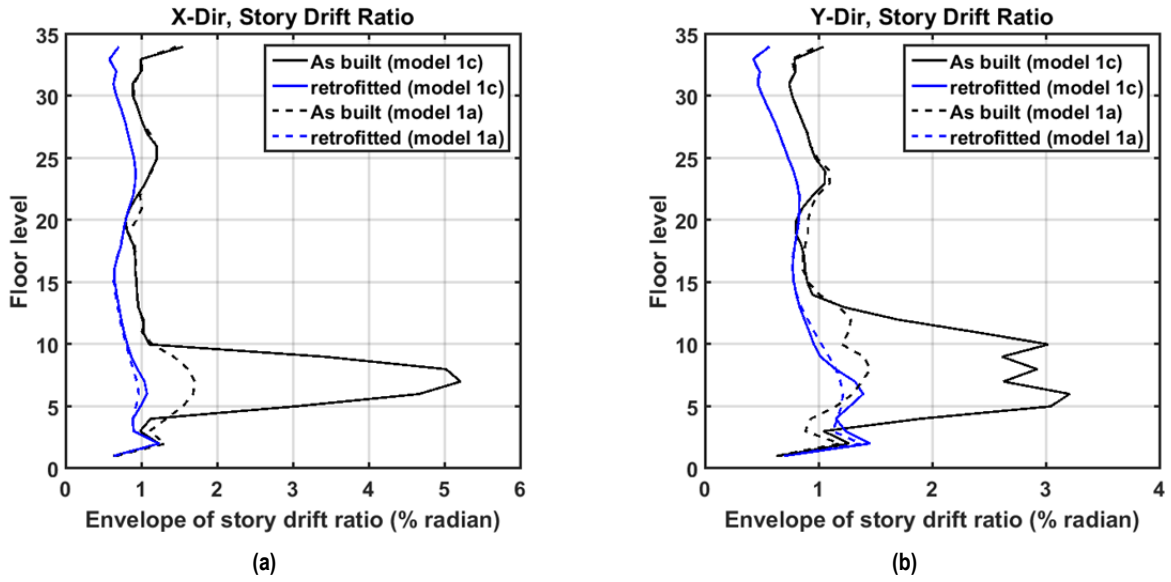

Figure 8.38 Peak drift ratio: (a) *X*-direction and (b) *Y*-direction.

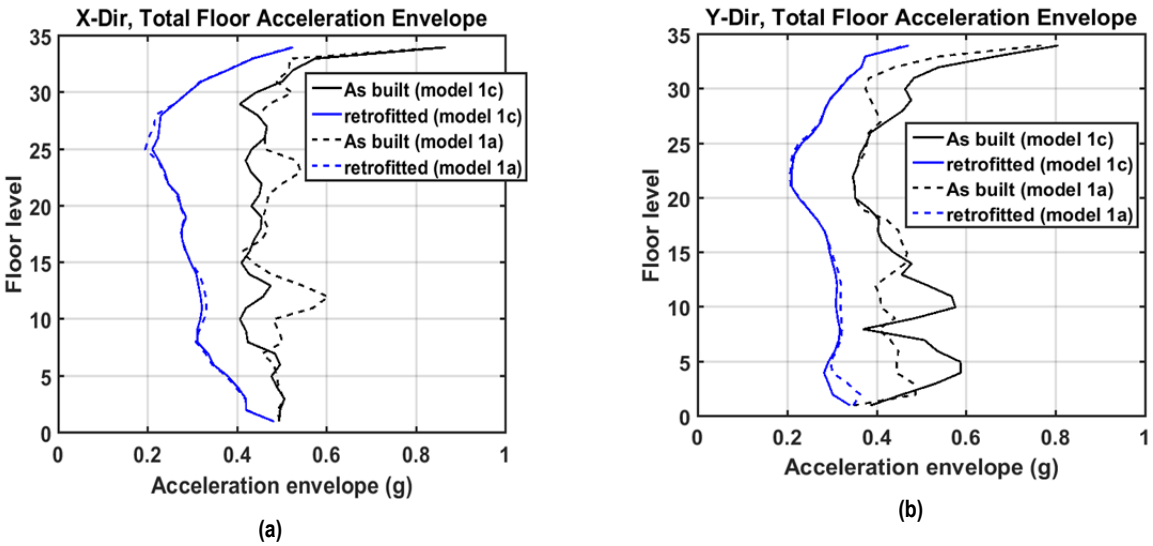

Figure 8.39 Peak floor acceleration: (a) *X*-direction and (b) *Y*-direction.

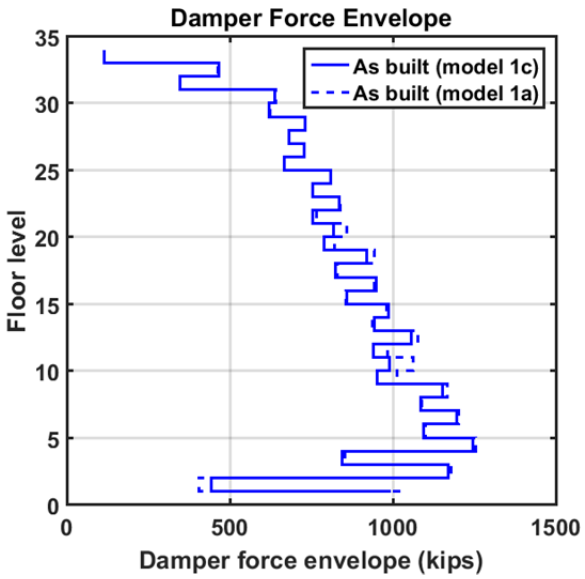

Figure 8.40 Peak damper forces.

8.7 CONCLUDING REMARKS

The preliminary study presented herein demonstrates that the stage 1 preliminary retrofit plan of repairing brittle column splices and the removal of concrete cladding was relatively inexpensive and easy to do, and performed adequately under the BSE-1E hazard level. When the BSE-2E hazard level was considered, however, these methods proved insufficient and further retrofit by using fluid viscous dampers was proposed and investigated. The results presented herein showed that FVDs were quite useful in improving the performance of the case-study building subjected to even the BSE-2E hazard level. They reduced the peak drift ratio by up to 30–40% and decreased the residual drift ratio by a similar amount. Incorporating FVDs also helped suppress floor accelerations and led to more rapid decay of vibrations, so that damage to structural and non-structural elements and discomfort to occupants would be diminished, especially for small and moderate earthquakes. For the BSE-2E level of excitation, some localized connection fractures may still be expected but were much reduced from as-built case. The analysis results indicate that large damper demands were needed to achieve the desired responses, especially in the most deformed stories. However, significant benefits and cost savings may be possible through more extensive assessment of damper configuration within the building, and systematic optimization procedures were possible.

A refining method that utilized simplified frame models to select damper locations, and performance and cost related indices to resize dampers were proposed, and their efficacy was verified. Nevertheless, continuing optimization studies are desirable to further reduce the damper demands while maintaining the improved structural response. Also, a more comprehensive cost index incorporating installation fees, connection detailing to ensure the force transfer, and non-structural components removal should be investigated so that such an index would be more informative. Moreover, coordination of damper placement with the needs of the building occupants in mind and the location of existing non-structural elements, interior spaces near stair and elevator access, require additional consideration; they were outside the scope of this study.

Extensive upgrade of column splices was used as part of the stage-1 plan, but the overloading of columns in compression remains as an issue. Extensive strengthening of these vulnerable columns, as well as other existing members of the building were deemed necessary; incorporating dampers alone might not solve all potential problems. Thus, it would be prudent to investigate other strategies to improve seismic performance, such as strengthening existing structural elements or connections, using other types of energy dissipation devices alone or in combination with FVDs, or adding lateral load resisting elements such as steel or reinforced concrete structural walls. Seismic isolation above the base of the structure may also be a viable strategy. The costs and benefits of such retrofits compared to those proposed herein or performance capabilities of the as-built building is an area of further and valuable study.

9 Economic Loss Estimates

9.1 LOSS ESTIMATE FRAMEWORK

The framework of FEMA P58 [2012a] was used to formulate repair costs and repair time. This framework is centered on the Performance Assessment Calculation Tool (PACT), which performs probabilistic loss calculations from fragility curves of structural and nonstructural components and consequence functions for damaged components to estimate repair costs and duration. User input to the PACT model includes structural response quantities, building components, and contents. Findings relied heavily on assumptions and recommendations made in the FEMA P58 framework.

9.2 PERFORMANCE ASSESMENT CALCULATION TOOL MODELING PARAMETERS

The PACT dollar values are based on 2011 estimates. To account for inflation, a 5% increase on this estimate was applied. A regional cost multiplier was assumed to be 5% above the national average for the site in San Francisco. A total replacement cost of $475 million and a replacement time of five years were assumed for present-day market conditions. A maximum number of workers per square foot of 0.001 and a total loss threshold of 40% were adopted based on PACT recommendations [FEMA 2012b]. Consequently, repair costs greater than 40% of the replacement cost will trigger full replacement. Modeling recommendations specific to tall buildings are limited to a height factor, see Volume 2, Table 2-1 [FEMA 2012b]. This accounts for increased costs of transporting materials and workers above four floors. Recommendations include an 8% increase for floors 5–10 and 16% thereafter. FEMA P58 [2012b] acknowledges that high-rise buildings may incur significant premiums for some items but combined with elements less sensitive to elevation, they anticipated only modest increases in most cases for tall buildings. The case study accounted for an office building occupancy with default parameters.

Non-structural components were allocated through the normative quantities available in PACT [FEMA 2012c] as recommendations for generic buildings based on occupancy. Contents obtained as normative quantities for an office building, see Table 9.1, were modified to reflect the most appropriate options based on limited knowledge of the case-study building. Modifications included changing the exterior curtain walls to 4-in. precast concrete panels and removal of the concrete tile roofing from each floor.

Structural elements such as beams, columns, and walls are building specific and require user input. Structural plans were used to identify member sizes. Components identified included

welded column splices on every other floor, bolted shear tab gravity connections, pre-Northridge WUF-B beam-column connections, and steel column base plates on the ground level; see Table 9.2.

Table 9.1 Nonstructural components included in loss estimations.

Raised access floor, non seismically rated
Wall partitions
Curtain walls (modified to precast concrete cladding)
Prefabricated steel with steel treads and landings with seismic joints that accommodate drift
Suspended ceiling
Recessed lighting
Independent pendant lighting
Traction elevator
Cold water piping
HVAC
Variable air volume box
Fire sprinkler water piping and standard threaded steel
Motor control center
Low voltage switchgear
Battery rack
Book case
Vertical filling cabinet
Storage rack

Table 9.2 Structural components included in loss estimations.

Welded column splices (every other floor)
Bolted shear tab gravity connections
Pre-Northridge WUF-B beam-column joints, beam one side of column
Pre-Northridge WUF-B beam-column joints, beam both sides of column
Steel column base plates, column w>300plf

Analysis results are dependent on assumptions made within the FEMA P58 framework since default parameters, damage fragility curves, and cost consequence functions were used unaltered. To the extent that the normative quantity components and structural elements encompass the majority of possible damage and repair costs, the repair scenarios should be reasonable. However, the list of nonstructural components is not exhaustive, and obvious office equipment such as computers were not included as these were absent from the normative quantity components. A potentially costly item for repairs is the unknown presence of asbestos. It is a likely scenario that asbestos is present in fireproofing, insulation, or finishing in buildings of this era, but hazardous materials were not considered present for this analysis. The hazardous

material factor was set to 1.0, whereas a building containing these materials could have a reasonably expected factor as high as 1.2.

9.3 RESULTS

Analysis results are presented in terms of median repair cost, median repair time, and probability of unsafe placarding. The main contributors to each of these are also presented. Repair time was calculated using a parallel repair strategy, meaning repair work could be conducted simultaneously on all floors. Neither this scenario nor the series repair strategy truly captures the sequence of work, but they are upper and lower bound estimates. The parallel strategy is presented for its optimistic view on repair time. The labor allocation is assumed to be 20 labors per floor based on the maximum number of workers per square foot (0.001) suggested by FEMA guideline [FEMA 2012] and the number used in similar high-rise buildings [Almufti and Willford, 2013].

Modeling scenarios analyzed included the "original" structure without any retrofit (see Section 4.3.4), the "as-built" model (with column splices strengthened and concrete cladding removed, see Section 4.3.7) and the "retrofitted" structure with fluid viscous dampers (see Section 8.5). Structural analysis results for these models were considered at the BSE-1E and BSE 2E hazard levels from ASCE 41 [2014]. Engineering demand parameters used in the cost analysis (peak drift ratio, peak floor acceleration, and peak floor velocity) were output from the nonlinear time history results of each hazard level. Residual drift ratios were estimated as a function of the peak drift ratio and yielding drift ratio following the FEMA P58 recommended equations. This is to avoid the high sensitivity of residual drift to the structural modeling assumptions [FEMA 2012b]. A results summary is presented in Table 9.3.

To be consistent with the structural analysis, the PACT analyses were based on the normally terminated cases or cases where the peak transient drift ratios exceed 10% for the "original" building. Other cases that failed due to unstable numerical issues are assumed to undergo collapse and thus excluded. This conforms to the FEMA P58 recommendation to discard analyses when numerical instability occurs [FEMA 2012b]. As a result, 11 analyses under BSE-1E hazard level and 7 analyses under BSE-2E hazard level were used for this model. All 20 analyses at both hazard levels were used for the both "as-built" model and damped model.

For the "as-built" case, the estimated residual drifts are quite large, with 63% and 100% probability of being irreparable due to excessive residual drifts. Consequently, the median repair costs and repair time predicted under both events default to the replacement value: $475 M replacement cost and 5 years replacement time. Note that the repair time in PACT does not account for the mobilization delay that prevent the initiation of repairs, nor the disruption to utilities, which might represent a large contributor to downtime [Almufti and Willford, 2013]. The probabilities of unsafe placarding were estimated to be 71% and 100% for the BSE-1E and -2E hazard levels, respectively. Both were due to excessive residual drifts. The cost analysis results are consistent with structural analysis results in that they anticipate high likelihood of structural failure under moderate to major earthquakes.

If the column splices are fixed and the concrete claddings are removed, the "as-built" case has much enhanced response at the BSE-1E hazard level. There is a 36% chance of being irreparable, and the median repair cost is estimated to be $26 M, which represents about 5.5% of

the replacement cost. The resulted median repair time is predicated to be 53 weeks, which is an overly optimistic repair strategy. Nevertheless, fixing vulnerable column splices everywhere and removing cladding do not help improve the structural behavior under BSE-2E hazard-level event. The structure still has a significant chance (86%) of being irreparable after the event. As such, the median results default to replacement cost ($475 M) and replacement time (5 years) under BSE-2E hazard level. The probability of unsafe placarding is estimated to be 41% and 92% for the BSE-1E and -2E hazards, respectively, with residual drift and column splices being the primary contributors. This correlates with structural analysis results that anticipate column splices fractures.

On the other hand, further retrofit by incorporating fluid viscous dampers (the "retrofitted" case) successfully reduced residual drifts; therefore, the resulting repair cost and repair time were reduced significantly under both BSE-1E and BSE-2E hazard levels. Under BSE-1E, the median repair cost was estimated as $10 M and median repair time as 17 weeks, representing a 98% reduction and 93% reduction from the "original" building, and a 61% reduction and 68% reduction from "as-built" case. The probability of unsafe placarding was reduced to only 3%. However, the residual drift ratios still remain a problem under the BSE-2E hazard level, with a 30% chance of being irreparable. Consequently, the probability of unsafe placarding remain as high as 45% due to large residual drift ratios and anticipated damage to pre-Northridge beam–column connections, especially for deep beams with section depth exceeding 30 in. The median repair cost is $24 M and median repair time is 37 weeks, which are much smaller than other cases without dampers.

Table 9.3 Loss estimations.

Scenario	ASCE 41-13 hazard level	Probability of being irreparble	Median repair cost (primary contributor)	Median repair time (primary contributor)	Probability of unsafe placard (primary contributor)
"Original"	BSE-1E	63%	$475 M* (Residual drift)	5 yrs.* (Residual drift)	71% (Residual drift)
	BSE-2E	100%	$475 M* (Residual drift)	5 yrs.* (Residual drift)	100% (Residual drift)
"As-built" (fixed columns splices and removed cladding)	BSE-1E	36%	$26 M (Interior const.)	53 weeks (Interior const., interior finishes)	41% (Residual drift, welded- column splices)
	BSE-2E	86%	$475 M* (Residual drift)	5 yrs.* (Residual drift)	92% (Residual drift, welded-column splices)
"Retrofitted" (further update with FVDs)	BSE-1E	2%	$10 M (Interior const., furnishings)	17 weeks (Interior const., furnishings)	3% (Residual drift, prefabricated steel stairs)
	BSE-2E	30%	$24 M (Interior const., super strucures)	37 weeks (Interior constr., furnishings)	45% (Residual drift, pre-Northridge beam-to-column connections with beam depth >W30)

* Default to replacement values for irreparable case

9.4 CONCLUDING REMARKS

Results indicate that the “original” building has a very high probability of being irreparable and requires replacement due to excessive residual drift ratios in the event of an earthquake. The expected median repair cost and repair time both default to the replacement values under BSE-1E and BSE-2E hazard levels. Fixing vulnerable column splices and removing exterior concrete cladding helped reduce consequences at the BSE-1E hazard level, but are much less effective under the BSE-2E hazard level. Further retrofitting with FVDs successfully brings down the residual drift ratios, reducing significant the median repair cost and repair time under both BSE-1E and BSE-2E hazard level.

Further cost analysis is warranted to have a more robust cost-benefit analysis. The initial damper cost along with the costs of driving braces, fixing connections, and installation need to be investigated in combination with the repair cost and business downtime.

10 Summary, Conclusions, and Recommendations

10.1 SUMMARY AND CONCLUSIONS

The majority of tall buildings constructed in California prior to 1990 are steel moment-resisting frame systems. Consequently, this type of structural system was selected for this initial evaluation. As demonstrated in past earthquakes, prior analytical studies, and the current study, these types of buildings have a variety of seismic vulnerabilities. In particular, steel moment-resisting frame systems constructed according to construction standards in place before the 1994 Northridge earthquake are vulnerable to brittle fracture of beam-to-column connections and column splices. Thus, seismic deficiencies common in the construction of older tall buildings include:

- Low required design base shear forces;
- Few or no drift limits imposed on the building during the design process;
- Use of simplified equivalent static lateral load analysis and design methods that were not able to address the complexities of dynamic response;
- Vertical irregularities, especially near the base of tall buildings, where partial mezzanines, tall ground story columns, discontinuous columns, large transfer girders, and sudden changes in framing systems may occur;
- Plan irregularities, including L, T, or other irregular floor plan layouts, and asymmetrical placement of lateral load-resisting systems;
- Member proportions and sizes not passing the "strong-column–weak-beam" checks;
- Capacity design principles not used in design;
- Column splice and similar details not being able to develop member capacity;
- Beam-to-column connections and panel zones not seismically designed;
- Built-up sections not being able to develop their full flexural or shear capacities;
- The demand-to-capacity ratios of columns in both tension and compression are excessive; and
- Column loads not adequately transferred to foundations.

Modern building codes have addressed many of these seismic deficiencies. However, questions linger about the seismic performance of earlier construction.

This study selected a 35-story steel moment-resisting space frame building designed and constructed around 1970 having typical pre-Northridge beam-to-column moment connection details and PJP weld column splice details. The building selected in the study addresses several key concerns in examining the safety and performance of existing tall buildings during future earthquakes.

The ASCE 41-13 standard was selected as the primary guideline to evaluate the seismic performance of the case-study building. The basic performance objectives for existing buildings were selected per ASCE 41. Both Tier 1 screening and Tier 3 systematic procedures were performed. Eight mathematical models were developed in OpenSees to capture the potential dynamic response of the case-study building considering different mechanical behaviors of beam-to-column moment connections and column splices, as well as the effect of cladding weight on global responses. The mathematical models used here followed the basic requirements described in ASCE 41. Because of the special features of the partial penetration welds employed on all column splices, an attempt was made to model the potential brittle fracture of column splices using OpenSees numerical models. Although ASCE 41-13 does not directly mention this mode of behavior as one to evaluate, the fracture of column splices and the early loss of capacity of the building's pre-Northridge beam-to-column connections had substantially detrimental effects on the seismic behavior for BSE-1E and especially BSE-2E seismic hazard levels. Various studies were also carried out to identify and discuss difficulties and uncertainties in modeling the mechanical behavior of the case-study building.

In addition to ASCE 41-13, evaluations were also made using FEMA 351: *Recommended Seismic Evaluation and Upgrade Criteria for Existing Welded Steel Moment-Frame Buildings* and FEMA P-58: *Seismic Performance Assessment of Buildings*. These methods suggest similar seismic responses, as does ASCE 41-13, but provide additional insight into the probability of achieving various performance goals and consequences of the expected performance in terms of repair costs, downtime, and expected tagging outcomes.

10.1.1 Seismic Performance of the Case-study building

The case-study building performed well under the 43-year mean return period hazard-level ground motions and one Loma Prieta earthquake ground motion recorded near the case-study building site. The building essentially remained elastic; median peak story drift ratios were less than 0.5%, and it could achieve the immediate occupancy performance level based on the FEMA 351 evaluation procedure for the global collapse evaluation.

However, the as-built building failed to satisfy the basic performance objectives targeted in the ASCE 41-13 standard for a building considered to be in Seismic Risk Category III: damage control state under BSE-1E hazard and limited safety state under BSE-2E hazard. In fact, the less stringent basic performance criteria corresponding to Seismic Category II are not satisfied either. Three major seismic deficiencies were identified during the Tier 3 evaluation procedure; (1) the case-study building had a tendency to form a weak-story region in the lower third of the building; (2) pre-Northridge beam-to-column connection details resulted in a high percentage of connection failure under BES-2E events; and (3) the partial joint penetration (PJP) column splice weld detail was insufficient for demands generated in the case-study building. These deficiencies were exacerbated by the low seismic design forces used in the original design of the building compared to today's expected demands. It was found that there were high

probabilities of brittle column splice failure under BSE-1E and BSE-2E hazard levels. The simulated seismic performance did not satisfy the target performance objectives even considering different basic seismic upgrade scenarios such as the removal of heavy cladding, removal of cladding plus strengthening all column splices, or removal of cladding plus fixing all brittle column splices.

The current condition of the case-study building failed to conform to the minimum 90% confidence level recommended for new buildings to achieve collapse prevention per FEMA 351 global performance evaluation procedure under both BSE-1E and BSE-2E hazard-level events. Even when the heavy cladding was removed from the case-study building in addition to having fully ductile beam-to-column connections and fully ductile column splices everywhere, the building still could not conform to a minimum 90% confidence level to achieve collapse prevention under BSE-2E hazard-level ground motions. It should be noted that the confidence level target for voluntary upgrading of existing buildings in FEMA 351 is left to the discretion of the owner and responsible building official.

Economic losses estimated in this report are anticipated to be significant. Based on the FEMA P-58 framework, the building has a very large probability of being irreparable, which justifies a total building replacement based on the damage levels sustained during the BSE-1E and BSE-2E hazard levels. Median repair cost and median repair time for both hazard levels thus defaults to the maximum economic loss and time assumed for demolition and replacement; that is, $475 million and five years, respectively. As a result, significant business interruption losses due to downtime are also anticipated. Substantial repair costs and a high probability of unsafe placarding were consequences of large residual drift, or post-earthquake leaning of the building, and fracture of welded column splices, respectively. These findings were based on structural elements specified in the building plans and nonstructural components recommended by FEMA P-58 for a typical office building occupancy. As such, to reduce losses and achieve the seismic performance objectives targeted in these studies, the basic remedial actions initially investigated were insufficient and additional seismic upgrade scenarios were considered.

10.1.2 Regarding Seismic Upgrading Procedures for Existing Tall Buildings

In evaluating the seismic performance of the case-study building, it became apparent that it was desirable to reduce story drift demands without significantly increasing force and acceleration demands. Traditional approaches that would stiffen and strengthen the structure might overload the already heavily loaded column elements and result in uplift in the unanchored column bases. As a result, a “two-stage” retrofit plan is proposed. In Stage-1, the brittle column splices are fixed everywhere and the heavy concrete cladding is removed. This method proved serviceable under BSE-1E hazard-level events, but were inadequate under BSE-2E events. Thus, in Stage-2, further upgrading by using fluid viscous dampers (FVD) was explored. Detailed studies presented in Chapter 8, demonstrated that this approach could be quite successful in improving the performance at even the BSE-2E hazard level. Structural improvements such as reduction of peak drift ratio and residual drift ratio, suppression of peak floor accelerations, and a more rapid decay of vibration were observed. Thus, retrofitting using FVDs substantially improves safety and reduces the severity of structural and nonstructural damage compared to the as-built condition.

Economic losses were significantly reduced compared to the as-built scenario when FVDs were employed as part of the retrofit. Repair costs for the Stage-2 retrofits were in large part associated with interior nonstructural components, but significant structural damage requiring repair before re-occupancy would still be expected. According to the FEMA P-58 framework, the as-built case has a large probability of being irreparable under both BSE-1E and BSE-2E hazard-level events, and thus the median repair cost and repair time are default to replacement values ($475 M and five years, respectively). Preliminary retrofitting by using Stage-1 plan reduces the consequences at BSE-1E, but was shown to be ineffective at the BSE-2E hazard level. Nevertheless, further retrofitting by incorporating FVDs in Stage-2 turned out to be very effective in reducing the economic and other consequences under both BSE-1E and BSE-2E hazard-level events due to much reduced structural responses. The probability of receiving an unsafe placard after retrofitting was reduced to 3% from the original 71% under the BSE-1E hazard level, and reduced to be 45% from the original 100% for BSE-2E hazard-level events. This unsafe placarding is due to anticipated residual drifts and damage to the pre-Northridge beam–column connections. Business interruption losses due to this downtime and placarding would be high. Findings were based on structural elements specified in the as-built building plans and nonstructural components recommended by FEMA P58 for a typical office building occupancy. Retrofit costs and repair to retrofit components were not considered in this study.

Studies where the damper sizes and configuration within the building were refined indicated that significant benefits and additional cost savings could be possible. However, coordination of damper locations with the pragmatic needs of the building occupants and the location of existing non-structural elements, especially exterior cladding and interior spaces near stair and elevator access, requires more careful consideration than was possible in this study.

Strengthening of the over-loaded columns and consideration of other existing features of the building—such as the potentially inadequate connections of the floor system to the supporting beams of the building—are still needed to complete a retrofit feasibility study. Adding dampers alone might not adequately resolve these potential issues. Specifically, column axial loads likely exceed allowable limits. Thus, strategies such as the addition of a strengthening box and other columns by filling them with concrete, strengthening beam-to-column connections by adding steel plates, using other types of energy-dissipation devices alone or in combination with FVDs, or adding lateral load-resisting elements such as steel braces or reinforced concrete structural walls, should be considered. Seismic isolation above the base of the structure may also be a viable strategy. The costs and benefits of such retrofits compared to those proposed herein or performance capabilities of the as-built building are areas of further and valuable study.

10.2 RECOMMENDATIONS

10.2.1 Regarding the Tier 1 Screenings in the ASCE 41-13 Standard

As mentioned previously, the Tier 1 structural evaluation screening identified a number of deficiencies in the case-study building, although such a Tier 1 screening is not a requirement for tall buildings like this one according to ASCE 41. Many of those seismic deficiencies were confirmed during the systematic Tier 3 nonlinear response history analyses. It is suggested that even for cases where only systematic procedures are required, conducting the Tier 1 deficiency

check can provide a rapid screening to identify potential problems and point out behavior modes and regions of the structure where special attention is needed while developing the computational models needed in the Tier 3 evaluations. However, not all vulnerabilities can be identified through the simple checklists screening, because the checklists do not consider all of the vulnerabilities found and do not consider the consequences of the deficiencies directly.

One of the limitations of the existing checklists is that they do not require calculation of the adequacy (shear capacity) of build-up sections in many older steel structures. Since allowable stress design was typically used in the design of such structures, and members were often sized on the basis of their stiffness and not strength, it is possible that members have inadequate shear capacities to develop the shear forces that would be expected if significant plastic hinging occurred in the members. While shear yielding of beam or column webs has been studied and is routinely checked in performance evaluations, the adequacy of the longitudinal welds that are used to connect the various plates of a built-up girder or column may be overlooked. In the case-study building, many of the built-up structural elements (columns and girders) are unable to fully yield in flexure because of the undersized welds used, indicating that the members may yield or fail in shear prior to forming plastic hinges at the both ends. This mode of behavior is not well understood, and the potential shear failure by this mechanism poses a potential vulnerability in existing tall buildings containing built-up sections. It is suggested to address this issue as part of the Tier 1 procedures by incorporating preliminary checks for some typical elements, as discussed in the Appendix C of this report. If shear failure poses a danger to the building under investigation, a more systematic check should be included as part of the Tier 3 systematic modeling and analysis process.

10.2.2 Modeling and Acceptance Criteria Issues

Results of dynamic analyses based on models constructed following ASCE 41-13 recommendations highlighted the complex nonlinear response of the structure, including large changes in geometry (associated with a side-sway mechanism between floor levels 5 and 12 that resulted in unacceptably large story drifts for many of the ground motions considered) and large inelastic deformations (including quasi-brittle behavior in beam-to-column connections and column splices). As a result, the building was susceptible to significant structural and nonstructural damage associate with large drifts and accelerations. Moreover, in many cases the building was predicted to suffer significant residual lateral displacement (>1%).

As discussed in Chapter 7, the inelastic dynamic and even quasi-static pushover response was quite sensitive to the mechanical behavior of beam-to-column connections. The actual behavior of these regions is difficult to predict with confidence. It was observed that the modeling parameters provided in Chapter 9 of ASCE 41-13 and used in these analyses may be optimistic (un-conservative) when compared with some laboratory experiments, such as those by Kim et al. [2003]. Thus, the formulae in Table 9-6 of ASCE 41-13 used to develop modeling parameters should be assessed and possibly refined based on new testing of large-scale moment connections incorporating realistic and representative details (such as built up and large-sized sections). More experimental data on large members are needed to provide the confidence in values for tall buildings found in Table 9-6 of ASCE 41.

Another critical modeling issue is how to properly model PJP welded column splices. Dynamic analysis results presented in Section 7.7 demonstrated the mechanical behavior of

column splices significantly affect the overall integrity of the structural system and importantly the stability of the analysis itself. Additional refined dynamic analyses are recommended where advanced finite solid or shell elements are used incorporating the ability to model fracture or rupture of the material due to local stress concentrations and ultra-low cycle fatigue (for example, Huang and Mahin [2010]). Of course, it is critical that additional tests be conducted of representative full-scale column splices to validate the numerical models, and to assess the effectiveness of economical retrofit schemes. Recommendations for modeling PJP column splices should be added to future versions of ASCE 41 based on experimental data and numerical analysis results.

ASCE 41-13 requires the modeling of some structural components such as floor diaphragms, column bases, and foundations, yet no specific information was provided therein to facilitate development of appropriate modeling assumptions. Thus, work is needed to develop more modeling parameters representative of structural components in older tall buildings. These recommendations again should depend on experimental or empirical data or results of refined analyses.

Very high column compression stresses were also identified in both Tier 1 and Tier 3 evaluation procedures. Many columns in the case-study building are considered force-controlled components per ASCE 41 because of high axial stress ratios. Acceptance criteria for columns in the fully restrained moment frames per ASCE 41 imply that there is no ductility capacity for columns having axial forces larger than 50% of their lower-bound compressive strengths, which were based on limited experimental data. Recent tests [Newell and Uang 2008] demonstrated that the column acceptance criteria are too conservative and suggested that it be updated in the future version. However, yielding of columns contributes significantly to the weak-story type sideways mechanism observed in the building. Strengthening of the columns sufficiently to achieve the elastic behavior required for force-controlled elements is not likely, either technically or economically feasible. Thus, some limited yielding might be considered for the columns, but lateral displacements need to be carefully controlled.

10.2.3 Retrofit Selection and Requirements

A possible Stage 2 retrofit was conducted by exploring the use of FVDs. The study was based on general requirements from ASCE 41, including specific guidance from Chapter 14 for base isolation and energy-dissipation systems. In the retrofit study covered in Chapter 8 of this report, FVDs were found to be effective in improving the seismic responses of the selected building. They reduced the peak drift ratio by up to 30% and decreased the residual drift ratio by a similar amount. The use of FVDs also helps suppress floor accelerations and leads to a more a rapid decay of vibrations, so that damage to structural and non-structural elements and discomfort to occupants would be reduced, especially for small and moderate earthquakes. Some localized connection fractures may still be expected for the retrofits designed herein, but at a significant reduction in the number of failures compared to the as-built condition is observed. General requirements for adding supplemental energy-dissipation devices were provided in Section 14.3 of the ASCE 41 standard. Possible recommendations are proposed below for several design considerations when use fluid viscous dampers and other types of supplemental energy dissipation devices.

10.2.3.1 Modeling of Flexible Elements in the Supplemental Energy-Dissipation system

The flexibility of energy dissipation systems, such as the driving braces in series with dampers, beams, and beam-to-column connections linking dampers and frames may significantly reduce the damper effectiveness. The loss of damper effectiveness is also dependent on damper configurations at each frame (e.g., diagonal or chevron configuration). These factors should be highlighted in the codes and call for special attention while setting up numerical models. In future version of standards and guidelines, modeling suggestions on flexible elements connecting dampers and frames should be provided for various damper configurations based on experimental data and more rigorous numerical analysis results.

10.2.3.2 Damper Stroke Capacity

For cases where near-collapse analyses are needed, the dampers may break if their stroke limits are reached. For new buildings, damper strokes are often based on the average damper stroke at the MCE level of excitation. In such a case, nearly 50% of the earthquake records considered might result in the stroke limit of the damper being exceeded. Miyamoto et al. [2010] indicated that a damper model that does not account for the damper stroke capacity or the damper force limit states would underestimate the forces that would develop in the structure and not account for possible failures of dampers if their force capacity is exceeded. In the future version of ASCE 41, modeling recommendations should account for damper stroke limits and limit states that might lead to failure of the damper should the stroke limits be exceeded.

10.3 RECOMMENDATIONS FOR FUTURE WORK

10.3.1 Regarding Improving Knowledge of the Probable Seismic Behavior of Existing Tall Buildings and Models to Predict their Performance

Based on the case-study building considered herein, a large number of connection failures were identified during a Tier 3 evaluation procedure. This evaluation considered nonlinear models that simulated the quasi-brittle behavior of beam-to-column connections and column splices. However, the confidence in the modeling parameters used for large pre-Northridge beam-to-column moment connections, column splices, and column bases of the type used in older tall buildings needs to be validated and improved where necessary by more representative large-scale tests. Results of such studies might have a large impact on the findings of studies such as ours.

The numerical models used in this study involved a number of simplifying assumptions. For example, they did not account for the basement region of the structure, soil-structure interaction, partial composite action of the slabs with the floor beams, or stiffening and damping effects of the cladding. A more comprehensive study should incorporate these and other aspects.

To develop improved modeling parameters for large members found in existing tall buildings, large-scale component tests are recommended. In particular, tests on columns (both built-up and hot-rolled sections) with high axial forces and large cyclic drift demands, full-scale cyclic loading tests on column splices with PJP weld details (combined axial forces and bi-directional bending moments), and sub-assemblage tests on wide flange beam-to-box column moment connections are recommended.

The vertical component of ground motions was seen to have an effect on the global dynamic response of the structure and especially the column axial force demands (Section 7.6). Further studies are required to assess the need to include the vertical component of ground shaking when analyzing tall buildings.

Two particular earthquake scenarios were presented in Section 7.9, with one representing a foreshock and a main shock combination (Scenario 1), and one representing a main shock and an aftershock combination (Scenario 2). These demonstrate the effect of multiple earthquake sequences on the dynamic responses of the case-study building. Cumulative increases in deformations and damages are observed under these two particular earthquake sequences. However, further study is required to derive solid conclusions on how multiple earthquakes affect the building dynamic response.

10.3.2 Regarding Improved Understanding of the Costs and Benefits of Various Retrofit and Upgrade Measures

10.3.2.1 Rigorous Cost Analysis under PBEE

Although the ASCE 41-13 standard does not predict that the existing case study structure would collapse under BSE-1E shaking, a significant cost is anticipated due to repair and downtown time. Retrofit strategies would reduce post-earthquake repair costs, but business downtime and associated economic losses might still be large. This is an area recommended for future work since refinement of costs and benefits may help understand the desired extent of retrofits and the return on investment expected. This issue is even more critical considering BSE-2E hazard level, where much more severe damage is anticipated, and the likely scope and cost of needed retrofits would be far greater.

Analyzing the trade-off of performance goals, retrofit strategies and return on investment are critical in the decision making process. The PEER performance-based design methodology is an efficient way to research on this issue by utilizing the performance assessment calculation tool (FEMA P58). A key question for owners, occupants, and public officials is what performance criteria should be used to make final assessments of this and other potentially vulnerable tall buildings containing large number of occupants that provide substantial economic benefit for the occupants and neighboring community, and that possibly raise risks for nearby buildings.

10.3.2.2 Cost Functions

The retrofit study presented showed that FVDs were quite useful in improving the response under BSE-2E level excitation. They reduced structural response, thus reducing damage to structural and non-structural elements and discomfort to occupants. The results also indicated that similar response could be achieved while reducing costs by fine-tuning the damper configuration and damper properties. Cost estimates including repair cost, damper installation costs, connection details to ensure adequate force transfer, and non-structural components removal and reinstallation should be considered in future studies. Moreover, coordination of damper placement with the needs of the building occupants and the location of existing non-structural elements, especially exterior cladding and interior spaces near stair and elevator access, requires careful consideration. In particular, the impact of a retrofit effort compared to a post-event repair effort on business interruption costs should be considered.

10.3.2.3 Other Retrofit Strategies

Other strategies to improve seismic performance, and address some seismic issues of existing tall buildings such as the overloaded columns need to be explored. Such strategies could include, but not limited to, strengthening existing structural elements/connections, using other types of energy-dissipation devices alone or in combination with FVDs, or adding lateral load-resisting elements such as steel or reinforced concrete structural walls should be explored. Seismic isolation above the base of the structure may also be a viable strategy. The cost-benefit analysis of each retrofit strategy should be conducted for comparison.

REFERENCES

AIJ (1995). *Reconnaissance Report on Damage to Steel Building Structures Observed from the 1995 Hyogoken-Nanbu (Hanshin/Awaji) Earthquake*, Steel Committee of Kinki Branch, Architectural Institute of Japan.

AISC (1994) *Manual of Steel Construction: Load and Resistance Factor Design*, 2nd Edition, Volume 1: Structural Members, Specifications, & Codes, American Institute of Steel Construction, Chicago, IL.

Almufti I., Hutt C.M., Willford M., Deierlein G.G. (2012) Seismic assessment of typical 1970s tall steel moment frame buildings in downtown San Francisco, *Proceedings, 15th World Conference on Earthquake Engineering*, Lisbon, Portugal.

Almufti I., Willford M. (2013). *REDi Rating System: resilient-based earthquake design initiative for the next generation of buildings*, Version 1.0, Arup.

Ancheta T.D., Darragh R.B., Stewart J.P., Seyhan E., Silva W.J., Chiou B. S.-J., Wooddell K.E., Graves R.W., Kottke A.R., Boore D.M., Kishida T., Donahue J.L. (2014). NGA-West2 Database, *Earthq. Spectra*, 30(3): 989–1005

Anderson J.C., Bertero V.V. (1997). Implications of the Landers and Big Bear earthquakes on earthquake resistant design of structures, *Report No. UCB/EERC-97/08*, Earthquake Engineering Research Center, University of California, Berkeley, CA.

Apostolakis G., Dargush G.F. (2010). Optimal seismic design of moment-resisting steel frames with hysteretic passive devices, *Earthq. Eng. Struct. Dyn*., 39: 355–376.

ASCE (2003). *Seismic Evaluation of Existing Buildings*, American Society of Civil Engineers, ASCE/SEI 31-03, Reston, VA.

ASCE (2007). *Seismic Rehabilitation of Existing Buildings*, American Society of Civil Engineers, ASCE/SEI 41-06, Reston, VA.

ASCE (2010). *Minimum Design Loads for Buildings and Other Structures*, American Society of Civil Engineers, ASCE/SEI 7-10, Reston, VA.

ASCE (2013). *Seismic Evaluation and Retrofit of Existing Buildings*, American Society of Civil Engineers, ASCE/SEI 41-13, Reston, VA.

ATC (1978). *Tentative Provisions for the Development of Seismic Regulations for Buildings,* Applied Technology Council, ATC-3-06 report, Palo Alto, CA.

ATC (1983). *Seismic Retrofitting Guidelines for Highway Bridges*, Applied Technology Council, ATC-6-2 report, Palo Alto, CA.

ATC (1987). *Evaluating the Seismic Resistance of Existing Buildings*, Applied Technology Council, ATC-14 report, Redwood City, CA.

ATC (1992). *Development of Guidelines for Seismic Rehabilitation of Buildings, Phase I: Issues Identification and Resolution*, prepared by Applied Technology Council (ATC-28 report) for Federal Emergency Management Agency (FEMA 237 report), Washington, D.C.

ATC (1993) *Development of Guidelines for Seismic Rehabilitation of Buildings, Phase I: Issues Identification and Resolution*, Proceedings of the Workshop to Resolve Seismic Rehabilitation Subissues, Applied Technology Council (ATC-28-2 report), Redwood City, CA.

Baker, J. (2014). *Personal Communication*.

Balling R.J., Pister K.S. (1983). Optimal seismic-resistant design of a planar steel frame, *Earthq. Eng. Struc. Dyn.*, 11: 541–556.

Bozorgnia Y. et al. (2014). NGA-West2 Research Project, *Earthq. Spectra*, 30(3), doi: http://dx.doi.org/10.1193/072113EQS209M, Earthquake Engineering Research Institute, Oakland, CA.

Bresler B., Okada T., Zisling D., Bertero V.V. (1977). Developing methodologies for evaluating the earthquake safety of existing buildings, *Report No. UCB/EERC-77/06,* Earthquake Engineering Research Center, University of California, Berkeley, CA.

CGS (2000). *Official Map of State of California Seismic Hazard Zones, City and County of San Francisco*, California Geological Survey, November 17, 2000.

CBSC (2013). *California Building Code," California Code of Regulations, Title 24, Part 2, Volumes 1 and 2*, California Building Standards Commission, Sacramento, CA.

CESMD (2015). Center for Engineering Strong Motion Data, doi: *http://strongmotioncenter.org/cgi-bin/NCESMD/StaEvent.pl?stacode=CE58480*, accessed January, 2015.

Chen Y.-T., Chai Y. H. (2011). Effects of brace stiffness on performance of structures with supplemental Maxwell model-based brace-damper systems, *Earthq. Eng. Struc. Dyn.,* 40(1): 75–92.

Comartin C.D., ed. (1995). Guam earthquake of August 8, 1993 reconnaissance report, *Earthq. Spectra*, Supplement B to Vol. 11, Earthquake Engineering Research Institute, Oakland, CA.

Comartin C.D., Greene M., Tubbesing S.K., eds. (1995). *The Hyogo-Ken Nanbu Earthquake, January 17, 1995, Preliminary Reconnaissance Report*, Earthquake Engineering Research Institute, Oakland, CA.

Constantinou M.C., Tsopelas P., Hammel W., Sigaher A.N. (2001). Toggle-brace-damper seismic energy dissipation systems, ASCE, *J. Struct. Eng*., 127: 105–112.

CSMIP (2015). California Strong Motion Implementation Program (CSMIP), doi: *http://strongmotioncenter.org/cgi-bin/NCESMD/stationhtml.pl?stationID=CE58480&network=CGS,* accessed January, 2015.

Culver C.G., Lew H.S, Hart G.C., Pinkham C.W. (1975). *Natural Hazards Evaluation of Existing Buildings*, U.S. Department of Commerce, National Bureau of Standards, Building Science Series 61, Washington, D.C.

DBI (2013). Department of Building Inspection, San Francisco, CA. (documents reviewed: structural drawings for the main tower, dated May 22nd, 1968, sheets S-2 through S–72)

Dobry R., Iai, S. (2000). Recent developments in the understanding of earthquake site response and associated seismic code implementation, *Proceedings, GeoEng2000: An International Conference on Geotechnical & Geological Engineering*, Melbourne, Australia.

EERI (1995). Slides of the Hyogo-ken Nanbu (Kobe) Earthquake, Set IV, Performance of Engineered Buildings, Earthquake Engineering Research Institute (EERI), Oakland, CA.

EERI (1997). Annotated Slide Set: A visual presentation of EERI Slide Sets on CD, Earthquake Engineering Research Institute, Oakland, CA.

EERI (2010a). Canterbury Earthquake Clearinghouse: Mw7.1 earthquake on September 3, 2010, *http://eqclearinghouse.org/co/20100903-christchurch/,* (last accessed March 25, 2015).

EERI (2010g). Chile Earthquake Clearinghouse: M8.8 earthquake on February 27, 2010, *http://eqclearinghouse.org/co/20100227-chile/* (last accessed March 25, 2015).

EERI (2012). Reconnaissance Team: "Performance of engineered structures in the Mw 9.0 Tohoku, Japan, Earthquake of March 11, 2011", EERI Special Earthquake Report, Earthquake Engineering Research Institute, Oakland, CA.

FEMA (1992a). *NEHRP Handbook for the Seismic Evaluation of Existing Buildings*, FEMA 178 report, Building Seismic Safety Council, Federal Emergency Management Agency, Washington, D.C.

FEMA (1992b). *NEHRP Handbook of Techniques for the Seismic Rehabilitation of Existing Buildings,* FEMA 172 report, Building Seismic Safety Council, Federal Emergency Management Agency, Washington, D.C.

FEMA (1997). *NEHRP Guidelines for the Seismic Rehabilitation of Buildings*, Federal Emergency Management Agency, FEMA 273 report, Washington, D.C.

FEMA (1998). *Handbook for the Seismic Evaluation of Buildings*, Federal Emergency Management Agency, FEMA 310 report, Washington, D.C.

FEMA (2000a). *Prestandard and Commentary for the Seismic Rehabilitation of Buildings*, Federal Emergency Management Agency, FEMA 356 report, Washington, D.C.

FEMA (2000b). *Recommended Seismic Design Criteria for New Steel Moment-Frame Buildings*, Federal Emergency Management Agency, FEMA 350 report, Washington, D.C.

FEMA (2000c). *Recommended Seismic Evaluation and Upgrade Criteria for Existing Welded Steel Moment-Frame Buildings*, Federal Emergency Management Agency, FEMA 351 report, Washington, D.C.

FEMA (2000d). *Recommended Postearthquake Evaluation and Repair Criteria for Welded Steel Moment-Frame Buildings,* Federal Emergency Management Agency, FEMA 352 report, Washington, D.C.

FEMA (2000e). *Recommended Specifications and Quality Assurance Guidelines for Steel Moment-Frame Construction for Seismic Applications*, Federal Emergency Management Agency, FEMA 353 report, Washington, D.C.

FEMA (2000f). *A Policy Guide to Steel Moment Frame Construction*, Federal Emergency Management Agency, FEMA 354 report, Washington, D.C.

FEMA (2000g). *State of the Art Report on Performance Prediction and Evaluation of Steel Moment-Frame Buildings,* Federal Emergency Management Agency, FEMA 355F report, Washington, D.C.

FEMA (2000h). *State of the Art Report on Past Performance of Steel Moment-Frame Buildings in Earthquakes*, Federal Emergency Management Agency, FEMA 355E report, Washington, D.C.

FEMA (2006). *Next-Generation Performance-Based Seismic Design Guidelines*, Federal Emergency Management Agency, FEMA 445 report, Washington, D.C.

FEMA, (2006). *NEHRP Recommended Provisions: Design Examples, FEMA* 451, Building Seismic Safety Council, Federal Emergency Management Agency.

FEMA (2012a). *Seismic Performance Assessment of Buildings, Volume 1 – Methodology,* Federal Emergency Management Agency, FEMA P-58-1 report, Washington, D.C.

FEMA (2012b). *Seismic Performance Assessment of Buildings, Volume 2 – Implementation Guide*, Federal Emergency Management Agency, FEMA P-58-2 report, Washington, D.C.

FEMA (2012c). *Seismic Performance Assessment of Buildings, Volume 3 – Supporting Electronic Materials and Background Documentation,* Federal Emergency Management Agency, FEMA P-58-3 report, Washington, D.C.

Freeman S.A., Nicoletti J.P., Tyrrell J.V. (1975). Evaluation of existing buildings for seismic risk - A case study of Puget Sound Naval Shipyard, Bremerton, Washington, *Proceedings, U.S. National Conference on Earthquake Engineering*, Earthquake Engineering Research Institute, Ann Arbor, MI.

Freeman S.A. (2007). Response spectra as a useful design and analysis tool for practicing structural engineers, ISET *J. Earthq. Tech*., 44(1): 25–37.

Fu Y., Kasai K. (1998). Comparative study of frames using viscoelastic and viscous dampers, *Struct. Eng*., pp. 513–552.

Garcia D.L., Soong T.T. (2002). Efficiency of a simple approach to damper allocation in MDOF structures, *J. Struct. Control*, 9: 19–30.

Ger J.F., Cheng F.Y. Lu L.W. (1993). Collapse behavior of Pino Suarez Building during 1985 Mexico City earthquake, ASCE, *J. Struct. Eng*., 119(3): 852–870.

Gluck N., Reinhorn A.M., Gluck J., Levy R. (1996). Design of supplemental dampers for control of structures, ASCE, *J. Struct. Eng*., 122: 1394–1399.

Hall J.F., ed. (1994). *Northridge Earthquake January 17, 1994: Preliminary Reconnaissance Report, Publ. No. 94–01*, Earthquake Engineering Research Institute, Oakland, CA.

Hall J.F, Heaton T., Halling M., Wald D.J. (1995). Near-source ground motion and its effects on flexible buildings, *Earthq. Spectra*, 11(4): 569–605.

Hall J.F. (1998). Seismic response of steel frame buildings to near-source ground motions, *Earthq. Eng. Struc. Dyn.,* 27(12): 1445–1464.

Holmes W., Kircher C., Petak W., Youssef N. (2008). Seismic performance objectives for tall buildings, *PEER Report No. 2008/101*, Pacific Earthquake Engineering Research Center, University of California, Berkeley, CA.

Huang, Y., Mahin, S. (2010). Simulating the inelastic seismic behavior of steel braced frames including the effects of low-cycle fatigue, *PEER Report No. 2010/104*, Pacific Earthquake Engineering Research Center, University of California, Berkeley, CA.

Hwang J.-S. (2008). *Seismic Design of Structures with Viscous Dampers*, International Training Programs for Seismic Design of Building Structures, pp. 123–138.

ICBO (1967) *Uniform Building Code*, International Conference of Building Officials, *1967 Edition*, Whittier, CA.

ICBO (1970) *Uniform Building Code*, International Conference of Building Officials, *1970 Edition*, Whittier, CA.

ICBO (1988) *Uniform Building Code*, International Conference of Building Officials, *1988 Edition*, Whittier, CA.

Kanvinde A. (2012). *Personal Communication*.

Kasai K., Ito H., Ogura T. (2008). Passive control design method based on tuning of equivalent stiffness of bilinear oil damper, *J. Struct. Construct. Eng*., AIJ, No 630, pp. 1281–1299

Kasai K., Lu. X., Pu W., Yamashita T., Arakawa Y., Zhou Y (2013). Effective retrofit using dampers for a steel tall buildings shaken by 2011 East Japan Earthquake—China-Japan Cooperation Program, *Proceedings, 20th International Conference on Urban Earthquake Engineering* (10CUEE), Tokyo, Japan.

Kim T., Stojadinovic B., Whittaker A.S (2003). Physical and numerical performance evaluation of steel moment-resisting frames, Part 1: existing building connection studies, *Report to California Department of Transportation (CalTrans), 2003-08*, Pacific Earthquake Engineering Research Center, University of California, Berkeley, CA.

Krawinkler H., Martinez-Romero E. (1989). Performance evaluation of steel structures in Mexico City, *Proceedings. 3rd U.S.-Mexico Workshop on 1985 Mexico Earthquake Research*, Mexico City, pp.113–119.

Krishnan S., Muto, M. (2011). Mechanism of collapse, sensitivity of ground motion features, and rapid estimation of response of tall steel moment frame buildings to earthquake excitation, *Technical Pre. EERL 2011-2, Earthquake Engineering Research Laboratory*, California Institute of Technology, Pasadena, CA.

LATBSDC (2014). *An Alternative Procedure for Seismic Analysis and Design of Tall Buildings Located in the Los Angeles Region*, Los Angeles Tall Buildings Structural Design Council, Los Angeles, CA.

Lavan O., Dargush G.F. (2009). Multi-objective evolutionary seismic design with passive energy dissipation systems*, J. Earth. Eng*, 13: 758–790.

Lee S.-H., Son D.-I., Kim J., Min K.-W. (2004). Optimal design of viscoelastic dampers using eigenvalue assignment, *Earthq. Eng. Struct. Dyn*., 33: 521–542.

Levy R., Lavan O. (2006). Fully stressed design of passive controllers in frames structures for seismic loading, *Struct. Multidiscipline Optimization*, 32: 485–498.

Liang X.-W., Dong Z.-P., Wang Y.-S., Deng M.-K. (2009). Damage to tall buildings in areas with large epicentral distance during M8.0 Wenchuan earthquake, *J. Earthq. Eng. Eng. Vibration,* 29(1): 24−31 (in Chinese).

Mahin S.A. (1998). Lessons from damage to steel buildings during the Northridge earthquake, *Eng. Struct*., 20(4–6): 261–270.

Martinez-Rodrigo M., Romero M.L. (2003). An optimum retrofit strategy for moment-resisting frames with nonlinear viscous dampers for seismic applications, *Eng. Struct.,* 25: 913–925.

McKenna F., Scott M., Fenves, G. (2010). Nonlinear finite-element analysis software architecture using object composition*, J. Computing Civil Eng*., 24(1): 95–107.

Mitchell A.D., Poland, C.D. (2007). A new seismic rehabilitation standard –ASCE/SEI 41-06, *Proceedings, ASCE Structures Congress*, American Society of Civil Engineers, Reston, VA.

Miyamoto H.K., Scholl R.E. (1996). Case study: seismic rehabilitation of a non-ductile soft story concrete structure using viscous dampers, *Proceedings, 11th World Conference on Earthquake Engineering*, Paper No. 315, Acapulco, Mexico.

Miyamoto K., Gilani A., Wada A., Ariyaratana C. (2010). Collapse risk of tall steel moment frame buildings with viscous dampers subjected to large earthquakes. Part I: damper limit states and failure modes of 10-story archetypes, *Struct. Design Tall Special Bldgs*., 19: 421–438.

Muto M., Krishnan S. (2011). Hope for the best, prepare for the worst: response of tall steel buildings to the shakeout scenario earthquake, ShakeOut Special Issue, *Earthq, Spectra*, 27(2): 375 –398.

Nakashima M., Inoue K., Tada, M. (1998). Classification of damage to steel buildings observed in the 1995 Hyogoken-Nanbu earthquake, *Eng. Struct*., 20 (4–6): 271–281.

Newell J.D., Uang C.M. (2008). Cyclic behavior of steel wide-flange columns subjected to large drift, ASCE, *J. Struct. Eng*., 134(8): 1334–1342.

NIST (2012). Soil-structure interaction for building structures, National Institute of Standards and Technology, NEHRP Consultants Joint Venture, *NIST GCR 12-917-21* (ATC-83 report). Gaithersburg, MD.

Osteraas J., Krawinkler H. (1989). The Mexico earthquake of September 19, 1985 - Behavior of steel buildings, *Earthq. Spectra*, 5(1): 51–88.

Osteraas J.D. (1990). *Strength and Ductility Considerations in Seismic Design*, Department of Civil Engineering, Ph.D. Dissertation, Stanford University, Stanford, CA.

PEER (2010a). Guidelines for performance-based seismic design of tall buildings, *PEER Report No. 2010/05*, Pacific Earthquake Engineering Research Center, University of California, Berkeley, CA.

PEER (2010b). Modeling and acceptance criteria for seismic design and analysis of tall buildings, *PEER Report No. 2010/111,* Pacific Earthquake Engineering Research Center, University of California, Berkeley, CA.

PEER (2011). Case studies of the seismic performance of tall buildings designed by alternative means, *PEER Report No. 2011/05*, Pacific Earthquake Engineering Research Center, University of California, Berkeley, CA.

PEER (2015). NGA-West2 Database, NGA-West2 -- Shallow Crustal Earthquakes in Active Tectonic Regimes, Pacific Earthquake Engineering Research Center, University of California, Berkeley, *http://ngawest2.berkeley.edu* (last accessed April 4, 2015).

Pekelnicky R., Poland, C. (2012). ASCE 41-13: Seismic evaluation and retrofit rehabilitation of existing buildings, *Proceedings, SEAOC 2012 Convention*, Santa Fe, NM.

Phipps M.T. (2000). Investigation of damage to WSMF by earthquakes other than Northridge, *SAC Joint Venture, Report SAC-BD-99-09*, Sacramento, CA.

Poland C.D., Hill J., Sharpe R.L. Soulages J.R. (1995). *Performance Based Seismic Engineering of Buildings*, Structural Engineers Association of California, Vision 2000 Committee, Sacramento, CA.

Porter K (2003). An overview of PEER's performance-based earthquake engineering methodology, *Proceedings, Ninth International Conference on Applications of Statistics and Probability in Civil Engineering (ICASP9)*, San Francisco, CA.

Ramirez O.M., Constantinou M.C., Kircher C.A., Whittaker A.S., Johnson M.W., Gomez J.D., Chrysostomou C.Z. (2001). Development and evaluation of simplified procedures for analysis and design of buildings with passive energy dissipation systems, *MCEER-00-0010*, Mid-American Center for Earthquake Engineering, Urbana, IL.

Reinhorn A.M., Li C., Constantinou M.C. (1995). Experimental and analytical investigation of seismic retrofit of structures with supplemental damping, part I: fluid viscous damping devices, *NCEER-95-0001*, National Center for Earthquake Engineering Research, Buffalo, NY.

Rezaeian S., Bozorgnia Y., Idriss I.M., Campbell K.W., Abrahamson N.A., Silva W.J. (2012). Spectral damping scale factors for shallow crustal earthquakes in active tectonic regions, *PEER Report No. 2012/01,* Pacific Earthquake Engineering Research Center, University of California, Berkeley, CA.

Ribeiro F., Barbosa A., Scott M., Neves L. (2015). Deterioration modeling of steel moment-resisting frames using finite-length plastic hinge force-based beam-column elements, ASCE, *J. Struct. Eng*., 141(2).

Rodgers J.E., Mahin, S.A. (2003). Effects of connection hysteretic degradation on the seismic behavior of steel moment-resisting frames, *PEER Report No. 2003/13*, Pacific Earthquake Engineering Research Center, University of California, Berkeley, CA.

Sexton H.J. & Associates, Engineers (1968). *Dynamic Earthquake Analysis*, A report to H.J. Brunnier Associates. San Francisco, CA.

SFDBI (2014). *Requirements and Guidelines for the Seismic Design of New Tall Buildings using Non-Prescriptive Seismic-Design Procedures*, *Administrative Bulletin 83*, San Francisco Building Code, San Francisco Department of Building Inspection, San Francisco, CA.

Stillmaker K., Kanvinde A., Galasso C. (2016). Fracture mechanics-based design of column splices with partial joint penetration welds, *J. Struct. Eng*., doi: 10.1061/(ASCE)ST.1943-541X.0001380.

Singh M.P., Moreschi L.M. (2001). Optimal seismic response control with dampers, *Earthq. Eng. Struct. Dyn*., 30: 553–572.

Singh M.P., Moreschi L.M. (2002). Optimal placement of dampers for passive response control, *Earthq. Eng. Struct. Dyn*., 31: 955–976.

Soong T.T., Dargush G.F. (1997). *Passive Energy Dissipation Systems in Structural Engineering*, Chichester, U.K.: John Wiley and Sons.

Stewart J.P., Tileylioglu S. (2010). Input ground motions for tall buildings with subterranean levels, *TBI Task 8 Final Report*, Pacific Earthquake Engineering Research Center, University of California, Berkeley, CA.

Symans M.D., Constantinou M.C. (1998). Passive fluid viscous damping systems for seismic energy dissipation, *ISET J. Earthq. Tech*., 35(4): 185–206.

Takewaki I. (2000). Optimal damper displacement for planar frames using transfer functions, *Struct. Multidisciplinary Optimization*, 20: 280–287.

Takewaki I., Moustafa A. Fujita K. (2013). *Earthquake Resilience of High-Rise Buildings -- Case Study of the 2011 Tohoku (Japan) Earthquake, Improving the Earthquake Resilience of Buildings*, Springer, DOI 10.1007/978-1-4471-4144-0_2.

Taylor Device Inc. (2010a). Damper mounting dimensions, retrieved from *http://taylordevices.com/pdf/web-damper.PDF*, accessed 2010.

Taylor Device Inc. (2010b). Structural applications of fluid viscous dampers, retrieved from *http://taylordevices.com/pdf/StructuralChart2010.pdf*, accessed 2010.

Taylor Device Inc. (2010c). Structural dampers and seismic protection products, retrieved from *http://taylordevices.com/dampers-seismic-protection.html*, accessed 2010.

Taylor D.P., Katz I. (2004). *Seismic Protection with Fluid Viscous Dampers for the Torre Mayor*, North Tonawanda: Taylor Devices, Inc.

Terzic V., Mahin S.A., Comerio, M. (2015). Using PBEE in seismic design to improve performance of moment-resisting frames by base isolation, *Earthq, Spectra*, in press, Earthquake Engineering Research Institute, Oakland, CA.

USGS (2008). 2008 Bay Area earthquake probabilities, *http://earthquake.usgs.gov/regional/nca/ucerf/*. U.S. Geological Survey, Menlo Park, CA.

Uzarski J., Arnold C., eds. (2001). "Chi-Chi, Taiwan, earthquake of September 21, 1999, reconnaissance report, *Earthq, Spectra*, Supplement A to Vol. 17, Earthquake Engineering Research Institute, Oakland, CA.

Veterans Administration (1973). Earthquake resistant design requirements for VA hospital facilities, *Handbook H-08-8*, Office of Construction, Washington, DC, 36 pgs.

Whittle J.K., Williams M.S., Karavasillis T.L., Blakeborough A. (2012). A comparison of viscous damper placement methods for improving seismic building design, *J. Earthq. Eng*., 16(4): 540–560.

Wright R.N, Kramer S., Culver, C. (1973). Building practices for disaster mitigation, *Proceedings, National Workshop on Building Practices for Disaster Mitigation*, Building Science Series 46, National Bureau of Standards, Gaithersburg, MD.

Wyllie L.A., ed. (1986). The Chile earthquake of March 3, 1985, *Earthq, Spectra*, 2(2): 249–513.

Wyllie L.A., Jr., Filson J.R., eds. (1989). Armenia earthquake reconnaissance report, *Earthq, Spectra*, Earthquake Engineering Research Institute, Oakland, CA.

Yang J.N., Lin S., Kim J.-H., Agrawal A.K. (2002). Optimal design of passive energy dissipation systems based on H∞ and H2 performances, *Earthq. Eng. Struct. Dyn*., 31: 921−936.

Youd T.L., Bardet J.P., Bray J.D., eds. (2000). Kocaeli, Turkey, earthquake of August 17, 1999 reconnaissance report, *Earthq. Spectra*, Supplement A to Vol. 16, Earthquake Engineering Research Institute, Oakland, CA.

Zhang R.-H., Soong T.T. (1992). Seismic design of viscoelastic dampers for structural applications, ASCE, *J. Struct. Eng*., 118: 1375−1392.

Appendix A: Ground Motion Selections and Scale Factors for the Hazards Considered

Table A.1 Ground-motion selections for ASCE 7-10.

No.	NGA#	Earthquake	Station	Mag.	Dist. (km)	V_{s30} (m/sec)	Scale Factor	NGAW 1	NGAW 2
1	285	Irpinia, Italy-01	Bagnoli Irpinio	6.9	8.2	650	1.906	0.113	0.125
2	737	Loma Prieta	Agnews State Hospital	6.9	24.6	240	1.765	0.104	0.250
3	827	Cape Mendocino	Fortuna - Fortuna Blvd	7.0	20.0	457	1.896	0.070	0.070
4	864	Landers	Joshua Tree	7.3	11.0	379	1.457	0.070	0.070
5	1104	Kobe, Japan	Fukushima	6.9	17.9	256	1.059	0.100	-
6	1110	Kobe, Japan	Morigawachi	6.9	24.8	256	1.596	0.100	-
7	1497	Chi-Chi, Taiwan	TCU057	7.6	11.8	555	1.484	0.038	0.038
8	1498	Chi-Chi, Taiwan	TCU059	7.6	17.1	273	1.043	0.038	0.038
9	1534	Chi-Chi, Taiwan	TCU107	7.6	16.0	409	1.135	0.038	0.038
10	3750	Cape Mendocino	Loleta Fire Station	7.0	25.9	516	1.231	0.063	NA
11	4757	Wenchuan, China	Dayiyinping	7.9	28.6	379	2.000	-	NA
12	4798	Wenchuan, China	Anxiantashui	7.9	0.1	376	1.428	-	NA
13	4806	Wenchuan, China	Bixianzoushi-shan	7.9	17.0	418	1.964	-	NA
14	4847	Chuetsu-oki	Joetsu Kakizakiku Kakizaki	6.8	11.9	383	0.859	0.088	NA
15	5823	El Mayor-Cucapah	Chihuahua	7.2	19.5	242	1.138	0.075	NA
16	5827	El Mayor-Cucapah	MICHOACAN DE OCAMPO	7.2	15.9	242	0.895	0.063	NA
17	5975	El Mayor-Cucapah	Calexico Fire Station	7.2	20.5	231	0.899	0.038	NA
18	6887	Darfield, New Zealand	Christchurch Botanical Gardens	7.0	18.1	187	1.044	0.050	NA
19	6927	Darfield, New Zealand	LINC	7.0	7.1	263	0.666	0.075	NA
20	6969	Darfield, New Zealand	Styx Mill Transfer Station	7.0	20.9	248	1.132	0.050	NA

Table A.2 Ground-motion selections for ASCE 41-13, BSE-1E.

No.	NGA#	Earthquake	Station	Mag.	Dist. (km)	V_{s30} (m/sec)	Scale Factor	NGAW 1	NGAW 2
1	776	Loma Prieta	Hollister - South & Pine	6.9	27.9	282	0.973	0.088	0.125
2	900	Landers	Yermo Fire Station	7.3	23.6	354	1.348	0.070	0.070
3	1100	Kobe, Japan	Abeno	6.9	24.9	256	1.956	0.025	NA
4	1158	Kocaeli, Turkey	Duzce	7.5	15.4	282	0.817	0.100	0.237
5	1198	Chi-Chi, Taiwan	CHY029	7.6	11.0	545	1.158	0.038	0.038
6	1484	Chi-Chi, Taiwan	TCU042	7.6	26.3	579	1.305	0.063	0.063
7	1491	Chi-Chi, Taiwan	TCU051	7.6	7.6	350	1.344	0.038	0.038
8	1496	Chi-Chi, Taiwan	TCU056	7.6	10.5	403	1.705	0.050	0.050
9	1605	Duzce, Turkey	Duzce	7.1	6.6	282	0.611	0.100	0.100
10	1787	Hector Mine	Hector	7.1	11.7	726	1.302	0.038	0.038
11	3744	Cape Mendocino	Bunker Hill FAA	7.0	12.2	566	1.310	NA	NA
12	3757	Landers	North Palm Springs Fire Sta #36	7.3	27.0	368	2.547	0.113	NA
13	4781	Wenchuan, China	Jiangyouchonghua	7.9	27.2	430	1.266	NA	NA
14	4866	Chuetsu-oki	Kawanishi Izumozaki	6.8	11.8	338	1.229	0.113	NA
15	5284	Chuetsu-oki	NIGH11	6.8	27.3	375	2.589	0.088	NA
16	5656	Iwate	IWTH24	6.9	5.2	486	0.943	0.063	NA
17	5829	El Mayor-Cucapah	RIITO	7.2	13.7	242	0.900	0.050	NA
18	5832	El Mayor-Cucapah	TAMAULIPAS	7.2	26.6	242	1.151	0.063	NA
19	5837	El Mayor-Cucapah	El Centro - Imperial & Ross	7.2	20.1	229	0.845	0.038	NA
20	6897	Darfield, New Zealand	DSLC	7.0	8.5	296	1.050	0.075	NA

Table A.3 Ground-motion selections for ASCE 41-13, BSE-2E.

No.	NGA#	Earthquake	Station	Mag.	Dist. (km)	V_{s30} (m/sec)	Scale Factor	NGAW 1	NGAW 2
1	776	Loma Prieta	Hollister - South & Pine	6.9	27.9	282	1.358	0.088	0.125
2	777	Loma Prieta	Hollister City Hall	6.9	27.6	199	1.682	0.100	0.125
3	778	Loma Prieta	Hollister Differential Array	6.9	24.8	216	1.740	0.088	0.125
4	827	Cape Mendocino	Fortuna - Fortuna Blvd	7.0	20.0	457	3.316	0.070	0.070
5	900	Landers	Yermo Fire Station	7.3	23.6	354	1.894	0.070	0.070
6	1104	Kobe, Japan	Fukushima	6.9	17.9	256	1.927	0.100	-
7	1158	Kocaeli, Turkey	Duzce	7.5	15.4	282	1.180	0.100	0.237
8	1493	Chi-Chi, Taiwan	TCU053	7.6	6.0	455	1.998	0.038	0.038
9	1605	Duzce, Turkey	Duzce	7.1	6.6	282	0.857	0.100	0.100
10	3744	Cape Mendocino	Bunker Hill FAA	7.0	12.2	566	1.833	-	NA
11	3750	Cape Mendocino	Loleta Fire Station	7.0	25.9	516	1.818	0.063	NA
12	4757	Wenchuan, China	Dayiyinping	7.9	28.6	379	3.283	-	NA
13	4798	Wenchuan, China	Anxiantashui	7.9	0.1	376	2.109	-	NA
14	4806	Wenchuan, China	Bixianzoushishan	7.9	17.0	418	3.048	-	NA
15	5832	El Mayor-Cucapah	TAMAULIPAS	7.2	26.6	242	1.541	0.063	NA
16	5837	El Mayor-Cucapah	El Centro - Imperial & Ross	7.2	20.1	229	1.442	0.038	NA
17	6906	Darfield, New Zealand	GDLC	7.0	1.2	344	0.616	0.063	NA
18	6927	Darfield, NZ	LINC	7.0	7.1	263	0.983	0.075	NA
19	6952	Darfield, NZ	Papanui High School	7.0	18.7	263	1.682	0.063	NA
20	6953	Darfield, NZ	Pages Road	7.0	24.6	206	1.638	0.088	NA

Table A.4 Ground-motion selections for a 43-year return period (50% in 30 years).

No.	NGA#	Earthquake	Station	Mag.	Dist. (km)	V_{s30} (m/sec)	Scale Factor	NGAW 1	NGAW 2
1	162	Imperial Valley-06	Calexico Fire Station	6.5	10.5	231	0.869	0.050	0.250
2	183	Imperial Valley-06	El Centro Array #8	6.5	3.9	206	0.397	0.038	0.125
3	316	Westmorland	Parachute Test Site	5.9	16.7	349	0.570	0.113	0.125
4	721	Superstition Hills-02	El Centro Imp. Co. Cent	6.5	18.2	192	0.504	0.088	0.125
5	728	Superstition Hills-02	Westmorland Fire Sta	6.5	13.0	194	0.605	0.088	0.125
6	882	Landers	North Palm Springs	7.3	26.8	345	1.151	0.050	0.276
7	1144	Gulf of Aqaba	Eilat	7.2	44.1	355	1.596	0.063	0.125
8	1794	Hector Mine	Joshua Tree	7.1	31.1	379	1.034	0.017	0.091
9	2650	Chi-Chi, Taiwan-03	TCU116	6.2	22.1	493	0.940	0.060	0.250
10	2715	Chi-Chi, Taiwan-04	CHY047	6.2	38.6	170	1.308	0.038	0.250
11	3264	Chi-Chi, Taiwan-06	CHY024	6.3	31.1	428	1.147	0.040	0.250
12	3747	Cape Mendocino	College of the Redwoods	7.0	31.5	493	0.772	0.063	NA
13	3943	Tottori, Japan	SMN015	6.6	9.1	617	1.130	0.075	NA
14	4031	San Simeon, CA	Templeton - Hospital	6.5	6.2	411	0.543	0.088	NA
15	4204	Niigata, Japan	NIG014	6.6	28.4	128	0.950	0.050	NA
16	4854	Chuetsu-oki	Nadachiku Joetsu City	6.8	35.9	571	1.376	0.100	NA
17	4881	Chuetsu-oki	Nagaoka Kouiti Town	6.8	20.8	294	1.145	0.050	NA
18	5990	El Mayor-Cucapah	El Centro Array #7	7.2	27.9	211	0.683	0.025	NA
19	6891	Darfield, NZ	CSHS	7.0	43.6	638	1.488	0.038	NA
20	8134	Christchurch, NZ	Styx Mill Transfer Sta.	6.2	11.3	248	0.754	0.050	NA

Table A.5 Ground-motion selections for a 224-year return period (20% in 50 years).

No.	NGA#	Earthquake	Station	Mag.	Dist. (km)	V_{s30} (m/sec)	Scale Factor	NGAW 1	NGAW 2
1	161	Imperial Valley-06	Brawley Airport	6.5	10.4	209	1.999	0.088	0.125
2	173	Imperial Valley-06	El Centro Array #10	6.5	8.6	203	1.541	0.100	0.125
3	182	Imperial Valley-06	El Centro Array #7	6.5	0.6	211	0.904	0.088	0.125
4	316	Westmorland	Parachute Test Site	5.9	16.7	349	1.559	0.070	0.070
5	721	Superstition Hills-02	El Centro Imp. Co. Cent	6.5	18.2	192	1.378	0.070	0.070
6	728	Superstition Hills-02	Westmorland Fire Sta	6.5	13.0	194	1.654	0.100	-
7	729	Superstition Hills-02	Imperial Valley Wildlife Liquefaction Array	6.5	23.9	179	1.403	0.100	0.237
8	776	Loma Prieta	Hollister - South & Pine	6.9	27.9	282	1.198	0.038	0.038
9	778	Loma Prieta	Hollister Differential Array	6.9	24.8	216	1.320	0.100	0.100
10	900	Landers	Yermo Fire Station	7.3	23.6	354	1.584	-	NA
11	1147	Kocaeli, Turkey	Ambarli	7.5	69.6	175	1.427	0.063	NA
12	1158	Kocaeli, Turkey	Duzce	7.5	15.4	282	1.008	-	NA
13	1605	Duzce, Turkey	Duzce	7.1	6.6	282	0.711	-	NA
14	1762	Hector Mine	Amboy	7.1	43.1	383	1.929	-	NA
15	3750	Cape Mendocino	Loleta Fire Station	7.0	25.9	516	1.596	0.063	NA
16	4798	Wenchuan, China	Anxiantashui	7.9	0.1	376	1.489	0.038	NA
17	4847	Chuetsu-oki	Joetsu Kakizakiku Kakizaki	6.8	11.9	383	1.089	0.063	NA
18	5827	El Mayor-Cucapah	MICHOACAN DE OCAMPO	7.2	15.9	242	0.995	0.075	NA
19	6013	El Mayor-Cucapah	El Centro - Meadows Union School	7.2	28.3	276	1.821	0.063	NA
20	8118	Christchurch, NZ	Papanui High School	6.2	9.1	263	1.428	0.088	NA

Table A.6 Ground-motion selections for a 475-year return period (10% in 50 years).

No.	NGA#	Earthquake	Station	Mag.	Dist. (km)	V_{s30} (m/sec)	Scale Factor	NGAW 1	NGAW 2
1	169	Imperial Valley-06	Delta	6.5	22.0	242	1.936	0.088	0.063
2	179	Imperial Valley-06	El Centro Array #4	6.5	7.1	209	1.460	0.063	0.125
3	185	Imperial Valley-06	Holtville Post Office	6.5	7.5	203	1.840	0.075	0.125
4	721	Superstition Hills-02	El Centro Imp. Co. Cent	6.5	18.2	192	1.924	0.088	0.125
5	728	Superstition Hills-02	Westmorland Fire Sta	6.5	13.0	194	2.000	0.088	0.125
6	776	Loma Prieta	Hollister - South & Pine	6.9	27.9	282	1.672	0.088	0.125
7	777	Loma Prieta	Hollister City Hall	6.9	27.6	199	1.824	0.100	0.125
8	778	Loma Prieta	Hollister Differential Array	6.9	24.8	216	1.842	0.088	0.125
9	900	Landers	Yermo Fire Station	7.3	23.6	354	2.000	0.070	0.070
10	1158	Kocaeli, Turkey	Duzce	7.5	15.4	282	1.407	0.100	0.237
11	1203	Chi-Chi, Taiwan	CHY036	7.6	16.0	233	1.691	0.063	0.063
12	1528	Chi-Chi, Taiwan	TCU101	7.6	2.1	389	1.887	0.050	0.050
13	1605	Duzce, Turkey	Duzce	7.1	6.6	282	0.993	0.100	0.100
14	3744	Cape Mendocino	Bunker Hill FAA	7.0	12.2	566	1.911	-	NA
15	4847	Chuetsu-oki	Joetsu Kakizakiku Kakizaki	6.8	11.9	383	1.520	0.088	NA
16	5827	El Mayor-Cucapah	MICHOACAN DE OCAMPO	7.2	15.9	242	1.389	0.063	NA
17	5975	El Mayor-Cucapah	Calexico Fire Station	7.2	20.5	231	1.655	0.038	NA
18	6888	Darfield, New Zealand	Christchurch Cathedral College	7.0	19.9	198	1.803	0.050	NA
19	6952	Darfield, New Zealand	Papanui High School	7.0	18.7	263	1.611	0.063	NA
20	6960	Darfield, New Zealand	Riccarton High School	7.0	13.6	293	1.956	0.050	NA

Table A.7 Ground-motion selections for a 975-year return period (5% in 50 years).

No.	NGA#	Earthquake	Station	Mag.	Dist. (km)	V_{s30} (m/sec)	Scale Factor	NGAW 1	NGAW 2
1	285	Irpinia, Italy-01	Bagnoli Irpinio	6.9	8.2	650	4.590	0.113	0.125
2	778	Loma Prieta	Hollister Differential Array	6.9	24.8	216	2.406	0.088	0.125
3	827	Cape Mendocino	Fortuna - Fortuna Blvd	7.0	20.0	457	4.840	0.070	0.070
4	900	Landers	Yermo Fire Station	7.3	23.6	354	2.889	0.070	0.070
5	1100	Kobe, Japan	Abeno	6.9	24.9	256	4.473	0.025	-
6	1104	Kobe, Japan	Fukushima	6.9	17.9	256	2.768	0.100	-
7	1148	Kocaeli, Turkey	Arcelik	7.5	13.5	523	5.000	0.088	0.088
8	1158	Kocaeli, Turkey	Duzce	7.5	15.4	282	1.838	0.100	0.237
9	1176	Kocaeli, Turkey	Yarimca	7.5	4.8	297	1.740	0.088	0.088
10	1194	Chi-Chi, Taiwan	CHY025	7.6	19.1	278	2.592	0.063	0.063
11	1208	Chi-Chi, Taiwan	CHY046	7.6	24.1	442	4.176	0.050	0.050
12	1605	Duzce, Turkey	Duzce	7.1	6.6	282	1.297	0.100	0.100
13	4757	Wenchuan, China	Dayiyinping	7.9	28.6	379	4.567	-	NA
14	4847	Chuetsu-oki	Joetsu Kakizakiku Kakizaki	6.8	11.9	383	1.985	0.088	NA
15	4855	Chuetsu-oki	Sanjo	6.8	27.2	245	4.923	0.100	NA
16	5975	El Mayor-Cucapah	Calexico Fire Station	7.2	20.5	231	2.162	0.038	NA
17	6887	Darfield, New Zealand	Christchurch Botanical Gardens	7.0	18.1	187	3.053	0.050	NA
18	6942	Darfield, New Zealand	North New Brighton School	7.0	26.8	211	2.997	0.050	NA
19	6960	Darfield, New Zealand	Riccarton High School	7.0	13.6	293	2.555	0.050	NA
20	8606	El Mayor-Cucapah	Westside Elementary School	7.2	11.4	242	1.892	0.050	NA

Table A.8 Ground motion selections for a 2475-year return period (2% in 50 years).

No.	NGA#	Earthquake	Station	Mag.	Dist. (km)	V_{s30} (m/sec)	Scale Factor	NGAW 1	NGAW 2
1	285	Irpinia, Italy-01	Bagnoli Irpinio	6.9	8.2	650	6.000	0.113	0.125
2	737	Loma Prieta	Agnews State Hospital	6.9	24.6	240	5.469	0.104	0.250
3	776	Loma Prieta	Hollister - South & Pine	6.9	27.9	282	2.939	0.088	0.125
4	778	Loma Prieta	Hollister Differential Array	6.9	24.8	216	3.239	0.088	0.125
5	900	Landers	Yermo Fire Station	7.3	23.6	354	3.888	0.070	0.070
6	1104	Kobe, Japan	Fukushima	6.9	17.9	256	3.726	0.100	-
7	1121	Kobe, Japan	Yae	6.9	27.8	256	4.955	-	-
8	1148	Kocaeli, Turkey	Arcelik	7.5	13.5	523	6.000	0.088	0.088
9	1158	Kocaeli, Turkey	Duzce	7.5	15.4	282	2.473	0.100	0.237
10	1176	Kocaeli, Turkey	Yarimca	7.5	4.8	297	2.342	0.088	0.088
11	1193	Chi-Chi, Taiwan	CHY024	7.6	9.6	428	2.963	0.025	0.025
12	1503	Chi-Chi, Taiwan	TCU065	7.6	0.6	306	1.429	0.075	0.075
13	1605	Duzce, Turkey	Duzce	7.1	6.6	282	1.746	0.100	0.100
14	3750	Cape Mendocino	Loleta Fire Station	7.0	25.9	516	3.916	0.063	NA
15	5774	Iwate	Nakashinden Town	6.9	29.4	276	4.234	0.113	NA
16	5831	El Mayor-Cucapah	EJIDO SALTILLO	7.2	17.3	242	3.937	0.050	NA
17	5838	El Mayor-Cucapah	El Centro - Meloland Geotechnic	7.2	29.0	186	4.617	0.063	NA
18	6889	Darfield, New Zealand	Christchurch Hospital	7.0	18.4	194	3.586	0.038	NA
19	6942	Darfield, New Zealand	North New Brighton School	7.0	26.8	211	4.034	0.050	NA
20	6952	Darfield, New Zealand	Papanui High School	7.0	18.7	263	2.832	0.063	NA

Appendix B ASCE 41-13 Tier 1 Checklist

Table B.1 ASCE 41-13 Tier 1 Life Safety (LS) Basic Configuration Checklist for case-study building.

Items	Evaluation Statement	Comments
General		
Load Path	☒C ☐NC ☐N/A ☐U	Bi-directional moment-resisting frames (Pre-Northridge connection details).
Adjacent Building	☒C ☐NC ☐N/A ☐U	Consider the main tower only.
Mezzanines	☒C ☐NC ☐N/A ☐U	Simple beam-to-column connections at mezzanine level. The mezzanine level is anchored to the box columns.
Building Configuration		
Weak Story	☒C ☐NC ☐N/A ☐U	
Soft Story	☐C ☒NC ☐N/A ☐U	The mezzanine level does not satisfy the soft story check criteria.
Vertical Irregularities	☐C ☒NC ☐N/A ☐U	All columns are continuous to the foundation but the building has a tall first story.
Geometry	☒C ☐NC ☐N/A ☐U	Consider the main tower only (It is not clear that the frames outside the main tower area are rigid beam-to-column connections or not; See lines G_E, J, K and M).
Mass	☒C ☐NC ☐N/A ☐U	Story weights are assumed based on the available information from the structural drawings.
Torsion	☒C ☐NC ☐N/A ☐U	Assume to be compliant (It is not clear that the frames outside the main tower area are rigid beam-to-column connections or not).
Geologic Site Hazards		
Liquefaction	☐C ☒NC ☐N/A ☐U	The building site is inside the regions that have potential for liquefaction during a seismic event (CGS, 2000).
Slope Failure	☒C ☐NC ☐N/A ☐U	
Surface Fault Rupture	☒C ☐NC ☐N/A ☐U	

Foundation Configuration		
Overturning	☒C ☐NC ☐N/A ☐U	$S_a = \frac{0.871}{0.035 \cdot \left(\frac{5879}{12}\right)^{0.8}} = 0.175$ $S_a < S_{XS} = 0.9$ for BSE-1E hazard level. And $\frac{1620}{5879} = 0.276 > 0.6 \cdot S_a = 0.105$
Ties Between Foundation Elements	☒C ☐NC ☐N/A ☐U	A 7-ft thick mat foundation is connecting the pile caps. The soil condition is Site Class E.

Note 1: Compliant (C), Noncompliant (NC), Not Applicable (N/A) and Unknown (U).

Note 2: For high seismicity case, Life Safety and Immediate Occupancy Basic Configuration Checklists are the same (Section 16.1.2).

Table B.2 ASCE 41-13 Tier 1 Life Safety (LS) Structural Checklist for case-study building (Type:S1).

Items	Evaluation Statement	Comments
Seismic-Force-Resisting System		
Drift Check	☒C ☐NC ☐N/A ☐U	Story drift ratio < 0.025
Axial Stress Check	☐C ☒NC ☐N/A ☐U	Columns < 0.1 F_y (gravity only) Alternatively, columns, equation (4-12) < 0.3 F_y (overturning alone)
Flexural Stress Check	☒C ☐NC ☐N/A ☐U	Columns and beams, equation (4-15) < F_y
Redundancy	☒C ☐NC ☐N/A ☐U	The number of lines of moment frames in *X*-direction is 6 (>2), and 5 (>2) is *Y*-direction. The number of bays of moment frames in each line is 4 (>2) in *X*-direction and 5 (>2) in *Y*-direction.
Interfering walls	☒C ☐NC ☐N/A ☐U	
Moment-resisting connections	☐C ☒NC ☐N/A ☐U	
Panel zones	☐C ☒NC ☐N/A ☐U	
Column splices	☐C ☒NC ☐N/A ☐U	Not able to develop the full strength of the column.
Strong column/weak beam	☐C ☒NC ☐N/A ☐U	> 50% satisfy SCWB check (each story of each line)
Compact members	☒C ☐NC ☐N/A ☐U	Moderately ductile members.
Connections		
Transfer to steel frames	☐C ☐NC ☐N/A ☒U	Metal decks are connected to steel frames with puddle welds, no shear studs exist.
Steel columns	☐C ☒NC ☐N/A ☐U	No anchor bolts exist between column base plates and mat foundations.
Stiff Diaphragms		
Openings at frames	☐C ☒NC ☐N/A ☐U	Openings are more than 25% of the frame length in both directions.

Note 1: Compliant (C), Noncompliant (NC), Not Applicable (N/A) and Unknown (U).

Appendix C: Preliminary Shear Capacity Check

Preliminary check for elements shear capacities were conducted in order to see whether the members are likely to lose shear resistance prior to forming plastic hinges.

C.1 SHEAR CHECK OF COLUMNS

Three categories of columns (Figure C.1) were checked for the shear capacity, each investigating both base metal and the welding area. Using capacity design philosophy, the shear demand was estimated from its probable strength assuming full plastic hinges were developed at both ends:

$$V = \frac{2M_p}{L_c} \qquad \tau_d = \frac{VQ_x}{I_x \sum t_{\text{web}}}$$

Shear capacity was obtained from the material properties:

$$\tau_c = 0.6 f_y$$

Table C.1 shows percentage of columns subjected to shear failure for each column category. A total of seven kinds of box-section columns, three kinds of H-box columns, and 15 kinds of H-section columns used in the case-study building were checked. The percentage is defined as the ratio between vulnerable sections and the total number of sections. H-section columns were the worst cases for both base metal and welds due to their insufficient web thickness.

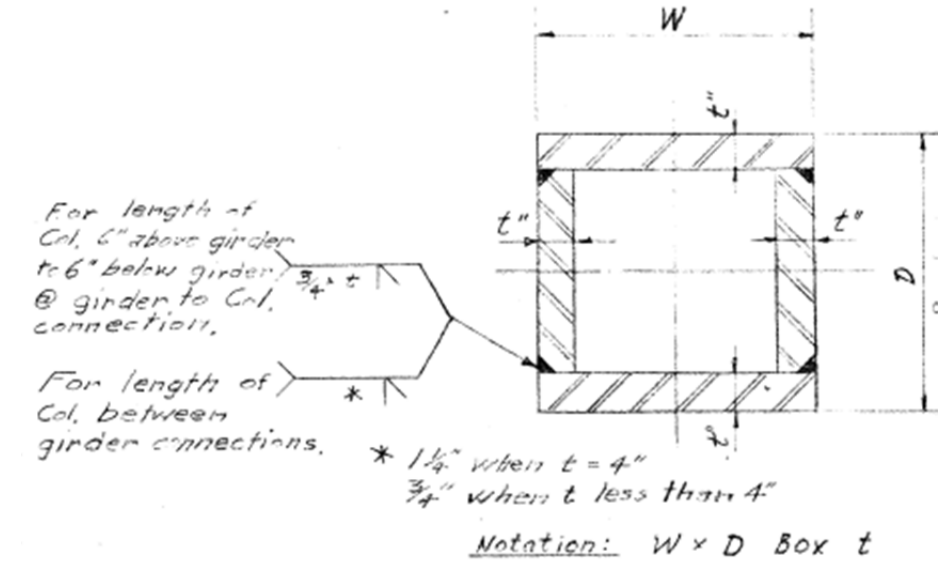

(a)

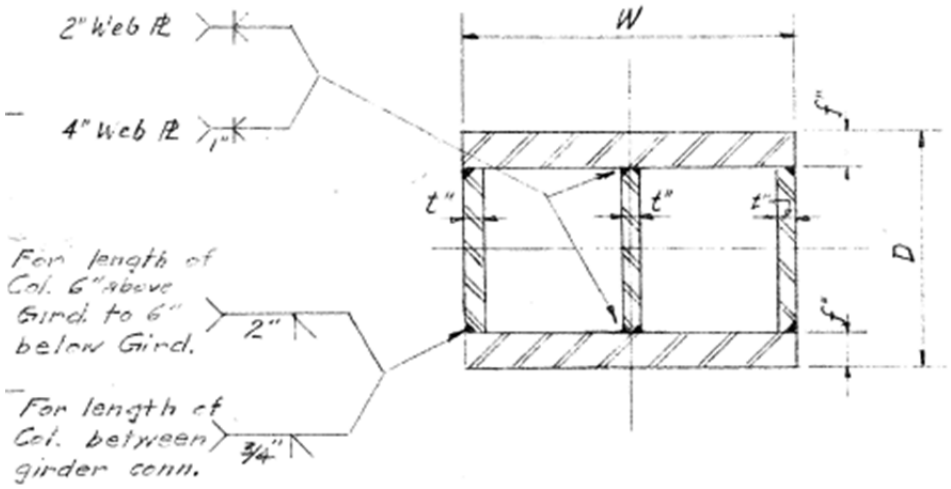

(b)

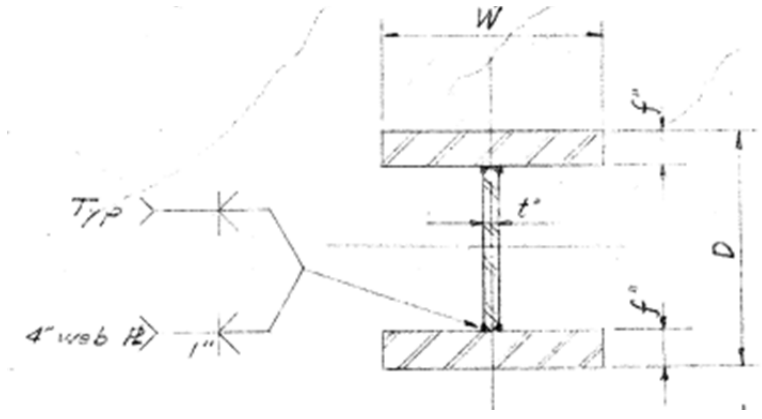

(c)

Figure C.1 Typical column sections: (a) box section; (b) H-box section; and (c) H section.

Table C.1 Percentage of column sections vulnerable to shear failure.

Column section	Base metal	Weld	Max. DCR*
Box	0	15%	1.2
H-box	0	0	0.8
H	90%	35%	2.3

Note 1: Maximum Demand to Capacity Ratio (DCR) indicates the worst scenario for each category

C.2 SHEAR CHECK OF GIRDERS

Two categories of girders were checked for their shear capacities, each investigating both base metal and the welding area. The built-up section was identified in Figure C.2. Following the same procedure as columns, the percentages of girders subjected to shear failure is listed in Table C.2. Note that the shear demand of girders also includes the shear force due to gravity, i.e., $v = 2M_p / L_c + V_g$.

W-section girders have sufficient capacity to transfer shears, while the built-up girders have a high chance (47% of all built-up girders) to fail in shear for the base metals. This is also due to the thin web for these kinds of sections; stiffeners or double plates might be used if further analysis confirms such vulnerabilities of structural elements.

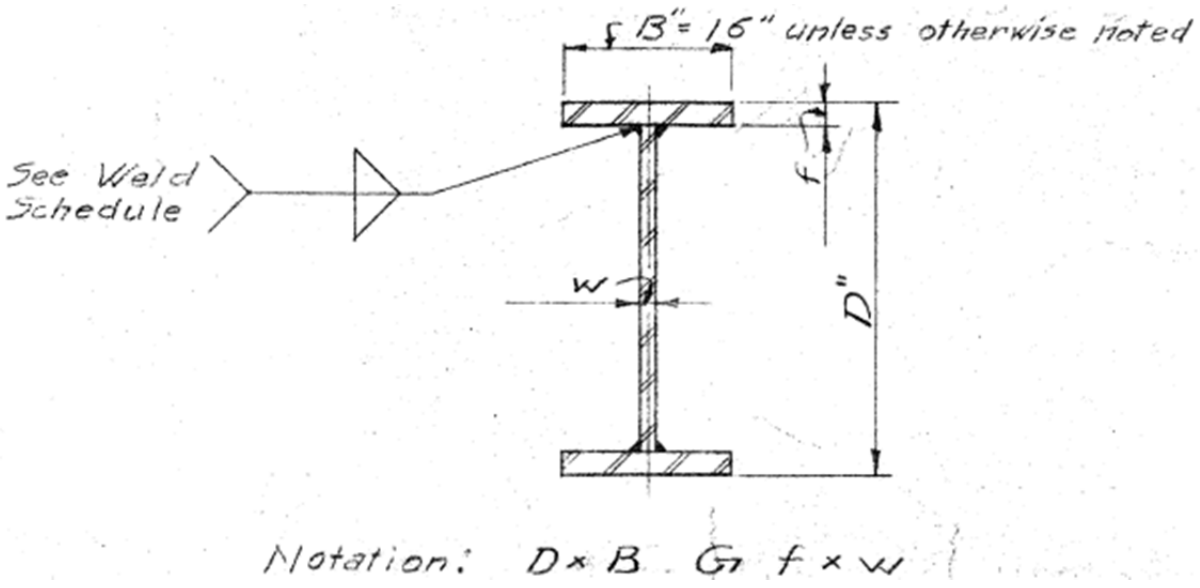

Figure C.2 Typical built-up girder section.

Table C.2 Percentage of girder sections vulnerable to shear failure

Girder Section	Base Metal	Weld	Max. DCR
Wide-flange	0	-	0.4
Built-up	47%	0	1.5

C.3 A FURTHER CHECK USING ACTUAL SHEAR DEMAND

Above-mentioned checks were based on the assumption that the probable strength of the gross Sections would be achieved following the capacity design philosophy. Nevertheless, the actual demands might be well below the probable strength and thus help alleviate the situation. To assess the difference between the actual demands and maximum demands, and better understand the shear resistance of various elements, comparisons were conducted for a few critical elements that having largest demand capacity ratios, as summarized in Table C.3 and C.4. The actual demands are extracted from the maximum response at BSE-2E hazard-level earthquake for each element.

Columns were checked at both the perimeter and inside frames. Preliminary check indicated that the columns at upper levels generally have larger demand-capacity ratio and thus selected for a further check. Given that the actual shear demands would be larger due to the formation of plastic hinges in the weak-story zone, the check was also extended to the lower stories for corresponding elements. Both base metal and welding area were investigated, with the critical case identified. A similar check was done for girders. The critical case was found in a built-up Section located in the lower stories (floor 5–7).

The results indicated that the actual shear demands would be much smaller than the maximum values, ranging from 30–60% of the maximum values for both columns and girders. As a result, the shear D/C would also be reduced in a similar extent. Therefore, it was concluded that the shear demand estimation using maximum probable strength was too conservative, and the shear capacity would be less of a concern in this case-study building. However, it should be noted that the D/C ratios were still close to 1.0, or even larger than 1.0 for some cases, thus it would be more prudent to conduct systematic shear capacity check.

Table C.3 Comparison of actual shear demands and maximum shear demands (columns).

Column Location	Location	Section	Actual Demands		Max. Demands	
			Shear	D/C	Shear	D/C
Perimeter frame	Lower level (3-7)	24×24 H 4×2*1	675 k	0.8	1575 k	1.8
		26×24 H 4×2*1	635 k	0.7	1750 k	1.8
	Upper level (19-23)	24×24 H 2.5×1*1	310 k	0.7	1061 k	2.3
		26×24 H 2.5×1*1	575 k	1.1	1169 k	2.3
Inside frame	Lower level (3-7)	30×30 Box 3.5*2	693 k	0.4	2321 k	1.2

*1 Base metal is more vulnerable.

*2 PJP Welding is more vulnerable.

Table C.4 Comparison of actual shear demands and maximum shear demands (girders).

Girder Section	Location	Actual Demands		Max. Demands	
		Shear	D/C	Shear	D/C
36×22 G 2.5×0.5*1	Floor level: lower (5–7) Inside frames	330 kips	0.9	540 kips	1.5

*1 Base metal is more vulnerable.

Appendix D: Column Splice Preliminary Check

A preliminary check of column splices was conducted. A total of 39 kinds of column splices were checked, covering four categories: box column to box column splice, H-box column to H-box column splice, H-box to H column splice, and H column to H column splice. Those Sections were checked for cases under pure tension. The demand was estimated from the probable strength of the gross Section of the upper column:

$$T_d = A_g F_y R_y$$

The capacity of the PJP welds were calculated following AISC requirement:

$$T_c = 0.8 \times t_{\text{weld}} \times L_{\text{weld}} \times 0.6 \times F_{y,\text{weld}}$$

Table D.1 showed that if the column gross Section is to reach the full Section yielding, the column splice regions where PJP welds are utilized would be quite vulnerable to tension. The maximum demand to capacity Ratio (DCR) identified in Table D.1 showed that the splice regions would be at least twice likely to failure in tension than the column gross Sections. Thereby those critical splice locations deserve special attention during later analysis, and possible upgrading might be needed.

Table D.1 Percentage of column splices subject to failure.

Splice Type	Tension*	Max. DCR*
Box & box	100%	2.4
H-box & H-box	100%	3.8
H-box & H	100%	2.5
H & H	100%	2.5

Note 1: Column splices were checked under pure tension

Note 2: Maximum Demand to Capacity Ratio (DCR) indicates the worst scenario for each category $T_d = A_g F_y R_y$

PEER REPORTS

PEER reports are available as a free PDF download from http://peer.berkeley.edu/publications/peer_reports_complete.html. Printed hard copies of PEER reports can be ordered directly from our printer by following the instructions at http://peer.berkeley.edu/publications/peer_reports.html. For other related questions about the PEER Report Series, contact the Pacific Earthquake Engineering Research Center, 325 Davis Hall Mail Code 1792, Berkeley, CA 94720. Tel.: (510) 642-3437; Fax: (510) 642-1655; Email: clairejohnson@berkeley.edu.

PEER 2015/14 *Seismic Evaluation and Retrofit of Existing Tall Buildings in California: Case Study of a 35-Story Steel Moment-Resisting Frame Building in San Francisco*. Jiun-Wei Lai, Shanshan Wang, Matthew J. Schoettler, and Stephen A. Mahin. December 2015.

PEER 2015/13 *Self-Centering Precast Concrete Dual-Steel-Shell Columns for Accelerated Bridge Construction: Seismic Performance, Analysis, and Design*. Gabriele Guerrini, José I. Restrepo, Athanassios Vervelidis, and Milena Massari. December 2015.

PEER 2015/12 *Shear-Flexure Interaction Modeling for Reinforced Concrete Structural Walls and Columns under Reversed Cyclic Loading*. Kristijan Kolozvari, Kutay Orakcal, and John Wallace. December 2015.

PEER 2015/11 *Selection and Scaling of Ground Motions for Nonlinear Response History Analysis of Buildings in Performance-Based Earthquake Engineering*. N. Simon Kwong and Anil K. Chopra. December 2015.

PEER 2015/10 *Structural Behavior of Column-Bent Cap Beam-Box Girder Systems in Reinforced Concrete Bridges Subjected to Gravity and Seismic Loads. Part II: Hybrid Simulation and Post-Test Analysis*. Mohamed A. Moustafa and Khalid M. Mosalam. November 2015.

PEER 2015/09 *Structural Behavior of Column-Bent Cap Beam-Box Girder Systems in Reinforced Concrete Bridges Subjected to Gravity and Seismic Loads. Part I: Pre-Test Analysis and Quasi-Static Experiments*. Mohamed A. Moustafa and Khalid M. Mosalam. September 2015.

PEER 2015/08 *NGA-East: Adjustments to Median Ground-Motion Models for Center and Eastern North America*. August 2015.

PEER 2015/07 *NGA-East: Ground-Motion Standard-Deviation Models for Central and Eastern North America*. Linda Al Atik. June 2015.

PEER 2015/06 *Adjusting Ground-Motion Intensity Measures to a Reference Site for which V_{S30} = 3000 m/sec*. David M. Boore. May 2015.

PEER 2015/05 *Hybrid Simulation of Seismic Isolation Systems Applied to an APR-1400 Nuclear Power Plant.* Andreas H. Schellenberg, Alireza Sarebanha, Matthew J. Schoettler, Gilberto Mosqueda, Gianmario Benzoni, and Stephen A. Mahin. April 2015.

PEER 2015/04 *NGA-East: Median Ground-Motion Models for the Central and Eastern North America Region*. April 2015.

PEER 2015/03 *Single Series Solution for the Rectangular Fiber-Reinforced Elastomeric Isolator Compression Modulus*. James M. Kelly and Niel C. Van Engelen. March 2015.

PEER 2015/02 *A Full-Scale, Single-Column Bridge Bent Tested by Shake-Table Excitation.* Matthew J. Schoettler, José I. Restrepo, Gabriele Guerrini, David E. Duck, and Francesco Carrea. March 2015.

PEER 2015/01 *Concrete Column Blind Prediction Contest 2010: Outcomes and Observations.* Vesna Terzic, Matthew J. Schoettler, José I. Restrepo, and Stephen A Mahin. March 2015.

PEER 2014/20 *Stochastic Modeling and Simulation of Near-Fault Ground Motions for Performance-Based Earthquake Engineering*. Mayssa Dabaghi and Armen Der Kiureghian. December 2014.

PEER 2014/19 *Seismic Response of a Hybrid Fiber-Reinforced Concrete Bridge Column Detailed for Accelerated Bridge Construction*. Wilson Nguyen, William Trono, Marios Panagiotou, and Claudia P. Ostertag. December 2014.

PEER 2014/18 *Three-Dimensional Beam-Truss Model for Reinforced Concrete Walls and Slabs Subjected to Cyclic Static or Dynamic Loading*. Yuan Lu, Marios Panagiotou, and Ioannis Koutromanos. December 2014.

PEER 2014/17 *PEER NGA-East Database*. Christine A. Goulet, Tadahiro Kishida, Timothy D. Ancheta, Chris H. Cramer, Robert B. Darragh, Walter J. Silva, Youssef M.A. Hashash, Joseph Harmon, Jonathan P. Stewart, Katie E. Wooddell, and Robert R. Youngs. October 2014.

PEER 2014/16 *Guidelines for Performing Hazard-Consistent One-Dimensional Ground Response Analysis for Ground Motion Prediction*. Jonathan P. Stewart, Kioumars Afshari, and Youssef M.A. Hashash. October 2014.

PEER 2014/15 *NGA-East Regionalization Report: Comparison of Four Crustal Regions within Central and Eastern North America using Waveform Modeling and 5%-Damped Pseudo-Spectral Acceleration Response*. Jennifer Dreiling, Marius P. Isken, Walter D. Mooney, Martin C. Chapman, and Richard W. Godbee. October 2014.

PEER 2014/14 *Scaling Relations between Seismic Moment and Rupture Area of Earthquakes in Stable Continental Regions*. Paul Somerville. August 2014.

PEER 2014/13 *PEER Preliminary Notes and Observations on the August 24, 2014, South Napa Earthquake*. Grace S. Kang and Stephen A. Mahin, Editors. September 2014.

PEER 2014/12 *Reference-Rock Site Conditions for Central and Eastern North America: Part II – Attenuation (Kappa) Definition*. Kenneth W. Campbell, Youssef M.A. Hashash, Byungmin Kim, Albert R. Kottke, Ellen M. Rathje, Walter J. Silva, and Jonathan P. Stewart. August 2014.

PEER 2014/11 *Reference-Rock Site Conditions for Central and Eastern North America: Part I - Velocity Definition*. Youssef M.A. Hashash, Albert R. Kottke, Jonathan P. Stewart, Kenneth W. Campbell, Byungmin Kim, Ellen M. Rathje, Walter J. Silva, Sissy Nikolaou, and Cheryl Moss. August 2014.

PEER 2014/10 *Evaluation of Collapse and Non-Collapse of Parallel Bridges Affected by Liquefaction and Lateral Spreading*. Benjamin Turner, Scott J. Brandenberg, and Jonathan P. Stewart. August 2014.

PEER 2014/09 *PEER Arizona Strong-Motion Database and GMPEs Evaluation*. Tadahiro Kishida, Robert E. Kayen, Olga-Joan Ktenidou, Walter J. Silva, Robert B. Darragh, and Jennie Watson-Lamprey. June 2014.

PEER 2014/08 *Unbonded Pretensioned Bridge Columns with Rocking Detail*. Jeffrey A. Schaefer, Bryan Kennedy, Marc O. Eberhard, and John F. Stanton. June 2014.

PEER 2014/07 *Northridge 20 Symposium Summary Report: Impacts, Outcomes, and Next Steps*. May 2014.

PEER 2014/06 *Report of the Tenth Planning Meeting of NEES/E-Defense Collaborative Research on Earthquake Engineering*. December 2013.

PEER 2014/05 *Seismic Velocity Site Characterization of Thirty-One Chilean Seismometer Stations by Spectral Analysis of Surface Wave Dispersion*. Robert Kayen, Brad D. Carkin, Skye Corbet, Camilo Pinilla, Allan Ng, Edward Gorbis, and Christine Truong. April 2014.

PEER 2014/04 Effect of Vertical Acceleration on Shear Strength of Reinforced Concrete Columns. Hyerin Lee and Khalid M. Mosalam. April 2014.

PEER 2014/03 *Retest of Thirty-Year-Old Neoprene Isolation Bearings.* James M. Kelly and Niel C. Van Engelen. March 2014.

PEER 2014/02 *Theoretical Development of Hybrid Simulation Applied to Plate Structures.* Ahmed A. Bakhaty, Khalid M. Mosalam, and Sanjay Govindjee. January 2014.

PEER 2014/01 *Performance-Based Seismic Assessment of Skewed Bridges.* Peyman Kaviani, Farzin Zareian, and Ertugrul Taciroglu. January 2014.

PEER 2013/26 *Urban Earthquake Engineerin*g. Proceedings of the U.S.-Iran Seismic Workshop. December 2013.

PEER 2013/25 *Earthquake Engineering for Resilient Communities: 2013 PEER Internship Program Research Report Collection.* Heidi Tremayne (Editor), Stephen A. Mahin (Editor), Jorge Archbold Monterossa, Matt Brosman, Shelly Dean, Katherine deLaveaga, Curtis Fong, Donovan Holder, Rakeeb Khan, Elizabeth Jachens, David Lam, Daniela Martinez Lopez, Mara Minner, Geffen Oren, Julia Pavicic, Melissa Quinonez, Lorena Rodriguez, Sean Salazar, Kelli Slaven, Vivian Steyert, Jenny Taing, and Salvador Tena. December 2013.

PEER 2013/24 *NGA-West2 Ground Motion Prediction Equations for Vertical Ground Motions*. September 2013.

PEER 2013/23 *Coordinated Planning and Preparedness for Fire Following Major Earthquakes*. Charles Scawthorn. November 2013.

PEER 2013/22 *GEM-PEER Task 3 Project: Selection of a Global Set of Ground Motion Prediction Equations.* Jonathan P. Stewart, John Douglas, Mohammad B. Javanbarg, Carola Di Alessandro, Yousef Bozorgnia, Norman A. Abrahamson, David M. Boore, Kenneth W. Campbell, Elise Delavaud, Mustafa Erdik, and Peter J. Stafford. December 2013.

PEER 2013/21 *Seismic Design and Performance of Bridges with Columns on Rocking Foundations*. Grigorios Antonellis and Marios Panagiotou. September 2013.

PEER 2013/20 *Experimental and Analytical Studies on the Seismic Behavior of Conventional and Hybrid Braced Frames*. Jiun-Wei Lai and Stephen A. Mahin. September 2013.

PEER 2013/19 *Toward Resilient Communities: A Performance-Based Engineering Framework for Design and Evaluation of the Built Environment.* Michael William Mieler, Bozidar Stojadinovic, Robert J. Budnitz, Stephen A. Mahin, and Mary C. Comerio. September 2013.

PEER 2013/18 *Identification of Site Parameters that Improve Predictions of Site Amplification*. Ellen M. Rathje and Sara Navidi. July 2013.

PEER 2013/17 *Response Spectrum Analysis of Concrete Gravity Dams Including Dam-Water-Foundation Interaction*. Arnkjell Løkke and Anil K. Chopra. July 2013.

PEER 2013/16 *Effect of Hoop Reinforcement Spacing on the Cyclic Response of Large Reinforced Concrete Special Moment Frame Beams.* Marios Panagiotou, Tea Visnjic, Grigorios Antonellis, Panagiotis Galanis, and Jack P. Moehle. June 2013.

PEER 2013/15 *A Probabilistic Framework to Include the Effects of Near-Fault Directivity in Seismic Hazard Assessment*. Shrey Kumar Shahi, Jack W. Baker. October 2013.

PEER 2013/14 *Hanging-Wall Scaling using Finite-Fault Simulations.* Jennifer L. Donahue and Norman A. Abrahamson. September 2013.

PEER 2013/13 *Semi-Empirical Nonlinear Site Amplification and its Application in NEHRP Site Factors*. Jonathan P. Stewart and Emel Seyhan. November 2013.

PEER 2013/12 *Nonlinear Horizontal Site Response for the NGA-West2 Project.* Ronnie Kamai, Norman A. Abramson, Walter J. Silva. May 2013.

PEER 2013/11 *Epistemic Uncertainty for NGA-West2 Models.* Linda Al Atik and Robert R. Youngs. May 2013.

PEER 2013/10 *NGA-West 2 Models for Ground-Motion Directionality.* Shrey K. Shahi and Jack W. Baker. May 2013.

PEER 2013/09 *Final Report of the NGA-West2 Directivity Working Group.* Paul Spudich, Jeffrey R. Bayless, Jack W. Baker, Brian S.J. Chiou, Badie Rowshandel, Shrey Shahi, and Paul Somerville. May 2013.

PEER 2013/08 *NGA-West2 Model for Estimating Average Horizontal Values of Pseudo-Absolute Spectral Accelerations Generated by Crustal Earthquakes*. I. M. Idriss. May 2013.

PEER 2013/07 *Update of the Chiou and Youngs NGA Ground Motion Model for Average Horizontal Component of Peak Ground Motion and Response Spectra*. Brian Chiou and Robert Youngs. May 2013.

PEER 2013/06 *NGA-West2 Campbell-Bozorgnia Ground Motion Model for the Horizontal Components of PGA, PGV, and 5%-Damped Elastic Pseudo-Acceleration Response Spectra for Periods Ranging from 0.01 to 10 sec.* Kenneth W. Campbell and Yousef Bozorgnia. May 2013.

PEER 2013/05 *NGA-West 2 Equations for Predicting Response Spectral Accelerations for Shallow Crustal Earthquakes*. David M. Boore, Jonathan P. Stewart, Emel Seyhan, and Gail M. Atkinson. May 2013.

PEER 2013/04 *Update of the AS08 Ground-Motion Prediction Equations Based on the NGA-West2 Data Set*. Norman Abrahamson, Walter Silva, and Ronnie Kamai. May 2013.

PEER 2013/03 *PEER NGA-West2 Database.* Timothy D. Ancheta, Robert B. Darragh, Jonathan P. Stewart, Emel Seyhan, Walter J. Silva, Brian S.J. Chiou, Katie E. Wooddell, Robert W. Graves, Albert R. Kottke, David M. Boore, Tadahiro Kishida, and Jennifer L. Donahue. May 2013.

PEER 2013/02 *Hybrid Simulation of the Seismic Response of Squat Reinforced Concrete Shear Walls*. Catherine A. Whyte and Bozidar Stojadinovic. May 2013.

PEER 2013/01 *Housing Recovery in Chile: A Qualitative Mid-program Review*. Mary C. Comerio. February 2013.

PEER 2012/08 *Guidelines for Estimation of Shear Wave Velocity.* Bernard R. Wair, Jason T. DeJong, and Thomas Shantz. December 2012.

PEER 2012/07 *Earthquake Engineering for Resilient Communities: 2012 PEER Internship Program Research Report Collection.* Heidi Tremayne (Editor), Stephen A. Mahin (Editor), Collin Anderson, Dustin Cook, Michael Erceg, Carlos Esparza, Jose Jimenez, Dorian Krausz, Andrew Lo, Stephanie Lopez, Nicole McCurdy, Paul Shipman, Alexander Strum, Eduardo Vega. December 2012.

PEER 2012/06 *Fragilities for Precarious Rocks at Yucca Mountain.* Matthew D. Purvance, Rasool Anooshehpoor, and James N. Brune. December 2012.

PEER 2012/05 *Development of Simplified Analysis Procedure for Piles in Laterally Spreading Layered Soils.* Christopher R. McGann, Pedro Arduino, and Peter Mackenzie–Helnwein. December 2012.

PEER 2012/04 *Unbonded Pre-Tensioned Columns for Bridges in Seismic Regions.* Phillip M. Davis, Todd M. Janes, Marc O. Eberhard, and John F. Stanton. December 2012.

PEER 2012/03 *Experimental and Analytical Studies on Reinforced Concrete Buildings with Seismically Vulnerable Beam-Column Joints*. Sangjoon Park and Khalid M. Mosalam. October 2012.

PEER 2012/02 *Seismic Performance of Reinforced Concrete Bridges Allowed to Uplift during Multi-Directional Excitation*. Andres Oscar Espinoza and Stephen A. Mahin. July 2012.

PEER 2012/01 *Spectral Damping Scaling Factors for Shallow Crustal Earthquakes in Active Tectonic Regions.* Sanaz Rezaeian, Yousef Bozorgnia, I. M. Idriss, Kenneth Campbell, Norman Abrahamson, and Walter Silva. July 2012.

PEER 2011/10 *Earthquake Engineering for Resilient Communities: 2011 PEER Internship Program Research Report Collection*. Heidi Faison and Stephen A. Mahin, Editors. December 2011.

PEER 2011/09 *Calibration of Semi-Stochastic Procedure for Simulating High-Frequency Ground Motions*. Jonathan P. Stewart, Emel Seyhan, and Robert W. Graves. December 2011.

PEER 2011/08 *Water Supply in regard to Fire Following Earthquake*. Charles Scawthorn. November 2011.

PEER 2011/07 *Seismic Risk Management in Urban Areas*. Proceedings of a U.S.-Iran-Turkey Seismic Workshop. September 2011.

PEER 2011/06 *The Use of Base Isolation Systems to Achieve Complex Seismic Performance Objectives*. Troy A. Morgan and Stephen A. Mahin. July 2011.

PEER 2011/05 *Case Studies of the Seismic Performance of Tall Buildings Designed by Alternative Means.* Task 12 Report for the Tall Buildings Initiative. Jack Moehle, Yousef Bozorgnia, Nirmal Jayaram, Pierson Jones, Mohsen Rahnama, Nilesh Shome, Zeynep Tuna, John Wallace, Tony Yang, and Farzin Zareian. July 2011.

PEER 2011/04 *Recommended Design Practice for Pile Foundations in Laterally Spreading Ground.* Scott A. Ashford, Ross W. Boulanger, and Scott J. Brandenberg. June 2011.

PEER 2011/03 *New Ground Motion Selection Procedures and Selected Motions for the PEER Transportation Research Program*. Jack W. Baker, Ting Lin, Shrey K. Shahi, and Nirmal Jayaram. March 2011.

PEER 2011/02 *A Bayesian Network Methodology for Infrastructure Seismic Risk Assessment and Decision Support*. Michelle T. Bensi, Armen Der Kiureghian, and Daniel Straub. March 2011.

PEER 2011/01 *Demand Fragility Surfaces for Bridges in Liquefied and Laterally Spreading Ground.* Scott J. Brandenberg, Jian Zhang, Pirooz Kashighandi, Yili Huo, and Minxing Zhao. March 2011.

PEER 2010/05 *Guidelines for Performance-Based Seismic Design of Tall Buildings.* Developed by the Tall Buildings Initiative. November 2010.

PEER 2010/04 *Application Guide for the Design of Flexible and Rigid Bus Connections between Substation Equipment Subjected to Earthquakes.* Jean-Bernard Dastous and Armen Der Kiureghian. September 2010.

PEER 2010/03 *Shear Wave Velocity as a Statistical Function of Standard Penetration Test Resistance and Vertical Effective Stress at Caltrans Bridge Sites.* Scott J. Brandenberg, Naresh Bellana, and Thomas Shantz. June 2010.

PEER 2010/02 *Stochastic Modeling and Simulation of Ground Motions for Performance-Based Earthquake Engineering.* Sanaz Rezaeian and Armen Der Kiureghian. June 2010.

PEER 2010/01 *Structural Response and Cost Characterization of Bridge Construction Using Seismic Performance Enhancement Strategies.* Ady Aviram, Božidar Stojadinović, Gustavo J. Parra-Montesinos, and Kevin R. Mackie. March 2010.

PEER 2009/03 *The Integration of Experimental and Simulation Data in the Study of Reinforced Concrete Bridge Systems Including Soil-Foundation-Structure Interaction.* Matthew Dryden and Gregory L. Fenves. November 2009.

PEER 2009/02 *Improving Earthquake Mitigation through Innovations and Applications in Seismic Science, Engineering, Communication, and Response*. Proceedings of a U.S.-Iran Seismic Workshop. October 2009.

PEER 2009/01 *Evaluation of Ground Motion Selection and Modification Methods: Predicting Median Interstory Drift Response of Buildings*. Curt B. Haselton, Editor. June 2009.

PEER 2008/10 *Technical Manual for Strata.* Albert R. Kottke and Ellen M. Rathje. February 2009.

PEER 2008/09 *NGA Model for Average Horizontal Component of Peak Ground Motion and Response Spectra.* Brian S.-J. Chiou and Robert R. Youngs. November 2008.

PEER 2008/08 *Toward Earthquake-Resistant Design of Concentrically Braced Steel Structures*. Patxi Uriz and Stephen A. Mahin. November 2008.

PEER 2008/07 *Using OpenSees for Performance-Based Evaluation of Bridges on Liquefiable Soils*. Stephen L. Kramer, Pedro Arduino, and HyungSuk Shin. November 2008.

PEER 2008/06 *Shaking Table Tests and Numerical Investigation of Self-Centering Reinforced Concrete Bridge Columns*. Hyung IL Jeong, Junichi Sakai, and Stephen A. Mahin. September 2008.

PEER 2008/05 *Performance-Based Earthquake Engineering Design Evaluation Procedure for Bridge Foundations Undergoing Liquefaction-Induced Lateral Ground Displacement*. Christian A. Ledezma and Jonathan D. Bray. August 2008.

PEER 2008/04 *Benchmarking of Nonlinear Geotechnical Ground Response Analysis Procedures.* Jonathan P. Stewart, Annie On-Lei Kwok, Yousseff M. A. Hashash, Neven Matasovic, Robert Pyke, Zhiliang Wang, and Zhaohui Yang. August 2008.

PEER 2008/03 *Guidelines for Nonlinear Analysis of Bridge Structures in California.* Ady Aviram, Kevin R. Mackie, and Božidar Stojadinović. August 2008.

PEER 2008/02 *Treatment of Uncertainties in Seismic-Risk Analysis of Transportation Systems*. Evangelos Stergiou and Anne S. Kiremidjian. July 2008.

PEER 2008/01 *Seismic Performance Objectives for Tall Buildings.* William T. Holmes, Charles Kircher, William Petak, and Nabih Youssef. August 2008.

PEER 2007/12 *An Assessment to Benchmark the Seismic Performance of a Code-Conforming Reinforced Concrete Moment-Frame Building.* Curt Haselton, Christine A. Goulet, Judith Mitrani-Reiser, James L. Beck, Gregory G. Deierlein, Keith A. Porter, Jonathan P. Stewart, and Ertugrul Taciroglu. August 2008.

PEER 2007/11 *Bar Buckling in Reinforced Concrete Bridge Columns.* Wayne A. Brown, Dawn E. Lehman, and John F. Stanton. February 2008.

PEER 2007/10 *Computational Modeling of Progressive Collapse in Reinforced Concrete Frame Structures*. Mohamed M. Talaat and Khalid M. Mosalam. May 2008.

PEER 2007/09 *Integrated Probabilistic Performance-Based Evaluation of Benchmark Reinforced Concrete Bridges*. Kevin R. Mackie, John-Michael Wong, and Božidar Stojadinović. January 2008.

PEER 2007/08 *Assessing Seismic Collapse Safety of Modern Reinforced Concrete Moment-Frame Buildings*. Curt B. Haselton and Gregory G. Deierlein. February 2008.

PEER 2007/07 *Performance Modeling Strategies for Modern Reinforced Concrete Bridge Columns*. Michael P. Berry and Marc O. Eberhard. April 2008.

PEER 2007/06 *Development of Improved Procedures for Seismic Design of Buried and Partially Buried Structures*. Linda Al Atik and Nicholas Sitar. June 2007.

PEER 2007/05 *Uncertainty and Correlation in Seismic Risk Assessment of Transportation Systems*. Renee G. Lee and Anne S. Kiremidjian. July 2007.

PEER 2007/04 *Numerical Models for Analysis and Performance-Based Design of Shallow Foundations Subjected to Seismic Loading.* Sivapalan Gajan, Tara C. Hutchinson, Bruce L. Kutter, Prishati Raychowdhury, José A. Ugalde, and Jonathan P. Stewart. May 2008.

PEER 2007/03 *Beam-Column Element Model Calibrated for Predicting Flexural Response Leading to Global Collapse of RC Frame Buildings*. Curt B. Haselton, Abbie B. Liel, Sarah Taylor Lange, and Gregory G. Deierlein. May 2008.

PEER 2007/02 *Campbell-Bozorgnia NGA Ground Motion Relations for the Geometric Mean Horizontal Component of Peak and Spectral Ground Motion Parameters*. Kenneth W. Campbell and Yousef Bozorgnia. May 2007.

PEER 2007/01 *Boore-Atkinson NGA Ground Motion Relations for the Geometric Mean Horizontal Component of Peak and Spectral Ground Motion Parameters*. David M. Boore and Gail M. Atkinson. May 2007.

PEER 2006/12 Societal Implications of Performance-Based Earthquake Engineering. Peter J. May. May 2007.

PEER 2006/11 *Probabilistic Seismic Demand Analysis Using Advanced Ground Motion Intensity Measures, Attenuation Relationships, and Near-Fault Effects*. Polsak Tothong and C. Allin Cornell. March 2007.

PEER 2006/10 *Application of the PEER PBEE Methodology to the I-880 Viaduct*. Sashi Kunnath. February 2007.

PEER 2006/09 *Quantifying Economic Losses from Travel Forgone Following a Large Metropolitan Earthquake*. James Moore, Sungbin Cho, Yue Yue Fan, and Stuart Werner. November 2006.

PEER 2006/08 *Vector-Valued Ground Motion Intensity Measures for Probabilistic Seismic Demand Analysis*. Jack W. Baker and C. Allin Cornell. October 2006.

PEER 2006/07 *Analytical Modeling of Reinforced Concrete Walls for Predicting Flexural and Coupled–Shear-Flexural Responses*. Kutay Orakcal, Leonardo M. Massone, and John W. Wallace. October 2006.

PEER 2006/06 *Nonlinear Analysis of a Soil-Drilled Pier System under Static and Dynamic Axial Loading*. Gang Wang and Nicholas Sitar. November 2006.

PEER 2006/05 *Advanced Seismic Assessment Guidelines.* Paolo Bazzurro, C. Allin Cornell, Charles Menun, Maziar Motahari, and Nicolas Luco. September 2006.

PEER 2006/04 *Probabilistic Seismic Evaluation of Reinforced Concrete Structural Components and Systems*. Tae Hyung Lee and Khalid M. Mosalam. August 2006.

PEER 2006/03 *Performance of Lifelines Subjected to Lateral Spreading*. Scott A. Ashford and Teerawut Juirnarongrit. July 2006.

PEER 2006/02 *Pacific Earthquake Engineering Research Center Highway Demonstration Project.* Anne Kiremidjian, James Moore, Yue Yue Fan, Nesrin Basoz, Ozgur Yazali, and Meredith Williams. April 2006.

PEER 2006/01 *Bracing Berkeley. A Guide to Seismic Safety on the UC Berkeley Campus.* Mary C. Comerio, Stephen Tobriner, and Ariane Fehrenkamp. January 2006.

PEER 2005/16 *Seismic Response and Reliability of Electrical Substation Equipment and Systems.* Junho Song, Armen Der Kiureghian, and Jerome L. Sackman. April 2006.

PEER 2005/15 *CPT-Based Probabilistic Assessment of Seismic Soil Liquefaction Initiation.* R. E. S. Moss, R. B. Seed, R. E. Kayen, J. P. Stewart, and A. Der Kiureghian. April 2006.

PEER 2005/14 *Workshop on Modeling of Nonlinear Cyclic Load-Deformation Behavior of Shallow Foundations.* Bruce L. Kutter, Geoffrey Martin, Tara Hutchinson, Chad Harden, Sivapalan Gajan, and Justin Phalen. March 2006.

PEER 2005/13 *Stochastic Characterization and Decision Bases under Time-Dependent Aftershock Risk in Performance-Based Earthquake Engineering*. Gee Liek Yeo and C. Allin Cornell. July 2005.

PEER 2005/12 *PEER Testbed Study on a Laboratory Building: Exercising Seismic Performance Assessment.* Mary C. Comerio, Editor. November 2005.

PEER 2005/11 *Van Nuys Hotel Building Testbed Report: Exercising Seismic Performance Assessment.* Helmut Krawinkler, Editor. October 2005.

PEER 2005/10 *First NEES/E-Defense Workshop on Collapse Simulation of Reinforced Concrete Building Structures.* September 2005.

PEER 2005/09 *Test Applications of Advanced Seismic Assessment Guidelines.* Joe Maffei, Karl Telleen, Danya Mohr, William Holmes, and Yuki Nakayama. August 2006.

PEER 2005/08 *Damage Accumulation in Lightly Confined Reinforced Concrete Bridge Columns.* R. Tyler Ranf, Jared M. Nelson, Zach Price, Marc O. Eberhard, and John F. Stanton. April 2006.

PEER 2005/07 *Experimental and Analytical Studies on the Seismic Response of Freestanding and Anchored Laboratory Equipment.* Dimitrios Konstantinidis and Nicos Makris. January 2005.

PEER 2005/06 *Global Collapse of Frame Structures under Seismic Excitations*. Luis F. Ibarra and Helmut Krawinkler. September 2005.

PEER 2005//05 *Performance Characterization of Bench- and Shelf-Mounted Equipment.* Samit Ray Chaudhuri and Tara C. Hutchinson. May 2006.

PEER 2005/04 *Numerical Modeling of the Nonlinear Cyclic Response of Shallow Foundations.* Chad Harden, Tara Hutchinson, Geoffrey R. Martin, and Bruce L. Kutter. August 2005.

PEER 2005/03 *A Taxonomy of Building Components for Performance-Based Earthquake Engineering.* Keith A. Porter. September 2005.

PEER 2005/02 *Fragility Basis for California Highway Overpass Bridge Seismic Decision Making*. Kevin R. Mackie and Božidar Stojadinović. June 2005.

PEER 2005/01 *Empirical Characterization of Site Conditions on Strong Ground Motion.* Jonathan P. Stewart, Yoojoong Choi, and Robert W. Graves. June 2005.

PEER 2004/09 *Electrical Substation Equipment Interaction: Experimental Rigid Conductor Studies.* Christopher Stearns and André Filiatrault. February 2005.

PEER 2004/08 *Seismic Qualification and Fragility Testing of Line Break 550-kV Disconnect Switches.* Shakhzod M. Takhirov, Gregory L. Fenves, and Eric Fujisaki. January 2005.

PEER 2004/07 *Ground Motions for Earthquake Simulator Qualification of Electrical Substation Equipment.* Shakhzod M. Takhirov, Gregory L. Fenves, Eric Fujisaki, and Don Clyde. January 2005.

PEER 2004/06 *Performance-Based Regulation and Regulatory Regimes.* Peter J. May and Chris Koski. September 2004.

PEER 2004/05 *Performance-Based Seismic Design Concepts and Implementation: Proceedings of an International Workshop.* Peter Fajfar and Helmut Krawinkler, Editors. September 2004.

PEER 2004/04 *Seismic Performance of an Instrumented Tilt-up Wall Building.* James C. Anderson and Vitelmo V. Bertero. July 2004.

PEER 2004/03 *Evaluation and Application of Concrete Tilt-up Assessment Methodologies.* Timothy Graf and James O. Malley. October 2004.

PEER 2004/02 *Analytical Investigations of New Methods for Reducing Residual Displacements of Reinforced Concrete Bridge Columns.* Junichi Sakai and Stephen A. Mahin. August 2004.

PEER 2004/01 *Seismic Performance of Masonry Buildings and Design Implications.* Kerri Anne Taeko Tokoro, James C. Anderson, and Vitelmo V. Bertero. February 2004.

PEER 2003/18 *Performance Models for Flexural Damage in Reinforced Concrete Columns.* Michael Berry and Marc Eberhard. August 2003.

PEER 2003/17 *Predicting Earthquake Damage in Older Reinforced Concrete Beam-Column Joints.* Catherine Pagni and Laura Lowes. October 2004.

PEER 2003/16 *Seismic Demands for Performance-Based Design of Bridges.* Kevin Mackie and Božidar Stojadinović. August 2003.

PEER 2003/15 *Seismic Demands for Nondeteriorating Frame Structures and Their Dependence on Ground Motions.* Ricardo Antonio Medina and Helmut Krawinkler. May 2004.

PEER 2003/14 *Finite Element Reliability and Sensitivity Methods for Performance-Based Earthquake Engineering*. Terje Haukaas and Armen Der Kiureghian. April 2004.

PEER 2003/13 *Effects of Connection Hysteretic Degradation on the Seismic Behavior of Steel Moment-Resisting Frames.* Janise E. Rodgers and Stephen A. Mahin. March 2004.

PEER 2003/12 *Implementation Manual for the Seismic Protection of Laboratory Contents: Format and Case Studies*. William T. Holmes and Mary C. Comerio. October 2003.

PEER 2003/11 *Fifth U.S.-Japan Workshop on Performance-Based Earthquake Engineering Methodology for Reinforced Concrete Building Structures*. February 2004.

PEER 2003/10 *A Beam-Column Joint Model for Simulating the Earthquake Response of Reinforced Concrete Frames.* Laura N. Lowes, Nilanjan Mitra, and Arash Altoontash. February 2004.

PEER 2003/09 *Sequencing Repairs after an Earthquake: An Economic Approach.* Marco Casari and Simon J. Wilkie. April 2004.

PEER 2003/08 *A Technical Framework for Probability-Based Demand and Capacity Factor Design (DCFD) Seismic Formats*. Fatemeh Jalayer and C. Allin Cornell. November 2003.

PEER 2003/07 *Uncertainty Specification and Propagation for Loss Estimation Using FOSM Methods.* Jack W. Baker and C. Allin Cornell. September 2003.

PEER 2003/06 *Performance of Circular Reinforced Concrete Bridge Columns under Bidirectional Earthquake Loading*. Mahmoud M. Hachem, Stephen A. Mahin, and Jack P. Moehle. February 2003.

PEER 2003/05 *Response Assessment for Building-Specific Loss Estimation.* Eduardo Miranda and Shahram Taghavi. September 2003.

PEER 2003/04 *Experimental Assessment of Columns with Short Lap Splices Subjected to Cyclic Loads*. Murat Melek, John W. Wallace, and Joel Conte. April 2003.

PEER 2003/03 *Probabilistic Response Assessment for Building-Specific Loss Estimation*. Eduardo Miranda and Hesameddin Aslani. September 2003.

PEER 2003/02 *Software Framework for Collaborative Development of Nonlinear Dynamic Analysis Program*. Jun Peng and Kincho H. Law. September 2003.

PEER 2003/01 *Shake Table Tests and Analytical Studies on the Gravity Load Collapse of Reinforced Concrete Frames.* Kenneth John Elwood and Jack P. Moehle. November 2003.

PEER 2002/24 *Performance of Beam to Column Bridge Joints Subjected to a Large Velocity Pulse.* Natalie Gibson, André Filiatrault, and Scott A. Ashford. April 2002.

PEER 2002/23 *Effects of Large Velocity Pulses on Reinforced Concrete Bridge Columns.* Greg L. Orozco and Scott A. Ashford. April 2002.

PEER 2002/22 *Characterization of Large Velocity Pulses for Laboratory Testing.* Kenneth E. Cox and Scott A. Ashford. April 2002.

PEER 2002/21 *Fourth U.S.-Japan Workshop on Performance-Based Earthquake Engineering Methodology for Reinforced Concrete Building Structures*. December 2002.

PEER 2002/20 *Barriers to Adoption and Implementation of PBEE Innovations.* Peter J. May. August 2002.

PEER 2002/19 *Economic-Engineered Integrated Models for Earthquakes: Socioeconomic Impacts.* Peter Gordon, James E. Moore II, and Harry W. Richardson. July 2002.

PEER 2002/18 *Assessment of Reinforced Concrete Building Exterior Joints with Substandard Details.* Chris P. Pantelides, Jon Hansen, Justin Nadauld, and Lawrence D. Reaveley. May 2002.

PEER 2002/17 *Structural Characterization and Seismic Response Analysis of a Highway Overcrossing Equipped with Elastomeric Bearings and Fluid Dampers: A Case Study*. Nicos Makris and Jian Zhang. November 2002.

PEER 2002/16 *Estimation of Uncertainty in Geotechnical Properties for Performance-Based Earthquake Engineering*. Allen L. Jones, Steven L. Kramer, and Pedro Arduino. December 2002.

PEER 2002/15 *Seismic Behavior of Bridge Columns Subjected to Various Loading Patterns*. Asadollah Esmaeily-Gh. and Yan Xiao. December 2002.

PEER 2002/14 *Inelastic Seismic Response of Extended Pile Shaft Supported Bridge Structures.* T.C. Hutchinson, R.W. Boulanger, Y.H. Chai, and I.M. Idriss. December 2002.

PEER 2002/13 *Probabilistic Models and Fragility Estimates for Bridge Components and Systems.* Paolo Gardoni, Armen Der Kiureghian, and Khalid M. Mosalam. June 2002.

PEER 2002/12 *Effects of Fault Dip and Slip Rake on Near-Source Ground Motions: Why Chi-Chi Was a Relatively Mild M7.6 Earthquake*. Brad T. Aagaard, John F. Hall, and Thomas H. Heaton. December 2002.

PEER 2002/11 *Analytical and Experimental Study of Fiber-Reinforced Strip Isolators*. James M. Kelly and Shakhzod M. Takhirov. September 2002.

PEER 2002/10 *Centrifuge Modeling of Settlement and Lateral Spreading with Comparisons to Numerical Analyses***.** Sivapalan Gajan and Bruce L. Kutter. January 2003.

PEER 2002/09 *Documentation and Analysis of Field Case Histories of Seismic Compression during the 1994 Northridge, California, Earthquake*. Jonathan P. Stewart, Patrick M. Smith, Daniel H. Whang, and Jonathan D. Bray. October 2002.

PEER 2002/08 *Component Testing, Stability Analysis and Characterization of Buckling-Restrained Unbonded Braces™*. Cameron Black, Nicos Makris, and Ian Aiken. September 2002.

PEER 2002/07 *Seismic Performance of Pile-Wharf Connections.* Charles W. Roeder, Robert Graff, Jennifer Soderstrom, and Jun Han Yoo. December 2001.

PEER 2002/06 *The Use of Benefit-Cost Analysis for Evaluation of Performance-Based Earthquake Engineering Decisions*. Richard O. Zerbe and Anthony Falit-Baiamonte. September 2001.

PEER 2002/05 *Guidelines, Specifications, and Seismic Performance Characterization of Nonstructural Building Components and Equipment*. André Filiatrault, Constantin Christopoulos, and Christopher Stearns. September 2001.

PEER 2002/04 *Consortium of Organizations for Strong-Motion Observation Systems and the Pacific Earthquake Engineering Research Center Lifelines Program: Invited Workshop on Archiving and Web Dissemination of Geotechnical Data, 4–5 October 2001*. September 2002.

PEER 2002/03 *Investigation of Sensitivity of Building Loss Estimates to Major Uncertain Variables for the Van Nuys Testbed*. Keith A. Porter, James L. Beck, and Rustem V. Shaikhutdinov. August 2002.

PEER 2002/02 *The Third U.S.-Japan Workshop on Performance-Based Earthquake Engineering Methodology for Reinforced Concrete Building Structures*. July 2002.

PEER 2002/01 *Nonstructural Loss Estimation: The UC Berkeley Case Study.* Mary C. Comerio and John C. Stallmeyer. December 2001.

PEER 2001/16 *Statistics of SDF-System Estimate of Roof Displacement for Pushover Analysis of Buildings.* Anil K. Chopra, Rakesh K. Goel, and Chatpan Chintanapakdee. December 2001.

PEER 2001/15 *Damage to Bridges during the 2001 Nisqually Earthquake.* R. Tyler Ranf, Marc O. Eberhard, and Michael P. Berry. November 2001.

PEER 2001/14 *Rocking Response of Equipment Anchored to a Base Foundation.* Nicos Makris and Cameron J. Black. September 2001.

PEER 2001/13 *Modeling Soil Liquefaction Hazards for Performance-Based Earthquake Engineering*. Steven L. Kramer and Ahmed-W. Elgamal. February 2001.

PEER 2001/12 *Development of Geotechnical Capabilities in OpenSees*. Boris Jeremić. September 2001.

PEER 2001/11 *Analytical and Experimental Study of Fiber-Reinforced Elastomeric Isolators*. James M. Kelly and Shakhzod M. Takhirov. September 2001.

PEER 2001/10 *Amplification Factors for Spectral Acceleration in Active Regions.* Jonathan P. Stewart, Andrew H. Liu, Yoojoong Choi, and Mehmet B. Baturay. December 2001.

PEER 2001/09 *Ground Motion Evaluation Procedures for Performance-Based Design.* Jonathan P. Stewart, Shyh-Jeng Chiou, Jonathan D. Bray, Robert W. Graves, Paul G. Somerville, and Norman A. Abrahamson. September 2001.

PEER 2001/08 *Experimental and Computational Evaluation of Reinforced Concrete Bridge Beam-Column Connections for Seismic Performance*. Clay J. Naito, Jack P. Moehle, and Khalid M. Mosalam. November 2001.

PEER 2001/07 *The Rocking Spectrum and the Shortcomings of Design Guidelines.* Nicos Makris and Dimitrios Konstantinidis. August 2001.

PEER 2001/06 *Development of an Electrical Substation Equipment Performance Database for Evaluation of Equipment Fragilities.* Thalia Agnanos. April 1999.

PEER 2001/05 *Stiffness Analysis of Fiber-Reinforced Elastomeric Isolators.* Hsiang-Chuan Tsai and James M. Kelly. May 2001.

PEER 2001/04 *Organizational and Societal Considerations for Performance-Based Earthquake Engineering*. Peter J. May. April 2001.

PEER 2001/03 *A Modal Pushover Analysis Procedure to Estimate Seismic Demands for Buildings: Theory and Preliminary Evaluation*. Anil K. Chopra and Rakesh K. Goel. January 2001.

PEER 2001/02 *Seismic Response Analysis of Highway Overcrossings Including Soil-Structure Interaction*. Jian Zhang and Nicos Makris. March 2001.

PEER 2001/01 *Experimental Study of Large Seismic Steel Beam-to-Column Connections.* Egor P. Popov and Shakhzod M. Takhirov. November 2000.

PEER 2000/10 *The Second U.S.-Japan Workshop on Performance-Based Earthquake Engineering Methodology for Reinforced Concrete Building Structures*. March 2000.

PEER 2000/09 *Structural Engineering Reconnaissance of the August 17, 1999 Earthquake: Kocaeli (Izmit), Turkey*. Halil Sezen, Kenneth J. Elwood, Andrew S. Whittaker, Khalid Mosalam, John J. Wallace, and John F. Stanton. December 2000.

PEER 2000/08 *Behavior of Reinforced Concrete Bridge Columns Having Varying Aspect Ratios and Varying Lengths of Confinement*. Anthony J. Calderone, Dawn E. Lehman, and Jack P. Moehle. January 2001.

PEER 2000/07 *Cover-Plate and Flange-Plate Reinforced Steel Moment-Resisting Connections.* Taejin Kim, Andrew S. Whittaker, Amir S. Gilani, Vitelmo V. Bertero, and Shakhzod M. Takhirov. September 2000.

PEER 2000/06 *Seismic Evaluation and Analysis of 230-kV Disconnect Switches.* Amir S. J. Gilani, Andrew S. Whittaker, Gregory L. Fenves, Chun-Hao Chen, Henry Ho, and Eric Fujisaki. July 2000.

PEER 2000/05 *Performance-Based Evaluation of Exterior Reinforced Concrete Building Joints for Seismic Excitation*. Chandra Clyde, Chris P. Pantelides, and Lawrence D. Reaveley. July 2000.

PEER 2000/04 *An Evaluation of Seismic Energy Demand: An Attenuation Approach*. Chung-Che Chou and Chia-Ming Uang. July 1999.

PEER 2000/03 *Framing Earthquake Retrofitting Decisions: The Case of Hillside Homes in Los Angeles.* Detlof von Winterfeldt, Nels Roselund, and Alicia Kitsuse. March 2000.

PEER 2000/02 *U.S.-Japan Workshop on the Effects of Near-Field Earthquake Shaking*. Andrew Whittaker, Editor. July 2000.

PEER 2000/01 *Further Studies on Seismic Interaction in Interconnected Electrical Substation Equipment.* Armen Der Kiureghian, Kee-Jeung Hong, and Jerome L. Sackman. November 1999.

PEER 1999/14 *Seismic Evaluation and Retrofit of 230-kV Porcelain Transformer Bushings*. Amir S. Gilani, Andrew S. Whittaker, Gregory L. Fenves, and Eric Fujisaki. December 1999.

PEER 1999/13 *Building Vulnerability Studies: Modeling and Evaluation of Tilt-up and Steel Reinforced Concrete Buildings*. John W. Wallace, Jonathan P. Stewart, and Andrew S. Whittaker, Editors. December 1999.

PEER 1999/12 *Rehabilitation of Nonductile RC Frame Building Using Encasement Plates and Energy-Dissipating Devices*. Mehrdad Sasani, Vitelmo V. Bertero, James C. Anderson. December 1999.

PEER 1999/11 *Performance Evaluation Database for Concrete Bridge Components and Systems under Simulated Seismic Loads*. Yael D. Hose and Frieder Seible. November 1999.

PEER 1999/10 *U.S.-Japan Workshop on Performance-Based Earthquake Engineering Methodology for Reinforced Concrete Building Structures*. December 1999.

PEER 1999/09 *Performance Improvement of Long Period Building Structures Subjected to Severe Pulse-Type Ground Motions*. James C. Anderson, Vitelmo V. Bertero, and Raul Bertero. October 1999.

PEER 1999/08 *Envelopes for Seismic Response Vectors.* Charles Menun and Armen Der Kiureghian. July 1999.

PEER 1999/07 *Documentation of Strengths and Weaknesses of Current Computer Analysis Methods for Seismic Performance of Reinforced Concrete Members*. William F. Cofer. November 1999.

PEER 1999/06 *Rocking Response and Overturning of Anchored Equipment under Seismic Excitations*. Nicos Makris and Jian Zhang. November 1999.

PEER 1999/05 *Seismic Evaluation of 550 kV Porcelain Transformer Bushings.* Amir S. Gilani, Andrew S. Whittaker, Gregory L. Fenves, and Eric Fujisaki. October 1999.

PEER 1999/04 *Adoption and Enforcement of Earthquake Risk-Reduction Measures.* Peter J. May, Raymond J. Burby, T. Jens Feeley, and Robert Wood. August 1999.

PEER 1999/03 *Task 3 Characterization of Site Response General Site Categories*. Adrian Rodriguez-Marek, Jonathan D. Bray and Norman Abrahamson. February 1999.

PEER 1999/02 *Capacity-Demand-Diagram Methods for Estimating Seismic Deformation of Inelastic Structures: SDF Systems*. Anil K. Chopra and Rakesh Goel. April 1999.

PEER 1999/01 *Interaction in Interconnected Electrical Substation Equipment Subjected to Earthquake Ground Motions*. Armen Der Kiureghian, Jerome L. Sackman, and Kee-Jeung Hong. February 1999.

PEER 1998/08 *Behavior and Failure Analysis of a Multiple-Frame Highway Bridge in the 1994 Northridge Earthquake*. Gregory L. Fenves and Michael Ellery. December 1998.

PEER 1998/07 *Empirical Evaluation of Inertial Soil-Structure Interaction Effects.* Jonathan P. Stewart, Raymond B. Seed, and Gregory L. Fenves. November 1998.

PEER 1998/06 *Effect of Damping Mechanisms on the Response of Seismic Isolated Structures*. Nicos Makris and Shih-Po Chang. November 1998.

PEER 1998/05 *Rocking Response and Overturning of Equipment under Horizontal Pulse-Type Motions*. Nicos Makris and Yiannis Roussos. October 1998.

PEER 1998/04 *Pacific Earthquake Engineering Research Invitational Workshop Proceedings, May 14–15, 1998: Defining the Links between Planning, Policy Analysis, Economics and Earthquake Engineering*. Mary Comerio and Peter Gordon. September 1998.

PEER 1998/03 *Repair/Upgrade Procedures for Welded Beam to Column Connections*. James C. Anderson and Xiaojing Duan. May 1998.

PEER 1998/02 *Seismic Evaluation of 196 kV Porcelain Transformer Bushings.* Amir S. Gilani, Juan W. Chavez, Gregory L. Fenves, and Andrew S. Whittaker. May 1998.

PEER 1998/01 *Seismic Performance of Well-Confined Concrete Bridge Columns.* Dawn E. Lehman and Jack P. Moehle. December 2000.

ONLINE PEER REPORTS

The following PEER reports are available by Internet only at http://peer.berkeley.edu/publications/peer_reports_complete.html.

PEER 2012/103 *Performance-Based Seismic Demand Assessment of Concentrically Braced Steel Frame Buildings.* Chui-Hsin Chen and Stephen A. Mahin. December 2012.

PEER 2012/102 *Procedure to Restart an Interrupted Hybrid Simulation: Addendum to PEER Report 2010/103.* Vesna Terzic and Bozidar Stojadinovic. October 2012.

PEER 2012/101 *Mechanics of Fiber Reinforced Bearings.* James M. Kelly and Andrea Calabrese. February 2012.

PEER 2011/107 *Nonlinear Site Response and Seismic Compression at Vertical Array Strongly Shaken by 2007 Niigata-ken Chuetsu-oki Earthquake.* Eric Yee, Jonathan P. Stewart, and Kohji Tokimatsu. December 2011.

PEER 2011/106 *Self Compacting Hybrid Fiber Reinforced Concrete Composites for Bridge Columns.* Pardeep Kumar, Gabriel Jen, William Trono, Marios Panagiotou, and Claudia Ostertag. September 2011.

PEER 2011/105 *Stochastic Dynamic Analysis of Bridges Subjected to Spacially Varying Ground Motions.* Katerina Konakli and Armen Der Kiureghian. August 2011.

PEER 2011/104 *Design and Instrumentation of the 2010 E-Defense Four-Story Reinforced Concrete and Post-Tensioned Concrete Buildings.* Takuya Nagae, Kenichi Tahara, Taizo Matsumori, Hitoshi Shiohara, Toshimi Kabeyasawa, Susumu Kono, Minehiro Nishiyama (Japanese Research Team) and John Wallace, Wassim Ghannoum, Jack Moehle, Richard Sause, Wesley Keller, Zeynep Tuna (U.S. Research Team). June 2011.

PEER 2011/103 *In-Situ Monitoring of the Force Output of Fluid Dampers: Experimental Investigation.* Dimitrios Konstantinidis, James M. Kelly, and Nicos Makris. April 2011.

PEER 2011/102 *Ground-Motion Prediction Equations 1964–2010.* John Douglas. April 2011.

PEER 2011/101 *Report of the Eighth Planning Meeting of NEES/E-Defense Collaborative Research on Earthquake Engineering.* Convened by the Hyogo Earthquake Engineering Research Center (NIED), NEES Consortium, Inc. February 2011.

PEER 2010/111 *Modeling and Acceptance Criteria for Seismic Design and Analysis of Tall Buildings.* Task 7 Report for the Tall Buildings Initiative - Published jointly by the Applied Technology Council. October 2010.

PEER 2010/110 *Seismic Performance Assessment and Probabilistic Repair Cost Analysis of Precast Concrete Cladding Systems for Multistory Buildings.* Jeffrey P. Hunt and Božidar Stojadinovic. November 2010.

PEER 2010/109 *Report of the Seventh Joint Planning Meeting of NEES/E-Defense Collaboration on Earthquake Engineering. Held at the E-Defense, Miki, and Shin-Kobe, Japan, September 18–19, 2009.* August 2010.

PEER 2010/108 *Probabilistic Tsunami Hazard in California.* Hong Kie Thio, Paul Somerville, and Jascha Polet, preparers. October 2010.

PEER 2010/107 *Performance and Reliability of Exposed Column Base Plate Connections for Steel Moment-Resisting Frames.* Ady Aviram, Božidar Stojadinovic, and Armen Der Kiureghian. August 2010.

PEER 2010/106 *Verification of Probabilistic Seismic Hazard Analysis Computer Programs.* Patricia Thomas, Ivan Wong, and Norman Abrahamson. May 2010.

PEER 2010/105 *Structural Engineering Reconnaissance of the April 6, 2009, Abruzzo, Italy, Earthquake, and Lessons Learned.* M. Selim Günay and Khalid M. Mosalam. April 2010.

PEER 2010/104 *Simulating the Inelastic Seismic Behavior of Steel Braced Frames, Including the Effects of Low-Cycle Fatigue.* Yuli Huang and Stephen A. Mahin. April 2010.

PEER 2010/103 *Post-Earthquake Traffic Capacity of Modern Bridges in California.* Vesna Terzic and Božidar Stojadinović. March 2010.

PEER 2010/102 *Analysis of Cumulative Absolute Velocity (CAV) and JMA Instrumental Seismic Intensity (I_{JMA}) Using the PEER–NGA Strong Motion Database.* Kenneth W. Campbell and Yousef Bozorgnia. February 2010.

PEER 2010/101 *Rocking Response of Bridges on Shallow Foundations.* Jose A. Ugalde, Bruce L. Kutter, and Boris Jeremic. April 2010.

PEER 2009/109 *Simulation and Performance-Based Earthquake Engineering Assessment of Self-Centering Post-Tensioned Concrete Bridge Systems.* Won K. Lee and Sarah L. Billington. December 2009.

PEER 2009/108 *PEER Lifelines Geotechnical Virtual Data Center.* J. Carl Stepp, Daniel J. Ponti, Loren L. Turner, Jennifer N. Swift, Sean Devlin, Yang Zhu, Jean Benoit, and John Bobbitt. September 2009.

PEER 2009/107 *Experimental and Computational Evaluation of Current and Innovative In-Span Hinge Details in Reinforced Concrete Box-Girder Bridges: Part 2: Post-Test Analysis and Design Recommendations.* Matias A. Hube and Khalid M. Mosalam. December 2009.

PEER 2009/106 *Shear Strength Models of Exterior Beam-Column Joints without Transverse Reinforcement.* Sangjoon Park and Khalid M. Mosalam. November 2009.

PEER 2009/105 *Reduced Uncertainty of Ground Motion Prediction Equations through Bayesian Variance Analysis.* Robb Eric S. Moss. November 2009.

PEER 2009/104 *Advanced Implementation of Hybrid Simulation.* Andreas H. Schellenberg, Stephen A. Mahin, Gregory L. Fenves. November 2009.

PEER 2009/103 *Performance Evaluation of Innovative Steel Braced Frames.* T. Y. Yang, Jack P. Moehle, and Božidar Stojadinovic. August 2009.

PEER 2009/102 *Reinvestigation of Liquefaction and Nonliquefaction Case Histories from the 1976 Tangshan Earthquake.* Robb Eric Moss, Robert E. Kayen, Liyuan Tong, Songyu Liu, Guojun Cai, and Jiaer Wu. August 2009.

PEER 2009/101 *Report of the First Joint Planning Meeting for the Second Phase of NEES/E-Defense Collaborative Research on Earthquake Engineering.* Stephen A. Mahin et al. July 2009.

PEER 2008/104 *Experimental and Analytical Study of the Seismic Performance of Retaining Structures.* Linda Al Atik and Nicholas Sitar. January 2009.

PEER 2008/103 *Experimental and Computational Evaluation of Current and Innovative In-Span Hinge Details in Reinforced Concrete Box-Girder Bridges. Part 1: Experimental Findings and Pre-Test Analysis.* Matias A. Hube and Khalid M. Mosalam. January 2009.

PEER 2008/102 *Modeling of Unreinforced Masonry Infill Walls Considering In-Plane and Out-of-Plane Interaction.* Stephen Kadysiewski and Khalid M. Mosalam. January 2009.

PEER 2008/101 *Seismic Performance Objectives for Tall Buildings.* William T. Holmes, Charles Kircher, William Petak, and Nabih Youssef. August 2008.

PEER 2007/101 *Generalized Hybrid Simulation Framework for Structural Systems Subjected to Seismic Loading*. Tarek Elkhoraibi and Khalid M. Mosalam. July 2007.

PEER 2007/100 *Seismic Evaluation of Reinforced Concrete Buildings Including Effects of Masonry Infill Walls*. Alidad Hashemi and Khalid M. Mosalam. July 2007.

The Pacific Earthquake Engineering Research Center (PEER) is a multi-institutional research and education center with headquarters at the University of California, Berkeley. Investigators from over 20 universities, several consulting companies, and researchers at various state and federal government agencies contribute to research programs focused on performance-based earthquake engineering.

These research programs aim to identify and reduce the risks from major earthquakes to life safety and to the economy by including research in a wide variety of disciplines including structural and geotechnical engineering, geology/seismology, lifelines, transportation, architecture, economics, risk management, and public policy.

PEER is supported by federal, state, local, and regional agencies, together with industry partners.

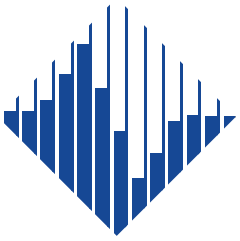

PEER Core Institutions:
University of California, Berkeley (Lead Institution)
California Institute of Technology
Oregon State University
Stanford University
University of California, Davis
University of California, Irvine
University of California, Los Angeles
University of California, San Diego
University of Southern California
University of Washington

PEER reports can be ordered at http://peer.berkeley.edu/publications/peer_reports.html or by contacting

Pacific Earthquake Engineering Research Center
University of California, Berkeley
325 Davis Hall, Mail Code 1792
Berkeley, CA 94720-1792
Tel: 510-642-3437
Fax: 510-642-1655
Email: peer_editor@berkeley.edu

ISSN 1547-0587X